Synthesis and Optical Spectroscopic Properties of Squaraine Superchromophores

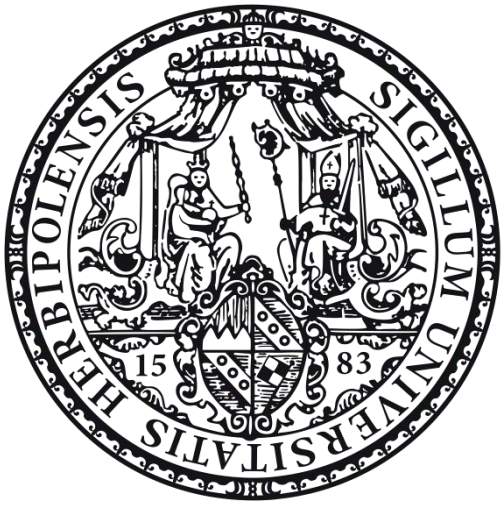

Dissertation zur Erlangung

des naturwissenschaftlichen Doktorgrades der

Julius-Maximilians-Universität Würzburg

vorgelegt von

Harald Ceymann

aus Kulmbach

Würzburg 2016

Eingereicht bei der Fakultät für Chemie und Pharmazie am

10.06.2016

Gutachter der schriftlichen Arbeit

1. Gutachter: Prof. Dr. Christoph Lambert

2. Gutachter: Prof. Dr. Matthias Lehmann

Prüfer des öffentlichen Promotionskolloquiums

1. Prüfer: Prof. Dr. Christoph Lambert

2. Prüfer: Prof. Dr. Matthias Lehmann

3. Prüfer: Prof. Dr. Tobias Hertel

Datum des öffentlichen Promotionskolloquiums

27.07.2016

Doktorurkunde ausgehändigt am

Die vorliegende Arbeit wurde in der Zeit von Oktober 2010 bis Juni 2016 am Institut für Organische Chemie der Universität Würzburg angefertigt.

Mein besonderer Dank gilt

Herrn Prof. Dr. Christoph Lambert

für die Überlassung des äußerst vielseitigen und interessanten Themas und das mit vielen Anregungen verbundene Interesse an dieser Arbeit.

COPYRIGHT

The following theses contributed also to this work:

3. Synthese und spektroskopische Characterisierung von Benzothiazol-Squarain-Farbstoffen, M. Mattenheimer, Bachelor Thesis, Julius-Maximilians-Universität (Würzburg), **2012**.
4. Synthese und spektroskopische Characterisierung von sternförmigen Squarain Trimeren, M. Balkenhohl, Bachelor Thesis, Julius-Maximilians-Universität (Würzburg), **2014**.
5. Synthese und spektroskopische Characterisierung von sternförmigen Squarain Trimeren zweiter Generation, C. Mützel, Bachelor Thesis, Julius-Maximilians-Universität (Würzburg), **2014**.

CONTENTS

Abbrevations

1PA	one-photon absorption
2PA	two-photon absorption
2PAF	two-photon absorption induced fluorescence
CV	cyclic voltammetry
DPV	differential pulse voltammetry
EADS	evolution associated difference spectrum
ESA	excited state absorption
FEA	fluorescence excitation emission
FLUC	fluorescence-upconversion spectroscopy
GPC	gel permeations chromatography
GSB	ground state bleaching
SADS	species associated difference spectra
SE	stimulated emission
SEC	spectroelectrochemistry
TCSPC	time-correlated single photon counting
TD-DFT	time dependent density functional theory

1 Introduction

1.1 Squaraines

1.1.1 Definition

The term squaraine was coined by *Schmidt*[1, 2] in 1980 and is a combination of squaric acid and betaine. These two terms describe the intrinsic structural properties of squaraines, the central quadratic cyclobutadiene acceptor unit and their zwitterionic character. Therefore, it is obvious that the expression “squaraine” is only used for the 1,3-dicondensation products of squaric acid, because the isomeric 1,2-dicondensation products do not have a zwitterionic character (see Scheme 1). Strictly speaking, squaraines are represented by two resonance forms, the dipolar cyanine (I) and the cyclobutenediyliumdiolate structure (II), but for reasons of simplicity, mostly (I) is used in this work.

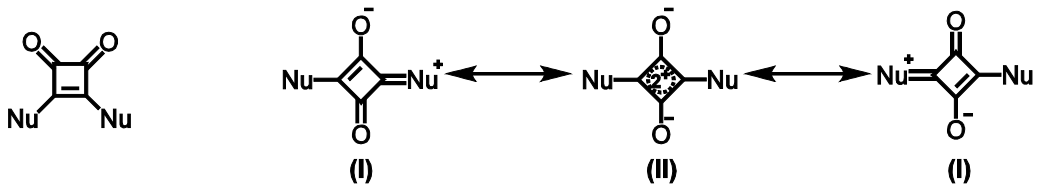

Scheme 1 1,2- and 1,3-dicondensation products of squaric acid with nucleophiles and their resonance forms.

Formally squaraines belong to the class of polymethine dyes as they usually consist of two heteroatoms that are connected by an odd number of repeating methine units, which results in conjugated systems. One exception are azulene squaraines, that do not have any heteroatoms. However, the donor-acceptor-donor (D–A–D) structure of the squaraines is unique for this class. The strong electron withdrawing oxocylcobutenolate core is stabilised by strong electron donating groups such as heterocycles, electron rich aromatic units or aniline derivatives.

1.1.2 Synthesis of Monomeric Squaraines

Over time many electron rich compounds were treated with squaric acid in order to form squaraines. The first reactions of this kind were reported by *Treibs* and *Jacob*[3] with highly reactive pyrroles (**I1**) and 1,3,5-trihydroxybenzene (**I2**) in ethanol. In the same publication

they claimed the synthesis of the first polymeric squaraine (**I3**) in refluxing acetic acid. While the monomers suffered only from poor solubility the polymer was completely insoluble.

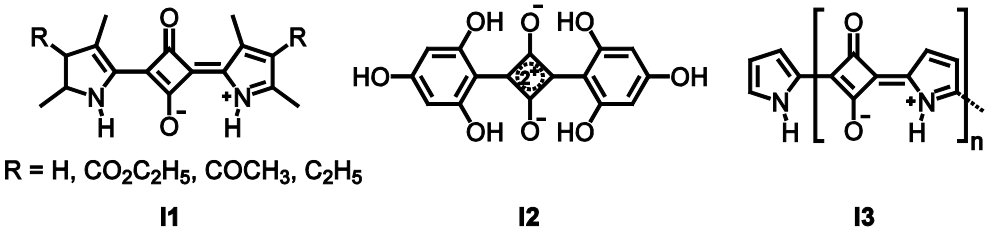

I1 **I2** **I3**

Figure 1 The first squaraines reported by *Treibs* and *Jacob*.[3]

In the following years many other symmetrical squaraines were synthesised by condensation reactions of two equivalents of an electron rich aromatic compound or a methylene base with one equivalent of squaric acid. The reaction conditions and especially the choice of the solvent play a crucial role in the synthesis of squaraines. While *Treibs* and *Jacob* used acetic anhydride as the solvent for the reaction of the *Fischer Base* with squaric acid (**I4**)[4] *Sprenger* and *Ziegenbein*[5] used a mixture of benzene and ^{n}BuOH with quinoline as a base. The latter method has a number of advantages; the use of a base allows the in situ preparation of the methylene base and the solvent mixture an azeotropic distillation of the water that is formed during the reaction. Therefore, this method is most commonly used today, although benzene is usually replaced by toluene. The use of butanol has a crucial significance as only in protic solvents a sufficient solubility of squaric acid is achieved.[6] *Sprenger* and *Ziegenbein* also reported the synthesis of squaraine dyes with benzothiazole (**I5**)[5], benzoselenazole (**I6**)[5], azulene (**I7**)[7], 2-methylchinoline (**I8**)[5], tertiary aromatic amines (**I9**)[8] and barbituric acid (**I10**)[9].

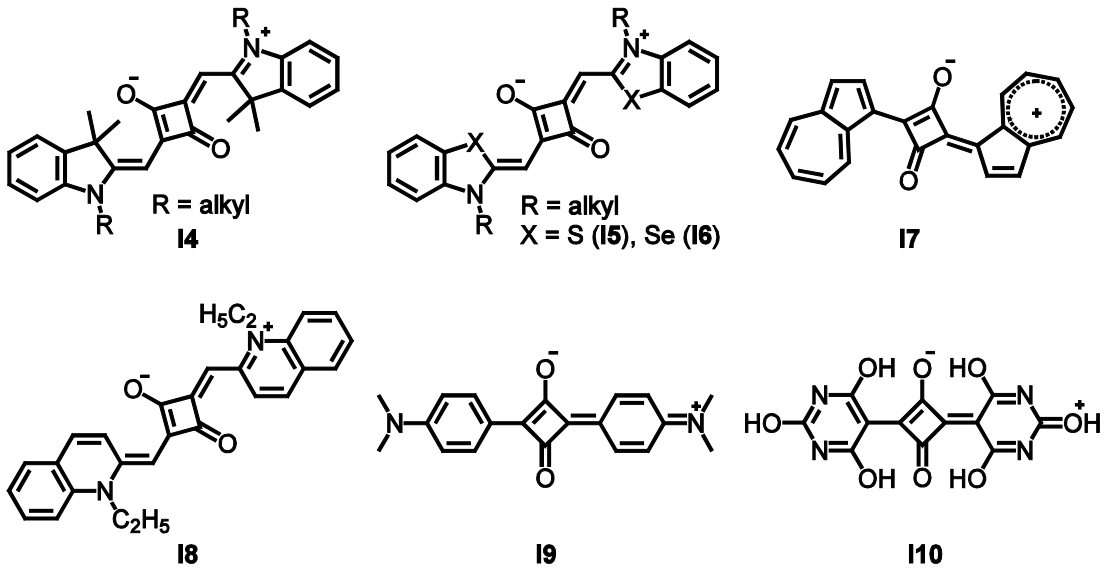

Figure 2 Selection of symmetrical squaraine dyes.

The general reaction mechanism for the formation of symmetrical squaraines was proposed by *Treibs* and *Jacob*[4] and later supplemented by *Sprenger* and *Ziegenbein*[6] for reactions in alcohols. In the latter squaric acid initially forms a half ester[7] (in brackets in Scheme 2) followed by the actual attack of the nucleophilic compound at the carbonyl carbon of the vinylogous ester and the subsequent elimination of an alcohol (or water, if the reaction takes place in non-alcoholic solvents). This leads to the formation of an intermediate semisquaraine. Usually another nucleophile attacks the semisquaraine in 2- or 3-position followed by the elimination of another water molecule. The higher reactivity at the 3-position makes the 1,3-substituted squaric acid the main product of this second condensation reaction. Since all reaction steps are reversible the best yields are achieved if the products are removed from the reaction mixture. This can be realised by e.g. azeotropic distillation of water, or precipitation of the squaraines.

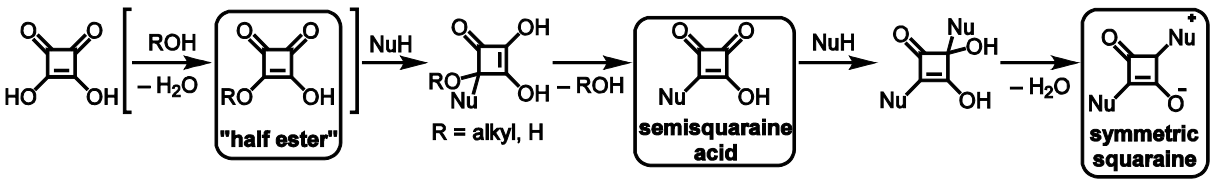

Scheme 2 Proposed reaction mechanism of the condensation reaction to symmetric squaraines.

The direct synthesis of asymmetrical squaraines starting from squaric acid is almost impossible. The 1:1:1 reaction of squaric acid with two nucleophiles results either in the almost exclusive formation of one symmetrical squaraine or in a varying mixture of two

symmetrical and one asymmetrical squaraine whose separation is challenging.[8] However, *Jyothish et al.*[9] reported that electron-rich derivatives of the quinoline series selectively yielded the semisquaraine (**I11**) in a 2:1 condensation reaction with squaric acid. If electron withdrawing substituents on the quinoline ring were used the intermediate semisquaraine reacted further to the squaraines (**I12**) (Scheme 3). This behaviour has its origin in the acidity of the hydrogen atoms of the 2-methyl group. In the case of **I11** the electron-donating groups at the benzene ring lower this acidity and thereby decrease the formation of the enamine nucleophile. Thus, the formation of the semisquaraine is slowed but not prohibited. The reactivity of the semisquaraine is lower than that of the squaric acid due to the addition of the first electron donor group and therefore the sole product of the reaction is the semisquaraine. In the presence of electronegative or electron-withdrawing groups the acidity of the hydrogen atoms of the 2-methyl group is higher, which results in a significantly higher concentration of the enamine nucleophile. Hence, in these cases the reaction does not stop at the semisquaraine but results in a quantitative conversion to the squaraines **I12**.

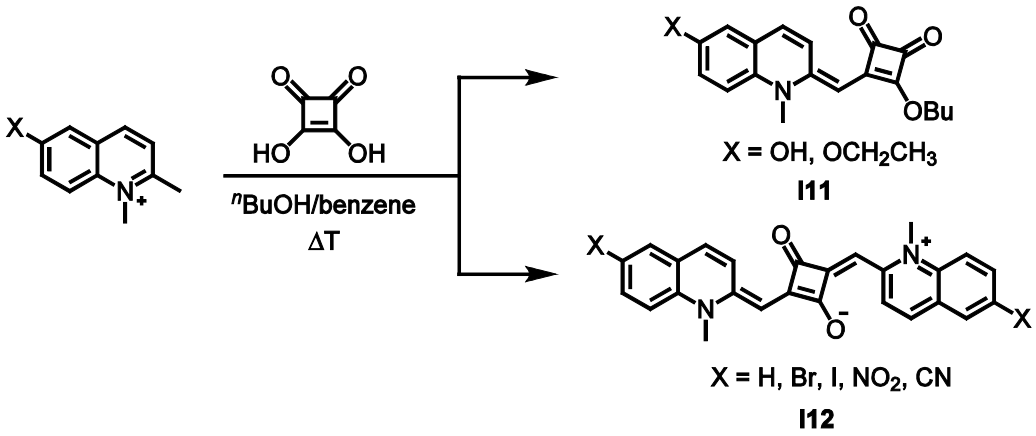

Scheme 3 Direct synthesis of semisquaraines.

Since the postulated mechanism for the squaraine synthesis contains the formation of a semisquaraine acid the most promising approach to the controlled formation of asymmetrical squaraines seems to be the isolation of this intermediate followed by a condensation reaction with a different nucleophile. Although the reactivity of the semisquaraine acid is usually lower than that of squaric acid this difference is not very large. Therefore, the isolation of a sufficient amount of semisquaraine acid from the reaction of a nucleophile with squaric acid is only possible if a very large excess of the latter is used. The required chromatographic purification is both tedious and inefficient. Therefore, the first rational synthesis of asymmetrical squaraines followed another approach. *Law* and *Bailey*[10,

[11] developed a synthetic route that utilises a modified version of a [2 + 2] cycloaddition reaction of 4-methoxyphenylacetyl chloride (**I13**) with tetraethoxyethene (**I14**) reported by *Bellušˇ*[12] (Scheme 4).

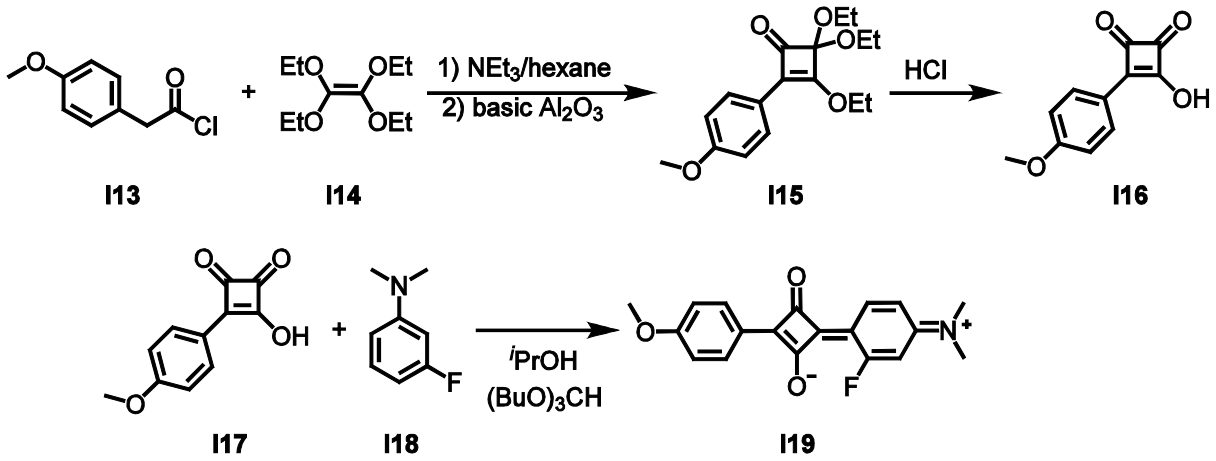

Scheme 4 Synthesis of an asymmetrical squaraine via a [2 + 2] cycloaddition.

The intermediate **I15**, a cyclobutenone, can be saponified with hydrochloric acid to the semisquaraine acid (**I16**). In the following condensation reaction in ^{i}PrOH with $(BuO)_3CH$ as a dehydrating agent the asymmetrical squaraine **I19** is synthesised. This type of reaction can be used for the selective incorporation of unreactive phenols or nitrobenzenes into squaraines or semisquaraines. However, the synthetic effort and the high possibility for polymerisation reactions if ketenes with a higher reactivity are used prohibit the general application of this method. Furthermore the commercialisation of pure squaric acid and its esters made a different approach more appealing.[13]

In this alternative method the reaction rate of the first condensation step is increased by the application of activated derivatives of squaric acid. If the reactants are used in an equimolar ratio the activated semisquaraines can be isolated. For the subsequent condensation to the asymmetrical squaraine these semisquaraines have to be deactivated, because otherwise the main product would be a 1,2-disubstituted cyclobutenedione. There are many possibilities for the activation of squaric acid[1, 8], the two most common of them are depicted in Scheme 5. The diesters of squaric acid can easily be prepared by simple heating in the respective alcohol. Similarly the semisquaraine chloride can be isolated from the reaction of squaric acid with $SOCl_2$ in benzene in the presence of a catalytic amount of DMF.

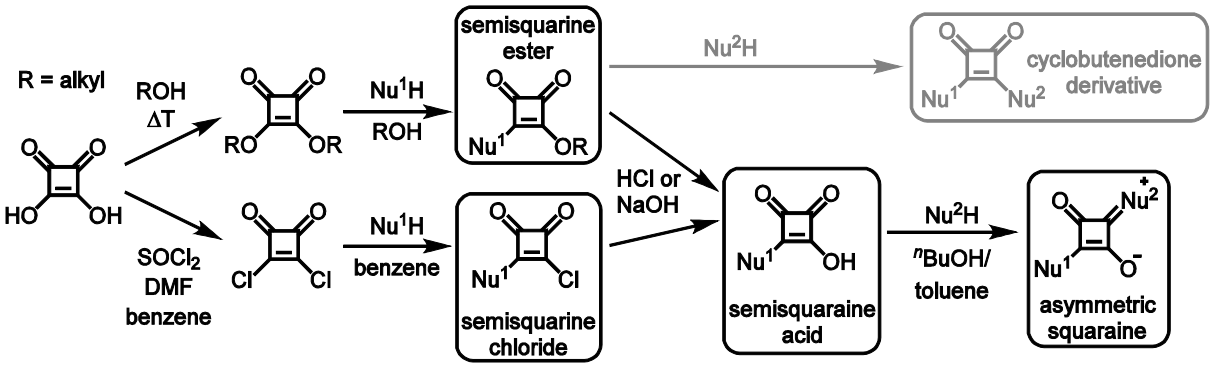

Scheme 5 Reaction pathways to asymmetric squaraines (black) and to cyclobutenedione derivatives (grey).

Both semisquaraine ester and semisquaraine chloride can conveniently be hydrolysed under either acidic or basic conditions. The resulting semisquaraine acid can then be employed in another condensation reaction to yield the asymmetric squaraine. For this last condensation step two already mentioned routes are possible and the choice depends on the nature of the second nucleophile. If it is an activated arene the best yields are achieved in an alcohol with an orthoformate as the dehydration agent as in Scheme 4. [10, 11] If the second nucleophile is a methylene base the azeotropic distillation in ^{n}BuOH/toluene yields the best results. Here, it is possible to generate the methylene base *in situ* by the addition of a base, *e.g.* quinoline or pyridine, or *ex situ*.

Semisquaraine esters can also be used for the synthesis of core substituted squaraine derivatives. The substitution of one oxygen atom of the central acceptor unit is a convenient way to tune the spectroscopic and electronic properties of squaraines. *Tatarets et al.*[14] described the synthesis of some acceptor substituted indolenine semisquaraines (Scheme 6). Most of these are obtained by a condensation reaction of the semisquaraine ester with methylene bases (**I20-24**). The chromophore (**I25**), where one oxygen atom is replaced by a sulphur atom, is the product of the reaction of the semisquaraine ester with sodium hydrosulphide.

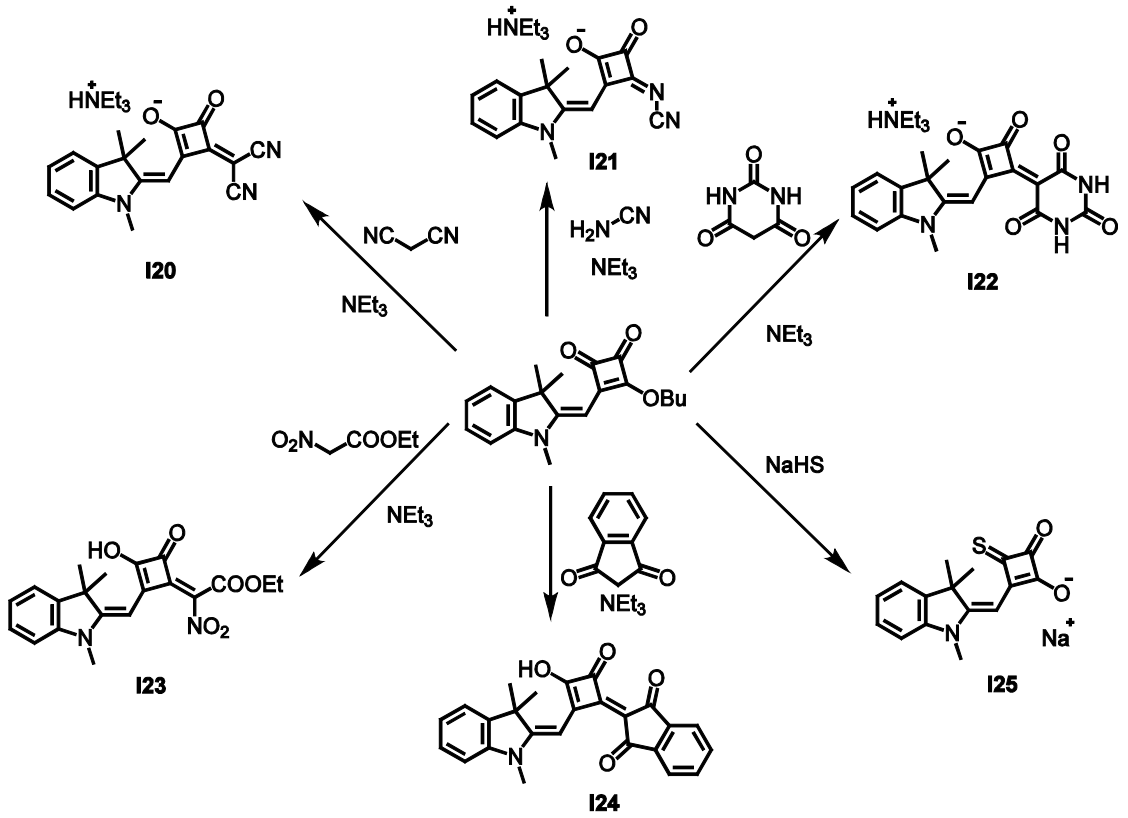

Scheme 6 Synthesis of some acceptor substituted semisquaraines.

Most of these acceptor substituted semisquaraines can then be used to obtain symmetric and asymmetric squaraines according to the general procedure depicted in Scheme 7.[14] The single exception is chromophore **I23**, probably due to electronic or steric reasons.

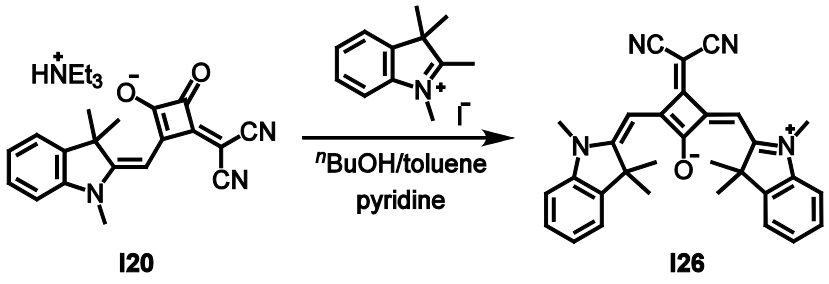

Scheme 7 General procedure for the second condensation reaction of an acceptor substituted semisquaraine.

For steric reasons, the large squaric acid substituents cause a change of the dominant structure of the squaraines from the transoid form of the “classic” squaraines (see Figure 2) to the cisoid form as shown for **I26**. In some cases the symmetric squaraines can also be synthesised by the utilisation of already functionalised squaric acid derivatives (Scheme 8).[15]

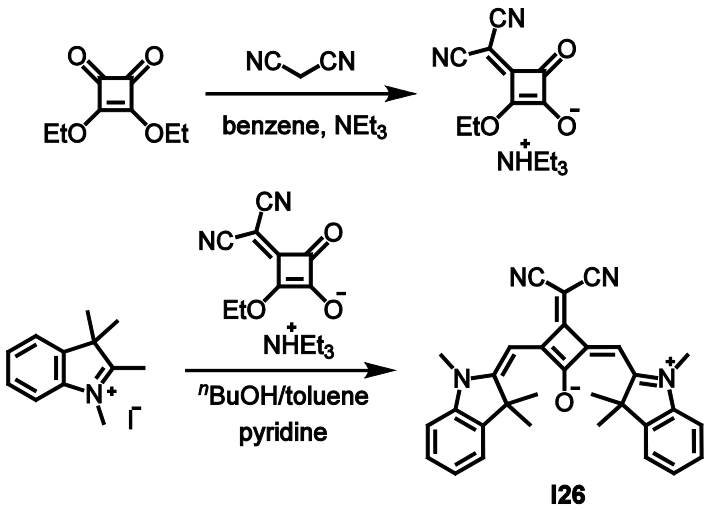

Scheme 8 Synthesis of a symmetrical acceptor substituted squaraine by the utilisation of functionalised squaric acid.

While *Tatarets et al.*[14] only reported about the synthesis of core functionalised squaraines containing indolenine, benzothiazole and quinoline derivatives *Mayerhöffer et al.*[15] added a few more compounds to the portfolio. These are mainly less reactive methylene bases such as quinoline, benzoxazole and benzoselenazole derivatives. For a few of these compounds there are no transoid squaraines known. The synthesis of the cisoid squaraines is possible due to the electron-withdrawing character of the dicyanovinylene group. The resulting higher electron deficiency of the squaric acid derivative in comparison to its parent compound leads to a higher reactivity towards nucleophiles. However, probably due to steric and electronic reasons the variety of core substituted compounds is still limited. For example, all reported acceptor core substituted squaraine compounds feature a methylene bridge between the outer donor groups and the central donor core.[14, 15]

1.1.3 Properties

The main optical property of squaraines is a sharp and intense absorption in the red to NIR region (Figure 3). Typically this absorption band shows a steep rise on the low energy side and vibronic shoulders with an average spacing of ~1000 – 1500 cm^{-1} on the high energy side.[16] The origin of this transition lies in the HOMO→LUMO ($\pi\pi^*$) excitation from the S_0 to the S_1 state. Its extinction coefficient is commonly on the order of 1–4 x 10^5 M^{-1} cm^{-1}. Due to the symmetrical structure of the example molecule the one photon excitation to the S_2 state in the vicinity of 25000 cm^{-1} has vanishing oscillator strength.[17, 18] The broad absorption at

higher energy is dependent on the used donor moieties and originates from a manifold of states with low oscillator strength.[16, 18] The emission spectrum is usually the mirror image of the main absorption peak, with a small *Stokes* shift. This is indicative of a delocalisation and small reorganisation energies in the excited state.

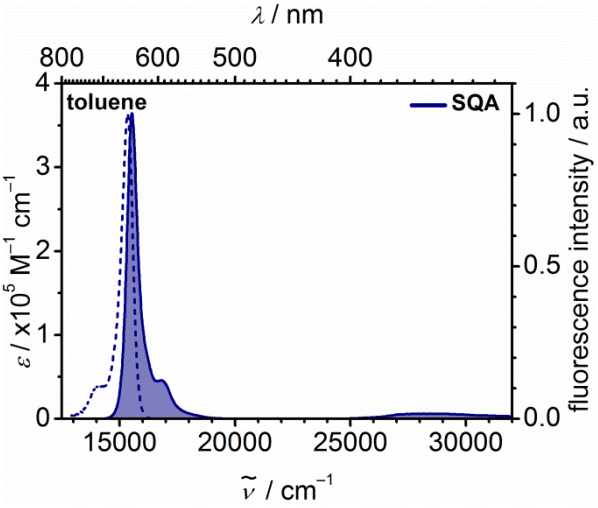

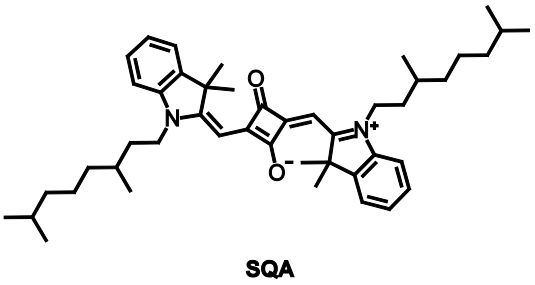

Figure 3 Absorption (solid line) and fluorescence (dashed line) of **SQA**, a typical symmetric indolenine squaraine, which will be discussed in chapter 3.3.2.

As already mentioned the position of the main absorption band can be tuned by the manipulation of the central acceptor core. A stronger electron acceptor leads to a decrease of the LUMO level which results in a red-shift of the HOMO→LUMO ($\pi\pi^*$) excitation. Likewise, the strength of the donor has an influence on the position of the HOMO and consequently also an impact on the position of the main absorption peak. [16-23] The variation of the donor strength can either be achieved by a change of the donor groups themselves, *e.g.* **I4** to **I5** or **I6** (Figure 2), or by substitution of the donor groups. For instance *Völker et al.*[24] reported a red shift of the main absorption of 700 cm^{-1} for the substitution of the first bromine in **I27** by one diarylamine group (**I28**) and another 500 cm^{-1} for the second (**I29**) (Figure 4). However, the shift of the absorption was also associated with a reduction of the extinction coefficient to less than 50 % compared to the brominated squaraine **I27**.

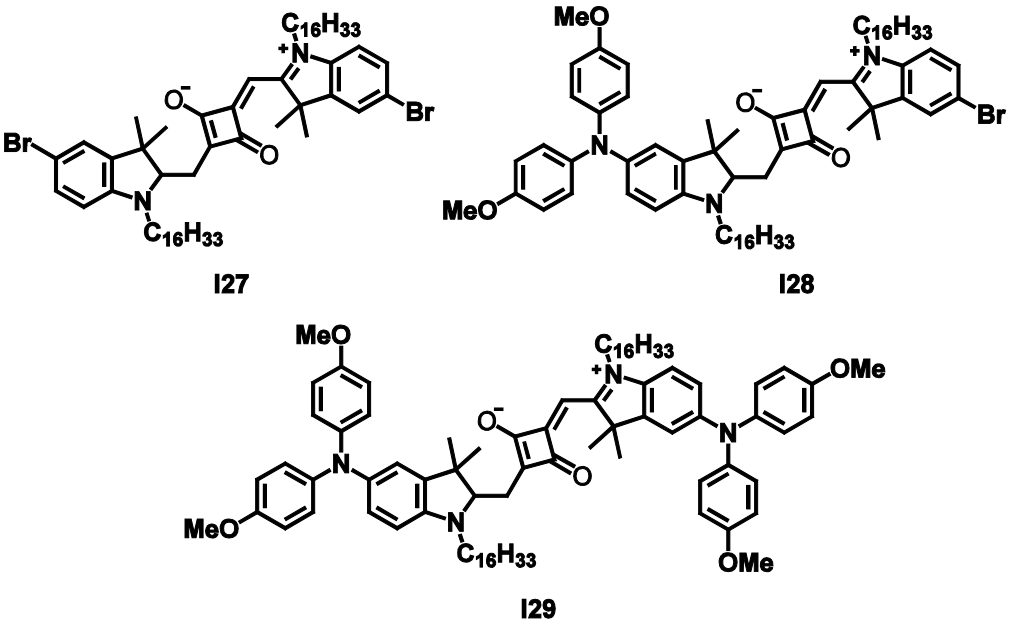

Figure 4 Indolenine squaraines with different donor groups.

The variation of the donor strength on the other hand can be achieved by the substitution of one oxygen atom of the central acceptor unit, as shown in Scheme 6 and Scheme 7.

1.1.4 Applications

The spectroscopic characteristics of squaraine dyes made them interesting for a number of applications. Over time they were used as photoconductors for xerographic processes[25, 26] and as absorbing agents for both optical data storage[27, 28] and bulk-heterojunction or dye-sensitised solar cells.[13, 29] Furthermore, squaraines are used as sensitive markers and detectors for ions.[30] Here, the binding of the substrate can occur either at an oxygen atom of the central cyclobutene ring or at an ionophore that is integrated into the squaraine structure. For example, the bis-dibenzo-18-crown-6-based squaraine **I30** can be used for the detection of Hg^{2+} ions in aqueous media (Scheme 9). Due to a perturbation of the D-π-A-π-D conjugation structure the change of the absorption intensity in the presence of Hg^{2+} ions can even be strong enough to be observed by the naked eye.[31]

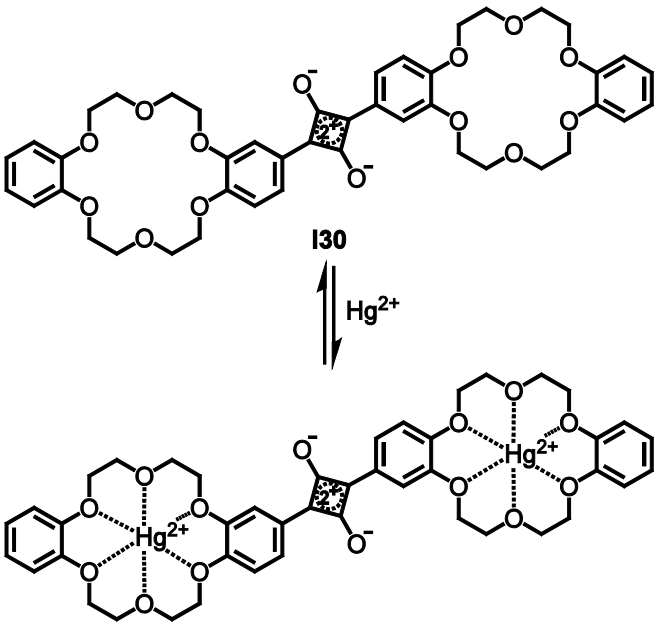

Scheme 9 Detection of Hg^{2+} by a bis-dibenzo-18-crown-6-based squaraine.

A similar concept is exploited for the self-assembly of supramolecular materials. *Yagi et al.*[32] used the central oxygen groups of two polymethylene-bridged squaraines of the **I9** type to form folded H-aggregates by the chelation of Ca^{2+} ions (Figure 5). *Ajayaghosh et al.*[33] even achieved spherical and extended micellar structures by the use of polyether chains for the bridging of the two squaraines.

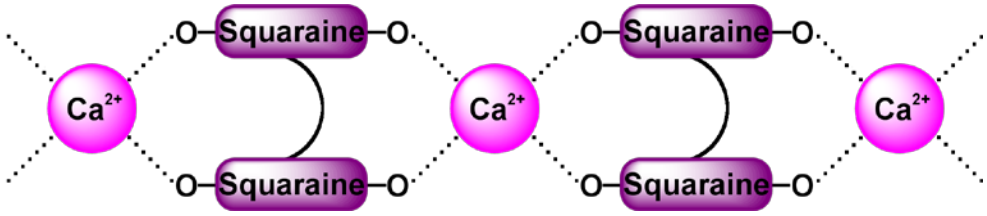

Figure 5 Extract of a self-assembled H-aggregate of polymethylene-bridged squaraines.

Squaraines are also tested as sensitisers in type II photodynamic therapy (PDT) reactions. Here, highly toxic singlet oxygen ($^1O_2$) is generated in *vivo* from ground-state molecular oxygen ($^3O_2$) through a sensitiser in the triplet excited state. This allows a high selectivity in the destruction of cancer cells. Although their absorption is well within the photodynamic window (600 – 850 nm) where the tissue penetration by light is high, squaraines were long considered as unsuitable sensitisers, because they have an inherently poor intersystem crossing efficiency and consequently a low efficiency in the generation of singlet oxygen. In case of the phloroglucinol squaraines **I31** (Figure 6) this efficiency could be improved significantly from >0.1% for the unsubstituted chromophore (X = H) to 0.22 (X = Br) and 0.5 (X = I) by halogenation of the donor moieties, due to the heavy atom effect.[34]

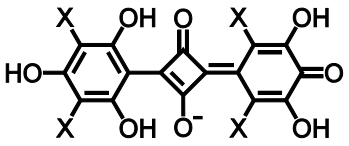

I31

Figure 6 Structure of squaraine compounds that are tested for photodynamic therapy.

In recent years squaraines were furthermore tested in nonlinear optical applications.[13] In particular the two-photon absorption (2PA) cross sections (δ_2) of squaraines were examined. For an easier understanding of 2PA the basic principles, design strategies for promising chromophores and measurement technics are elucidated before some applications are presented.

1.2 2-Photon Absorption

1.2.1 Theory

2-photon absorption (2PA) is a third order nonlinear optical effect that was first described theoretically by *Göppert-Mayer* in the 1930s.[35] It is defined as the simultaneous absorption of two photons *via* a virtual state that gains no population during the excitation (Figure 7) and exists only up to a few femtoseconds. This means, that the absorption of the second photon has to take place within this short timescale after the absorption of the first photon.[36-38] The two photons can either have the same energy (degenerate or one-color 2PA) or different energies (non-degenerate 2PA). In contrast, the stepwise absorption of two photons consists of the population of an existing, real state, such as S_1, by one-photon absorption (1PA) followed by excited state absorption (ESA).

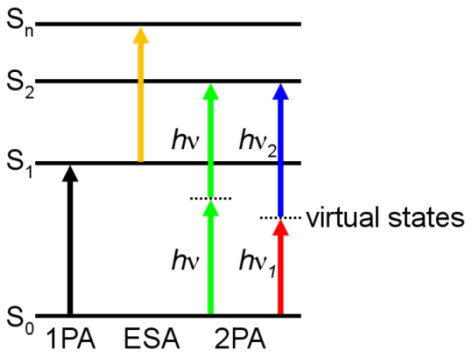

Figure 7 Energy diagram of one photon absorption (1PA, black arrow), excited state absorption (ESA, orange arrow), degenerate (green arrows) and non-degenerate (red and blue arrows) 2-photon absorption (2PA).

The probability for 2PA depends on the product of the intensities of the laser beams ($(I)^2$ or $I_1 \times I_2$), while the transition energy is the sum of the energies of the two photons ($2h\nu$ or $h\nu_1 + h\nu_2$). This means, that in order to observe two-photon absorption an intense monochromatic light source with short pulse duration is needed. Therefore, it took 30 years until the first observation of the effect by *Kaiser et al.*[39] with a ruby optical maser. The availability of lasers, especially focused sub-picosecond pulsed lasers, led to an increased activity in the field of TPA.[40, 41]

For reasons of simplicity only the degenerated case is considered in the following. Here, the attenuation of the intensity I after the distance z in the medium resulting solely from 2PA can be expressed by eq. (1):

$$\frac{dI}{dz} = -N\alpha_2 I^2 \tag{1}$$

N is the number of molecules per unit volume, α_2 is a molecular absorption coefficient for 2PA. The attenuation can also be written using the 2PA molecular cross section $\delta_2 = \alpha_2/h\nu$ in Göppert-Mayer (1 GM = 10^{-50} cm^4 s photons^{-1} molecule^{-1}) and the photon flux $F = I/h\nu$.[42]

$$\frac{dI}{dz} = -N\delta_2 h\nu I^2 = -N\delta_2 F I \tag{2}$$

There are a few approaches to the theoretical calculation of δ_2 in the literature that result in slightly different formulas.[42-47] Especially the different definitions (S.I. vs. CGS) and abbreviations that are used for the laser frequency, energy and the line shape make a comparison of the formulas confusing.[48] With eq. (3) the maximum of the 2PA cross section of a 2PA-band with a Lorentzian shape can be calculated for light with only one plane of polarisation in S.I. units.[40]

$$\delta_{\max} = \frac{2\pi h\nu^2}{\varepsilon_0^2 n^2 c^2} L^4 \left(\frac{1}{\Gamma}\right) S_{fg}$$
$$\text{with } S_{fg} = \left[\sum_i \frac{\langle \mu_{gi}\mu_{if} \rangle}{(E_{gi} - h\nu)}\right]^2 \tag{3}$$

Here, Γ is the half-width at half-maximum of the 2PA band in energy units. L is the local field factor, that can be calculated by $L = (n^2 + 2)/3$ (with the refractive index n). The indices g, i and f represent the ground, intermediate and final state. Therefore, E_{gi} is the energy gap between the two denoted states. μ_{ab} are the amplitudes of the transition-dipole moments

induced by the electric field of a light wave, whose frequency is in resonance with the energy difference between the a and b states. In solution the molecules and consequently their transition-dipole moment vectors are randomly oriented. Hence, for a mathematical solution the average of their projections onto the direction of the electrical field has to be calculated as indicated by the pointed brackets in eq. (3).[41, 45] For the majority of the absorbers with high 2PA cross sections most of the transition moments are oriented parallel to each other. Therefore, the term that describes the parallel transition moments has the greatest influence and the other orientations can be neglected. With this, eq. (4) can be derived.[40]

$$S_{fg} = \frac{1}{5}\left[\underbrace{\left(\frac{\Delta\mu_{gf}\,\mu_{gf}}{h\nu}\right)^2}_{\mathrm{D}} + \underbrace{\sum_{i\neq f,g}\left(\frac{\mu_{gi}^2\,\mu_{if}^2}{(E_{gi}-h\nu)^2}\right)}_{\mathrm{T}}\right] \tag{4}$$

Here, $\Delta\mu_{gf}$ is the change of the static dipole moment from the ground state to the final state. The first term of eq. (4) is abbreviated as D (dipolar-term), the second as T (2PA-term).[43, 49] These abbreviations can be explained with the three-level model for centrosymmetric systems (Figure 8a) and the two-level model for non-centrosymmetric systems (Figure 8b).[40]

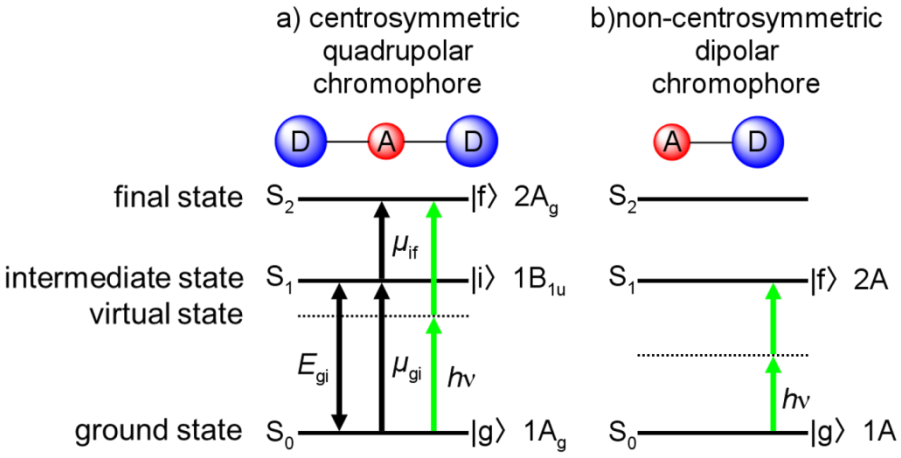

Figure 8 Schematic representation of the energy level diagram for the essential states in a centrosymmetric donor-acceptor-donor (D-A-D) quadrupolar (a) and a non-centrosymmetric acceptor-donor (A-D) dipolar (b) chromophore.

The dipolar-term corresponds to a two-photon resonance with a low-lying intermediate state. For a centrosymmetric quadrupolar chromophore (like squaraines) this term is zero (Figure 8a), because the static dipole moments do not change between the ground and the

final state. The states for such chromophores with D_{2h} symmetry are denoted as $1A_g$, $1B_{1u}$ and $2A_g$ from the ground state to the final state. According to the selection rules, transitions between states with different parity (gerade and ungerade) are allowed as one-photon transitions.[50] This is the case for g↔i and i↔f. For the two-photon transition the selection rules are different.[51, 52] The first photon induces a virtual state that is a superposition between $|g\rangle$ and $|i\rangle$. The induced polarisation of this state is detuned from that of the intermediate state by a frequency that corresponds to the difference between E_{gi} and $h\nu$. Due to the transient presence of the ungerade intermediate state, the second photon can induce an electric-dipole transition to the gerade final state. Hence, for centrosymmetric molecules the two-photon transition is allowed between states with the same parity.[37, 40]

If the molecule is not centrosymmetric as depicted in Figure 8b the transition rules are different. Here, in theory the transition from the ground state to the first excited state is both 1PA and 2PA allowed. In this case the dipolar-term in eq. (4) is different from zero. However, in dipolar molecules the 2PA term gets smaller, because it is related to an intermediate state that is now above the final state. As a result the observed δ_2 are commonly much lower in such molecules, compared to centrosymmetric analogues.[40]

For the case that the photon energy $h\nu$ is close to E_{gi}, the 2PA-term in eq. (4) and consequently, if an adequate final state is available, the 2PA cross section value increases dramatically. This effect is called “double resonance”, and can only be determined correctly if there is no overlap with the 1PA.[46] Thus, molecules with sharp 1PA bands are needed.

According to eq. (4), reliable values for the transition-dipole moments are needed to predict accurately strong two-photon absorbers. The transition moments μ_{gi} and μ_{gf} can be easily calculated from the integration of the respective 1PA bands ($\int \frac{\varepsilon}{\tilde{\nu}} d\tilde{\nu}$) using the following equation:[53]

$$\mu^2 = \frac{3hc\varepsilon_0 \ln 10}{2000\pi^2 N_{Av}} \frac{9n}{(n^2+2)^2} \int \frac{\varepsilon}{\tilde{\nu}} d\tilde{\nu} \qquad (5)$$

The transition-dipole moment from the intermediate to the final state μ_{if} cannot be determined that easily. The observation of such transitions is *e.g.* possible as ESA in transient absorption measurements. However, the measurements often have to cope with overlays of ESA, ground state bleaching (GSB) and stimulated emission (SE). Therefore, μ_{if} is often

estimated theoretically and used in an empiric approach for the design of new efficient two-photon absorbing molecules.

1.2.2 Design of 2-Photon Absorption Materials

In the following a few promising design strategies for molecules with high two-photon absorption cross sections will be presented. The main focus will be on squaraines and the concepts that will be applied in the experimental part of this work. A more detailed overview can be achieved in one of the many reviews on this subject.[38, 40, 41, 48, 54]

Linear Molecules

In Figure 9 different substitution patterns of linear chromophores are depicted that were tested for their 2PA cross section. As already described above, dipolar molecules normally have smaller δ_2 values compared to the centrosymmetric quadrupolar molecules. Therefore, only the modifications of quadrupolar chromophores are discussed. The most simple quadrupolar molecules consist of either two acceptor (A) or two donor (D) groups that are connected *via* a π-conjugated bridge resulting in either an A-π-A (I) or a D-π-D (II) structure.

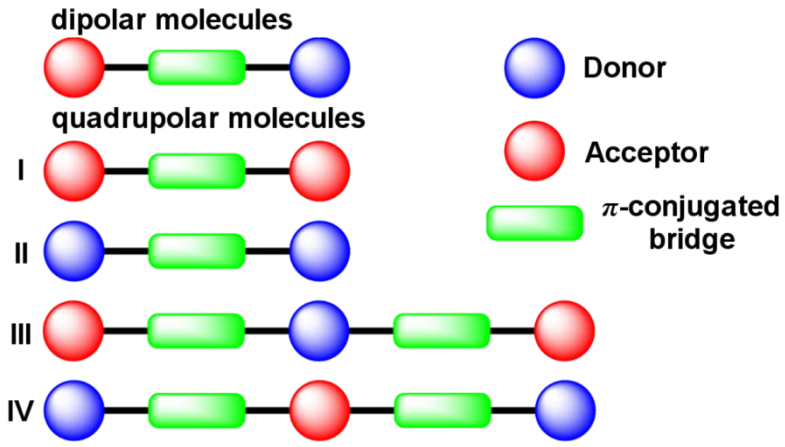

Figure 9 Schematic representations of linear chromophores with different substitution patterns.

Many different terminal groups for quadrupolar molecules were investigated. The general result is that chromophores with terminal donor groups (II and IV in Figure 9) have higher 2PA cross sections than chromophores with terminal acceptor groups (I and III in Figure 9).[38, 40, 55, 56]

The length of the π-conjugated bridge is an easy way to manipulate the 2PA cross section. *Rumi et al.*[44] have shown that the extension of the bridge in α,ω-diphenylpolyenes **I32** resulted in an increase of δ_2 from 260 GM (n = 2) to 1300 GM (n = 5). This effect is caused by the higher charge separation between the terminal donors and the centre of the molecule, resulting in an increase of μ_{gi} and consequently of the cross section. With increasing chain length the terminal groups will eventually become decoupled, leading to a saturation of δ_2. For that reason, the ratio of the 2PA cross section and the length of the chromophore or rather the effective number of the π-electrons N_e (δ_2/N_e) is used for the comparison of different molecules.[57]

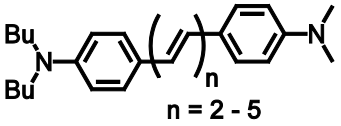

I32

Figure 10 D-π-D α,ω-diphenylpolyenes with different lengths of the π conjugated bridge.

If two identical chromophores are coupled and there is no electronic delocalisation between them, the value of the 2PA cross section should approximately double ($\delta_2 \propto N_e$). This behaviour is termed as additive. With increasing delocalisation the transition-dipole moments μ_{gi} and μ_{if} become larger and with them the 2PA cross section (cooperative behaviour). The linear dependency on both transition-dipole moments means, that if full cooperativity is observed the 2PA cross section should scale with $(N_e)^2$.[40, 57-59]

The nature of the π-conjugated bridge is also an important factor. For example a planarisation of the core moiety leads to a distinctly larger 2PA cross section of diphenyl (**I33**) compared to fluorene (**I34**) (Figure 11).[56]

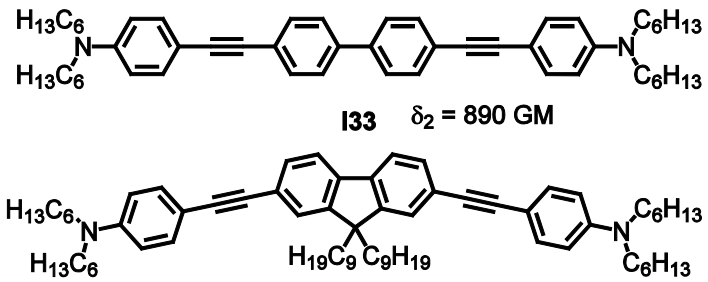

I33 δ_2 = 890 GM

I34 δ_2 = 1200 GM

Figure 11 Effect of the planarisation of the core on δ_2.

Van Stryland et al.[17, 60] varied the strength of the bridge between two nearly identical heterocyclic terminal donor groups (Figure 12). The D-π-D system **I35** with a polymethine bridge has the lowest 2PA response. The introduction of the acceptor functionality in **I36** and **I37** increases this response distinctly. The authors concluded that in these D-π-A-π-D systems the density of final states and therefore the number of possible electronic transitions between the $S_1 \leftarrow S_0$ band and twice that energy is raised. For the squaraine **I36** they also noticed a large intermediate state resonance ("double resonance") enhancement, because of the sharply rising low-energy side of the 1PA.

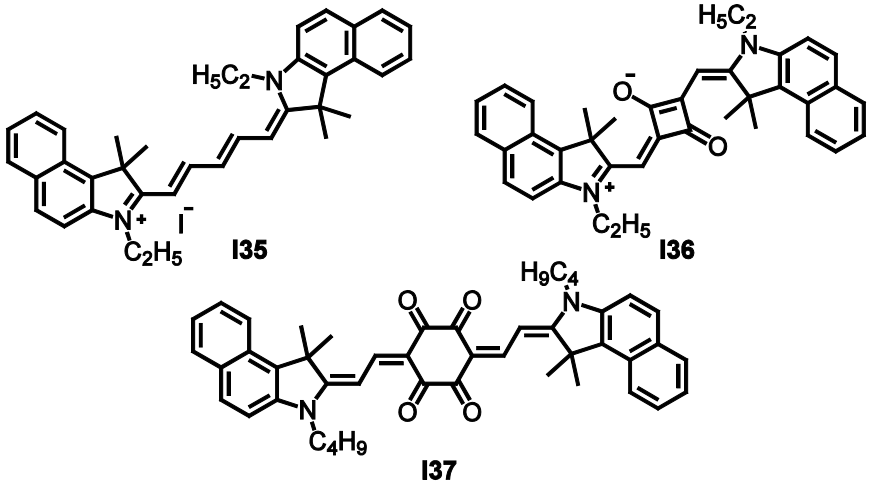

Figure 12 Comparison of a polymethine (**I35**) D-π-D chromophore with a squaraine (**I36**) and a tetraone (**I36**) D-π-A-π-D chromophore.

The combinations of the above mentioned promising concepts have also been tested. For example, *Moreshead et al.*[61] linked two D-π-A-π-D indolenine squaraines with a rigid fluorene bridge (Figure 13). Due to the coupling of the squaraine moieties the low energy 1PA of **I38** was much larger compared to an analogue monomer. The 2PA bands were also broader and more intense as a result of several efficient charge transfer transitions across the bridge.

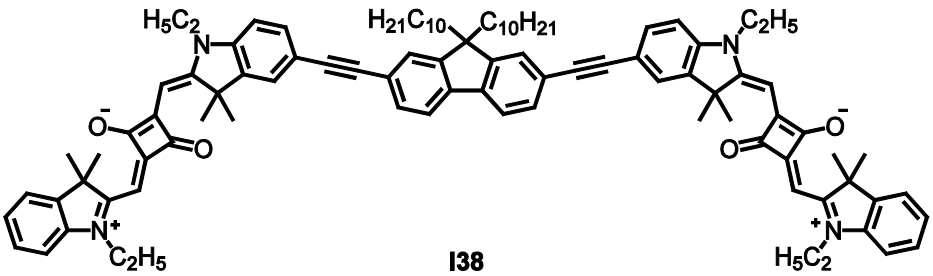

Figure 13 Two indolenine squaraines that are linked by a rigid bridge.

In another study an indolenine squaraine was used as a bridge between two porphyrins (Figure 14).[21] The formed superchromophore **I39** combined and improved the characteristics of the monomeric chromophores. In **I39** not only transitions within the porphyrins and the squaraine, but also intramolecular charge transfer transitions from the porphyrins to the central squaraine are observed. For example, the low energy side of the 1PA is red-shifted by ~2000 cm^{-1} in comparison to the monomeric squaraine. The efficient charge transfer bands are furthermore the reason, why the superchromophore has a broad 2PA spectrum with distinctly enhanced cross sections. This explanation was also confirmed by DFT frontier orbital calculations.

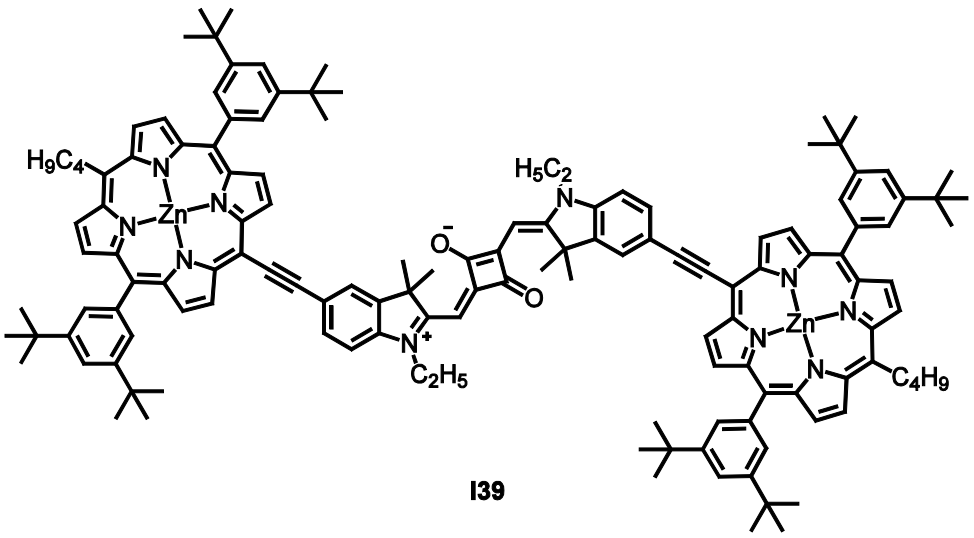

Figure 14 A porphyrin-squaraine-porphyrin superchromophore.

Scherer et al.[62] examined squaraine oligomers (up to a pentamer) that are connected *via* thienyl spacers (Figure 15). Here, the 1PA spectra could be explained by electrostatic exciton coupling. On the other hand the conjugational effects that led to the low-lying 2PA allowed states could not be explained by purely electrostatic exciton coupling.

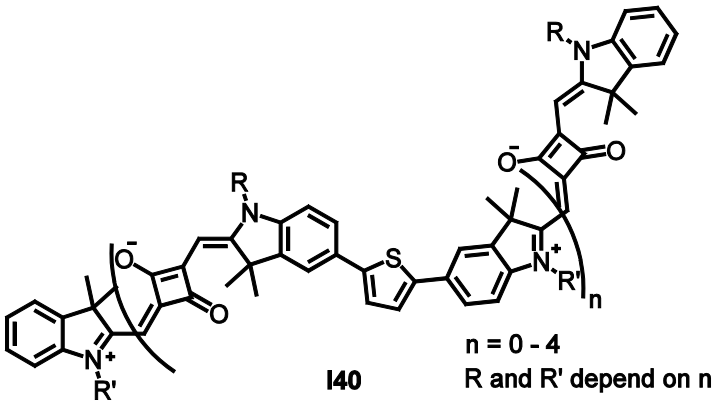

Figure 15 A homologues series (monomer-pentamer) of squaraines that are connected *via* thienyl spacers.

Multibranched Dyes

In comparison to their linear counterparts multibranched dyes sometimes exhibit significantly larger 2PA cross sections.[40, 41, 48] A simple rating for the branching effect was introduced with eq. (6).[43]

$$F_{(n)} = \frac{\delta_2^{(n)}}{\delta_2^{(1)}} \tag{6}$$

Here, $\delta_2^{(n)}$ is the 2PA cross section of a superchromophore consisting of *n* monomers and $\delta_2^{(1)}$ is the 2PA cross section of the monomer. Depending on the ratio $F_{(n)}$ the effect is called additive behaviour ($F_{(n)} = n$), cooperative behaviour ($F_{(n)} > n$) and weakening ($F_{(n)} < n$). Again the full potential for cooperative behaviour is observed for n^2.

One example for a cooperative behaviour is the quite small octupolar chromophore crystal violet (**I41**, Figure 16). It showed a remarkable δ_2 value of 2000 GM, which was explained by an efficient crosstalk among the conjugated arms.[63]

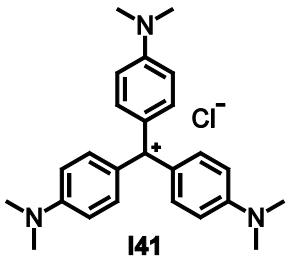

I41

Figure 16 Crystal violet.

Such crosstalk is often, but not always, observed in systems that have 4,4',4''-substituted triphenylamine or 1,3,5-substituted benzene as the core unit.[48] The star-shaped chromophores **I42** [45, 64] (Figure 17) consist formally of three dipolar molecules that share one central donor group. The triphenylamine moiety adopts a propeller like geometry. The 2PA spectra of these chromophores show a first low energy maximum close to twice the one-photon absorption maximum. Due to interactions between the branches this absorption is red-shifted in comparison to the monomeric dipolar reference compounds. The δ_2 of this band shows roughly additive behaviour. However, there is another 2PA maximum on the blue side of the spectrum, which is about four times larger than in the monomers. The authors suggest that for **I42** the coupling of the dipolar chromophores is responsible for a mixing of single-branch excited states, with important consequences on the nature of the excited states themselves.[41]

In the branched chromophores **I43** [65] the central nitrogen atom is replaced by a benzene unit. Again the branches adopt a propeller like geometry. The 1PA spectra show a slight red-shift compared to the monomers, indicating that there is only weak coupling between the branches. The 2PA spectra of the star-shaped trimers show almost additive behaviour compared to that of the monomers. Overall the spectroscopic data suggests that the branches behave as nearly independent subchromophores.

The different behaviour of the triarylamine and the benzene core cannot be ascribed to the geometries of the branches since both chromophores adopt a propeller like geometry. Based on high-level quantum-mechanical calculations, the authors concluded that not only dipolar interactions but also coherent interactions mediated by substantial wave function overlaps are important in defining the coupling values and, consequently, the spectroscopic properties of branched chromophores.[41, 45]

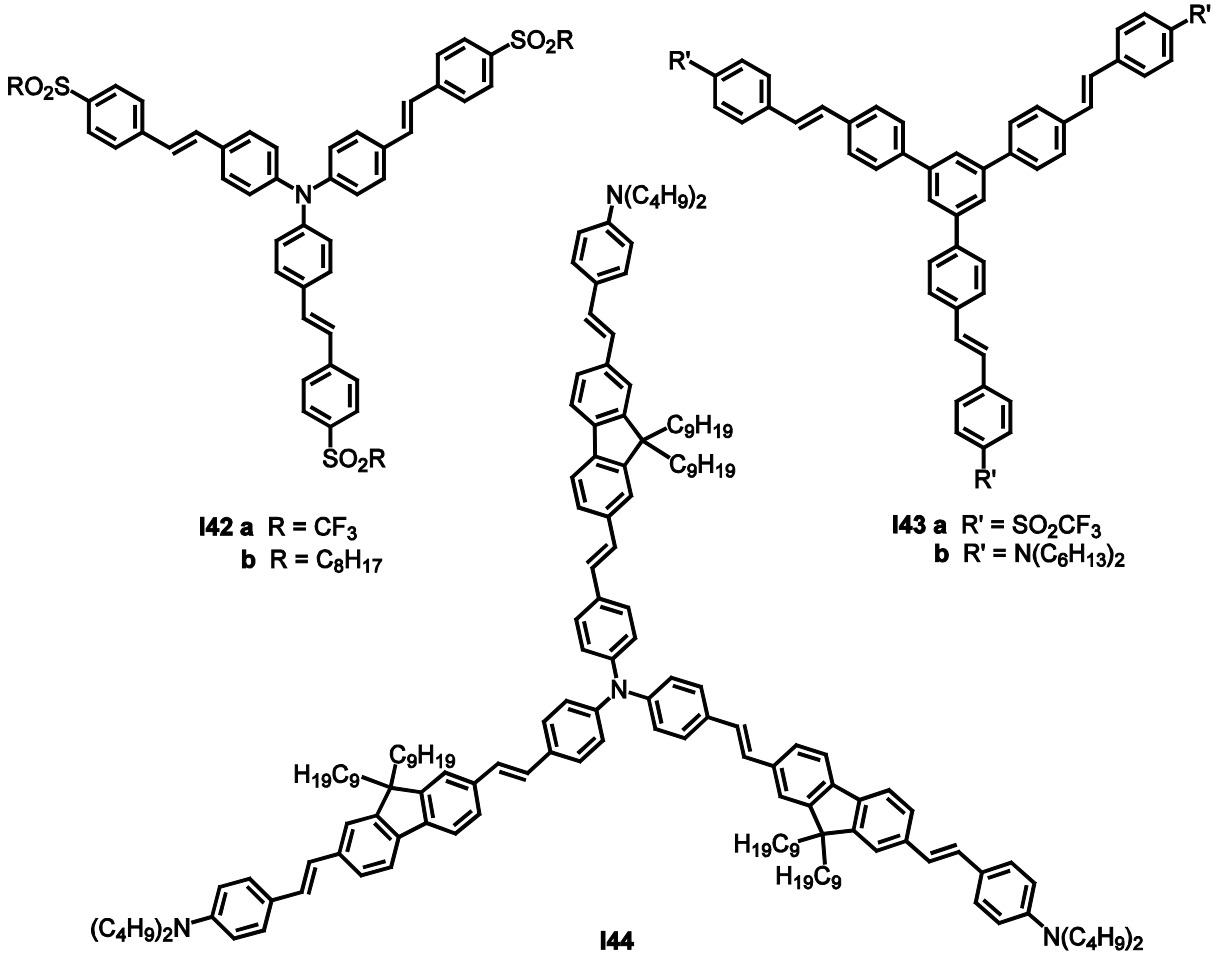

Figure 17 Star-shaped 2PA chromophores.

The star-shaped chromophore **I44** [66] consists of three quadrupolar chromophores **I34** that share one central donor group. The 1PA spectrum of **I44** is red-shifted and the molar extinction coefficient is approximately three times larger than that of **I34.** Although the central nitrogen core still promotes the cross-branch talk, like in **I42**, the trimer only displays nearly additive behaviour for the 2PA cross sections. The reason behind that is the dissymmetry that is introduced by the branching. Quadrupoles are commonly centrosymmetric or nearly centrosymmetric and have an inversion centre. Therefore, the selection rules that were already discussed above apply. As a result the transition to the first excited state is 2PA forbidden and the transition to the second excited state is 2PA allowed. Surprisingly the 2PA response of the trimer **I44** looks very much like that of the monomer. Although the 1PA is red-shifted the maxima of the 2PA bands are slightly broader but remain at the same energy. The authors argue that due to symmetry breaking by the incorporation of quadrupolar chromophores into a three-branched system additional two-photon allowed excited states are formed.[41, 66]

In principle all design strategies that are already discussed above for the linear compounds can be applied for the star-shaped chromophores as well. For example, larger 2PA cross sections can be achieved by elongation of the single branches. Furthermore, terminal donor groups are again superior to terminal acceptor groups in their 2PA response.[48]

1.2.3 Measuring Methods

For the degenerate case (see Figure 7) the 2PA properties of a sample can be measured by direct methods or by indirect methods. The direct methods are based on the attenuation of the beam after it crossed the sample (see eq. (1) and (2)). In the indirect methods an effect that is caused by 2PA, such as fluorescence/phosphorescence or generated heat, is quantified.

Direct Methods

In the z-scan technique a sample is translated along the path of a focused laser beam (z-axis). The setup is depicted in Figure 18.

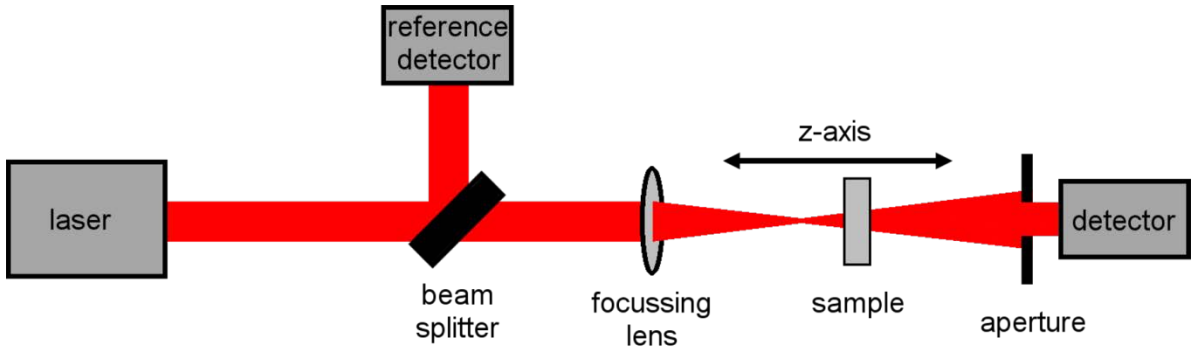

Figure 18 Experimental setup for a z-scan.

The aperture allows the measurement of two nonlinear effects. If the aperture is small ("closed-aperture" setup) self-focusing or defocusing of the beam due to intensity-dependent changes in the refractive index can be observed. These are caused by thermal effects or third-order nonlinear polarisability. Otherwise, if there is no limit to the collection of the light from the sample by the aperture ("open-aperture" setup), the measurement reflects the intensity-dependent transmission, which can be used to determine TPA cross sections according to eq. (7).

$$\frac{dI}{dz} = -\sigma_1 N I - N \delta_2 F I \qquad (7)$$

This equation is the extended version of eq. (2). In this case the 1PA with its cross section σ_1 is also considered. In a typical 2PA z-scan measurement the concentration of the sample is thin in order to minimise 1PA. The transmittance of the beam is unaffected by the sample if its position is far from the focus of the beam. During the translation of the sample the

transmittance decreases and reaches a minimum at the focus. After the focus is passed the transmittance increases again.

The measured cross sections can be influenced by two effects, additional to true simultaneous TPA.

1. High populations of excited states, either by one photon or by two photon absorption, can lead to nonlinear transmission through excited states absorption (ESA). In order to minimise this effect short laser pulses (<1 ps) and low repetition rates should be used.
2. If the aperture of the detector is too narrow or too far from the sample, self-defocusing can result in a loss of measured light. Nonlinear scattering can also induce a drop of transmittance.

These problems tend to enhance the apparent TPA cross sections especially if the 1PA is not negligible at the used wavelength.[37, 40, 67] Furthermore, the z-scan technique is quite insensitive. Therefore, concentrated samples are needed, which can be a problem due to solubility of the compound in the solvent of interest and/or aggregation phenomena.[41]

In an alternate setup the sample is stationary while the laser intensity is altered. Again the difference of the intensity before and after the sample is determined. In this so called nonlinear transmission experiment the optical configuration and the pulse characteristics have to be known in order to determine the 2PA cross section. Therefore, this setup is not prevalent.[37]

Indirect Methods

In the indirect methods one of the processes is monitored that can happen after an upper excited state is populated by 2PA and the nonradiative relaxation to S_1 has taken place. For example, a pump-probe approach can be used. In that case, the absorbance of the ESA process is proportional to the population of the S_1-state and consequently to δ_2 and the square of the beam energy.[68] If the molecule is deactivated by non-radiative decay pathways the 2PA cross section can also be determined by the local increase of temperature or one of its consecutive processes. For example, these are a change of the refractive index,

pressure changes or acoustic waves generated by the thermal gradient.[37] These methods are generally associated with quite high effort and therefore not that common.

Provided that the sample is fluorescent, its TPA cross sections can be determined by two-photon excited fluorescence (2PEF). This experiment uses the same principles as the one-photon excited fluorescence (1PEF). After the excitation, in this case by two-photon absorption, the molecule is in an upper excited state. The excited molecule relaxes by internal conversion to the lowest excited state S_1. From there the molecule fluoresces to the ground state (Figure 19).

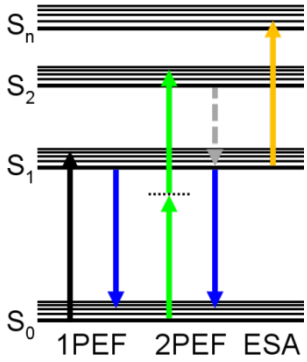

Figure 19 Energy diagram for one-photon excited fluorescence (1PEF), two-photon excitation fluorescence (2PEF) and excited state absorption (ESA).

Assuming the molecule follows "Kasha´s rule"[69], the observed fluorescence spectrum is equal to the spectrum obtained by one-photon excited fluorescence. If stimulated emission and self-quenching are excluded the measured signal is the number of photons, that are created by spontaneous fluorescence, collected per unit time $F_2(t)$. Using eq. (8) the 2PA cross section δ_2 at wavelength λ_2 can be determined.[70]

$$F_2(t) = \frac{1}{2} g \Phi \eta C \delta_2(\lambda_2)(I_0(t))^2 \int_V dV S^2(r) \qquad (8)$$

The factor 1/2 reflects that for one excitation event two photons are needed. $g = (I_0^2(t))/(I_0(t))^2$ is a measure of the second-order temporal coherence of the excitation source, Φ is the fluorescence collection efficiency of the system, C is the dye concentration (< 0.1 OD in order to minimise reabsorption), η is the differential fluorescence quantum efficiency, $(I_0(t))^2$ is the square of the incident intensity and $\int_V dV S^2(r)$ is the spatial distribution of the incident light with V as the illuminated sample volume. As eq. (8) indicates many parameters relating to the excitation light and the setup have to be distinguished in this absolute measurement in order to get reliable values for the TPA cross

section. Therefore, relative measurements are a much simpler approach. In that case the one- and two-photon excited fluorescence signals of the sample (s) are compared to a reference compound (r) under identical conditions. With this method most of the setup specific parameters are cancelled out as shown in eq. (9).

$$\delta_2^{(s)}(\lambda_2) = \frac{F_2^{(s)}(\lambda^{(s)})\eta^{(r)}(\lambda^{(r)})\Phi^{(r)}(\lambda^{(r)})C^{(r)}}{F_2^{(r)}(\lambda^{(r)})\eta^{(s)}(\lambda^{(s)})\Phi^{(s)}(\lambda^{(s)})C^{(s)}}\delta_2^{(r)}(\lambda_2) \tag{9}$$

The ratio of the one-photon excited fluorescence signals is shown in eq. (10).

$$\frac{F_1^{(r)}(\lambda^{(r)})}{F_1^{(s)}(\lambda^{(s)})} = \frac{\eta^{(r)}(\lambda^{(r)})\Phi^{(r)}(\lambda^{(r)})C^{(r)}\sigma_1^{(r)}(\lambda_1)}{\eta^{(s)}(\lambda^{(s)})\Phi^{(s)}(\lambda^{(s)})C^{(s)}\sigma_1^{(s)}(\lambda_1)} \tag{10}$$

The combination of eq. (9) and (10) leads to eq. (11). Here, all the values on the right-hand side of the equation are easy to determine.[71]

$$\delta_2^{(s)}(\lambda_2) = \frac{F_2^{(s)}(\lambda^{(s)})F_1^{(r)}(\lambda^{(r)})\sigma_1^{(s)}(\lambda_1)}{F_2^{(r)}(\lambda^{(r)})F_1^{(s)}(\lambda^{(s)})\sigma_1^{(r)}(\lambda_1)}\delta_2^{(r)}(\lambda_2) \tag{11}$$

The method was refined by *Makarov et al.*[72] by the publication of 2PA standards in a wide excitation wavelength range. With these values the cross sections can be determined by eq. (12).

$$\delta_2^{(s)}(\lambda_{obs}) = \frac{F_2^{(s)}(\lambda_{obs})\phi^{(r)}(\lambda_{obs})C^{(r)}}{F_2^{(r)}(\lambda_{obs})\phi^{(s)}(\lambda_{obs})C^{(s)}}\delta_2^{(r)}(\lambda_{obs}) \tag{12}$$

In that case the unknown $\delta_2^{(s)}$ is referenced to the $\delta_2^{(r)}$ of a 2PA standard that has its fluorescence maximum close to that of the sample. Here λ_{obs} is the fluorescence observation wavelength. The differential quantum efficiency $\phi(\lambda_{obs})$ can be obtained by a regular spectrofluorimeter or in the same setup. The detector responses have not to be determined as they conveniently cancel in both ratios $F_2^{(s)}(\lambda_{obs})/F_2^{(r)}(\lambda_{obs})$ and $\phi^{(r)}(\lambda_{obs})/\phi^{(s)}(\lambda_{obs})$.

The optical arrangement that is needed to perform a two-photon excited fluorescence measurement is in principle an advanced 1PEF setup (Figure 20). The main difference is the utilisation of a tuneable laser with pulses that are shorter than 1 ps, in order to minimise excited state absorption.

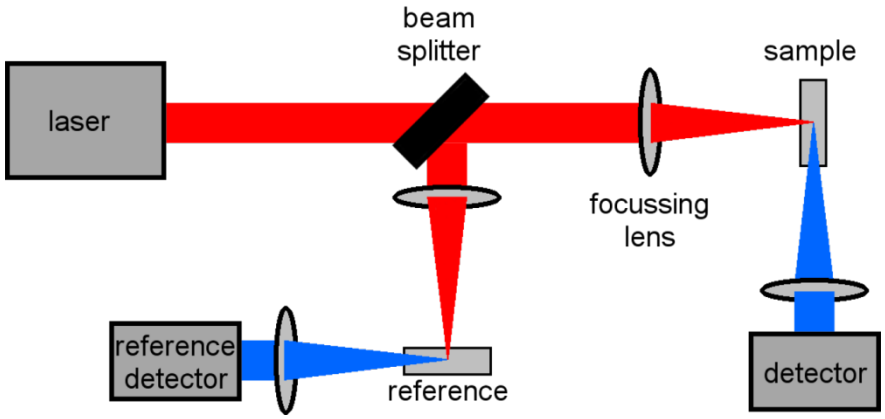

Figure 20 Schematic of an optical arrangement for a two-photon excited fluorescence setup.

The filters and pinholes that are used to configure the optical path are left out. The laser beam is split in two parts. One portion is used as a reference, in order to correct for fluctuations in intensity from pulse to pulse during the course of the measurement. However, other issues such as variations in spectral responsivity of diffraction gratings and detectors may introduce errors. Of course, a similar setup can be built without the beam splitter. In this one arm version the sample and the reference are measured successively. In that case the beam fluctuations are a source for deviations. *Makarov et al.*[73] have developed an improved version of this one arm setup, by building a two channel type. Here, the sample is located in the first channel and the reference in the second channel. They are aligned in the same laser beam with its focus located between them. The fluorescence after 2PA is simultaneously collected from both channels. The authors assumed that the depletion of the laser beam by the first channel is negligible. Differences in excitation and collection geometries and variations in detector response are excluded with a second measurement in which the sample and reference are exchanged. The 2PA cross section at one wavelength can then be obtained by eq. (13).

$$\delta_2^{(s)}(\lambda) = \delta_2^{(r)}(\lambda)\frac{C^{(r)}}{C^{(s)}}\sqrt{\frac{F_1^{(s)}(\lambda)F_2^{(s)}(\lambda)}{F_1^{(r)}(\lambda)F_2^{(r)}(\lambda)}}\frac{\phi^{(r)}(\lambda')}{\phi^{(s)}(\lambda')} \tag{13}$$

In that case the indices of the fluorescence signals *F* refer to the position of the sample and the reference.

As shown earlier δ_2 and of course the two-photon fluorescence signal depends on the square of the laser intensity. Regardless which setup is used, this dependence has to be checked throughout the experiment to exclude effects such as linear absorption, stimulated emission and excited state absorption. Due to the 90° geometry of the setups, the reabsorption of the

emitted light has to be minimised. This means that especially for chromophores with a small Stokes shift the incident beam should be focused near the cell window next to the detector.

Of course the same methods can be utilised for molecules with large intersystem crossing rates. Here, either the intensity of 2PA induced phosphorescence[74] or phosphorescence from singlet oxygen, produced by oxygen quenching of the triplet state of the chromophore[75] are measured.[37, 40]

1.2.4 Application of 2-Photon-Absorption

Especially its quadratic dependence on the photon intensity made 2PA an interesting technique for technologies that rely on high precision. The 3D resolution of 2PA is even higher, because the intensity of a focussed laser beam decreases also quadratically with the distance from the focal point. Therefore, 2PA falls off as the fourth power of distance from the focal plane.[76]

As already explained above, molecules that show high absorption within the photodynamic window (600 – 850 nm), where the light penetration of tissue is high are interesting for photodynamic therapy. Chromophores with high 2PA cross sections in this region can be used as “photon-harvesters”. The energy of their absorbed two-photons can then be transferred to a photosensitiser, which can generate singlet oxygen in the presence of atmospheric oxygen.[77] Molecules that combine high 2PA absorbance and good quantum yields of singlet oxygen generation allow an even more precise treatment of cancer cells due to the 3D resolution of 2PA.[78] Furthermore, 2PA is used *in vivo* for photoactivation and drug delivery. Although the cross section of most of the currently employed molecules is below 1 GM, the high spectral resolution and the depth of penetration are significant advantages in those applications.[40]

Two-photon absorption is also used in optical microscopy. In a confocal microscope only a small area of the sample is illuminated and the emitted light is collected through a pinhole, to eliminate the out-of-focus signal. The 2D or 3D image is generated at a computer by scanning over a regular raster and combining the single measurements. The resolution of this technique depends on the volume of the sample that is illuminated, which is much smaller in case of 2PA compared to 1PA because of the different dependencies on the beam intensity.[79, 80]

Another application is 3D multiphoton fabrication. In this lithographic process light induced polymerisation or depolymerisation processes are used to generate contrasts in solubility. The first process is already used in commercially available liquid 1PA 3D-printers.[81] The desired component is built up layer by layer through illumination of a photoactive liquid. The focus of the illumination, and the polymerisation, is close to the bottom of the liquid tank. After one layer is printed the component is lifted by the thickness of the layer and the next layer can be printed. The advantage of 2PA for this process lies in the spatial resolution. The printed structures could be much smaller (<µm) with clearly defined edges and could be printed without the need of lifting the component after one layer is printed. However, the intrinsic printing speed is significantly slower. In the depolymerisation technique the procedure is the other way around. Here, a solid is used and everything that gets illuminated liquefies while the rest forms the desired component. In that case the 1PA has the disadvantage, that only solid components can be printed, while in theory 2PA is capable to produce hollow structures.[82-84]

The three dimensional raster process can also be used to create 3D optical data storage memory. *Rentzepis et al.*[85] developed a write-once-read-many system that is capable to store up to 1 Tbyte of data in a 1 mm thick disc with a diameter of 120 mm. A standard DVD with the same diameter can only store 5 GB. For the disc the authors used a colourless precursor molecule that produces the Rhodamine 700 dye in the presence of acid. The second component is a light-sensitive photo acid generator that generates acid upon 2PA. The write process is done with a 532 nm laser (7 nJ per written bit) and the read process with a low-power 630 nm laser. The induced fluorescence of the Rhodamine with a wavelength of 670 nm is used in the read process. The whole system is thermally stable and the stored bits can be read over 10^6 times. However, the recording rate of only 25 Mbit/s means that the writing of the whole 1 Tbyte of data took nearly 90 h. Nevertheless the authors seem to be confident that the recording speed can be increased to 250 Mbit/s. Similar to Blu-rays, which have a larger capacity than DVD because they use blue light, the capacity of the disc can be increased if lasers with shorter wavelength are used for the writing process.[85-88]

All described applications of 2PA can benefit strongly from the development of materials that have higher 2PA cross sections. In the case of the *in vivo* application this means that lower laser intensities have to be used, which results in a minimisation of the damage to the

nearby tissue. In case of the technical applications the resolution and the speed can be increased.

1.3 Exciton Coupling Theory

The photophysical behaviour of organic superchromophores is often described by the *Frenkel*[89] exciton model. The term exciton is used for a bound electron-hole pair that is formed upon excitation and held together by electrostatic *Coulomb* forces. In *Frenkel* excitons these forces are strong, therefore, the electron and the hole are tightly bound and localised. This applies to clusters of weakly interacting molecules, such as organic molecules or aggregates.[41] If the Coulomb forces are weak, as *e.g.* in inorganic semiconductor crystals, the electron and the corresponding hole are loosely bound and the radius of the exciton is consequently large. In this case one speaks of *Wannier-Mott*[90, 91] excitons.

In the following the *Frenkel* exciton model is used to estimate the eigenvalues, the normalised eigenvectors and the transition-dipole moments for a dimer that consists either of two identical or different molecules. The description follows the work of *Amerongen et al.*[92] and *Kasha et al.*[93-95] The single molecules are considered to have two energy levels, ground state and excited state, with the according wave functions of the eigenstates ψ and ψ^*. The asterisk marks the excited state. The estimation was also done for a linear homotrimer and the star-shaped homo- and heterotrimers that are the main topic of this work. The results are listed in the appendix and depicted in Figures throughout this work (see appendix table S1-4).

Eigenvalues and Normalised Eigenvectors

The simplest system in which exciton coupling effects can be considered are two interacting molecules. These two molecules can be spatially separated or, like in this work, chemically bonded. The wave functions of the eigenstates of the isolated molecules can be determined with a Hamiltonian $\hat{H}$ and the *Schrödinger* equation:

$$\hat{H}_n \psi_n = \varepsilon_n \psi_n \tag{14}$$

The subscript *n* identifies the molecules (either molecule 1 or 2). In the case that the molecules interact (perturbed case) the *Hamiltonian* of the dimer can be described by the following equation

$$\hat{H} = \left(\hat{H}_1 + \hat{H}_2 + \hat{V}\right) \tag{15}$$

Additional to the Hamiltonians of the single molecules the Coulombic Potential term $\hat{V}$ has to be taken into account. For the combined wavefunction (Ψ) we chose the product of the wavefunctions of the monomers ($\Psi = \psi_1 \psi_2$).

The ground state energy of the dimer (E) is expressed by

$$E = \left\langle \psi_1 \psi_2 \middle| \hat{H}_1 + \hat{H}_2 + \hat{V} \middle| \psi_1 \psi_2 \right\rangle = E_1 + E_2 + \left\langle \psi_1 \psi_2 \middle| \hat{V} \middle| \psi_1 \psi_2 \right\rangle = E_1 + E_2 + V_{00} \tag{16}$$

We are only interested in the relative energies and set the ground state energies of the single molecules E_1 and E_2 equal to 0. The term V_{00} describes the displacement of the ground state energy.

The excited state wave functions can formally be written as the linear combination of two terms, where either one or the other molecule is excited. This ansatz is called *Heitler-London* approximation. We also assume that the electrons are not exchanged between the two molecules. Therefore, the wavefunction of the dimer does not have to be symmetrised.

$$\Psi_f = c_{f1} \psi_1^* \psi_2 + c_{f2} \psi_1 \psi_2^* \tag{17}$$

The relative contribution of the terms are determined by the coefficients c_{f1} and c_{f2}, which are normalised and orthogonal.

$$c_{f1}^{\,2} + c_{f2}^{\,2} = 1 \tag{18}$$

$$c_{f1} \times c_{g1} + c_{f2} \times c_{g2} = 0 \tag{19}$$

The *f* and *g* represent different eigenstates. These are the stationary solutions of the *Schrödinger* equation

$$\hat{H}\,\Psi_f = \left(\hat{H}_1 + \hat{H}_2 + \hat{V}\right)\Psi_f = \varepsilon_f\,\Psi_f \tag{20}$$

We multiply both sides from the left with either $\psi_1^* \psi_2$ or $\psi_1 \psi_2^*$ and integrate over the entire space.

$$c_{f1}\left(E_1^* + \left\langle \psi_1^* \psi_2 \middle| \hat{V} \middle| \psi_1^* \psi_2 \right\rangle\right) + c_{f2}\left\langle \psi_1^* \psi_2 \middle| \hat{V} \middle| \psi_1 \psi_2^* \right\rangle = c_{f1}\varepsilon_f \tag{21}$$

$$c_{f1}\left(\left\langle \psi_1 \psi_2^* \middle| \hat{V} \middle| \psi_1^* \psi_2 \right\rangle\right) + c_{f2}\left\langle E_2^* + \psi_1 \psi_2^* \middle| \hat{V} \middle| \psi_1 \psi_2^* \right\rangle = c_{f2}\varepsilon_f \tag{22}$$

For a simplification we introduce

the Coulomb interaction terms

$$H_{11} = E_1^* + \left\langle \varphi_1^* \varphi_2 \middle| \hat{V} \middle| \varphi_1^* \varphi_2 \right\rangle = E_1^* + V_{11} \tag{23}$$

$$H_{22} = E_2^* + \left\langle \varphi_1 \varphi_2^* \middle| \hat{V} \middle| \varphi_1 \varphi_2^* \right\rangle = E_2^* + V_{22} \tag{24}$$

and the resonance interaction terms

$$V_{12} = V_{21} = \left\langle \varphi_1^* \varphi_2 \middle| V \middle| \varphi_1 \varphi_2^* \right\rangle \tag{25}$$

With them the eq. (21) and (22) can be written in a shorthand notation.

$$c_{f1}\left(H_{11} - \varepsilon_f\right) + c_{f2}V_{12} = 0 \tag{26}$$

$$c_{f1}V_{12} + c_{f2}\left(H_{22} - \varepsilon_f\right) = 0 \tag{27}$$

The non-trivial solutions of this system of equations can be obtained by solving the secular determinant

$$\begin{vmatrix} H_{11} - \varepsilon_f & V_{12} \\ V_{12} & H_{22} - \varepsilon_f \end{vmatrix} = 0 \tag{28}$$

In the case of identical molecules with degenerate excited states the coulomb interactions are equal ($H_{11} = H_{22}$) and the secular determinant gives

$$\left(H_{11} - \varepsilon_f\right)^2 - V_{12}^2 = 0 \tag{29}$$

This quadratic formula yields two eigenenergies

$$\varepsilon_1 = H_{11} - V_{12} \tag{30}$$

$$\varepsilon_2 = H_{11} + V_{12} \tag{31}$$

This means that the former degenerated eigenstates of the dimer are split by

$$\delta E = 2V_{12} \tag{32}$$

This splitting is called *Davydov* splitting (see Figure 21). In eq. (23) and (24) one can see that the average energies of the excited states are shifted in comparison to the ground state (eq. (16)) by an amount of $V_{11} - V_{00}$ (since the molecules are identical $V_{11} = V_{22}$). This so called displacement energy is not important for our further discussion and is therefore disregarded ($V_{11} = 0$). With the values for the eigenstates one can determine the coefficients c_{f1} and c_{f2}. This can be accomplished with the eq. (26)and (27). The normalised and orthogonal values are

$$c_{11} = -\frac{1}{2}\sqrt{2}, \quad c_{12} = \frac{1}{2}\sqrt{2} \tag{33}$$

$$c_{21} = \frac{1}{2}\sqrt{2}, \quad c_{22} = \frac{1}{2}\sqrt{2} \tag{34}$$

The probability that the excitation is localised at one molecule for one excitonic state can be calculated by taking the square of the absolute values of the coefficients (*e.g.* $|c_{11}|^2$). In this simple case all values are identical. This means, that the excitation is completely delocalised over the molecules.

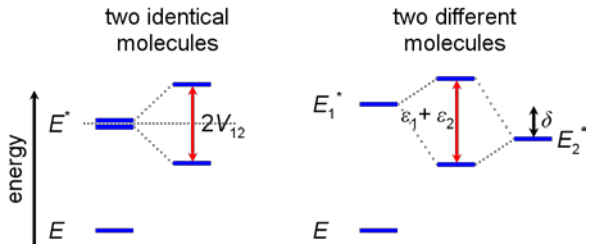

Figure 21 Schematic energy diagram showing exciton splitting in molecular dimers.

If the two molecules are not identical their excited state energies are no longer degenerate. The difference between the excited states is called δ (Figure 21). Nevertheless, the calculation of the excitonic eigenstates and eigenenergies can be done in an analogous way as for the degenerate dimer above. Therefore, the average energy between the two excited states is defined as the new zero-energy of the transition energies of the two molecules. The excited state energies can then be written as either

$$E_n^* = \frac{\delta}{2} = \Delta E \quad \text{or} \quad E_n^* = -\frac{\delta}{2} = -\Delta E$$

The equations that are obtained by solving the *Schrödinger* equation are

$$c_{f1}\left(\Delta E - \varepsilon_f\right) + c_{f2}V_{12} = 0 \tag{35}$$

$$c_{f1}V_{12} + c_{f2}\left(-\Delta E - \varepsilon_f\right) = 0 \tag{36}$$

Again the eigenenergies ε_1 and ε_2 of the dimer can be calculated by solving the secular determinant

$$\begin{vmatrix} \Delta E - \varepsilon_f & V_{12} \\ V_{12} & -\Delta E - \varepsilon_f \end{vmatrix} = 0 \tag{37}$$

which leads to

$$\varepsilon_1 = \sqrt{(V_{12})^2 + (\Delta E)^2} \tag{38}$$

$$\varepsilon_2 = -\sqrt{(V_{12})^2 + (\Delta E)^2} \tag{39}$$

In the same way as above the eigenstates can be used to determine the coefficients.

$$c_{11} = \frac{1}{\sqrt{1+\left(\left(-\frac{\Delta E}{V_{12}}\right)+\sqrt{1+\left(\frac{\Delta E}{V_{12}}\right)^2}\right)^2}}, \quad c_{12} = c_{11}\sqrt{1+\left(\left(-\frac{\Delta E}{V_{12}}\right)+\sqrt{1+\left(\frac{\Delta E}{V_{12}}\right)^2}\right)^2} \tag{40}$$

$$c_{21} = \frac{1}{\sqrt{1+\left(\left(-\frac{\Delta E}{V_{12}}\right)-\sqrt{1+\left(\frac{\Delta E}{V_{12}}\right)^2}\right)^2}}, \quad c_{22} = c_{21}\sqrt{1+\left(\left(-\frac{\Delta E}{V_{12}}\right)-\sqrt{1+\left(\frac{\Delta E}{V_{12}}\right)^2}\right)^2} \tag{41}$$

It is obvious that on the one hand if $\Delta E << V_{12}$ the case of identical molecules is approached and on the other hand if $\Delta E >> V_{12}$ no excitonic coupling is observed.

The value for the intermolecular Coulombic potential term V, that describes the interactions between the electrons and the nuclei of both molecules can be determined with the following equation:

$$V = V_{\text{mono-mono}} + V_{\text{mono-di}} + V_{\text{di-di}} + V_{\text{di-quad}} + V_{\text{quad-quad}} + \dots \tag{42}$$

We assume a neutral total charge distribution and that the distance between the molecules is considerably larger than the size of the charge distribution of the single molecules. In that case the monopole interactions are zero and V is dominated by the dipole-dipole potential term. The higher multipole potential terms depend quite strongly on the distance between the molecules, which makes them comparatively small.

For our case of two interacting molecules with strong absorption bands this means, that the intermolecular coulombic potential term can be expressed by a point-dipole point-dipole approximation.

$$V \cong V_{\text{di-di}} = \frac{1}{hc4\pi\varepsilon_0}\frac{|\mu_1||\mu_2|}{r_{12}^3}\left(\hat{e}_{\mu_1}\cdot\hat{e}_{\mu_2} - 3\left(\hat{e}_{\mu_1}\cdot\hat{e}_{r_{12}}\right)\left(\hat{e}_{\mu_2}\cdot\hat{e}_{r_{12}}\right)\right) \tag{43}$$

Here, ε_0 is the electric permittivity, the $\hat{e}_a$ are the eigenvectors of the transition-dipole moments μ_n of molecule n and the distance between the point-dipoles r_{12}.

Transition-Dipole Moment

The change of the excited states of two monomers due to intermolecular interactions also has an influence on the transition-dipole moments.

The electric part E of a plane electromagnetic wave passing through the dimer can be described by

$$E = E_0 \cos(k \cdot r - \omega t) \tag{44}$$

E_0 is the polarisation direction and the amplitude of the wave, k is the wave vector, ω is the frequency and r the size of the molecule. The influence of the light wave on the molecule is considered in the overall Hamiltonian $\hat{H}$.

$$\hat{H} = \hat{H}_0 + \hat{H}_1 \tag{45}$$

Here, $\hat{H}_0$ is the Hamiltonian of the molecule in the absence of light and $\hat{H}_1$ describes the interaction energy of the light with the molecule. The main part of this interaction depends on the electric dipole moment operator $\hat{\mu}$ of the molecule and the electric part of the light E. According to Fermi´s golden rule the transition probability from the ground state to the first excited state W_{0f} depends on the square of the matrix element $\left|\left\langle \psi^* \middle| \hat{H} \middle| \psi \right\rangle\right|^2$. We apply the long-wave approximation (kr <<1), which means that the wavelength of the light is much larger than the size of the molecule, and get

$$W_{0f} \propto {E_0}^2 \cdot \left|\hat{e}_E \cdot \left\langle \psi^* \middle| \hat{\mu} \middle| \psi \right\rangle\right|^2 = \left|E_0\right|^2 \cdot {\mu_{0f}}^2 \cdot \left(\cos(\hat{e}_E \cdot \hat{e}_\mu)\right)^2 \tag{46}$$

The last term of eq. (46) depends on the orientation of the transition-dipole moments and the linear polarisation of the light wave. If we assume an isotropic sample all orientations of the transition-dipole moment are equally likely and averaging over all orientations leads to

$$\left\langle \left(\cos(\hat{e}_E \cdot \hat{e}_{\mu_{0f}})\right)^2 \right\rangle = \frac{1}{3} \tag{47}$$

which is independent of the polarisation of the light wave.

For any molecule the square of the transition-dipole moment is proportional to the intensity of the absorption band and can be calculated according to the already mentioned eq. (5).

In our singly excited dimer the square of the magnitude of the dipole strengths for the transition between the ground state and the two excited states can be estimated from the

eigenvectors of the transition-dipole moments of the single molecules ($\hat{e}_{\mu_1}$ and $\hat{e}_{\mu_2}$) and their respective coefficients.

$$\mu_{0f}{}^2 = \left\langle \Psi^* \middle| \hat{\mu} \middle| \Psi \right\rangle = \left(c_{f1}\hat{e}_{\mu_1} + c_{f2}\hat{e}_{\mu_2}\right)^2 = c_{f1}{}^2\hat{e}_{\mu_1}{}^2 + 2c_{f1}c_{f2}\left(\hat{e}_{\mu_1}\cdot\hat{e}_{\mu_2}\right) + c_{f2}{}^2\hat{e}_{\mu_2}{}^2 \tag{48}$$

Actually, the equation is simpler for the magnitude of the vector of the transition-dipole moments.

$$\mu_{0f} = c_{f1}\hat{e}_{\mu_1} + c_{f2}\hat{e}_{\mu_2} \tag{49}$$

The orientation of the molecules to each other is considered by their projection on a Cartesian coordinate system (Figure 22 and Figure 23). We assume planarity in all our molecules. Therefore, the projection on the *z*-axis is always zero and neglected in our estimations.

$$\mu_{0f} = c_{f1}\hat{e}_{\mu_1} + c_{f2}\hat{e}_{\mu_2} = c_{f1}\mu_1\begin{pmatrix}\cos\alpha_1\\ \sin\alpha_1\end{pmatrix} + c_{f2}\mu_2\begin{pmatrix}\cos\alpha_2\\ \sin\alpha_2\end{pmatrix} \tag{50}$$

If we assume a linear head to tail arrangement for our dimer of two identical molecules ($\mu_1 = \mu_2$, see Figure 22), the transition-dipole moments for the two excited states can be estimated with the coefficients of eq. (33) and (34).

$$\begin{aligned}\mu_{01} &= c_{11}\mu_1\begin{pmatrix}\cos 180°\\ \sin 180°\end{pmatrix} + c_{12}\mu_2\begin{pmatrix}\cos 0°\\ \sin 0°\end{pmatrix} = -\frac{1}{2}\sqrt{2}\mu_1\begin{pmatrix}-1\\ |0|\end{pmatrix} + \frac{1}{2}\sqrt{2}\mu_1\begin{pmatrix}1\\ 0\end{pmatrix}\\ &= \begin{pmatrix}0.5\sqrt{2}\mu_1\\ 0\end{pmatrix} + \begin{pmatrix}0.5\sqrt{2}\mu_1\\ 0\end{pmatrix} = \begin{pmatrix}\sqrt{2}\mu_1\\ 0\end{pmatrix}\\ \mu_{01} &= \sqrt{\left(\sqrt{2}\mu_1\right)^2 + (0)^2} = \sqrt{2}\mu_1\end{aligned} \tag{51}$$

$$\begin{aligned}\mu_{02} &= c_{21}\mu_1\begin{pmatrix}\cos 180°\\ \sin 180°\end{pmatrix} + c_{22}\mu_2\begin{pmatrix}\cos 0°\\ \sin 0°\end{pmatrix} = \frac{1}{2}\sqrt{2}\mu_1\begin{pmatrix}-1\\ 0\end{pmatrix} + \frac{1}{2}\sqrt{2}\mu_1\begin{pmatrix}1\\ 0\end{pmatrix}\\ &= \begin{pmatrix}-0.5\sqrt{2}\mu_1\\ 0\end{pmatrix} + \begin{pmatrix}0.5\sqrt{2}\mu_1\\ 0\end{pmatrix} = \begin{pmatrix}0\\ 0\end{pmatrix}\\ \mu_{02} &= 0\end{aligned} \tag{52}$$

According to this calculation and the relationship in eq. (46) the transition to the first excited state has a quite large transition-dipole moment and should be quite intense in the absorption spectrum. The transition to the second excited state should not be observed, because it has no dipole strength (Figure 22 right side).

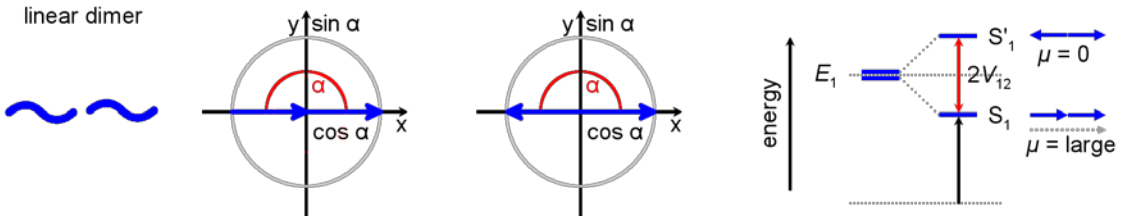

Figure 22 Orientation of a linear dimer in a Cartesian coordinate system. On the right side the exciton eigenstates that are formed by exciton interaction are depicted, together with the localised transition-dipole moments of the monomers (blue) and the resulting sum of the transition-dipole moments (grey dashed).

In solution the two molecules of the dimer can assume many orientations to each other. In the following the transition-dipole moments for a bent dimer with an angle of 120° are calculated (Figure 23).

$$\begin{aligned}\mu_{01} &= c_{11}\mu_1\begin{pmatrix}\cos 120°\\ \sin 120°\end{pmatrix} + c_{12}\mu_2\begin{pmatrix}\cos 0°\\ \sin 0°\end{pmatrix} = -\frac{1}{2}\sqrt{2}\mu_1\begin{pmatrix}-0.5\\ 0.87\end{pmatrix} + \frac{1}{2}\sqrt{2}\mu_1\begin{pmatrix}1\\ 0\end{pmatrix}\\ &= \begin{pmatrix}0.25\sqrt{2}\mu_1\\ -0.435\sqrt{2}\mu_1\end{pmatrix} + \begin{pmatrix}0.5\sqrt{2}\mu_1\\ 0\end{pmatrix} = \begin{pmatrix}0.75\sqrt{2}\mu_1\\ -0.435\sqrt{2}\mu_1\end{pmatrix}\\ \mu_{01} &= \sqrt{\left(0.75\sqrt{2}\mu_1\right)^2 + \left(-0.435\sqrt{2}\mu_1\right)^2}\end{aligned} \tag{53}$$

$$\begin{aligned}\mu_{02} &= c_{21}\mu_1\begin{pmatrix}\cos 120°\\ \sin 120°\end{pmatrix} + c_{22}\mu_2\begin{pmatrix}\cos 0°\\ \sin 0°\end{pmatrix} = \frac{1}{2}\sqrt{2}\mu_1\begin{pmatrix}-0.5\\ 0.87\end{pmatrix} + \frac{1}{2}\sqrt{2}\mu_1\begin{pmatrix}1\\ 0\end{pmatrix}\\ &= \begin{pmatrix}-0.25\sqrt{2}\mu_1\\ 0.435\sqrt{2}\mu_1\end{pmatrix} + \begin{pmatrix}0.5\sqrt{2}\mu_1\\ 0\end{pmatrix} = \begin{pmatrix}0.25\sqrt{2}\mu_1\\ 0.435\sqrt{2}\mu_1\end{pmatrix}\\ \mu_{02} &= \sqrt{\left(0.25\sqrt{2}\mu_1\right)^2 + \left(0.435\sqrt{2}\mu_1\right)^2}\end{aligned} \tag{54}$$

This time both transition-dipole moments differ from zero and therefore should be observed in the absorption spectrum. Actually this is the case for every alignment that is different from the linear case. However, the transition-dipole moment of the second excited state is always smaller than the one of the first excited state. Due to the direct proportionality of μ and the transition probability (see eq. (46)) the absorption spectrum of our dimer in solution should have one intense band and one less intense band at higher energy ($\sim 2V_{12}$).

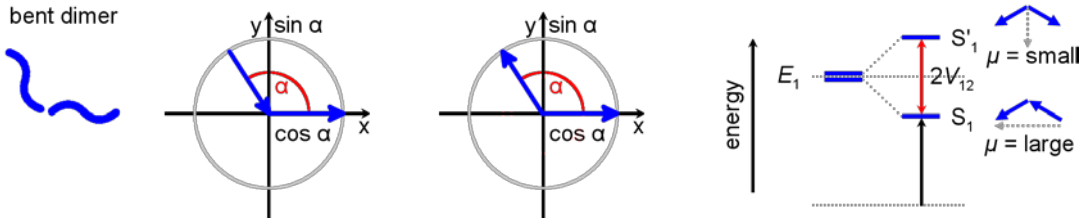

Figure 23 Orientation of a bent dimer in a Cartesian coordinate system. On the right side the exciton eigenstates that are formed by exciton interaction are depicted, together with the localised transition dipole moments of the monomers (blue) and the resulting sum of the transition-dipole moments (grey dashed).

Despite the number of assumptions and simplifications, which were described above, the *Frenkel* exciton model[41] is a powerful tool to interpret the linear spectroscopic properties of organic chromophores. In this work it is used to explain the photophysical properties of the superchromophores based on the properties of their respective monomers.

2 Scope of the Work

This thesis partly follows the work of *Lawrentz et al.* [62, 96] who investigated the linear and nonlinear properties of a series of thiophene-**SQA** co-oligomers. These oligomers showed a red-shift and a broadening of the main absorption band that can be explained by exciton coupling theory. The elongation of the π-system had also a beneficial influence on the nonlinear properties of the chromophores. (Figure 15). Besides that, they investigated the structure and the linear properties of a number of chromophores that are based on the parent squaraine **SQ** that is red-shifted by 900 cm^{-1} in comparison to **SQA**.

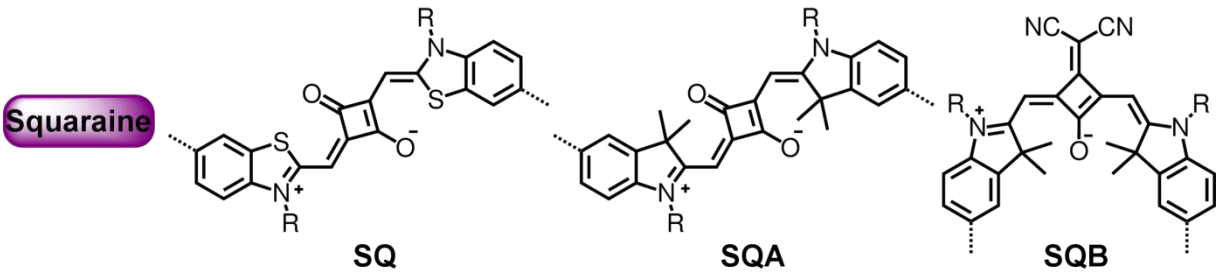

Figure 24 Monomeric benzothiazole (**SQ**) and indolenine (**SQA** and **SQB**) squaraine units that are used in this work.

The present thesis furthermore builds upon the work of *Völker et al.* on polymers and co-polymers that are based on the indolenine squaraines **SQA** and **SQB**. [97, 98] In the course of the synthesis of a **SQB**-based homopolymer they observed the formation of cyclic compounds, which showed atypical spectroscopic behaviour. *E.g.* the cyclic trimer has an absorption band that is located at lower energies than the main absorption band and its vibronic shoulder. In addition the emission of the trimer has not only an unusually large Stokes-shift, but also two distinct maxima besides the vibronic shoulders. This behaviour could not be explained by the exciton coupling theory of the symmetrical chromophore (Figure 25). Theoretical studies interpreted the shifts of the absorption and the emission bands to be caused by deviations of the excited state geometries from the strictly symmetric configuration.[99] In this work the squaraines in Figure 24 should be used to synthesise trimers that are connected *via* a shared core unit, as shown in Figure 25. The benzothiazole squaraine **SQ** is chosen, because of its main absorption that is already further in the red to NIR region than **SQA**.[96] The indolenine squaraines **SQA** and **SQB** on the other hand are well established and known for their stability.[97, 98]

The star-shaped superchromophores should display spectroscopic properties that are superior to their parent squaraines (see Chapter 1.1.3). Due to excitonic coupling their main absorption band should be red-shifted, broader and more intense. Their geometry, especially if the symmetry is broken, might also be beneficial for the nonlinear properties of the squaraines (see Chapter 1.2.2).

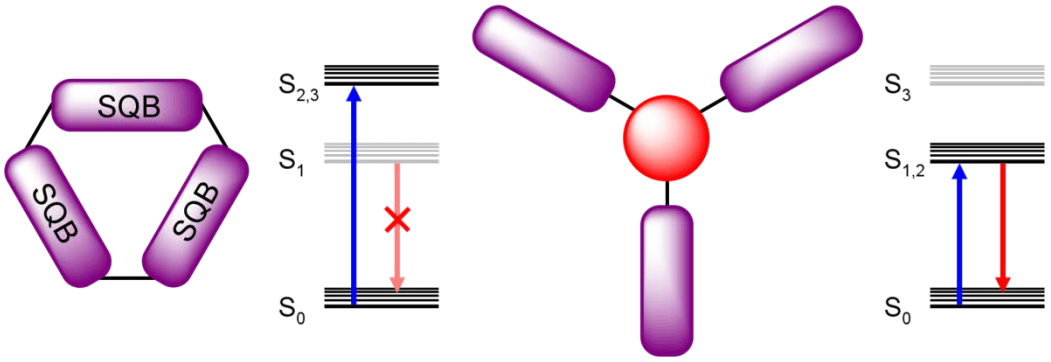

Figure 25 Cyclic squaraine trimer of *Völker et al.*[97] and a star-shaped trimer with their respective energy diagrams derived from excitonic coupling theory.

The selected core units are partly based on the work on the addition of electron donating and electron withdrawing groups to the squaraines **SQA** and **SQB** by *Völker et al.*[24, 98] While the acceptor unit triarylamine (**TAA**) lead to a red shift of the absorption of the Donor-Squaraine-Donor compound, the acceptor unit tris-duryl-boryl (**bor**) had nearly no influence on the properties of the chromophore. This means, that although both units are tilted out of the squaraine plane, **TAA** is still able to promote an efficient π-overlap to influence the spectroscopic properties of the squaraine. In the **bor** unit the sterically demanding duryl group prohibits this overlap. Based on that, we expect that due to excitonic coupling the **TAA** trimer shows a broadening and a red-shift of the main absorption band. The **bor** core in the opposite should not promote excitonic coupling between the branches of the trimer. Therefore, the spectroscopic properties of the star-shaped trimer should simply resemble three mono-squaraines.

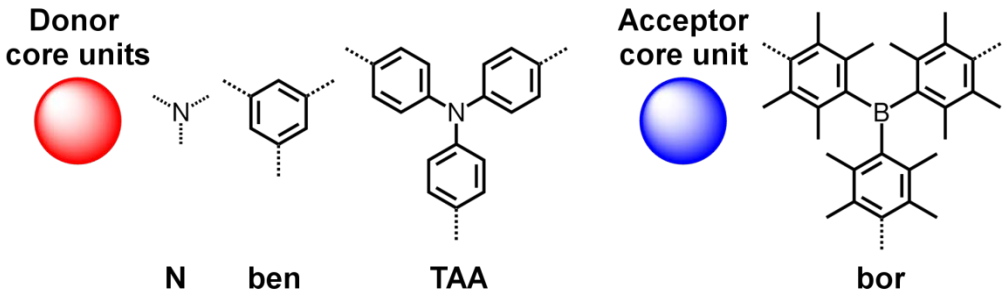

Figure 26 Core units for the trimerisation of squaraine chromophores.

Furthermore, the cores benzene (**ben**) and **TAA** already proved to be beneficial for the nonlinear properties in the trimerisation of dipolar and quadrupolar chromophores (see Chapter 1.2.2). This should also be the case for the trimerisation of squaraines.

The smallest core consists of a single nitrogen (**N**) atom and might therefore lead to a good electronic communication between the three arms. In addition the synthesis of the **N**-trimer enables a simple route to attach different squaraines to one single core unit. This might provide energy transfer from one arm to another.

Due to excitonic coupling the directly linked linear squaraine dimer and trimer should also show a red-shift and a broadening of the linear absorption properties and have superior nonlinear properties compared to the monomer (Figure 27).

Figure 27 Linear squaraine chromophores.

The combination of the star-shaped and the linear concept should be tested with a superchromophore that has a **ben** core and two directly linked squaraines on each branch.

In addition the equilibrium of the cisoid and the transoid structure of donor substituted azulene squaraines should be investigated.[100] With the help of sterically demanding groups the chromophore should be forced into a pure transoid structure.

3 Results and Discussion

3.1 Donor Substituted Azulene Squaraines

3.1.1 Introduction

In an earlier work[100] donor substituted azulene squaraine monomers were synthesised and characterised. Thereby, triarylamine induced a bathochromic shift of the absorption of 1500 cm^{-1} compared to the unsubstituted parent chromophore. A further red shift of 1500 cm^{-1} was achieved by diphenylamine due to the shorter distance between the azulene squaraine and the additional donor.[101] NMR studies of the diphenylamine substituted squaraine with a 600 MHz spectrometer revealed that at rt the molecule exists in a dynamic equilibrium between the assumed transoid structure[102] and the cisoid structure (Scheme 10). It was expected, that the substitution of the protons in 2-position of the azulenes (blue and red protons) with sterically demanding groups might force the chromophore into a pure transoid structure. In a similar way the replacement of an oxygen atom (green) of the central cyclobutadiene by a sterically demanding group might lead to a pure cisoid structure. In addition carbazoles were used as donors and the influence of the coupling position on the structure and the absorption was investigated.

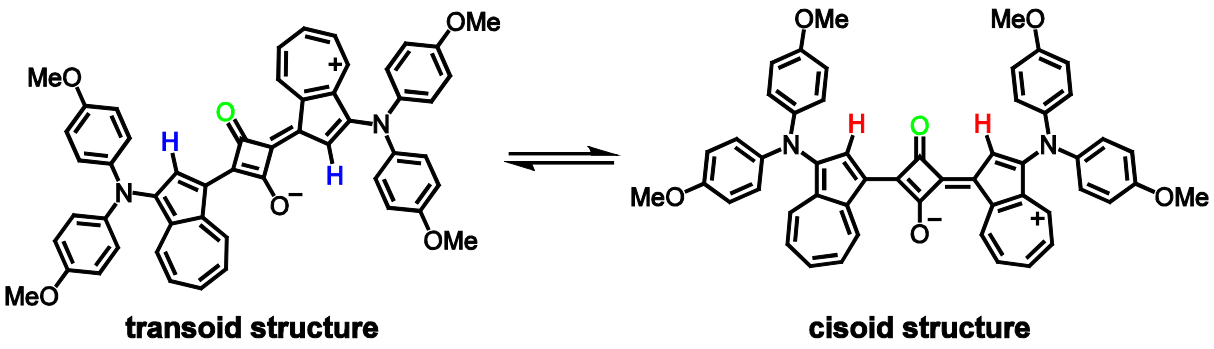

Scheme 10 Transoid (left) and cisoid (right) structure of the diphenylamine azulene squaraine.

3.1.2 Synthesis of Azulene Carbazole Squaraines

The bromination of azulene was done with *N*-bromosuccinimide according to the literature (Scheme 11).[100, 103] After a short column chromatography not only 1-bromoazulene (**2**) but also 1,3-dibromoazulene and azulene (**1**) were present in the crude product. Given that 1-iodoazulene crystals are known for explosive decomposition at 20°C[103] the crude mixture was used in the following coupling reactions without further purification.

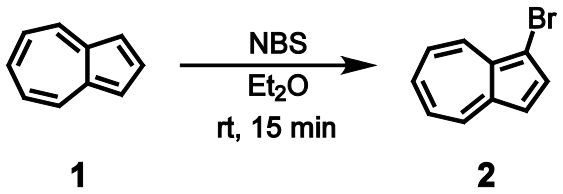

Scheme 11 Synthesis of 1-bromoazulene (2).

9-(azulen-1-yl)-9*H*-carbazole (**3**) was synthesised in a *Buchwald-Hartwig* coupling reaction of 9H-carbazole with 1-bromoazulene (**2**) (Scheme 12). The carbazole boronic esters **4** and **6** were synthesised according to the literature.[98] In subsequent palladium catalysed *Suzuki* coupling reactions of the boronic esters and 1-bromoazulene (**2**) the precursors for the condensation reaction were prepared.

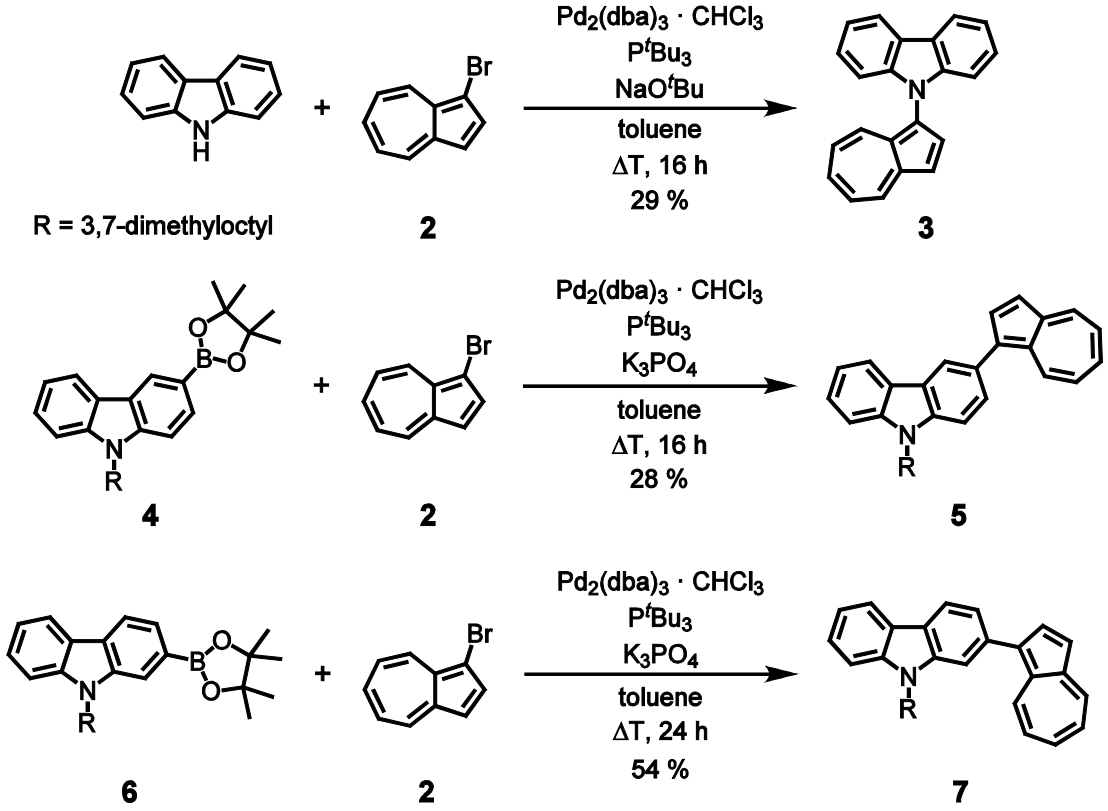

Scheme 12 Synthesis of 9-(azulen-1-yl)-9H-carbazole (**3**), 3-(azulen-1-yl)-9-(3,7-dimethyloctyl)-9H-carbazole (**5**) and 2-(azulen-1-yl)-9-(3,7-dimethyloctyl)-9H-carbazole (**7**).

The symmetrical squaraines **Az1**, **Az2** and **Az3** were synthesised in dicondensation reactions of the precursors with half an equivalent of squaric acid in a 6/4 mixture of *n*-butanol and toluene with azeotropic distillation of water using a *Dean-Stark*-trap.

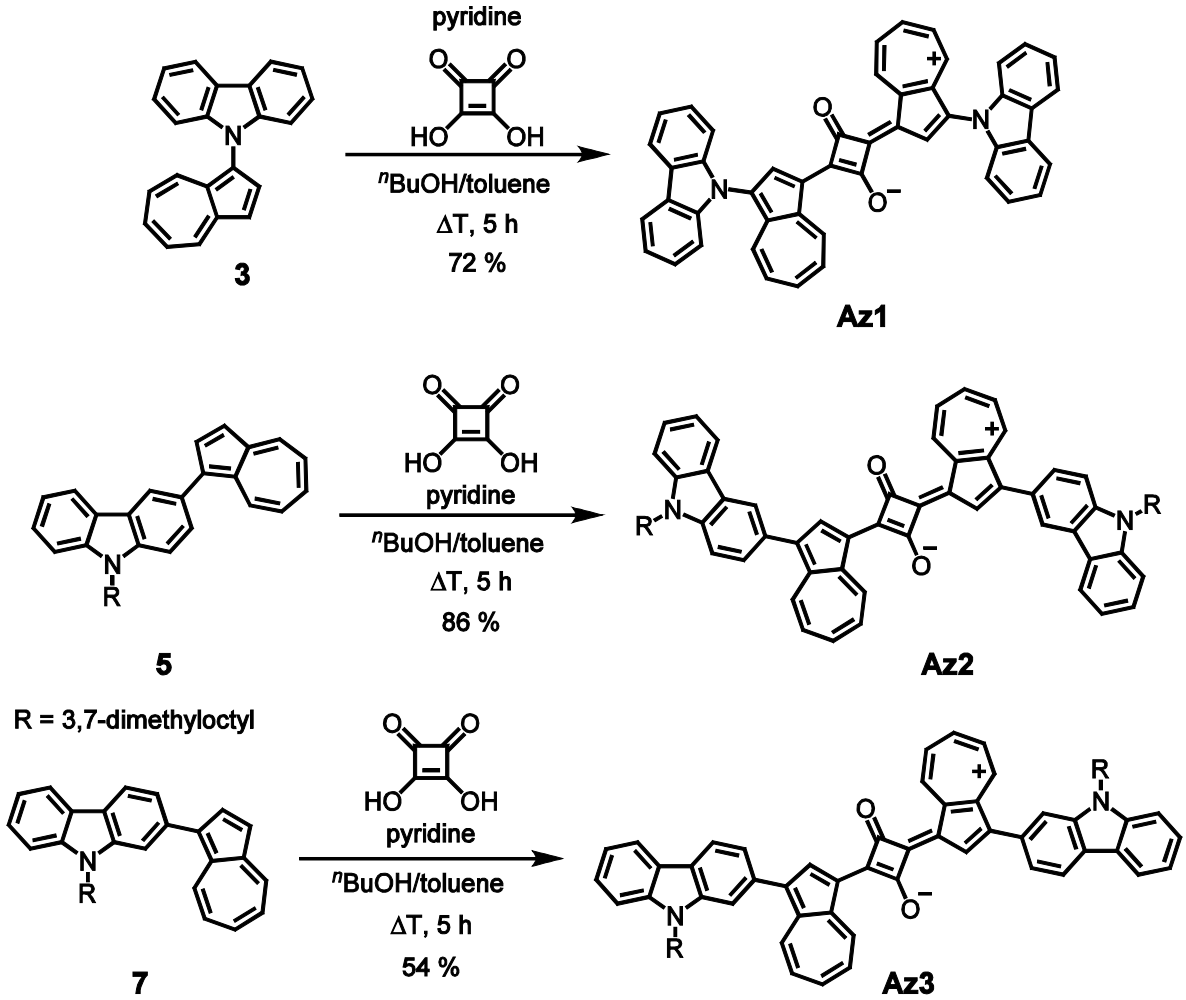

Scheme 13 Synthesis of the carbazole-azulene squaraines **Az1**, **Az2** and **Az3**.

3.1.3 Structure of the Azulene Carbazole Squaraines

In an earlier work[100] an azulene squaraine showed an additional proton signal in the 600 MHz ^{1}H-NRM spectrum that was not detectable in the 400 MHz spectrum. The signal could be assigned to the hydrogen in the five ring of the azulene. The carbazole-azulene squaraines **Az2** and **Az3** show a similar behaviour. For **Az1** the differences of the spectra were even more significant.

While the spectra of a low concentration of **Az1** with the 400 MHz spectrometer at rt show only one set of signals the measurements of a higher concentration with the 600 MHz spectrometer show a complete additional set of signals. At 293 K the ratio between the signals is 2:1, and at 273 K 3:2 respectively. It is assumed that the larger signals belong to the transoid structure and the smaller to the cisoid structure (Figure 28). Since squaraines are

known to form aggregates at higher concentrations[104, 105] the measurement at 273 K was repeated with a lower concentration but the ratio between the peaks remained unchanged.

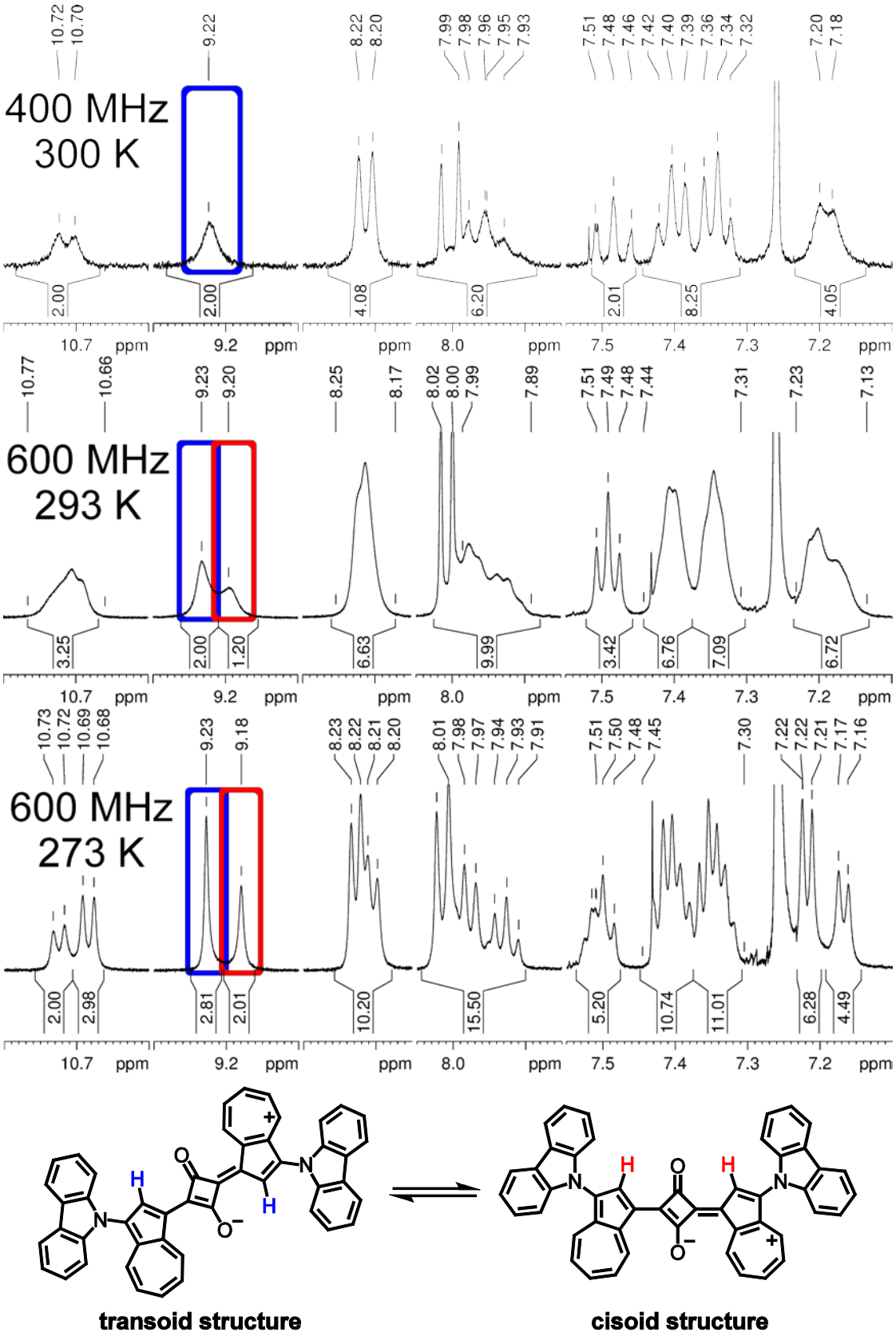

Figure 28 1H-NMR spectra of **Az1** in $CHCl_3$ measured at a 400 MHz spectrometer at 300 K (top), at a 600 MHz spectrometer at 293 K (middle) and at 276 K (bottom).

The tautomerization might be prevented if sterically demanding groups are used to replace either the hydrogen atom in the five ring of the azulene or one oxygen atom of the cyclobutadiene. In addition a hydroxyl group might form hydrogen bonds to the oxygens of the central cyclobutadiene ring and therefore stabilise one structure.

The replacement of the hydrogen was not successful because either the bromination of the 1-position of the substituted azulene resulted in unstable compounds (in case of 2-hydroxyazulene and ethyl azulene-2-carboxylate) or the condensation reaction to the squaraine failed (N,N-2-tris(4-methoxyphenyl)azulene-1-amine) (Scheme 14).

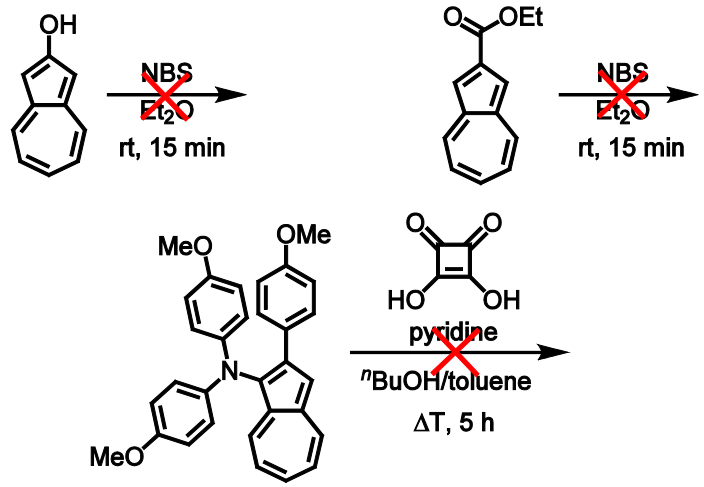

Scheme 14 Attempted bromination of the 1-position of substituted azulenes and condensation of a 1,2-substituted azulene.

The replacement of the oxygen by dicyanomethylene, which is known to result in cisoid squaraines[14, 15, 106], was not successful either. The reaction of the squaraine with malononitrile in the dark at rt in the presence of a base (triethylamine or *N*,*N*-dimethyl-4-aminopyridine) resulted in a rapid decolouration of the solution. If only one reagent was added to the dissolved squaraine no decomposition was observed. The condensation reaction of the precursor **3** with an already functionalised squaric acid resulted in a decolouration of the solution as well.

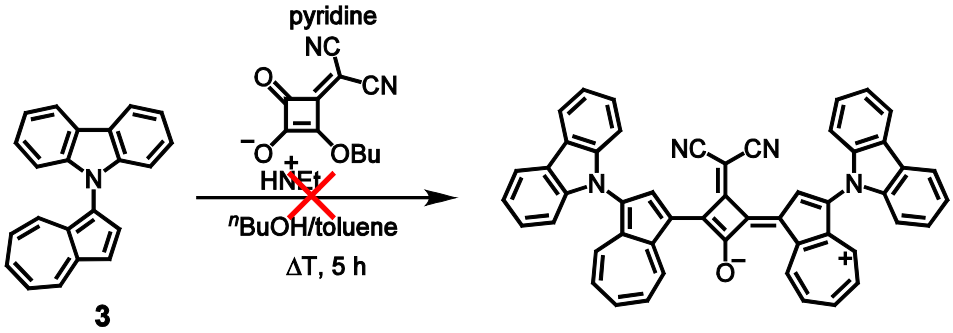

Scheme 15 Attempted reaction of **3** with a functionalised squaric acid.

3.1.4 Absorption Spectroscopy

The absorption spectra of the squaraines **Az1**, **Az2** and **Az3** were only recorded in CH_2Cl_2 and $CHCl_3$ due to the poor solubility of the chromophores in other solvents. The absorption data are listed in Table 1.

In Figure 29 the spectra of the squaraines in $CHCl_3$ are shown together with the spectrum of the unsubstituted azulene squaraine **Az**. All squaraines show the typical sharp absorption in the red region with a vibronically shoulder to the higher energy side. The extinction coefficients of a bit more than 100000 M cm^{-1} and the squares of the transition-dipole moments for this transition are very similar for the four chromophores.

The position of the connection of the carbazole moieties to the azulene has an effect on the red shift of the main absorption of the chromophores. While the smallest shift with only 800 cm^{-1} occurs for the connection via the nitrogen atom, the largest shift is observed for the connection via the 3-position. The absorption bands at higher energies differ significantly for the three connection positions.

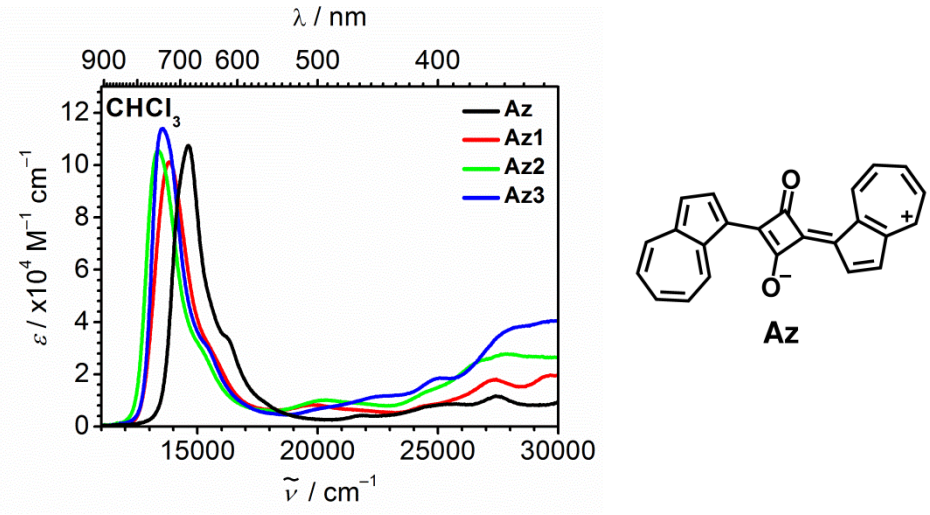

Figure 29 Absorption spectra of **Az1**, **Az2**, **Az3** and the parent chromophore **Az** in $CHCl_3$ at rt.

In order to investigate if there are several tautomers present in solution the absorption spectrum of **Az1** in $CHCl_3$ was measured at different temperatures. The density corrected measurements are depicted in Figure 30. The absorption maximum shifts with higher temperature slightly to the blue while the extinction coefficient shrinks and the one of the shoulder at 15600 cm^{-1} rises. The transition-dipole moment stays the same for the different temperatures.

The temperature range is limited due to the boiling point of the solvent and water condensation at the outside of the cuvettes. Hence only small differences of the concentration of the tautomers are observable.

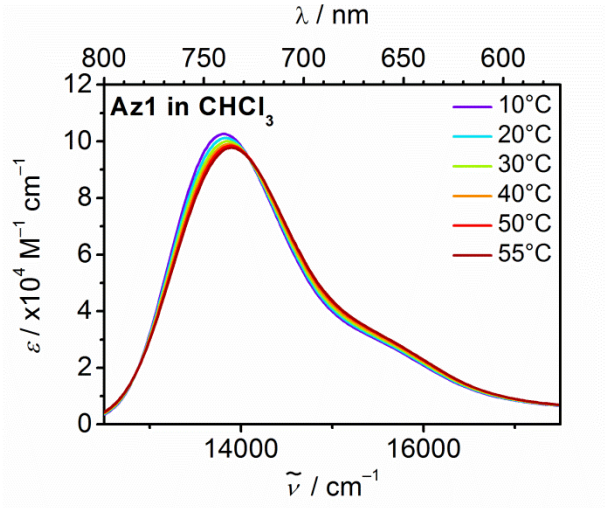

Figure 30 Absorption spectra of the main absorption of **Az1** in $CHCl_3$ at different temperatures.

Table 1 Absorption maxima, extinction coefficients and transition moments of the carbazole-azulene squaraines **Az**, **Az1**, **Az2** and **Az3**.

	solvent	$\tilde{\nu}_{max}$ / cm^{-1} (nm)	ε_{max} / M^{-1} cm^{-1}	μ^2 / D^2
Az	CH_2Cl_2	14600 (685)	122200	112
	$CHCl_3$	14600 (684)	107500	102
Az1	CH_2Cl_2	13900 (718)	100900	105
	$CHCl_3$	13800 (725)	101200	103
Az2	CH_2Cl_2	13400 (744)	113100	116
	$CHCl_3$	13400 (746)	105600	106
Az3	CH_2Cl_2	13700 (730)	120200	115
	$CHCl_3$	13500 (741)	114000	110

3.1.5 Fluorescence Spectroscopy

The fluorescence of the chromophores **Az**, **Az1**, **Az2** and **Az3** in $CHCl_3$ was examined. Neither excitation at the squaraine band nor excitation at the $S_2 \leftarrow S_0$ transition of azulene[107] at 29400 cm^{-1} yielded any fluorescence. The excitation at the higher energy was used because of the anomalous light emission behaviour of azulene from the S_2 state.[108]

3.1.6 Cyclic Voltammetry

The cyclic voltammetry experiments of the carbazole-azulene squaraines were carried out in CH_2Cl_2 solution with $^nBu_4PF_6$ (0.2 M) as electrolyte. The voltammograms of the chromophores and the reduction process of the unsubstituted azulene squaraine **Az** are depicted in Figure 31. The oxidation potential for **Az** was not determinable because it polymerises upon oxidation.[109] The half wave potentials of the other processes are summarised in Table 2.

The substitution of the 3-position of the azulene leads to a shift of the irreversible reduction to a higher voltage. The first oxidation process of the three substituted chromophores is reversible. The electrochemical polymerisation of the azulene is prohibited because the 1 and 3 positions of the azulene are both blocked by substituents. The at the 3-position of the carbazole coupled **Az2** has the lowest half wave potential for the first oxidation, followed by the in 2-postion coupled **Az3** and the via the nitrogen coupled **Az1**. The second oxidation process is irreversible in all three compounds.

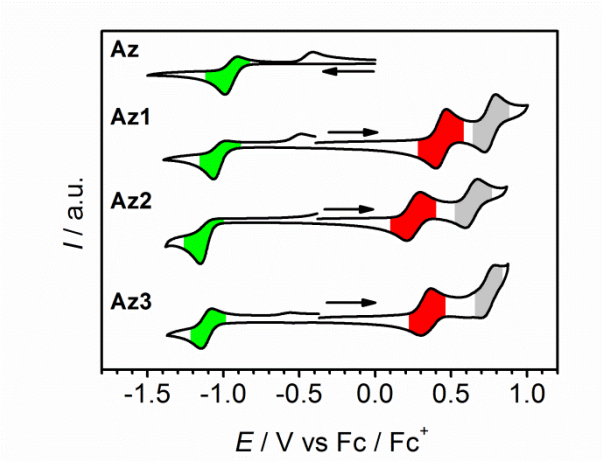

Figure 31 Cyclic voltammograms of **Az**, **Az1**, **Az2** and **Az3** in $CH_2Cl_2/^nBu_4PF_6$ (0.2 M) at a scan rate of 100 mV s^{-1}. All voltammograms are referenced against (Fc/Fc^+) and normalised. The scanning direction is indicated by the arrows.

Table 2 Redox potentials ($E_{1/2}$) of **Az**, **Az1**, **Az2** and **Az3** in $CH_2Cl_2/^nBu_4PF_6$ (0.2 M) at a scan rate of 100 mV s^{-1} and referenced against (Fc/Fc^+).

	$E^{red}_{1/2}$ / mV	$E^{ox}_{1/2}$ / mV	$E^{ox}_{1/2}$ / mV
Az	-950[i,*]	–	–
Az1	-1020[i,*]	433[r]	760[i]
Az2	-1080[i,*]	225[r]	637[i]
Az3	-1110[i,*]	337[r]t	744[i]

[i] irreversible, [r] reversible, [*] crude estimate

3.1.7 Conclusion

To sum up, three carbazole-azulene squaraines could be synthesised in good yields by condensation reactions of functionalised azulene derivatives. NMR-studies suggest that in solution the chromophores are existent in a dynamic equilibrium of the transoid and the cisoid structure. The syntheses of squaraines with only one preferred structure failed due to the instability of the precursors. Temperature dependent absorption measurements show no significant change of the absorption spectra.

Depending on the coupling position the carbazole substituents red-shift the main absorption compared to the unsubstituted chromophore. The extinction coefficient and the transition-dipole moments remain almost unchanged.

Although azulene and squaraines are typically known for strong fluorescence the combination of the two compounds leads to no observable fluorescence.

The addition of the carbazoles prohibits the electrochemical polymerisation of the azulene and results in a reversible 1st oxidation.

3.2 Star-Shaped Benzothiazole Squaraine Trimers[1]

3.2.1 Introduction

For the synthesis of star-shaped trimers asymmetric precursors are necessary. Therefore, mono brominated and mono aminated squaraines were synthesised. For the trimerisation two strategies were pursued. On the one hand the palladium catalysed *Buchwald-Hartwig* coupling reaction of one equivalent of the aminated with two equivalents of the brominated species. On the other hand different triboronic ester moieties were deployed in palladium catalysed *Suzuki* coupling reactions with the brominated squaraines.

In order to achieve a high solubility of the final chromophores different linear and one branched alky chains were utilised.

[1] Parts of this chapter have been investigated in a Bachelor thesis under the supervision of H. Ceymann: M. Mattenheimer, Bachelor Thesis, Julius-Maximilians-Universität (Würzburg), 2012.

3.2.2 Synthesis

Benzothiazole Precursors

The synthesis of 6-amino-2-methylbenzothiazole (**9**) was carried out according to the literature (Scheme 16).[110] First 2-methylbenzothiazole was nitrated with nitrosulphuric acid. Then 2-methyl-6-nitrobenzothiazole (**8**) was reduced with iron in EtOH and HCl in an ultrasonic bath. For the alkylation in 3-postion and the following condensation reaction the amino functionality had to be protected. The protective group had to be stable in alkaline conditions at temperatures of ca. 140°C and had to be removable at conditions in which squaraines are stable. The acetyl group met these conditions. It was introduced by the reaction of acetic anhydride and the amine in the presence of a catalytic amount of 4-(dimethylamino)-pyridine (DMAP).[111]

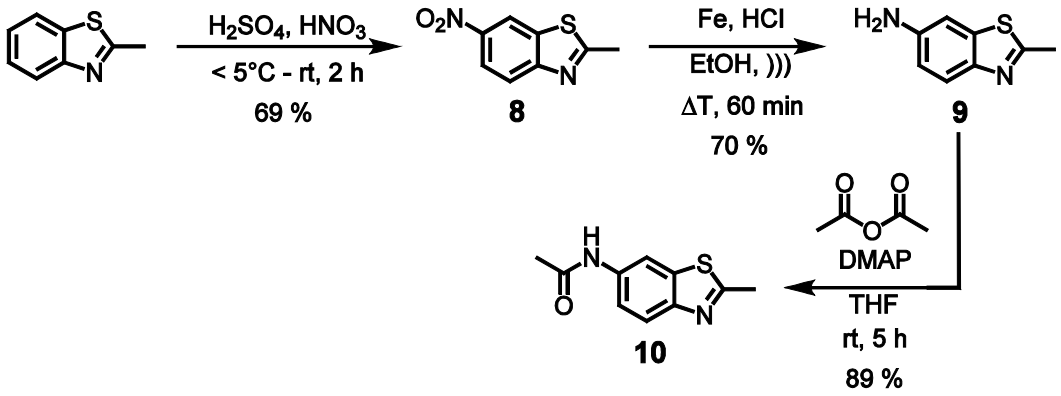

Scheme 16 Synthesis of 6-acetamido-2-mehtylbenzothiazole (**10**).

The reaction of 2-methylbenzothiazole with standard bromination reagents, like bromine or n-bromosuccinimide, results in mono or multi bromination of the methyl group. The bromination in 6-position was achieved with dibromoisocyanuric acid, a reagent for the bromination of deactivated aromatic compounds (Scheme 17).[112] In order to minimise dibromination 2-methylbenzothiazole was solubilised in concentrated sulfuric acid and half an equivalent dibromoisocyanuric acid (**11**) in concentrated sulfuric acid was added slowly.[96]

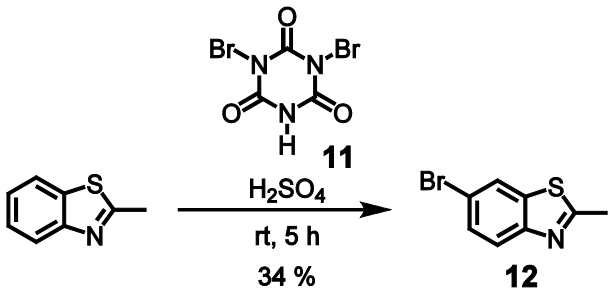

Scheme 17 Synthesis of 6-bromo-2-mehtylbenzothiazole (**12**).

Quaternary Salts of the Benzothiazoles

The alkylation of 6-substituted 2-methylbenzothiazoles proved to be challenging, hence, various reaction conditions were tested first with the unsubstituted and commercial available 2-methylbenzothiazole (Scheme 18). The alkylation with 1-iodohexane and 1-iodohexadecane in refluxing CH_3NO_2 according to the literature resulted in good yields.[24, 29, 62] Another literature procedure without solvent either did not give the product or only in low yields.[113] In order to improve the solubility of the final squaraine compounds the branched 3,7-dimethyloctyl chain was used as well. Therefore the alkylation reagents 3,7-dimethyloctyl tosylate (**13**)[114], 1-bromo-3,7-dimethyloctane (**14**)[115] and 1-iodo-3,7-dimethyloctane (**15**)[116] were synthesised according to the given literatures starting from 3,7-dimethyloctan-1-ol. The alkylation with **13** and **14** using the established conditions[97] or a microwave procedure[111] only gave small amounts of the product. The change of the counterion to iodine improved the yield distinctly. All findings are summarised in Table 3.

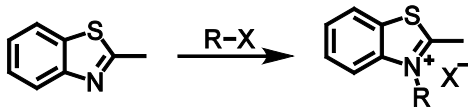

Scheme 18 Alkylation of 2-methylbenzothiazole.

Table 3 Conditions for the alkylation of 2-methylbenzothiazole.

R	X	reaction conditions	yield	compound name
3,7-dimethyloctyl	tos	CH_3NO_2, 120°C, 15 h [97]	22 %	
3,7-dimethyloctyl	tos	95°C; 48 h [113]	–	
3,7-dimethyloctyl	tos	CH_3NO_2, 120°C, 45 min Microwave [111]	4 %	
3,7-dimethyloctyl	Br	CH_3NO_2, 120°C, 15 h [97]	1 %	
3,7-dimethyloctyl	I	CH_3NO_2, 120°C, 15 h	36 %	**16**
hexadecyl	I	120°C, 16 h [113]	13 %	**17**
hexadecyl	I	CH_3NO_2, 120°C, 20 h [24, 29, 62]	59 %	**18**
hexyl	I	CH_3NO_2, 120°C, 16 h [62]	92 %	**18**

The alkylation of 6-bromo-2-methylbenzothiazole (**12**) (Scheme 19) with the conditions that proved suitable for the alkylation of 2-methylbenzothiazole, was not successful (Table 4). However, the extension of the reaction time to 5 - 7 d resulted in the desired products.

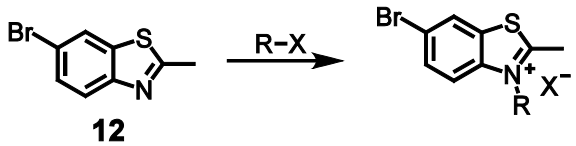

12

Scheme 19 Alkylation of 6-bromo-2-methylbenzothiazole (**12**).

Table 4 Conditions for the alkylation of 6-bromo-2-methylbenzothiazole (**12**).

R	X	reaction conditions	yield	compound name
3,7-dimethyloctyl	tos	CH_3NO_2, 120°C, 16 h	–	
3,7-dimethyloctyl	I	CH_3NO_2, 120°C, 16 h	–	**12**
3,7-dimethyloctyl	I	CH_3NO_2, 120°C, 3 h, Microwave [111]	–	**12**
3,7-dimethyloctyl	I	CH_3NO_2, 120°C, 5 d	31 %	**12**
hexadecyl	I	CH_3NO_2, 120°C, 20 h	–	**13**
hexadecyl	I	CH_3NO_2, 120°C, 7 d	29 %	**13**
hexyl	I	CH_3NO_2, 120°C, 7 d	80 %	**14**

The alkylation of 6-acetamido-2-methylbenzothiazole (**10**) was done in refluxing CH_3NO_2 with 1-iodohexane (Scheme 20).

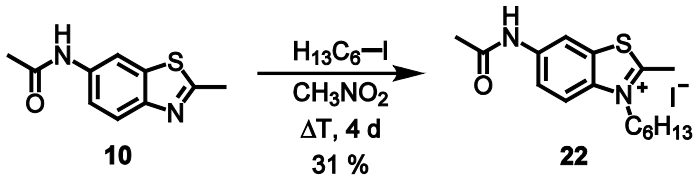

Scheme 20 Alkylation of 6-acetamido-2-mehtylbenzothiazole (**10**).

Monofunctionalised Benzothiazole Squaraines

The unsymmetrical squaraines of the non-functionalised benzothiazole salts were obtained in a three-step synthesis (Scheme 21). Initially the semisquaraine butyl esters were obtained in a condensation reaction of the quaternary salt with one equivalent of 3,4-dibutoxy-3-cyclobutene-1,2-dione in the presence of triethylamine. Subsequent saponification yielded the semisquaraine acids. An additional condensation reaction with a functionalised quaternary benzothiazole salt in a 6/4 mixture of refluxing ^{n}BuOH/toluene in the presence of pyridine with azeotropic distillation of water using a *Dean-Stark*-trap yielded the asymmetrical squaraine.

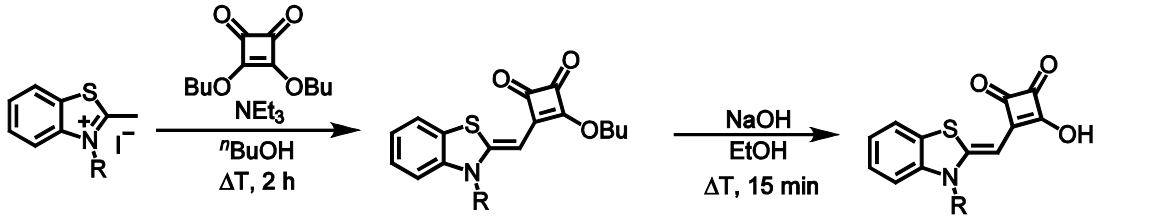

16 (R = 3,7-dimethyloctyl) **23** (R = 3,7-dimethyloctyl) 68 % **26** (R = 3,7-dimethyloctyl) 92 %
17 (R = hexadecyl) **24** (R = hexadecyl) 61 % **27** (R = hexadecyl) 94 %
18 (R = hexyl) **25** (R = hexyl) 52 % **28** (R = hexyl) 96 %

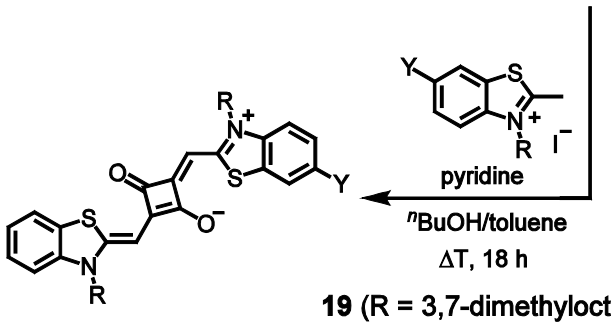

B1 = 26 + 19
(R = 3,7-dimethyloctyl, Y = Br) 41 %
B2 = 27 + 20
(R = hexadecyl, Y = Br) 49 %
B3 = 28 + 21
(R = hexyl, Y = Br) 48 %
B4 = 28 + 22
(R = hexyl, Y = NHAc) 20 %

19 (R = 3,7-dimethyloctyl, Y = Br)
20 (R = hexadecyl, Y = Br)
21 (R = hexyl, Y = Br)
22 (R = hexyl, Y = NHAc)

Scheme 21 Synthesis of the unsymmetrical benzothiazole squaraines.

The acetyl group was removed under acidic conditions in ethanol under exclusion of light (Scheme 22).

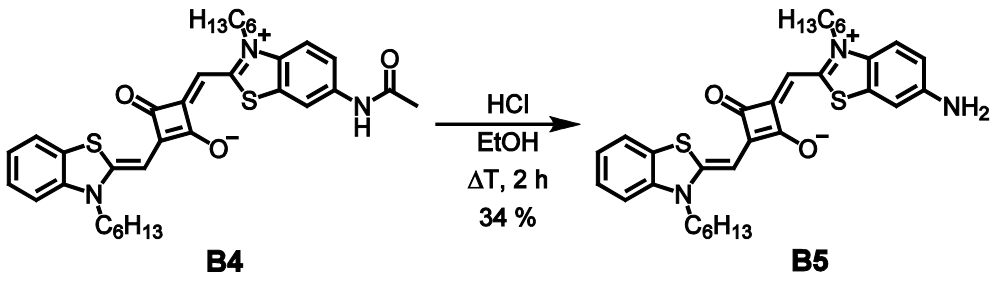

Scheme 22 Removal of the protecting group of the amine.

Star-Shaped Benzothiazole Squaraine Trimers

In theory the nitrogen core squaraine trimer could be build up in a palladium catalysed *Buchwald-Hartwig* coupling reaction using $Pd_2(dba)_3 \cdot CHCl_3$ as catalyst, P^tBu_3 as co-catalyst and NaO^tBu as base. One equivalent of the aminated squaraine **B5** and about 2.5 equivalents of the brominated benzothiazole squaraine **B3** were used as reactants. Even though thin layer chromatograms indicated that multiple squaraine compounds have formed during the reaction, the work up after 4 d in refluxing toluene under exclusion of light only yielded very small amounts of the dimer as confirmed by mass spectrometry (Scheme 23).

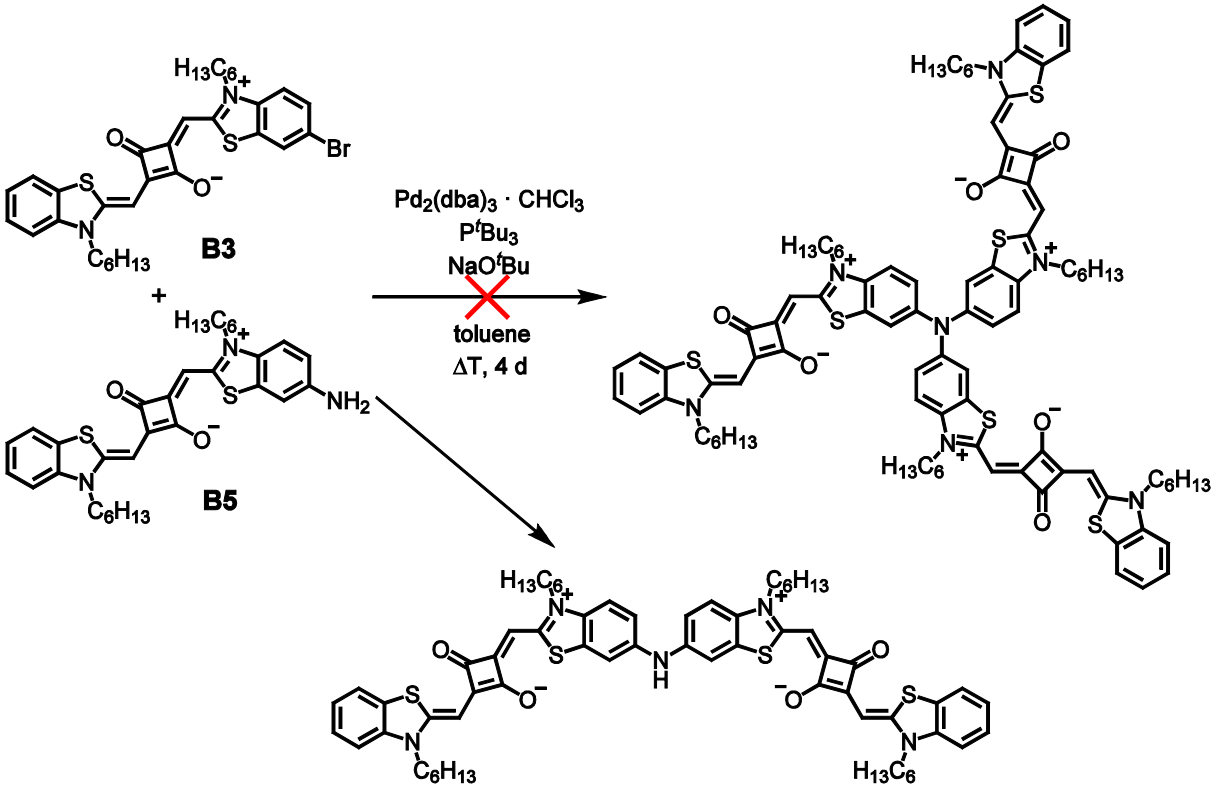

Scheme 23 Attempted synthesis of the nitrogen core benzothiazole squaraine trimer.

As a test if the trimerisation of benzothiazoles takes place under the chosen conditions the reaction of one equivalent of 6-amino-2-methylbenzothiazole (**9**) with 2.2 equivalents of 6-bromo-2-methylbenzothiazole (**12**) was carried out. After the workup 50 % of tris(2-methylbenzothiazol-6-yl)amine **29** could be isolated (Scheme 24).

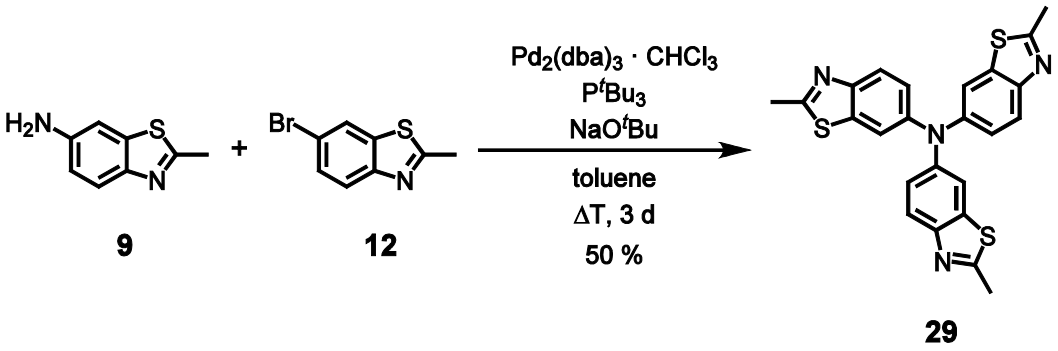

Scheme 24 Test of the conditions for the *Buchwald-Hartwig* coupling reaction.

Moreover the palladium catalysed *Suzuki* coupling reactions of 3.3 equivalents of the brominated unsymmetrical benzothiazole squaraines **B1**, **B2** and **B3** with one equivalent of 1,3,5-tris-(4, 4, 5, 5-tetramethyl-1,3,2-dioxaborolan-2-yl)benzene (**30**) (Scheme 25) as well as with tris(4-(4, 4, 5, 5-tetramethyl-1,3,2-dioxaborolan-2-yl)phenyl)amine (**31**) were tested (Scheme 26). In the reactions with R = hexyl some blue insoluble solid was noticed, therefore the reaction was carried out with the linear hexadecyl and the branched 3,7-dimethyloctyl chain as well in order to achieve a better solubility. In all reactions two new squaraines, most likely dimer and trimer, were observed after the first short column filtration. These two compounds were inseparable by column chromatography and unstable on the GPC. Literature suggests that benzothiazole squaraines are prone to degradation in the presence of oxygen and/or light.[117] This could be the reason that no pure products could be isolated.

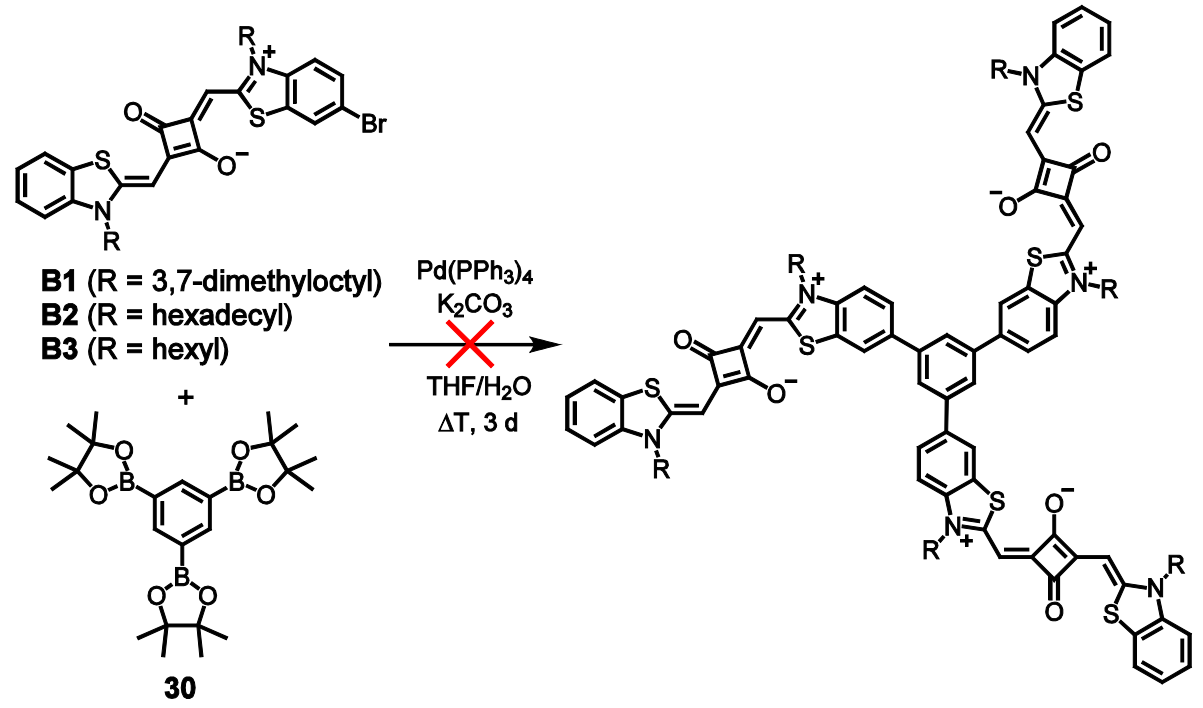

Scheme 25 Attempted synthesis of the star-shaped benzene core benzothiazole squaraine trimer.

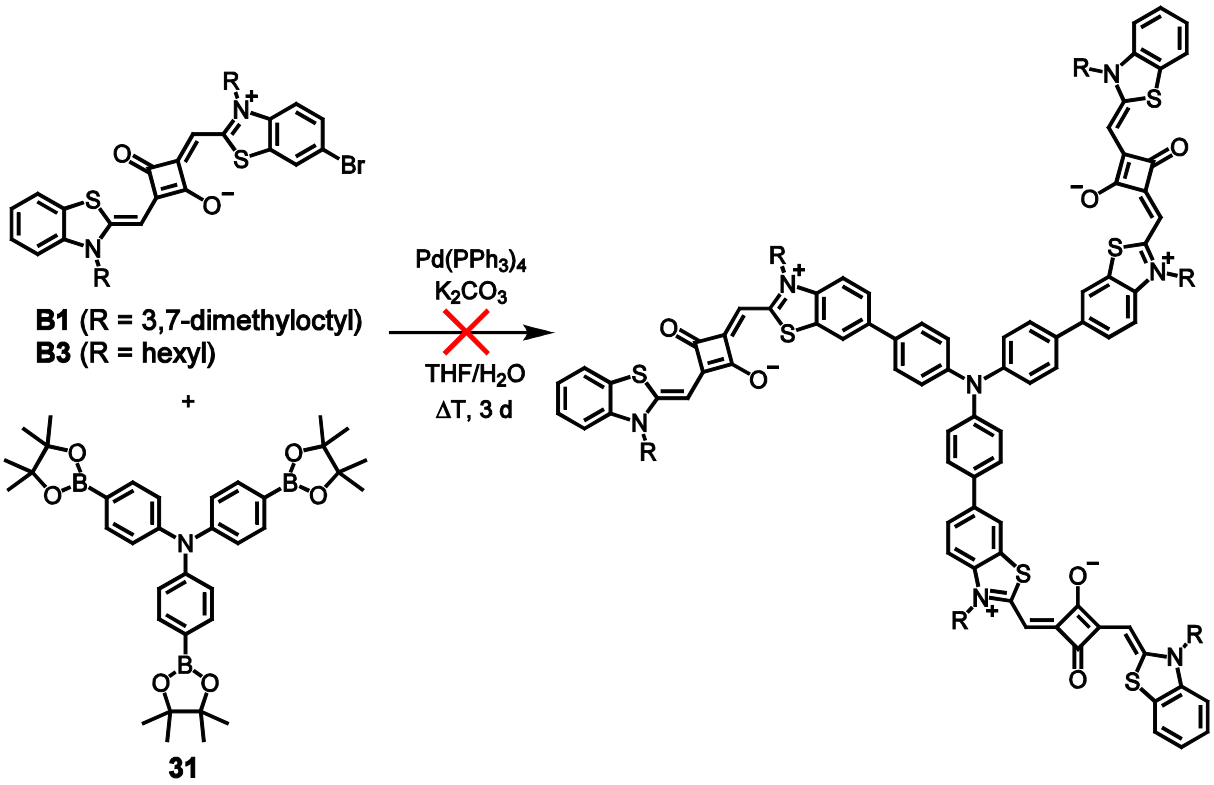

Scheme 26 Attempted synthesis of the star-shaped triarylamine core benzothiazole squaraine trimer.

3.2.3 Conclusion

Despite the indications that the trimers were formed during the reactions, no pure product could be isolated. In the case of the benzothiazoles with hexyl chains this might be because the product was insoluble as a blue solid formed in the *Suzuki* coupling reactions. The compounds with the longer and the branched chain seemed to decompose during flash-column chromatography on silica as well as during recycling Gel-Permeation-Chromatography with $CHCl_3$ as mobile phase.

Nevertheless, some useful insight into the preparation of the precursors and the trimerisation reactions could be gained.

3.3 Linear and Star-Shaped Indolenine Squaraine Trimers[1]

Introduction

Due to the problems regarding the synthesis of the benzothiazole squaraine trimers the basic squaraine unit was changed to the well-established 2,3,3-trimethylindolenine analogues. The educts for the trimerisations were synthesised using the insight that was gained in the benzothiazole synthesis. For example only 1-iodo-3,7-dimethyloctyl was used as alkylation reagent, because it combined the highest yield for the quaternary salts and the best solubility for the squaraines.

Synthesis of the Indolenine precursors

The alkylation of commercially available 2,3,3-trimethyl-3H-indole with 1-iodo-3,7-dimethyloctane (**15**) in refluxing nitromethane yielded 84 % of the quaternary salt 1-(3,7-dimthely)-2,3,3-trimethyl-3H-indole-1-ium iodine (**31**) (Scheme 27).

[1] Text and Figures are reproduced or adapted in part with permission from: a) H. Ceymann, M. Balkenhohl, A. Schmiedel, M. Holzapfel and C. Lambert, *Phys. Chem. Chem. Phys.*, 2016, **18**, 2646-2657. b) H. Ceymann, A. Rosspeintner, M. H. Schreck, C. Mützel, A. Stoy, E. Vauthey and C. Lambert, Phys. Chem. Chem. Phys., 2016, DOI: 10.1039/C6CP02312F.
Parts of this chapter have been investigated in two Bachelor thesis under the supervision of H. Ceymann: M. Balkenhohl, Bachelor thesis, Julius-Maximilians-Universität (Würzburg), 2014 and C. Mützel, Bachelor thesis, Julius-Maximilians-Universität (Würzburg), 2014.

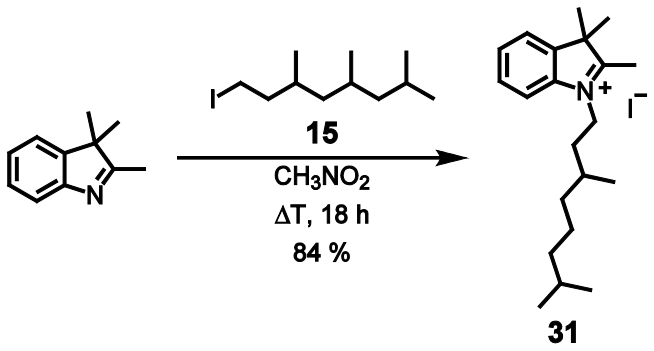

Scheme 27 Synthesis of 1-(3,7-dimethyloctyl)-2,3,3-trimethyl-3H-indole (**31**).

The bromine functionalised indole derivative 5-bromo-2,3,3-trimethyl-3H-indole (**33**) was synthesised via a *Fisher* indole synthesis of *p*-bromophenylhydrazine hydrochloride with isopropylmethyl ketone in pure acetic acid according to the literature.[118] The alkylation yielded 63 % of 5-bromo-1-(3,7-dimethyloctyl)-2,3,3-trimethyl-3H-indole-1-ium iodine (**34**) (Scheme 28).

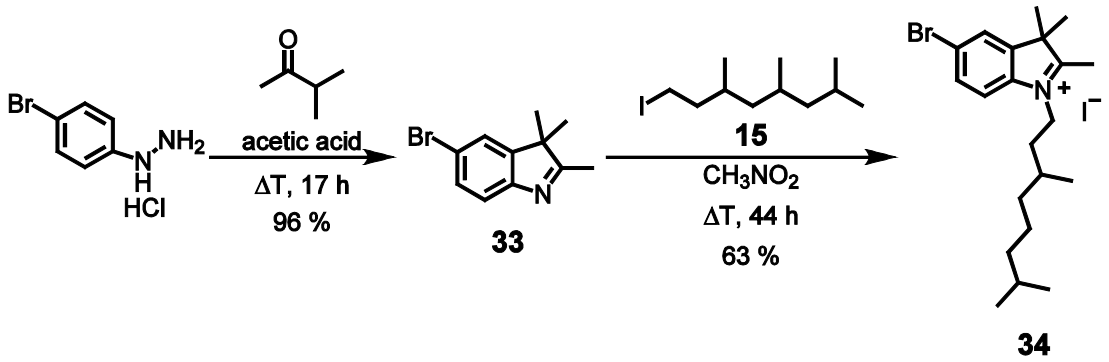

Scheme 28 Synthesis of 5-bromo-1-(3,7-dimethyloctyl)-2,3,3-trimethyl-3H-indole-1-ium iodine (**34**).

The synthesis of 5-amino-2,3,3-trimethyl-3H-indole (**36**) was accomplished by a slightly different protocol compared to the synthesis of 6-amino-2-methylbenzothiazole (**9**) (Scheme 29).[119] The reduction of 5-nitro-2,3,3-trimethyl-3H-indole (**35**) was carried out with tin chloride in refluxing hydrochloric acid. The protection of the amine group using the conditions for the benzothiazole equivalent resulted in no product whatsoever. A similar attempt in pure acetic anhydride according to the literature[120] only gave yields of up to 12 %. After a few further attempts and even the change of the protecting group[121] the reaction of a slight excess of 5-amino-2,3,3-trimethylindole (**36**) with one equivalent of acetic anhydride and one equivalent of triethylamine in dry CH_2Cl_2 at room temperature resulted in a nearly quantitative conversion. During the reaction ethylene was generated, as verified by the decolouration of bromic water by the collected gas. The endothermic

reaction was finished when the gas formation ceased. When an excess of acetic anhydride and triethylamine was used the second nitrogen became alkylated as well. The quaternary salt **38** was finally obtained by the alkylation with 1-iodo-3,7-dimethyloctane (**15**).

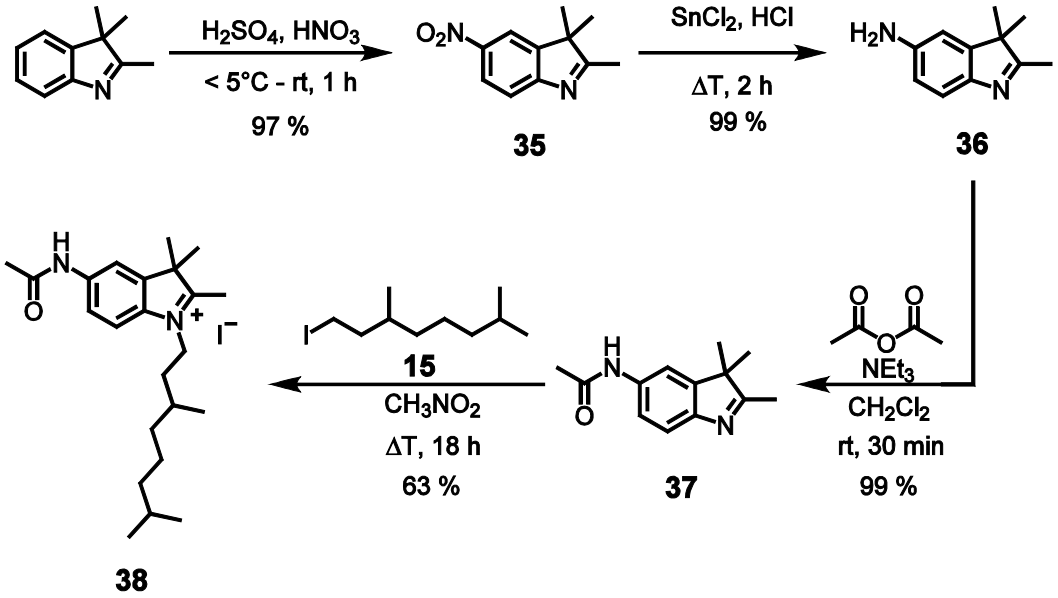

Scheme 29 Synthesis of 5-acetamido-1-(3,7-dimethyloctyl)-2,3,3-trimethyl-3H-indole-1-ium iodine (**38**).

Synthesis of the Monomeric Indole Squaraines

The symmetrical squaraines **SQA** and **SQA-Br$_2$** were synthesised in a one pot reaction starting with an *in situ* deprotonation of the quaternary salt resulting in the highly nucleophilic methylene base. A consecutive dicondensation reaction with half an equivalent of squaric acid in a 6/4 mixture of ^{n}BuOH and toluene with azeotropic distillation of water using a *Dean-Stark*-trap gave the symmetrical transoid squaraines.

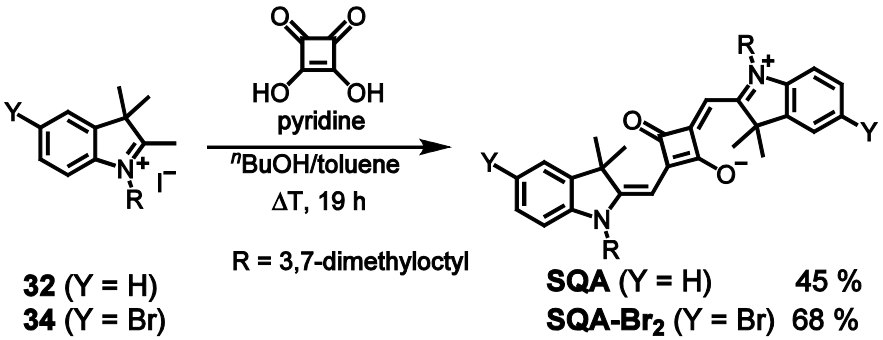

Scheme 30 Synthesis of the symmetrical transoid squaraines **SQA** and **SQA-Br$_2$**.

The semisquaraines were synthesised in a similar manner as the benzothiazole derivatives. In this case the condensation of the quaternary salt was carried out with 3,4-diethoxy-3-cyclobutene-1,2-dione because it was simpler to separate from the product. Then the semisquaraine esters were either converted into the semisquaraine acid via a saponification with sodium hydroxide or into the dicyanomethylene-substituted semisquaraine with malononitrile and triethylamine. The acid **41** was used to synthesise the squaraines that adopt the *trans*-configuration while the dicyanomethylene-substituted semisquaraines **42** and **43** were used to get the squaraines that adopt the *cis*-configuration (Scheme 31).

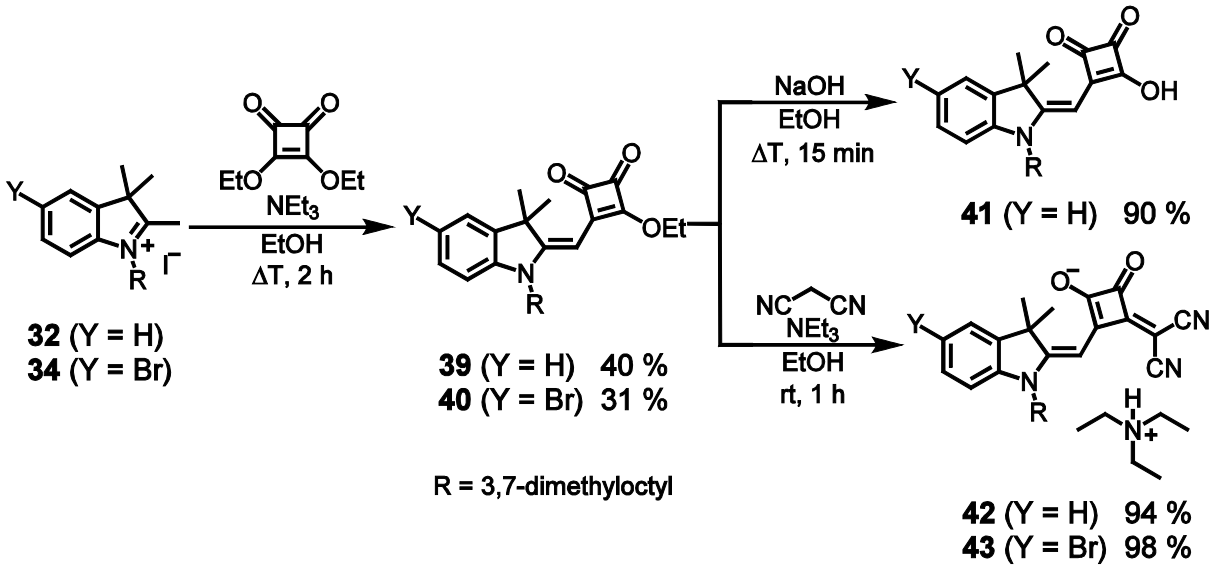

Scheme 31 Synthesis of the semisquaric acid **41** and the dicyanovinylene analogues **42** and **43**.

The unsymmetrical mono functionalised *trans*-configured squaraines **SQA-Br** and **SQA-NHAc** were synthesised in a condensation reaction of the semisquaraine acid **41** with the quaternary salts **34** and **38** in a 6/4 mixture of refluxing ^{n}BuOH and toluene in the presence of pyridine with azeotropic distillation of water using a *Dean-Stark*-trap (Scheme 32).

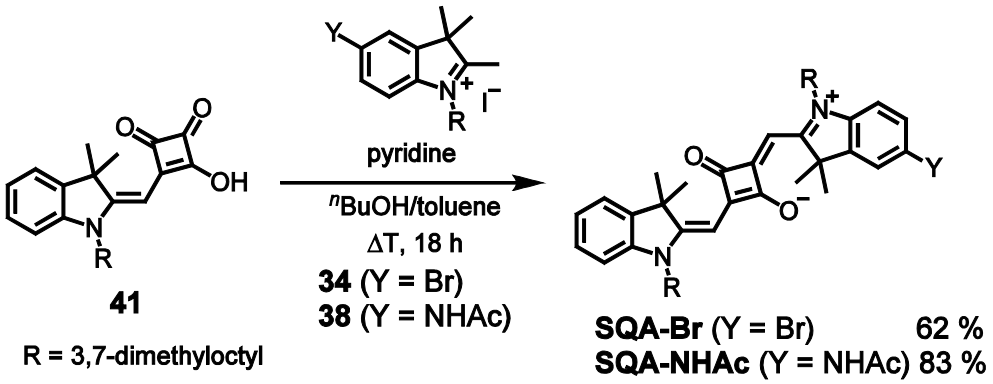

Scheme 32 Synthesis of the unsymmetrical trans-squaraines **SQA-Br** and **SQA-NHAc**.

Analogue reactions of the dicyanomethylene-substituted semisquaraines **42** and **41** with the quaternary salts **32** and **38** yielded the unsymmetrical cis-configured mono functionalised squaraines **SQB-NHAc** and **SQB-Br**.

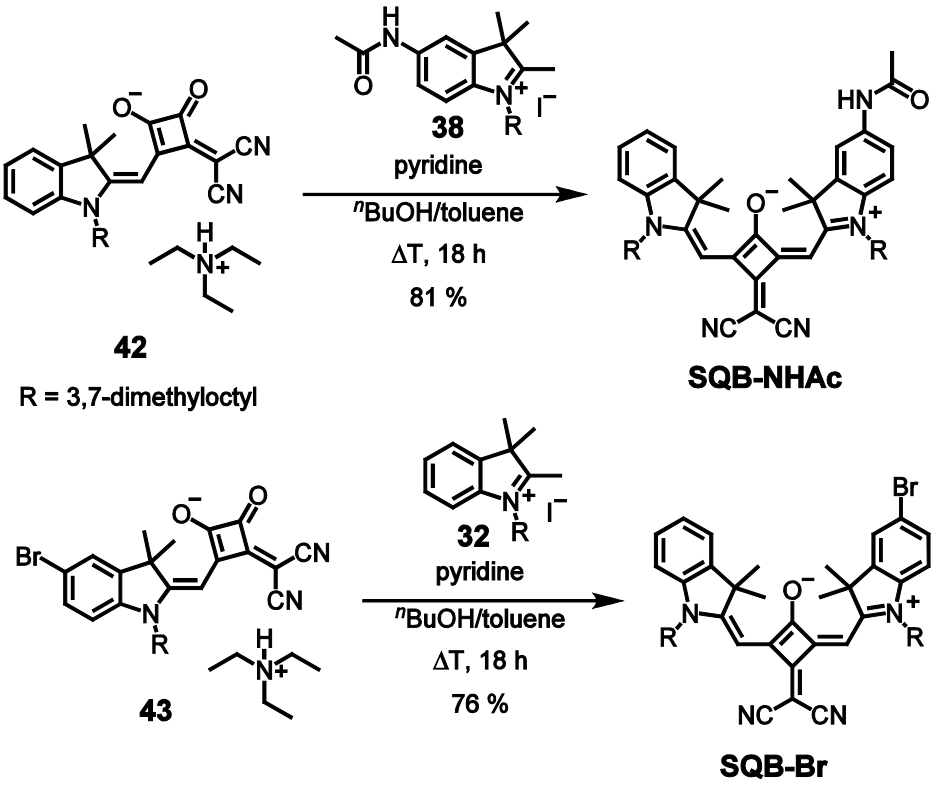

Scheme 33 Synthesis of the unsymmetrical cis-squaraines **SQB-NHAc** and **SQB-Br**.

The acetyl groups of **SQA-NHAc** and **SQA-NHAc** were removed under acidic conditions in ethanol under exclusion of light (Scheme 34).

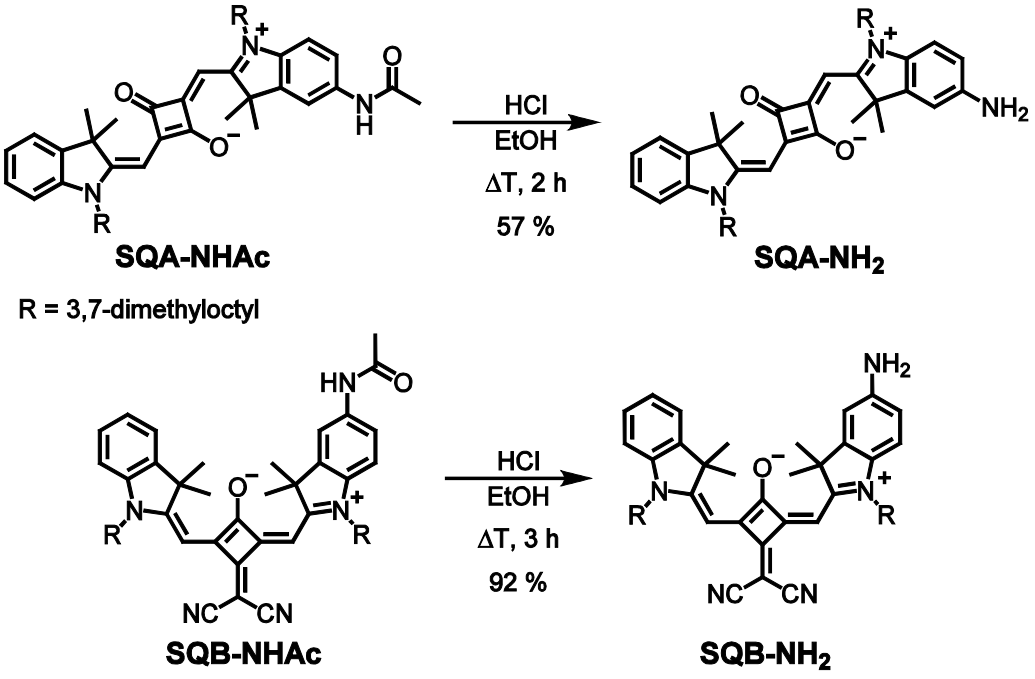

Scheme 34 Removal of the protecting group of the amine.

The condensation reaction of the semisquaraine acid **41** with 6-bromo-3-(3,7-dimethyloctyl)-2-methylbenzothiazol-3-ium iodide (**19**) yielded the mixed benzothiazole-indole squaraine **SQC-Br**. **SQD-Br** where the functionality is located at the indolenine part of the molecule was synthesised in the reaction of the benzothiazole semisquaraine acid **26** with 6-bromo-1-(3,7-dimethyloctyl)-2,3,3-trimethyl-3H-indol-1-ium iodide (**34**).

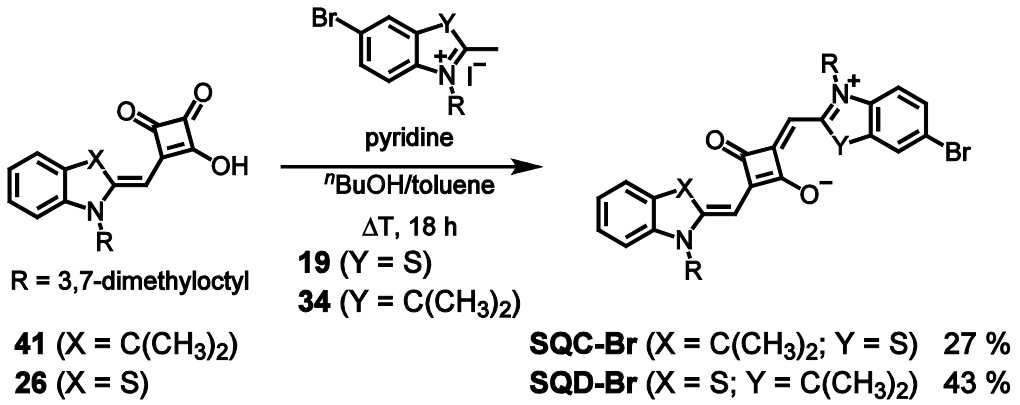

Scheme 35 Synthesis of the indole-benzothiazole trans-squaraines **SQC-Br** and **SQD-Br**.

The bromine atoms of the symmetrical squaraine **SQA-Br$_2$** and the unsymmetrical squaraine **SQA-Br** were substituted by boronic ester groups via the palladium catalysed *Miyaura* borylation reaction with 4,4,4',4',5,5,5',5'-octamethyl-2,2'-bi(1,3,2-dioxaborolane), $Pd(PhCN)_2Cl_2$, 1,1'-bis(diphenylphosphino)ferrocene (dppf) and the base KOAc.

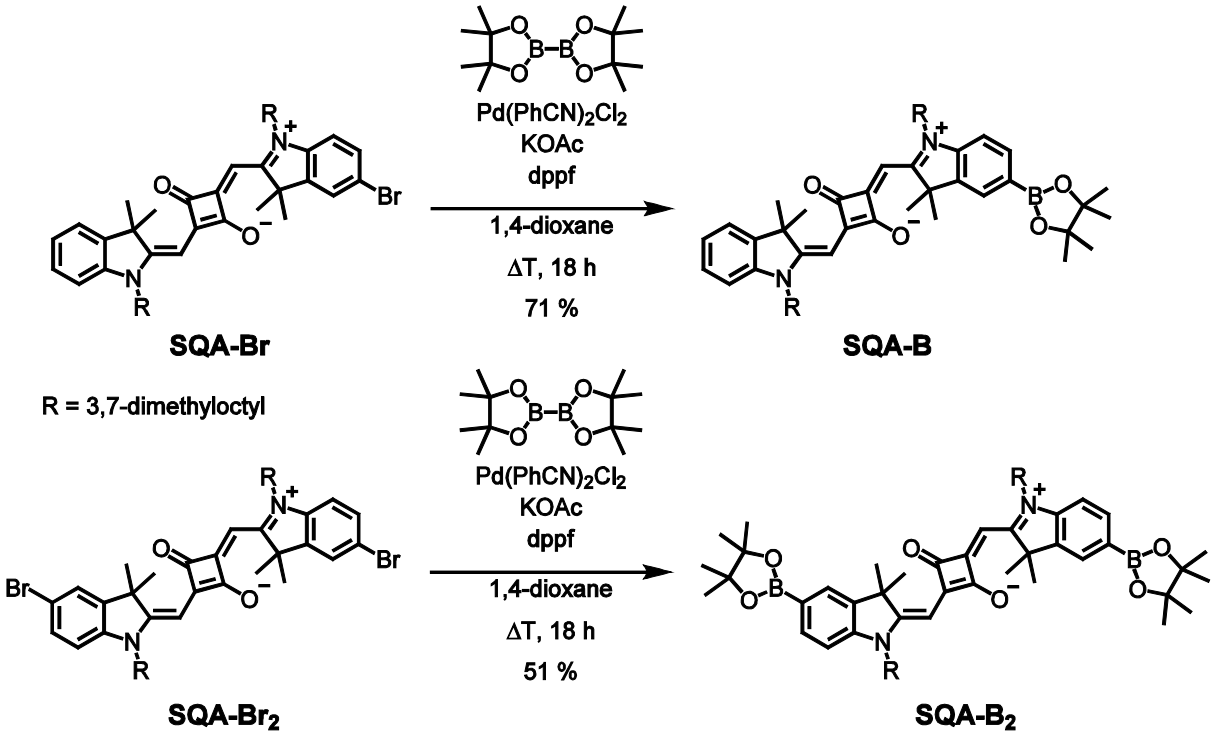

Scheme 36 Synthesis of boronic esters of the trans indolenine squaraines.

3.3.1 Star-Shaped Trimers with a Nitrogen Core

Synthesis

The squaraine homotrimers **$(SQA)_3$-N** (Scheme 37) and **$(SQB)_3$-N** (Scheme 38) were synthesised in a palladium catalysed *Buchwald-Hartwig* coupling reaction using the conditions that were used for the synthesis of *tris*(2-methylbenzothiazol-6-yl)amine (**29**) (Scheme 24). One equivalent of the aminated and 2.2 equivalents of the brominated unsymmetrical squaraines were used. The separation of the dimer and trimer was quite challenging[121] and was finally achieved by slowly changing of the methanol ratio of the eluent for the flash-column chromatography by steps of 0.1 ‰ over several hours. During that time the column had to be kept in the dark to prevent degradation of the product. The yields for the isolated trimers are quite low with only a few per cent.

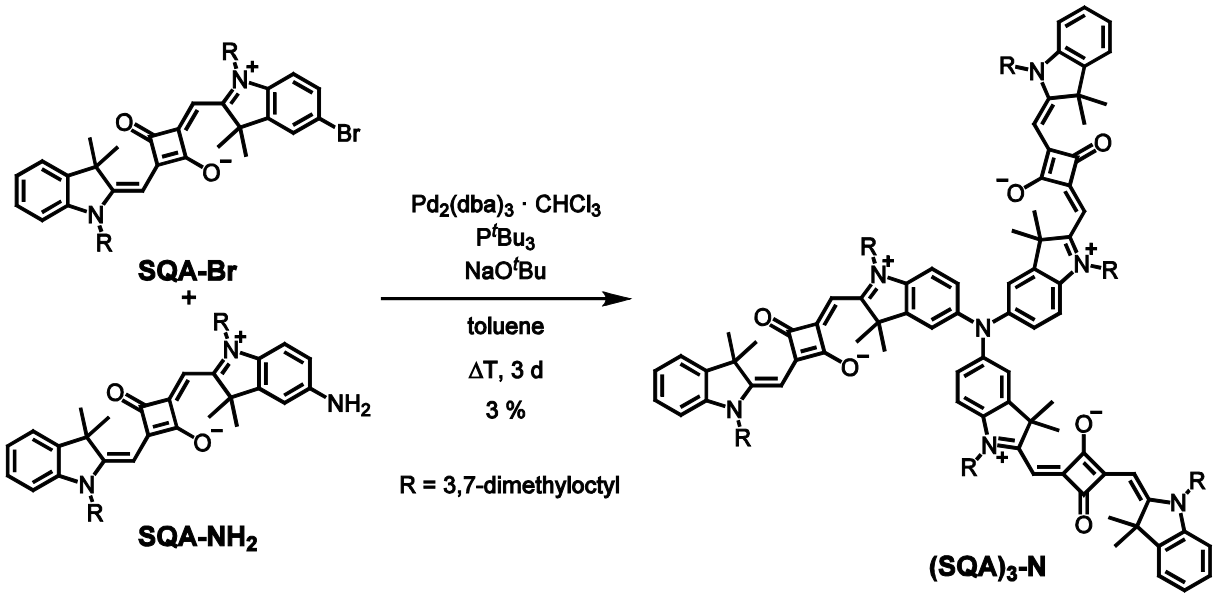

Scheme 37 Synthesis of the *N*-core *trans* squaraine trimer **$(SQA)_3$-N**.

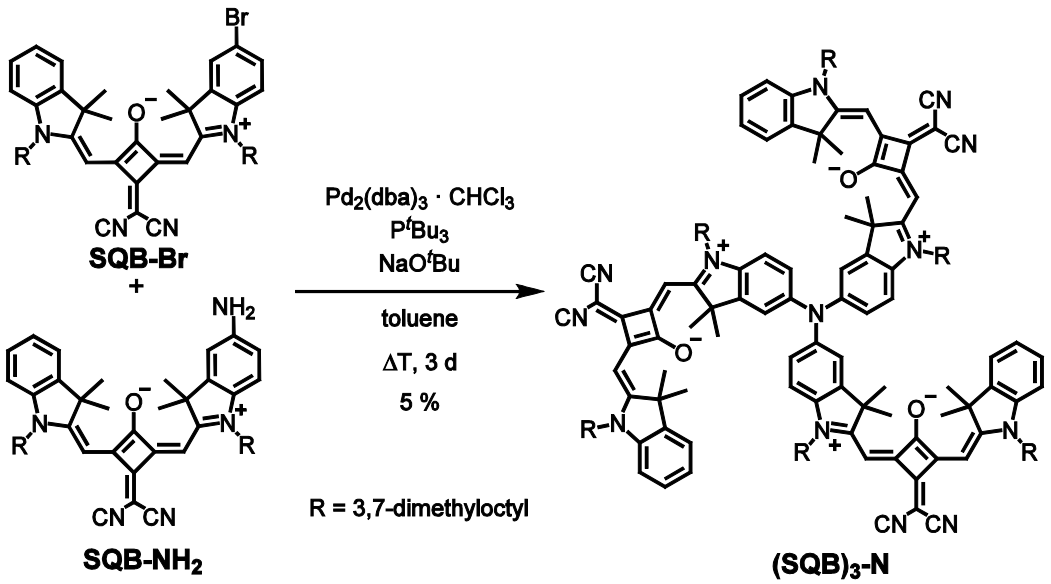

Scheme 38 Synthesis of the *N*-core *cis* squaraine trimer **(SQB)$_3$-N**.

The heterotrimers **(SQA)(SQB)$_2$-N** (Scheme 39) and **(SQA)$_2$(SQB)-N** (Scheme 40) were synthesised using the same conditions but this time the brominated and the aminated squaraines had different structures. The workup for **(SQA)(SQB)$_2$-N** was similar to the one used for the homotrimers. In this case not only 11 % of the trimer, but also 8 % of the dimer **(SQA)(SQB)-NH** could be isolated.

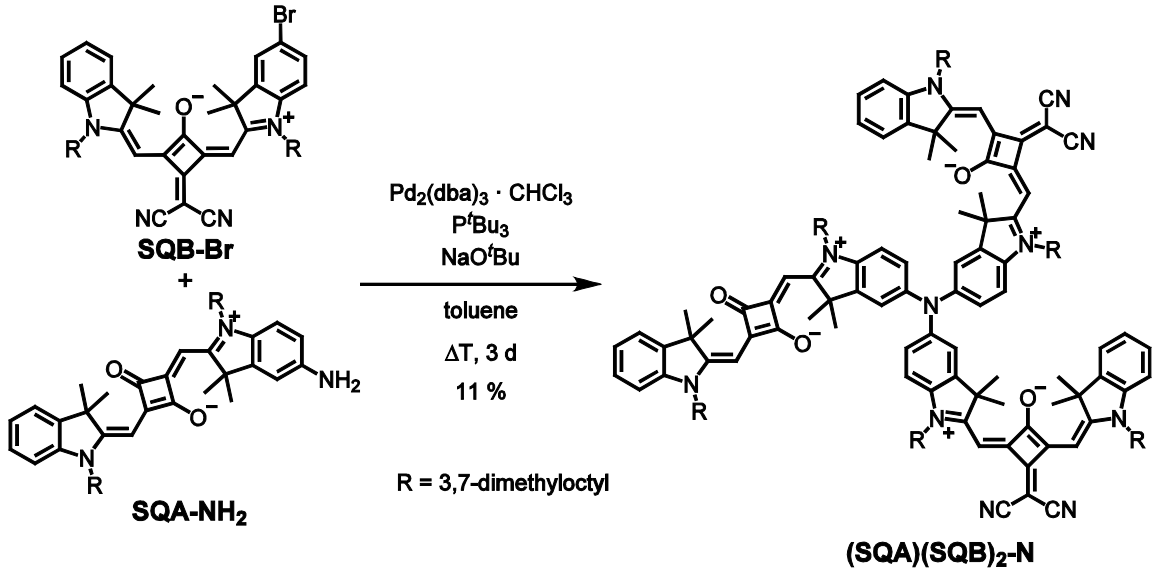

Scheme 39 Synthesis of the *N*-core *trans-cis-cis* squaraine trimer (**SQA)(SQB)$_2$-N**.

For the other mixed trimer **(SQA)$_2$(SQB)-N** the purification was even more challenging. After a short column filtration the crude product did not show any traces of the desired product. However, the mixture contained 45 % of the dimer. This dimer was then used for another palladium catalysed *Buchwald-Hartwig* coupling reaction with 1.2 equivalents of the brominated unsymmetrical squaraine. The trimer **(SQA)$_2$(SQB)-N** was unstable on silica over a longer timescale and a separation following the procedure for the other trimers was not possible. Therefore, the crude product after a short column filtration was purified by GPC. The GPC workup, next to some others[121], was tested for **(SQA)$_3$-N** as well. Unfortunately **(SQA)$_3$-N** proved unstable on the GPC even after the first cycle. This might be due to a faulty degassing unit of the GPC setup at the time the purification of **(SQA)$_3$-N** was attempted.

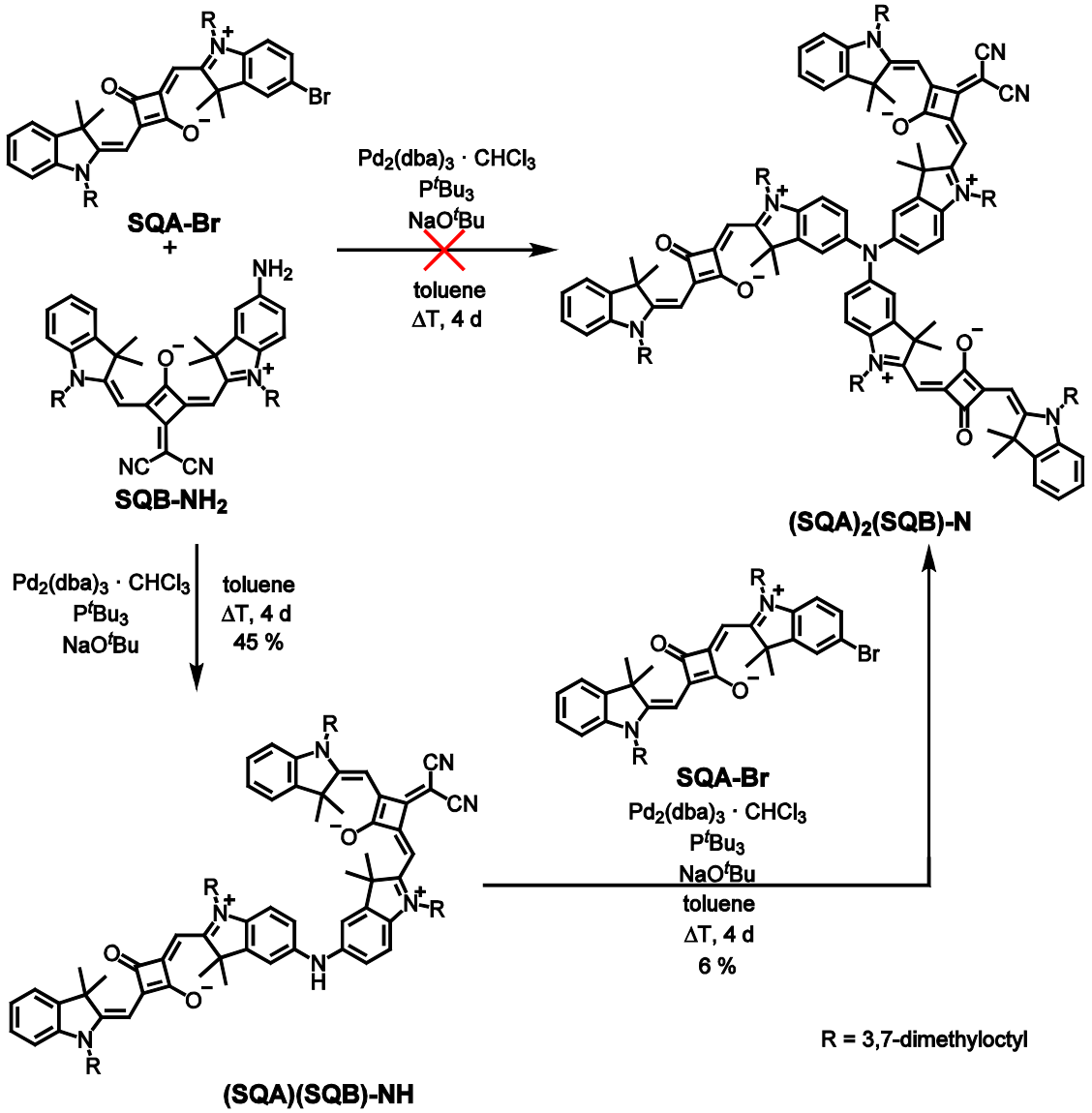

Scheme 40 Synthesis of the *cis-trans* dimer **(SQA)(SQB)-NH** and the *N*-core *trans-trans-cis* squaraine trimer **(SQA)$_2$(SQB)-N**.

Absorption Spectroscopy

The absorption spectra of the unsymmetrical squaraines **SQA-NHAc** and **SQB-NHAc** (Figure 32) show the typical properties of squaraine dyes and serve as reference compounds for the homo- and heterotrimers with one N-atom as core unit. The sharp and very intense absorption band in the red region of the visible spectrum originates from the HOMO→LUMO transition. While this band rises steeply on the low energy side there is a small shoulder on the high energy side which stems from vibronic progression. In **SQB-NHAc** the electron acceptor strength of the central squaric acid ring is increased by the substitution of one oxygen atom by a dicyanomethylene group. This leads to a lowering of the LUMO energy level, which in turn, because the rest of the molecule is the same, results in a bathochromic shift of the absorption maximum by about 1100 cm^{-1}. In addition **SQB-NHAc** shows prominent transitions between 20000 and 28000 cm^{-1} (HOMO-1→LUMO and HOMO→LUMO+1) which are typical of dicyanomethylene-substituted squaraines.[15]

The solvent has nearly no influence on the absorption spectra of **SQA-NHAc**. The main absorption in toluene is at 15300 cm^{-1} with an extinction coefficient of 281000 M^{-1} cm^{-1}. This is a red shift of 200 cm^{-1} compared to the unsubstituted parent squaraine **SQA**. In **SQB-NHAc** the main absorption in toluene is again 200 cm^{-1} bathochromically shifted, relative to the unsubstituted squaraine **SQB**, at 14100 cm^{-1} with an extinction coefficient of 233000 cm^{-1}. The influence of the solvent leads to a shift to higher energies of 300 cm^{-1}, if toluene is exchanged by acetone.

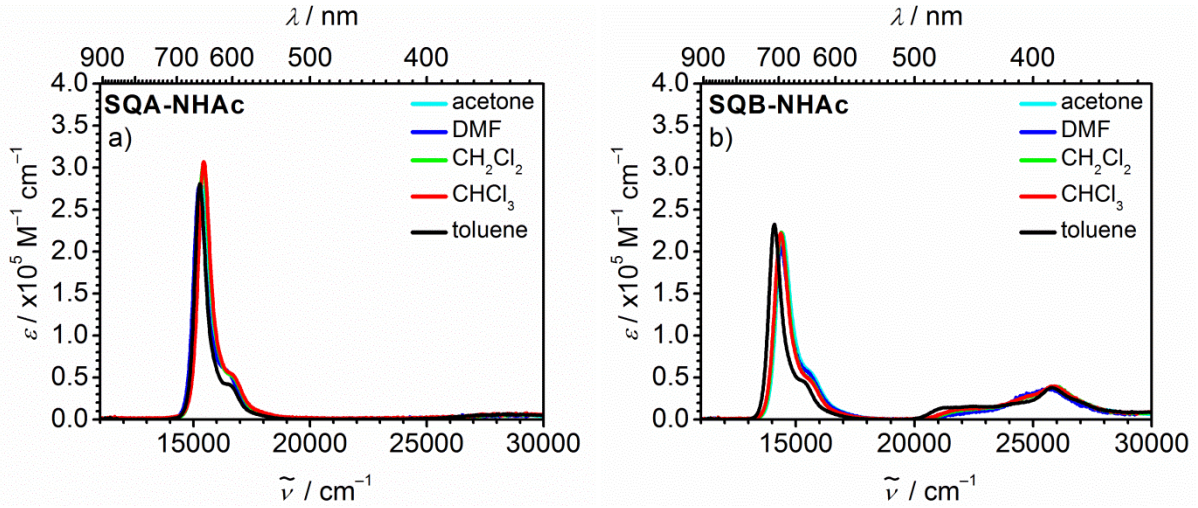

Figure 32 Absorption spectra of the unsymmetrical squaraines **SQA-NHAc** (a) and **SQB-NHAc** (b) in different solvents.

The investigation of the homo- and heterotrimers and the heterodimer focus on the low energy squaraine absorption only, therefore the spectra in Figure 33 are magnified in the red to NIR region.

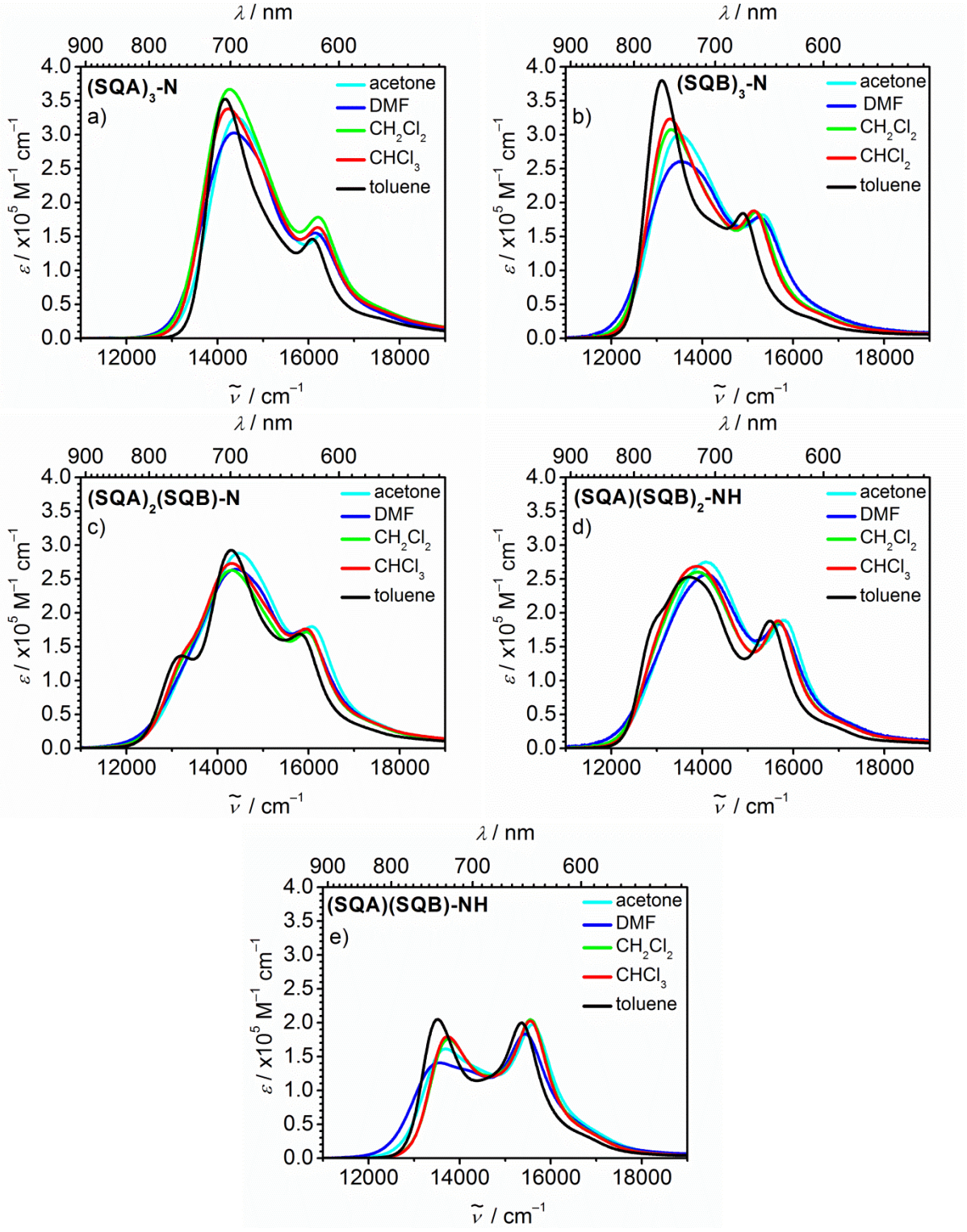

Figure 33 Absorption spectra of the low energy absorption of the homotrimers **(SQA)$_3$-N** (a) and **(SQB)$_3$-N** (b), the heterotrimers **(SQA)(SQB)$_2$-N** (c) and **(SQA)$_2$(SQB)-N** (d) and the heterodimer **(SQA)(SQB)-N** (e) in different solvents at rt.

The absorption spectra of the homotrimers **(SQA)$_3$-N** and **(SQB)$_3$-N** (Figure 33a and b) display a strong red shift of the HOMO→LUMO transition in comparison to their monomeric reference compounds **SQA-NHAc** and **SQB-NHAc** (Figure 32) of ca. 1000 cm^{-1} in all measured solvents. This shift is caused by excitonic coupling due to the delocalisation of the excitation over all three branches (Figure 34). The absorption peak at higher energy, which should be forbidden for a truly C_3-symmetric superchromophore, is visible as a result of structural disorder. The difference of this transition to the main peak can be used to estimate the exciton coupling energy J (see appendix Table S2-4).

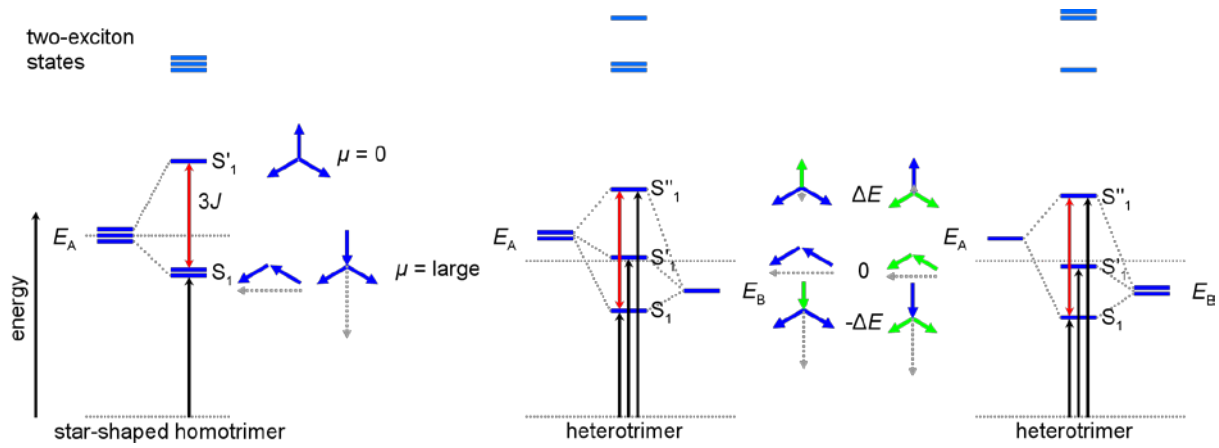

Figure 34 Exciton eigenstates formed by exciton interaction in case of a C_3-symmetric homotrimer (left) and two heterotrimers (middle and right). The excited state energies of the isolated monomers are given as E_A and E_B. The excited state energies in the heterotrimers are arbitrary and depend on the relative magnitude of J and ΔE. The blue and green arrows indicate the phase relations of the localised transition moments. Allowed transitions from the ground state are given as black arrows.

The absorption spectra of the heterotrimers show a more complex pattern. Superchromophore **(SQA)$_2$(SQB)-N** (Figure 33c) shows in toluene three defined peak maxima in the red region. In the other solvents the small peak with the lowest energy merges with the most intense at intermediate energy and only a shoulder is observable. The maxima are associated to the three excited states that are predicted by exciton-coupling theory. In **(SQA)(SQB)$_2$-N** (Figure 33d) the difference between the first two states is even smaller than in **(SQA)$_2$(SQB)-N**. Therefore, even in toluene, only a shoulder is visible for the absorption with the lowest energy. In toluene the heterodimer **(SQA)(SQB)-NH** (Figure 33e) shows two distinct peaks at 13500 cm^{-1} and 15400 cm^{-1} with similar intensities. In the other solvents the peak at lower energy is less intense than the peak at higher energy. In DMF the difference in intensities is most pronounced. Absorption measurements in toluene with

differing temperatures showed a negligible temperature dependence of the absorption in this region (Figure 35).

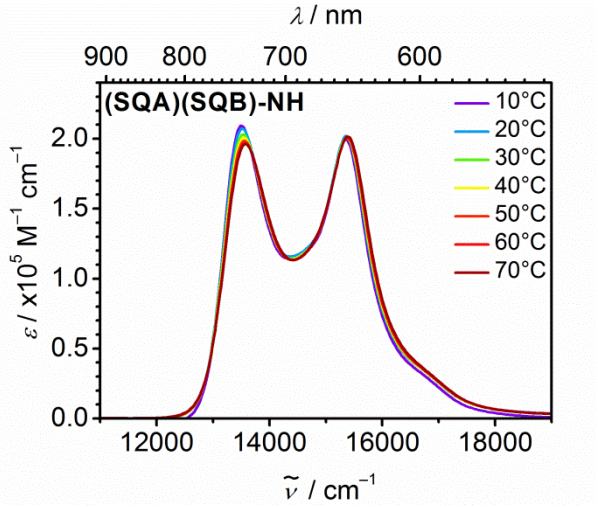

Figure 35 Absorption spectra of **(SQA)(SQB)-NH** in toluene at various temperatures.

In **(SQA)(SQB)-NH** only one coupling between the two squaraines is possible. Therefore, the difference of the absorption peaks is used to predict the splitting of the bands by exciton coupling theory (see chapter 1.3) and further to determine the coupling constant *J* according to eq. (55).[122]

$$\delta E = 2\sqrt{\Delta E^2 + J^2} \tag{55}$$

In toluene this leads to a value of 736 cm^{-1} for *J*. With this coupling constant for different squaraines and the constants for couplings between identical squaraines, which can be determined from the absorption spectra of the monomers, a crude estimation for the constants of the heterotrimers can be achieved. For example *J* of **$(SQA)_2$(SQB)-N** in toluene = 2 x 736 cm^{-1} + 630 cm^{-1} /3 = 701 cm^{-1}. [1]

The squared transition moments of the chromophores can be calculated using eq. (5). Compared to the monomeric reference compounds the trimers and the dimer show roughly additivity of μ^2 and therefore follow the *Thomas-Reiche-Kuhn* sum rule.[123] This means, that no other transitions are involved besides those generated by exciton coupling.

[1] The formulas for the determination of the eigenvalues and eigenvectors of the exciton coupling theory for the trimers can be found in the appendix in Tables S2-4.

Fluorescence Spectroscopy

The fluorescence of the chromophores was investigated in toluene and $CHCl_3$ (Figure 36). While the monomers **SQA-NHAc** and **SQB-NHAc** fluoresce with a substantial quantum yield in both solvents (see Table 6), the values for the superchromophores are significantly smaller in toluene and hardly detectable in $CHCl_3$. This may be understood in terms of the energy gap rule. A smaller energy difference between the HOMO and the LUMO leads to a higher possibility for nonradiative deactivation processes and therefore, the observed quantum yields get smaller.

The monomeric reference compounds show the typical fluorescence behaviour of squaraines (Figure 36f), that is small *Stokes* shifts and mirror images to the absorption bands. In comparison the signals of the homotrimers (Figure 36a and b) represent the shape of monomer fluorescence shifted to smaller wavenumbers. Therefore these compounds follow *Kasha's* rule that fluorescence only occurs with appreciable quantum yield from the lowest excited state.[69] The hetero compounds behave quite differently. If they are excited at the high energy side of the exciton manifold complex fluorescence spectra, which overlap strongly with the absorption, can be observed. In toluene the heterotrimer **$(SQA)_2$(SQB)-N** (Figure 36c) shows two signals with vibronic shoulders, one at 14900 cm^{-1} and a second much weaker one at 12700 cm^{-1}. While the one at lower wavenumber resembles the typical monomer fluorescence shape and *Stokes* shift from the lowest excited state, the second one should have its origin from a higher lying state. In **(SQA)$(SQB)_2$-N** (Figure 36d) there are also two signals at 12600 cm^{-1} and at 13600 cm^{-1} observable. But in this superchromophore the signal at higher energy is less intense. The fluorescence spectrum of the heterodimer **(SQA)(SQB)-NH** (Figure 36e) has two signals as well. One at 13200 cm^{-1} and one at 14500 cm^{-1}, whereby the difference in intensity is less pronounced.

In order to investigate this unusual emission behaviour, excitation spectra of the three heterochromophores were measured at different emission wavenumbers. The spectra measured at the low energy emission peak (solid black lines in Figure 36) look very similar to the absorption. The intensity of the low energy side of the spectra is lower than at the high energy side. This deviation is present at all excitation spectra of squaraines that are measured at emissions below ~13500 cm^{-1} and might be caused by an improper correction of the excitation monochromator in this wavelength region. Nevertheless the excitation spectra at the high energy emission maxima (solid white lines in Figure 36) do not resemble

the absorption spectra in this region. Their shape and position are reminiscent of a monomeric squaraine absorption spectrum.

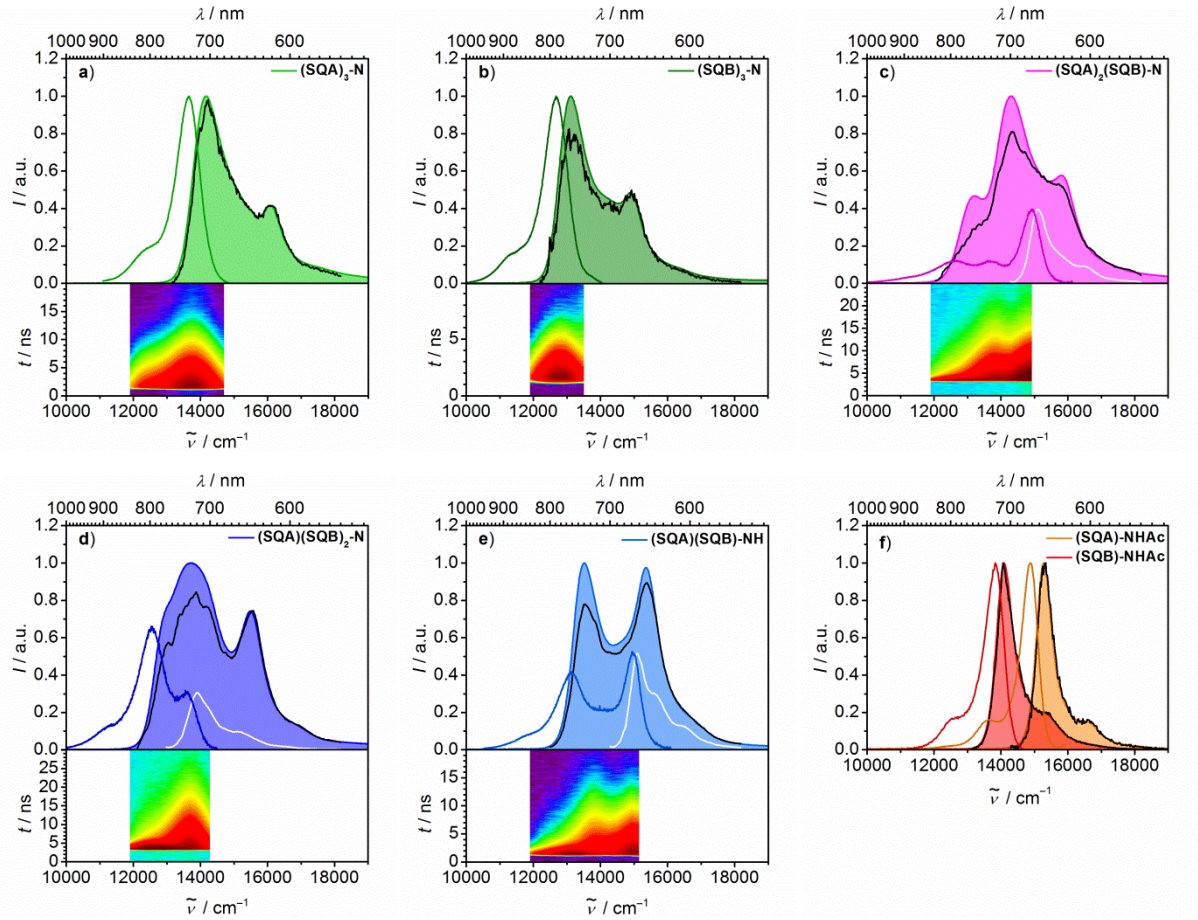

Figure 36 Absorption spectra (shaded areas), fluorescence spectra (coloured solid lines), excitation spectra measured at low energy emission (black solid lines) and at high energy emission (solid white lines) of superchromophore squaraines **(SQA)$_3$-N** (a), **(SQB)$_3$-N** (b), **(SQA)$_2$(SQB)-N** (c), **(SQA)(SQB)$_2$-N** (d), **(SQA)(SQB)-N** (e) and the monomers **(SQA)-NHAc** (f) and **(SQB)-NHAc** (f) in toluene at rt. The fluorescence emission maps reflect intensity and decay dynamics for excitation at 15200 cm^{-1}. The excitation wavenumbers (ex) for the fluorescence spectra and the emission wavenumbers (em) for the excitation spectra were as follows: a) ex: 15200 cm^{-1}; em: 13300 cm^{-1} b) ex: 14300 cm^{-1}; em: 12700 cm^{-1} c) ex: 16700 cm^{-1}; em: 14900 cm^{-1}, 12700 cm^{-1} d) ex: 14900 cm^{-1}; em: 13700 cm^{-1}, 12300 cm^{-1} e) ex: 16700 cm^{-1}; em: 14900 cm^{-1}, 13000 cm^{-1} f) **(SQA)NHAc**: ex: 16100 cm^{-1}; em: 13900 cm^{-1}; **(SQB)NHAc**: ex: 15600 cm^{-1}; em: 12500 cm^{-1}.

Table 5 Absorption maxima, extinction coefficients, transition moments, fluorescence maxima, fluorescence quantum yields and coupling constants of the squaraine compounds **(SQA)-NHAc**, **$(SQA)_3$-N**, **$(SQB)_3$-N**, **$(SQA)_2$(SQB)-N**, **(SQA)$(SQB)_2$-N**, **(SQA)(SQB)-N** and **(SQB)-NHAc** in various solvents at rt.

	solvent	$\tilde{\nu}_{abs}$ / cm^{-1} (nm)	ε / $M^{-1}\,cm^{-1}$	μ^2 / D^2	$\tilde{\nu}_{fl}$ / $cm^{-1\,a}$	ϕ_{fl} ($\tilde{\nu}_{fl}$ / cm^{-1})^b	$\lvert J \rvert$ / cm^{-1}
SQA-NHAc	acetone	15400 (649)	278000	132			
	DMF	15200 (658)	279000	129			
	CH_2Cl_2	15400 (649)	303000	132			
	$CHCl_3$	15400 (649)	307000	133	15200	0.56±0.067 (16100)	
	toluene	15300 (654)	281000	107	15100	0.65±0.035 (16100)	
SQB-NHAc	acetone	14400 (694)	221000	129			
	DMF	14400 (694)	204000	116			
	CH_2Cl_2	14400 (694)	223000	116			
	$CHCl_3$	14300 (699)	222000	115	14100	0.42±0.073 (15600)	
	toluene	14100 (709)	233000	108	13800	0.61±0.030 (15600)	
(SQA)(SQB)-NH	acetone	13700 (730) 15600 (641)	161000 197000	282			808
	DMF	13600 (735) 15400 (649)	141000 183000	262			807
	CH_2Cl_2	13800 (725) 15600 (641)	176000 205000	252			748
	$CHCl_3$	13700 (730) 15600 (641)	180000 203000	248	(14100) 15100	x	775
	toluene	13500 (741) 15400 (649)	205000 200000	239	(13200) 14900	0.12±0.010 (16700)	736
$(SQA)_3$-N	acetone	14400 (694)	326000	397			630
	DMF	14400 (694)	303000	380			600
	CH_2Cl_2	14300 (699)	367000	437			630
	$CHCl_3$	14200 (704)	338000	398	13400	0.01±0.001 (14700)	670
	toluene	14200 (704)	352000	314	13700	0.35±0.009 (15200)	630
$(SQA)_2$(SQB)-N	acetone	14500 (690)	288000	426			749
	DMF	14400 (694)	264000	395			738
	CH_2Cl_2	14300 (699)	263000	385			709
	$CHCl_3$	14300 (699)	273000	393	15100 (14000)	x	740
	toluene	14300 (699)	292000	347	(12700) (13700) 14900	0.04±0.005 (16700)	701
(SQA)$(SQB)_2$-N	acetone	14100 (709)	275000	423			739
	DMF	14100 (709)	257000	397			728
	CH_2Cl_2	13900 (710)	260000	391			709
	$CHCl_3$	13900 (719)	269000	389	13800 (12600)	x	717
	Toluene	13700 (730)	253000	350	12600 (13600)	0.06±0.007 (14900)	691

	solvent	$\tilde{\nu}_{abs}$ / cm^{-1} (nm)	ε / M^{-1} cm^{-1}	μ^2 / D^2	$\tilde{\nu}_{fl}$ / cm^{-1} [a]	ϕ_{fl} ($\tilde{\nu}_{fl}$ / cm^{-1})[b]	$\lvert J \rvert$ / cm^{-1}
	acetone	13500 (740)	300000	421			600
	DMF	13500 (740)	261000	392			570
$(SQB)_3$-N	CH_2Cl_2	13300 (751)	308000	390			630
	$CHCl_3$	13300 (751)	323000	380	12700	0.01±0.001 (14300)	600
	toluene	13100 (763)	380000	347	12700	0.10±0.002 (15200)	600

[a] Less intense maxima in parentheses [b] Fluorescence quantum yield and excitation wavenumber used for measuring the fluorescence spectra in parentheses. The quantum yields that are marked with an x are smaller than 1%.

Time Dependent Measurements

The fluorescence lifetime of all squaraines in toluene was measured by TCSPC (Table 7, page 96). The lifetimes of the monomers are with 2 ns (**SQA-NHAc**) and 3 ns (**SQB-NHAc**) in the same region as their unsubstituted equivalents.[124] In the cisoid homotrimer **$(SQB)_3$-N** the lifetime is with 0.83 ns significantly shorter than in the monomer while the lifetimes of the transoid **$(SQA)_3$-N** are in the same range as the monomer. Due to the complexity of the emission spectra of the heterochromophores fluorescence decay spectra at various wavelengths using TCSPC were measured. The contour spectra are shown in Figure 36 and the decay associated spectra from a global fit are given in Figure 37. In all cases except for **$(SQB)_3$-N** four components were necessary to fit the emission map adequately. The maxima of the shorter lifetimes of the heterochromophores are predominantly at the lower emission wavenumbers, while the maxima of the longer lifetimes are at higher emission wavenumbers. This indicates that the fluorescence stems from at least two different states, where the higher energy state possesses the longer lifetime. Taking a more detailed look, the components at the higher wavenumbers of the fluorescence spectra of **$(SQA)_2$(SQB)-N** (τ = 1.74 ns) and of **(SQA)(SQB)-NH** (τ = 1.90 ns) have similar lifetimes as **SQA-NHAc** (τ = 1.93 ns), the one of **$(SQA)_2$(SQB)-N** (τ = 3.07 ns) and of **(SQA)$(SQB)_2$-N** (τ = 3.20 ns) as **SQB-NHAc** (τ = 2.98 ns). In addition to the spectral similarity to the emission spectra of the monomeric compounds (see Figure 36f) it can most probably be concluded that the emission stems from states/species that are very similar to the pure monomer states.

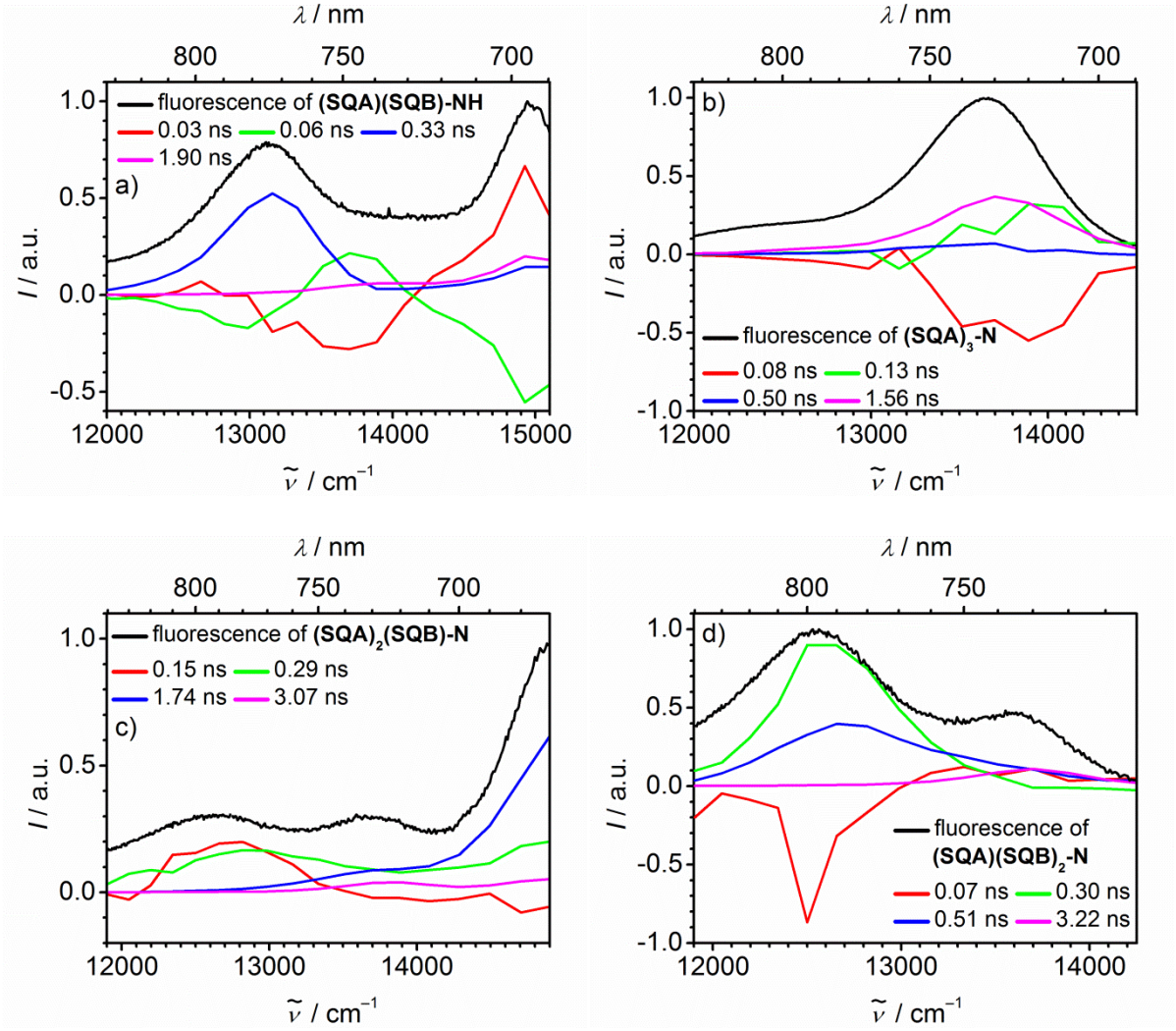

Figure 37 Fluorescence of **(SQA)(SQB)-NH** (a), **$(SQA)_3$-N** (b), **$(SQA)_2(SQB)$-N** (c) and **$(SQA)(SQB)_2$-N** (d) together with decay associated spectra (parallel model) of their lifetimes in toluene.

Cyclic Voltammetry

For all squaraines cyclic voltammetry measurements in CH_2Cl_2 were carried out with $^nBu_4PF_6$, (0.2 M) as supporting electrolyte. The voltammograms are referenced against the ferrocene/ferrocenium redox couple (Fc/Fc^+) (Figure 38). The obtained data are summarised in Table 6.

The monomeric reference compounds **SQA-NHAc** and **SQB-NHAc** show one reduction process and two oxidation processes. This is the typical result of cyclic voltammetry measurements of squaraines. Measurements at different scan rates (10–4000 mV) displayed irreversibility for the reduction and the second oxidation while the first oxidation is

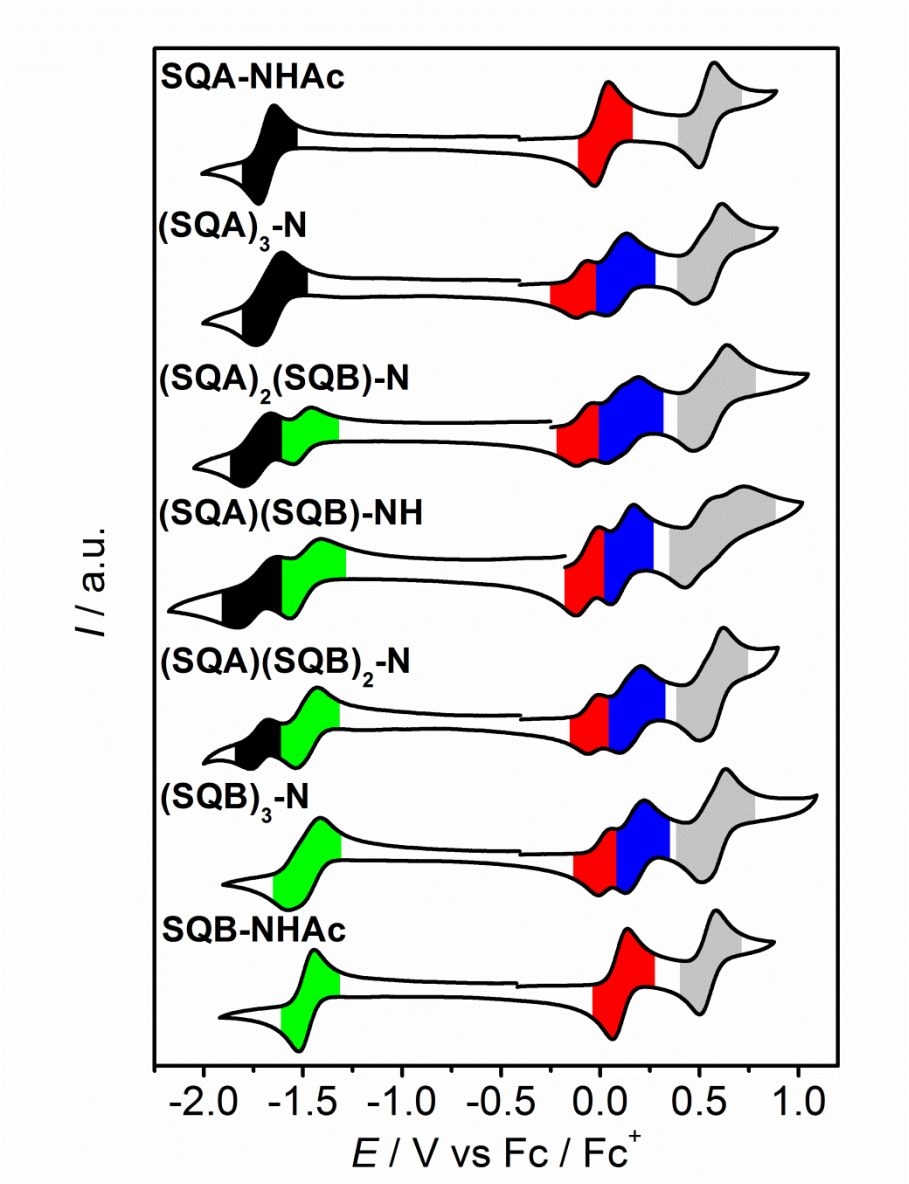

Figure 38 Cyclic voltammograms of **SQA-NHAc**, **$(SQA)_3$-N**, **$(SQA)_2$(SQB)-N**, **(SQA)(SQB)-NH**, **(SQA)$(SQB)_2$-N**, **$(SQB)_3$-N**, and **SQB-NHAc** in $CH_2Cl_2/{}^nBu_4PF_6$ (0.2 M) at a scan rate of 100 mV s^{-1}. All voltammograms are referenced against (Fc/Fc^+), normalised and recorded by first scanning into the oxidative direction. The first reduction of **SQA** is marked with black and the first reduction of **SQB** with green. The first oxidation of the squaraines is marked with red, in case of the star-shaped trimers the first oxidations of the other two branches are marked with blue. The grey area marks the second oxidations of the squaraines.

reversible. The same behaviour was observed in thin layer measurements. Compared to the symmetrical squaraines **SQA** and **SQB** the mono substituted compounds are shifted to lower energies. This effect is with 40 mV (1st oxidation) and 20 mV (reduction and 2nd oxidation) appreciably smaller for **SQA-NHAc** compared to the 110 mV (reduction and 1st oxidation) and 50 mV (2nd oxidation) for **SQB-NHAc**.

The trimerisation to the homotrimers **$(SQA)_3$-N** and **$(SQB)_3$-N** has nearly no effect on the half wave potentials of the reduction. The first oxidation splits into two signals with a ratio of one (red area in Figure 38) to two (blue area in Figure 38) as determined by differential pulse voltammetry. This indicates that the oxidation of the first branch of the trimers has an effect on the other two branches while the oxidation of the second one has no noticeable effect on the third branch. The shift of the first oxidation is more pronounced for the transoid trimer compared to the cisoid. The second oxidation of the individual branches (grey area in Figure 38) splits into two half wave potentials as well. But this time the effect is much smaller and hardly to determine.

The dimer **(SQA)(SQB)-NH** and the heterotrimers **$(SQA)_2$(SQB)-N** and **(SQA)$(SQB)_2$-N** show a combination of the half wave potentials of the reference compounds. They display two well distinguishable reduction processes where the first one (green area in Figure 38) is related to the cisoid squaraine and the second one (black area in Figure 38) to the transoid squaraine. The same correlation can be determined for the oxidation processes. First the transoid branch/branches are oxidised followed by the cisoid branch/braches.

The HOMO and LUMO levels of the squaraines can be calculated from the half wave potentials.[1] While the addition of the protected amine has nearly no influence on the energy levels and the electrochemically determined band gap (see *e.g.* **SQA** and **SQA-NHAc**), the trimerisation leads to a shift of the HOMO by ~0.1 eV (**$(SQA)_3$-N**) and therefore a smaller band gap. In the mixed compounds the band gap gets even smaller, because the HOMO energy level derives from the cisoid and the LUMO energy level from the transoid parent chromophore.

[1] The process is described in chapter 5.1.7.1

Table 6 Redox potentials ($E_{1/2}$), HOMO and LUMO energy levels and band gaps of **SQA-NHAc**, **$(SQA)_3$-N**, **$(SQA)_2(SQB)$-N**, **(SQA)(SQB)-NH**, **$(SQA)(SQB)_2$-N**, **$(SQB)_3$-N**, and **SQB-NHAc** in $CH_2Cl_2/^nBu_4PF_6$ (0.2 M) at a scan rate of 100 mV s^{-1} and referenced against (Fc/Fc^+).

	$E^{red}_{1/2}$ / mV	$E^{red}_{1/2}$ / mV	$E^{ox}_{1/2}$ / mV	$E^{ox}_{1/2}$ / mV	$E^{ox}_{1/2}$ / mV	$E^{ox}_{1/2}$ / mV	E_{HOMO} / eV	E_{LUMO} / eV	E_{gap} / eV
SQA	-1665[i]		50[r]		555[i]		-5.21	-3.50	1.71
SQA-NHAc	-1690[i]		5[r]		540[i]		-5.17	-3.47	1.70
$(SQA)_3$-N	-1670[i]		-90[r]	85[r]	500[i]	590[i]	-5.07	-3.49	1.58
$(SQA)_2(SQB)$-N	-1725[i]	-1500[i]	-85[r]	70/150 [r, fit]	510[i]	590[i]	-5.07	-3.66	1.41
(SQA)(SQB)-NH	-1740[i]	-1490[i]	-70[r]	110[r]	500[i]	650[i]	-5.09	-3.67	1.42
$(SQA)(SQB)_2$-N	-1720[i]	-1475[i]	-40[r]	150[r]	560[i]		-5.12	-3.69	1.43
$(SQB)_3$-N		-1490[i]	20[r]	180[r]	570[i]		-5.18	-3.67	1.51
SQB-NHAc		-1480[i]	100[r]		545[i]		-5.26	-3.68	1.58
SQB		-1370[i]	215[r]		595[i]		-5.38	-3.79	1.59

[i] irreversible, [r] reversible, [fit] fitted with Digi Elch.

Spectroelectrochemistry (SEC)

In order to get some insight into the changes that occur upon electrochemical excitation, spectroelectrochemical measurements were performed in $CH_2Cl_2/^nBu_4PF_6$ (0.2 M). In this setup the negative or positive electrochemical potential of a solution is increased stepwise while the UV/Vis/NIR spectrum after each change is monitored. With this technique, the spectra of the reduced or oxidised species can be measured.

The monomeric compound **SQA-NHAc** shows the typical behaviour of squaraine chromophores and is therefore used as an example for most of the compounds that are discussed in this work. Figure 39 depicts the evolution of the radical anion (a) and the radical cation (b) features when reducing or oxidising. The reduction proved irreversible as the back oxidation process did not fully recover the neutral spectrum. The estimated degradation is 5–10%. The main change upon stepwise reduction of the squaraine is the decrease of the intense absorption peak and its vibronic shoulder by 20-30%. After the first oxidation the neutral spectrum could be fully recovered. Here again the main squaraine feature decreases, but this time two peaks at lower energy (14300 cm^{-1} and 10000 cm^{-1}) gain intensity. At the high energy side one broad band at 35000 cm^{-1} gets smaller while another band at 23800 cm^{-1} gets higher.

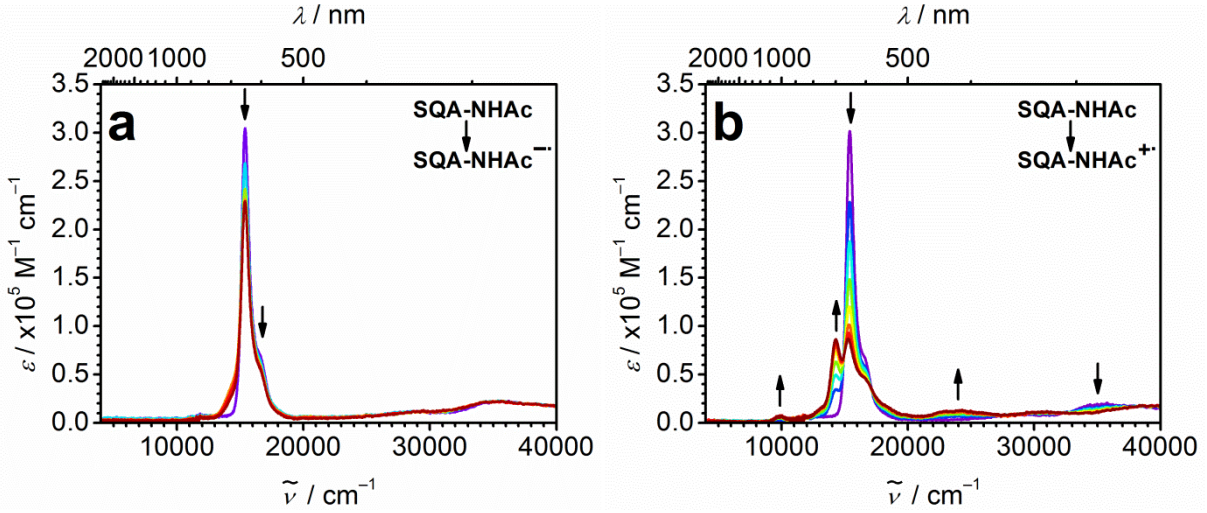

Figure 39 UV/Vis/NIR-Spectroelectrochemistry of the first reduction (a) and the first oxidation process (b) of **SQA-NHAc** in $CH_2Cl_2/^nBu_4PF_6$ (0.2 M). In purple: the spectrum of the neutral chromophore which act as calibration for ε_{abs}. Early spectra are shown in blue and late spectra in red colours.

The homo- and heterotrimers show a slightly different behaviour than **SQA-NHAc**. **$(SQA)_3$-N** and **$(SQA)(SQB)_2$-N** serve as model compounds for star-shaped superchromophores with identical or different branches (Figure 40). The first reduction process shows the same degree of irreversibility as the monomer. The main absorption peaks to the states that derive from the S_1 state via exciton coupling (see Figure 34) show less intensity. But in contrast to the monomers there is a new peak at ~20000 cm^{-1}. In the heterotrimer **$(SQA)(SQB)_2$-N** (Figure 40b) the absorption band at 25000 cm^{-1}, that is associated to the dicyanomethylene moiety, gets smaller as well while a new peak at 28000 cm^{-1} rises.

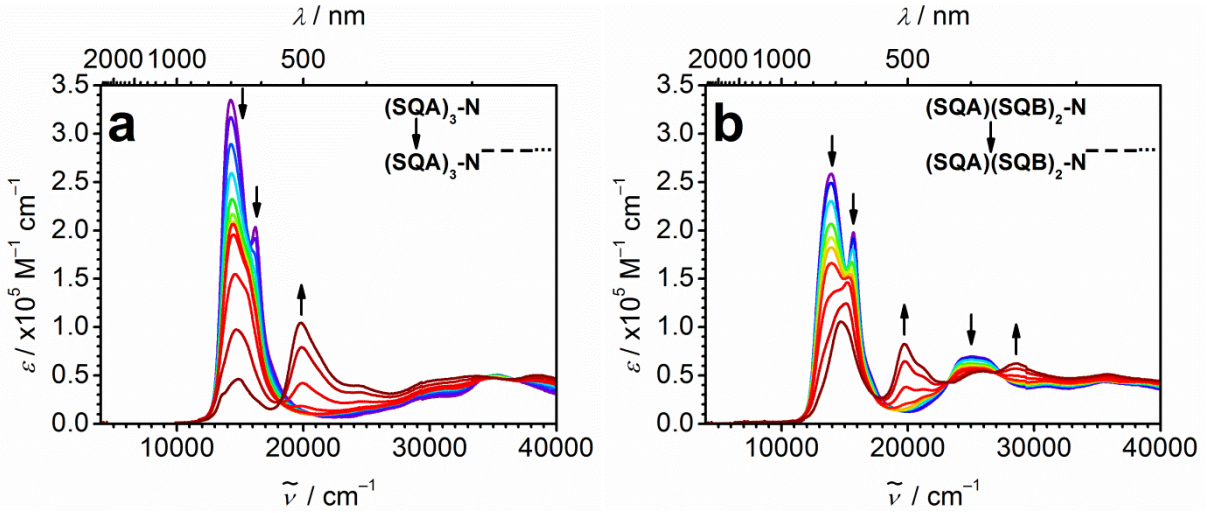

Figure 40 UV/Vis/NIR-Spectroelectrochemistry of the first reduction process of **$(SQA)_3$-N** (a) and **$(SQA)(SQB)_2$-N** (b) in $CH_2Cl_2/^nBu_4PF_6$ (0.2 M). In purple: the spectrum of the neutral chromophore which act as calibration for ε_{abs}. Early spectra are shown in blue and late spectra in red colours.

The first oxidation process can be separated into two consecutive processes like in the cyclovoltammetric experiments. Although the processes overlap and there will be no pure mono cation the spectra for this compound will at least show some trends.

In Figure 41 the oxidation of just one branch of each **(SQA)$_3$-N** molecule (a) and the successive oxidation of the other two branches (b) is presented. While in the first step the main absorption at 14300 cm^{-1} loses intensity the peak at 16000 cm^{-1}, which represents the transition to the S'$_1$, state gets higher. In addition there are new peaks at 10500 cm^{-1} and 12100 cm^{-1} and a broad band in the region below 8000 cm^{-1}. In the following oxidations of the other branches the transitions to the S$_1$ and the S'$_1$ states both decrease, as well as the broad band below 8000 cm^{-1} and the peak at 10500 cm^{-1}. The newly formed peak at 12100 cm^{-1} gains intensity next to a new peak at 13400 cm^{-1}. In the region around 7400 cm^{-1} a further broad peak rises.

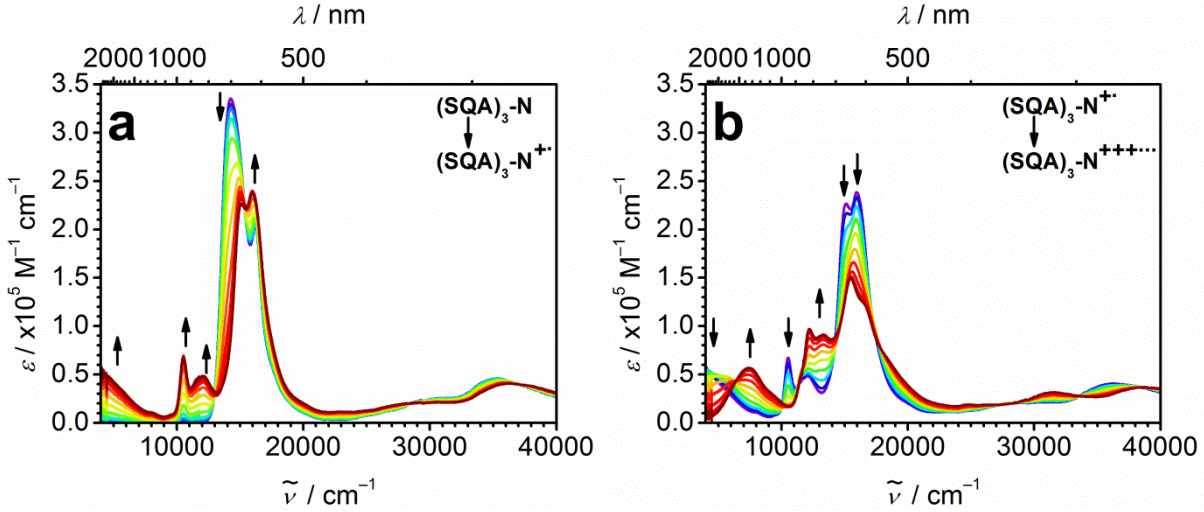

Figure 41 UV/Vis/NIR-Spectroelectrochemistry of the first oxidation process of one branch (a) and the first oxidation processes of the other two branches (b) of **(SQA)$_3$-N** in $CH_2Cl_2/^nBu_4PF_6$ (0.2 M). The purple spectrum of a represents the neutral chromophore and acts as calibration for ε_{abs}. Early spectra are shown in blue and late spectra in red colours.

The oxidation processes of the heterotrimer **(SQA)(SQB)$_2$-N** show very similar behaviour as for the homotrimer **(SQA)$_3$-N**. The main difference is that during the oxidation process of the first branch the transition to the S'$_1$ state does not gain intensity but gets smaller.

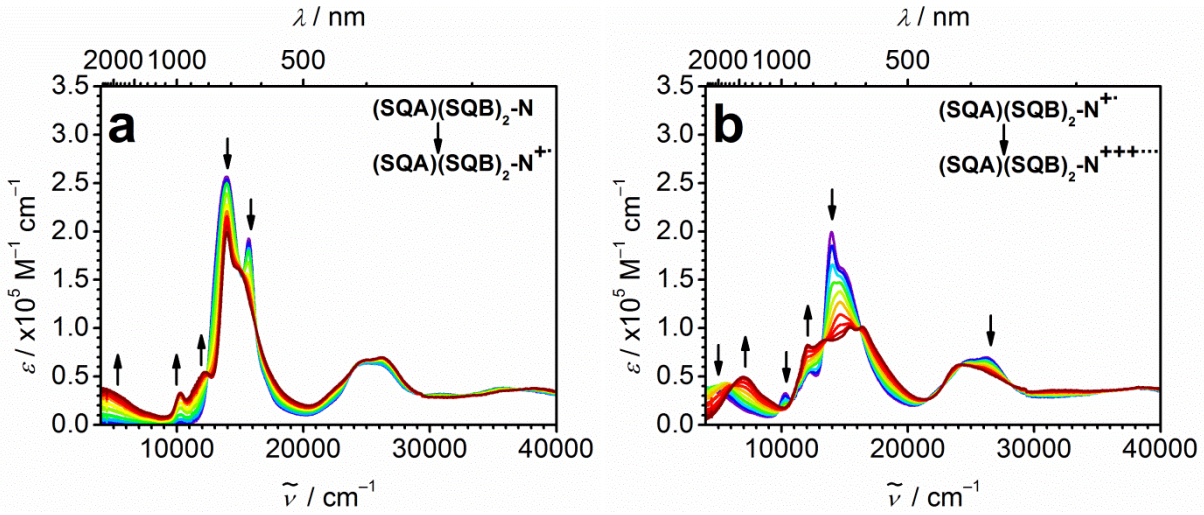

Figure 42 UV/Vis/NIR-Spectroelectrochemistry of the first oxidation process of one branch (a) and the first oxidation processes of the other two branches (b) of **(SQA)(SQB)$_2$-N** in CH_2Cl_2/^{n}Bu$_4$PF$_6$ (0.2 M). The purple spectrum of a represents the neutral chromophore and acts as calibration for ε_{abs}. Early spectra are shown in blue and late spectra in red colours.

Time Resolved Spectroscopy with fs-Time Resolution

The steady state and time resolved fluorescence measurements of the heterochromophores hint that in the toluene solution a second species/state is present that is deactivated by fluorescence at higher energy. For a further investigation of this unusual emission behaviour time resolved pump-probe spectroscopy were performed with fs-time resolution, namely fluorescence upconversion (FLUC) of the homotrimer **(SQA)$_3$-N** and the heterotrimer **(SQA)(SQB)$_2$-N** and transient absorption (TA) spectroscopy of all trimers and the dimer **(SQA)(SQB)-NH**. In the FLUC measurements the relative orientation of the transition-dipole moments and possible energy transfer processes can be observed. In the TA measurements the time-dependent change of the absorption after excitation at a certain wavenumber can be detected. This technique allows the interpretation of the photoinduced dynamics in the superchromophores.

***Fluorescence Upconversion Spectroscopy* (FLUC)**

Due to the small *Stokes* shift of the fluorescence near the gate wavenumber, the FLUC measurements were performed by excitation of the exciton manifold at higher wavenumbers. The time resolution was on the order of ca. 300 fs because of the wavelength dispersion of the solvent and the necessity to use a set of filters to suppress stray light. The measurements were performed exemplarily for the transoid homotrimer **(SQA)$_3$-N** and one heterotrimer **(SQA)(SQB)$_2$-N** at magic angle, parallel and perpendicular orientation of pump and gate pulse (Figure 43). A combined deconvolution fit of the measurements gave, besides the isotropic decay time constants, the fluorescence anisotropy decay *r*(t) and its initial amplitude (Table 7). The latter gives information about relative orientation of transition-dipole moments and, hence, possible energy transfer processes. The isotropic decay is multiexponential in both cases which suggests some structural reorganisation in the excited state. The theoretical values for the anisotropy are 0.4, -0.2, 0.1 and 0 for parallel, perpendicular, 2D and 3D polarisation. The initial anisotropies of the trimers are quite small with 0.03 (**(SQA)$_3$-N**) and 0.06 (**(SQA)(SQB)$_2$-N)** which indicates at least two-dimensional delocalisation of excitation within the time resolution of the measurement (see Fig. S3 in the appendix). The amplitude of the measurements is quite small; therefore, the decay constants are rather imprecise. They are with 1.5 ns (**(SQA)$_3$-N**) and 0.9 ns (**(SQA)(SQB)$_2$-N**) on the order of diffusional rotation expected for the size of these chromophores.[125, 126]

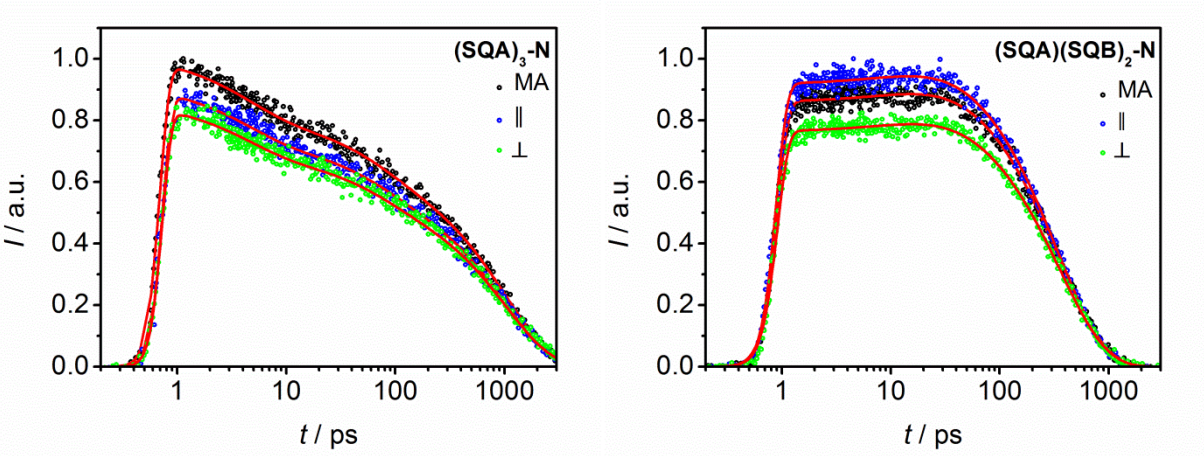

Figure 43 Fluorescence upconversion measurements of **(SQA)$_3$-N** (left, pump at 16100 cm^{-1}, fluorescence at 13600 cm^{-1}) and **(SQA)(SQB)$_2$-N** (right, pump at 14400 cm^{-1}, fluorescence at 11100 cm^{-1}) in toluene with pump pulse at magic angle (MA, black circles), parallel (∥, blue circles) and perpendicular orientation (⊥, green circles) relative to the gate pulse. Global convoluted fit curves (red lines).

Transient Absorption Spectroscopy (TA)

The TA measurements have a better time resolution (instrument response function ca. 140 fs) and were measured at the maximum of the lowest energy absorption and at the maximum of the highest energy absorption of the exciton manifold (see Figure 34 and Figure 44). In the dimer **(SQA)(SQB)-NH** a third measurement was performed at the shoulder of the high energy side of the exciton manifold in order to exclude a coherent artefact. The excited states were probed by white light between 400 – 800 nm and in one case between 500 – 900 nm (Figure 50a-b). The transient maps were analysed with a heuristic target model given in Figure 44 under the assumption that the excited state absorption (ESA) of all species associated difference spectra (SADS) have (almost) equal intensity at ca. 18000 cm^{-1}.[1] This required in most cases that the efficiency for each particular step was adjusted by the values that are given in the respective SADS. The transient absorption spectra, the time scans at selected wavenumbers and the SADS of **$(SQA)_3$-N** (Figure 45), **$(SQB)_3$-N** (Figure 47), **$(SQA)_2(SQB)$-N** (Figure 48), **$(SQA)(SQB)_2$-N** (Figure 50) and **(SQA)(SQB)-NH** (Figure 53) in toluene are shown and discussed in the following. The globally fitted lifetimes are summarised in Table 7.

[1] The shortest component (τ < 1 ps) was not adjusted as this would in most cases require direct ground state recovery which is unlikely at this short time scale.

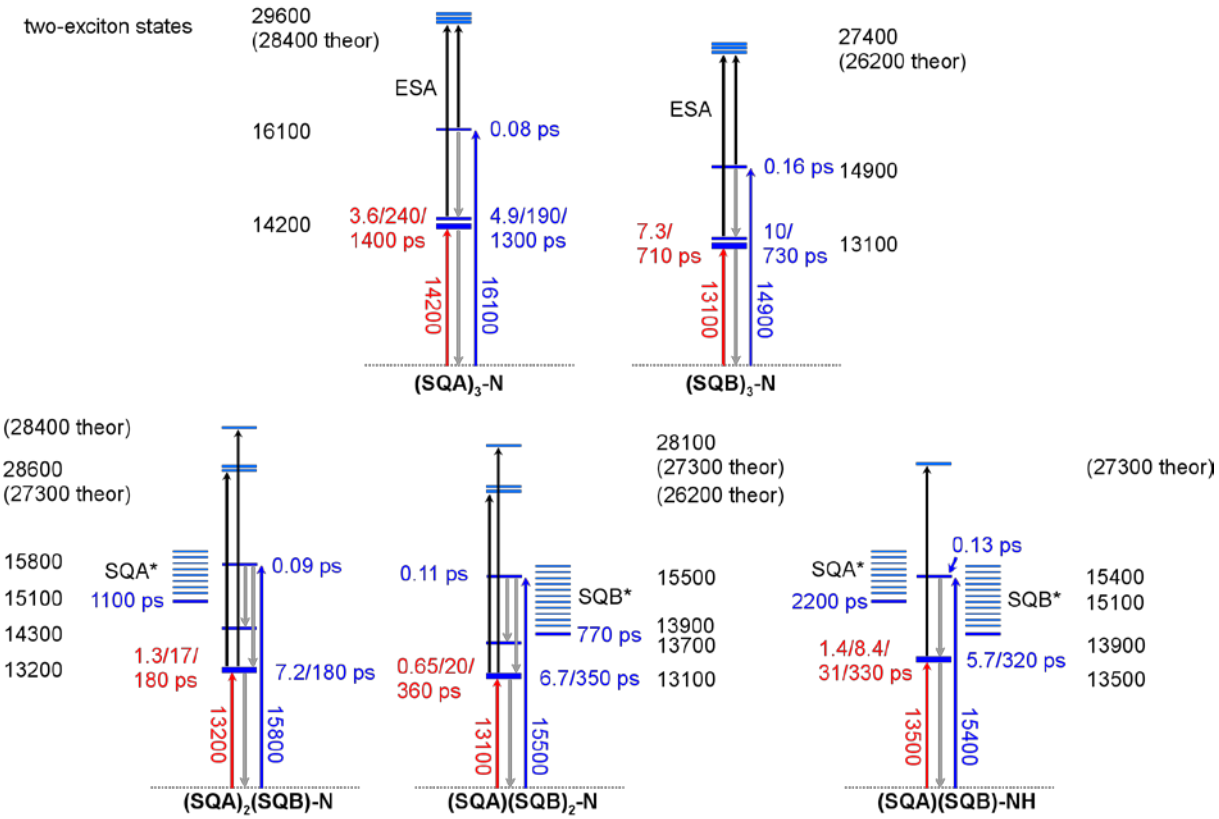

Figure 44 State diagram used for the heuristic target analysis of the transient absorption spectra. Lifetimes in red are for excitation into the maximum of the lowest exciton band, those in blue for excitation into the maximum of the the lowest exciton band at the given wavenumbers. The state energies were estimated by the peak positions of respective absorption bands. The two-exciton states were estimated (= theor) from the respective energies of the mono-exciton states in the homotrimers. The localised excited SQA* and SQB* states are given with their respective vibrational manifold to indicate spectral overlap with excitation at high energy. Lifetimes separated by a slash indicate multiexponential decay process from multiple levels with slightly different energy (given as one bold bar). All the energies are not to scale.

The transient maps of **(SQA)$_3$-N** show upon excitation at 14200 cm^{-1} into the lowest exciton level (Figure 45b) a strong ground state bleaching (GSB) signal at 14200 cm^{-1} merged with an also negative signal at the lower energy flank of the GSB caused by stimulated emission (SE). This GSB/SE signal forms within instrument response time as an initially narrow negative peak at 14200 cm^{-1} which broadens within ca. 100 fs. This process has frequently been assigned to transient hole-burning of the ground state population.[127-133] However there is doubt whether this effect can really be discerned from coherent artefacts when pump and probe pulse overlap in time.[134] Therefore, this effect is not discussed further. The GSB at the highest exciton level at 16100 cm^{-1} is hardly noticeable. This is probably because there is an excited-state absorption (ESA) in the immediate proximity at 15000–16000 cm^{-1}, which is

formed by excitation into two-exciton states (see Figure 44). They are populated by simultaneous excitation of two chromophore branches, a process that is forbidden from the ground state but allowed as consecutive processes in the TA experiment.[92, 135] The state energy can easily be estimated by adding the energies of the two individual excited states of the chromophore branches. In the case of the homotrimers this is simply two times the absorption maximum. In the wavenumber region above 16500 cm^{-1} there are also two additional weak and unstructured excited state absorptions. All signals decay multiexponentially with only little shift/broadening of the principal GSB/SE signal.

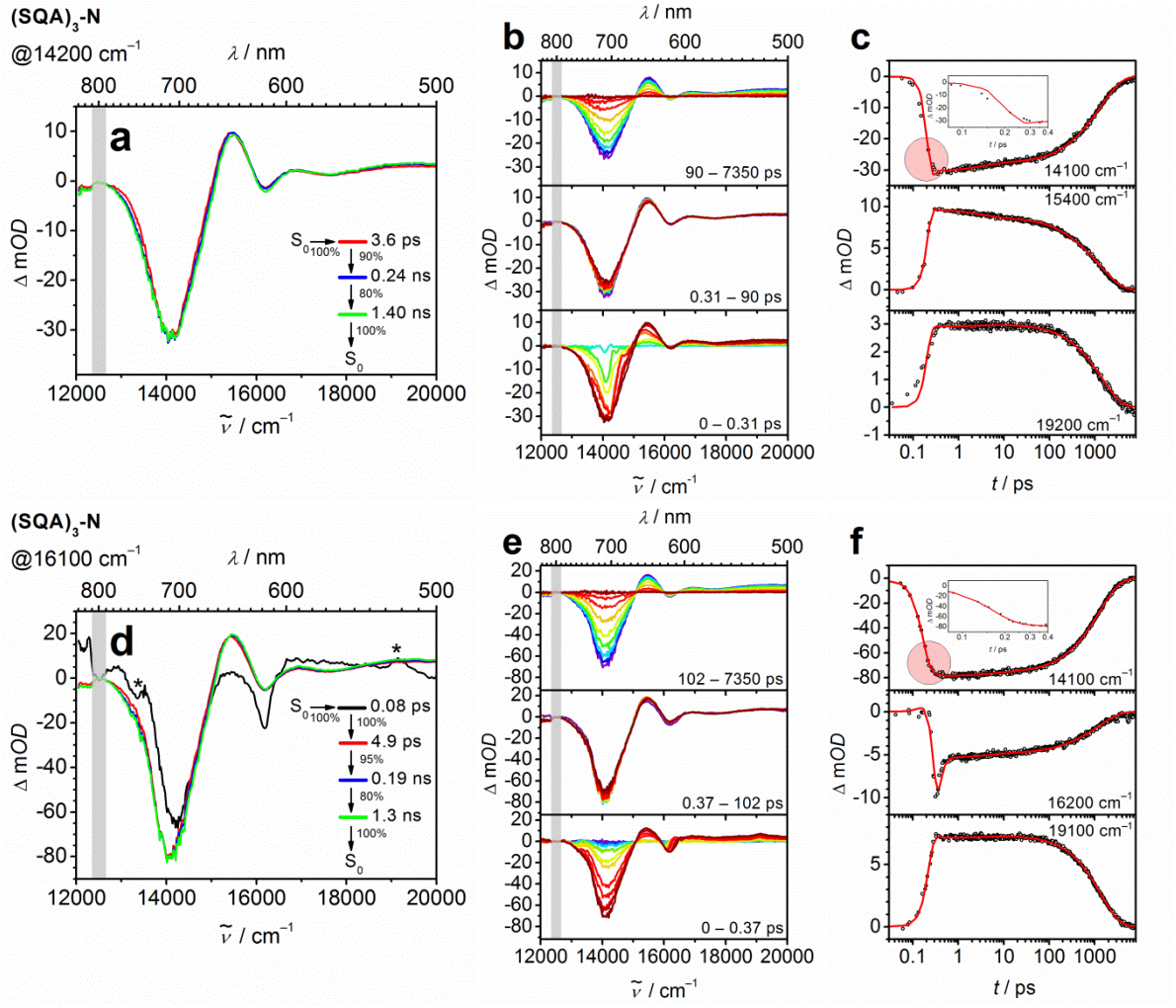

Figure 45 Species associated difference spectra (SADS) of **$(SQA)_3$-N** in toluene for excitation at 14200 cm^{-1} (a) and at 16100 cm^{-1} (d) obtained by a heuristic target model (Figure 44). The percentages at the arrows indicate the efficiency for each step. The deviations from 100% are relaxations to the ground state. The spectra at 12500 cm^{-1} ± 200 cm^{-1} (grey bar) are influenced by the laser fundamental and should be taken with caution. The signals indicated with * are caused by the coherent artefact. The colour code of the SADS refers to the dimension of lifetime. The transient absorption spectra (b, e) and the time scans at selected wavenumbers (c, f) were corrected for chirp and scattered light. Early spectra are given in blue, the later spectra in red.

After excitation into the highest exciton band at 16100 cm^{-1} the TA spectra show altered behaviours. The GSB are more pronounced in comparison to the ESA. Especially the signal at the highest exciton band shows an initially rapid decay within ca. 100 fs (see time profile at 16200 cm^{-1} in Figure 45f). This signal may be caused by diverse processes which are hard to discern given the short timescale. It might be caused by a coherent artefact, since similar behaviours are also visible in the other superchromophores after excitation into the highest exciton band. This consideration can be discarded, because the excitation of **(SQA)(SQB)-NH** at somewhat higher energy (16100 cm^{-1}) than the S'_1 state (15400 cm^{-1}) shows the same signal contribution (Figure 53g-i). The second possible reason for the signal is the preferred population of an exciton state in a mixture of conformers with slightly varying absorption spectra. This can also be discarded because the stiff dimer **pySQB** (Figure 46) that cannot possess different conformers shows the same behaviour.[136]

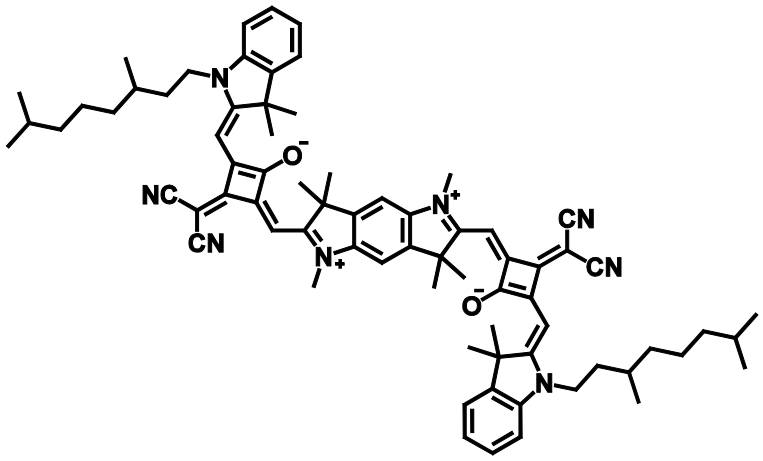

Figure 46 Stiff squaraine dimer pySQB.

Another cause of the signal might be SE from a higher exciton level in addition to the GSB. Here the SE signal from the higher exciton level would decrease as the population of the S'_1 state is transferred to the S_1 state, while the GSB signal would remain nearly unchanged as the GSB only depends on the depopulation of the ground state and not which excited state is populated. With the rising population of the S_1 state the SE from this state should increase. Exactly this behaviour can be observed in the comparison of the time scans at 14100 cm^{-1} for the two excitation energies in Figure 45c and f (red circles and inlets). In the case of the excitation to the higher exciton band the increase of the SE from the S_1 state is visible as a smooth curvature at around $t = 0.3$ ps. In addition the population of the S_1 state at the expense of the S'_1 state (= interband relaxation) leads to an increase of the energy of the ESA to the two-exciton states.

The global fit, with the heuristic target model, of **(SQA)$_3$-N** for the excitation at 14200 cm^{-1} resulted in three SADS (Figure 45a). The short lifetime (3.6 ps) is presumably associated with fast vibrational relaxation or intramolecular vibrational energy redistribution[137-139], while the longest lifetime (1.4 ns) is caused by ground state recovery. The intermediate lifetime (0.24 ns) is frequently observed in the relaxation of squaraine dyes[122, 125] and is probably related to a slow structural reorganisation. The longer lifetimes are similar to the ones that were acquired by global deconvolution of the TCSPC measurements (0.13/0.50 and 1.56 ns).

The TA experiment for the excitation at 16100 cm^{-1} gave four SADS (Figure 45d). In addition to three SADS that are very similar in structure and lifetimes to the ones already observed in the experiment with the lower pump energy there is a component with a very short lifetime (0.08 ps). Here an intense GSB at 16100 cm^{-1}, a reduced SE at 13300–14300 cm^{-1} and a reduced ESA at 15100–15900 cm^{-1} are observed in comparison to the species with longer lifetimes. This short lived species would support the above mentioned interpretation as an intraband relaxation process.

The TA spectra of the cisoid homotrimer **(SQB)$_3$-N** are similar to the one of the transoid homotrimer. The GSB and SE signals are red-shifted by ~1100 cm^{-1} while the ESA is shifted by the two fold value (see Figure 44). In this case the excitation at the higher exciton band at 14900 cm^{-1} shows less pronounced intraband relaxation features at 15000 cm^{-1} (Figure 47f). The global fit resulted in two (low excitation energy) and three (high excitation energy) SADS for the two different pump energies. The lifetime that is associated to the ground state recovery (0.71 ns) is shorter than in **(SQA)$_3$-N** (1.30 ns) but similar to the one that was acquired by global deconvolution of the TCSPC measurements (0.83 ns). This shorter lifetime might be a result of the smaller energy gap. Since the intraband relaxation is small in **(SQB)$_3$-N** (0.16 ps) the additional SADS for the excitation at the highest exciton level (15000 cm^{-1}) (Figure 47d) shows only slight differences to the other SADS.

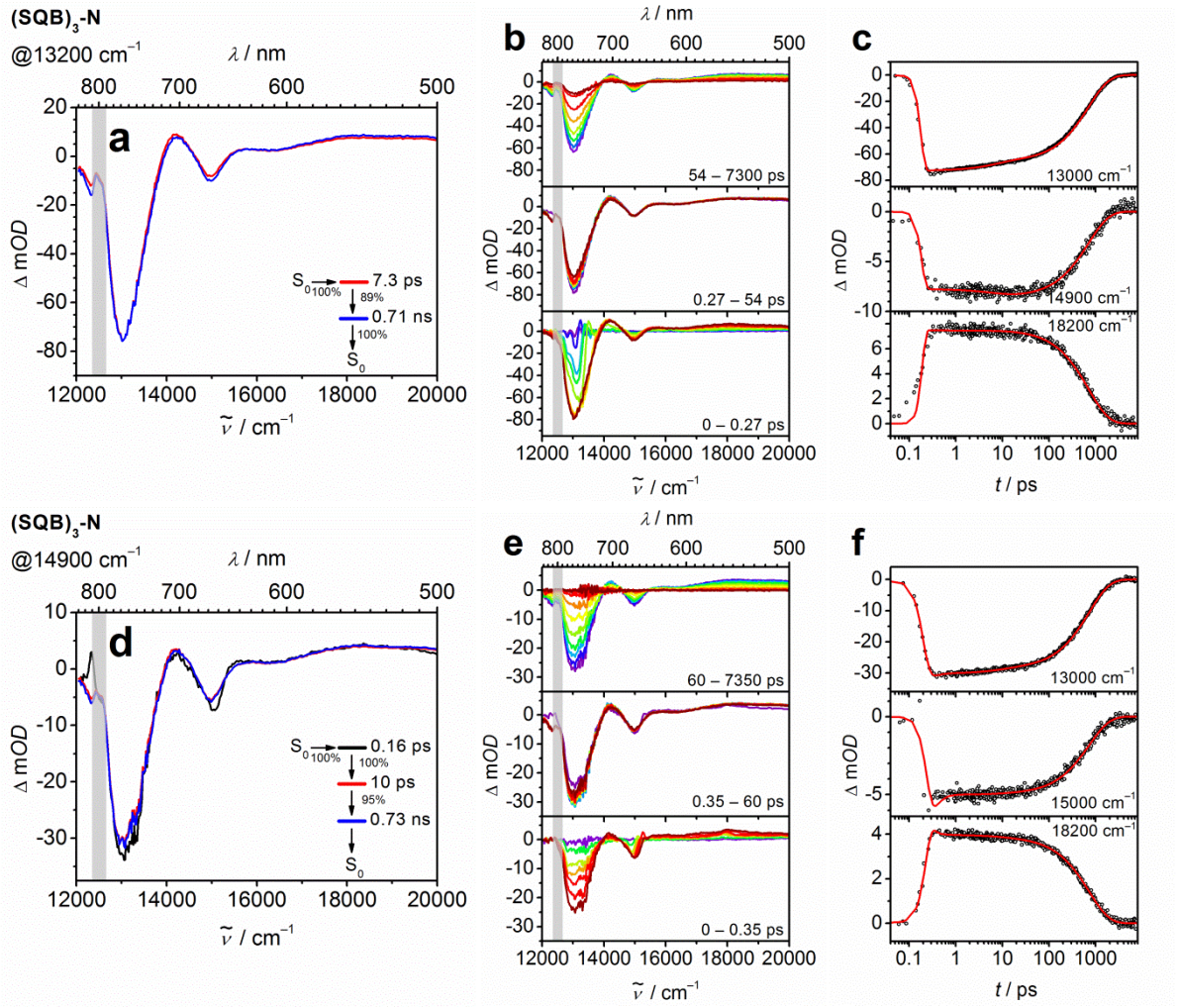

Figure 47 Species associated difference spectra (SADS) of **$(SQB)_3$-N** in toluene for excitation at 13200 cm^{-1} (a) and at 14900 cm^{-1} (d) obtained by a heuristic target model (Figure 44). The percentages at the arrows indicate the efficiency for each step. The deviations from 100% are relaxations to the ground state. The spectra at 12500 cm^{-1} ± 200 cm^{-1} (grey bar) are influenced by the laser fundamental and should be taken with caution. The colour code of the SADS refers to the dimension of lifetime. The transient absorption spectra (b, e) and the time scans at selected wavenumbers (c, f) were corrected for chirp and scattered light. Early spectra are given in blue, the later spectra in red.

After excitation into the lowest exciton band at 13200 cm^{-1} the heterotrimer **$(SQA)_2(SQB)$-N** displays two intense negative signals at 13000 cm^{-1} and 14200 cm^{-1} representing the GSB of the two absorption peaks of the lower energies and their SE (Figure 48a-c). The third absorption peak at 16100 cm^{-1} is hardly to discern because the GSB/SE is overlaid by the ESA at 15300 cm^{-1}. Since the second photon can promote the molecule in a like (two SQA branches) and an unlike (one SQA and one SQB branch) fashion the ESA is quite broad and leads to the difference of the intensities of the negative signals. During the measurement

the value of the signal at 13000 cm^{-1} shrinks while the peak at 15300 cm^{-1} remains at the same intensity until the molecule relaxes to the ground state (Figure 48b). This means that the SE and/or the ESA vary because the GSB remains the same independently which excited state is populated. That behaviour is easily explained by slight conformational changes between the three chromophore branches. This leads to a variation of the exciton coupling strength which in turn influences the oscillator strengths. The global fit gives three SADS (Figure 48a). The first two with 1.3 ps and 17 ps are related to structural relaxation and the third with 0.18 ns to the ground state recovery.

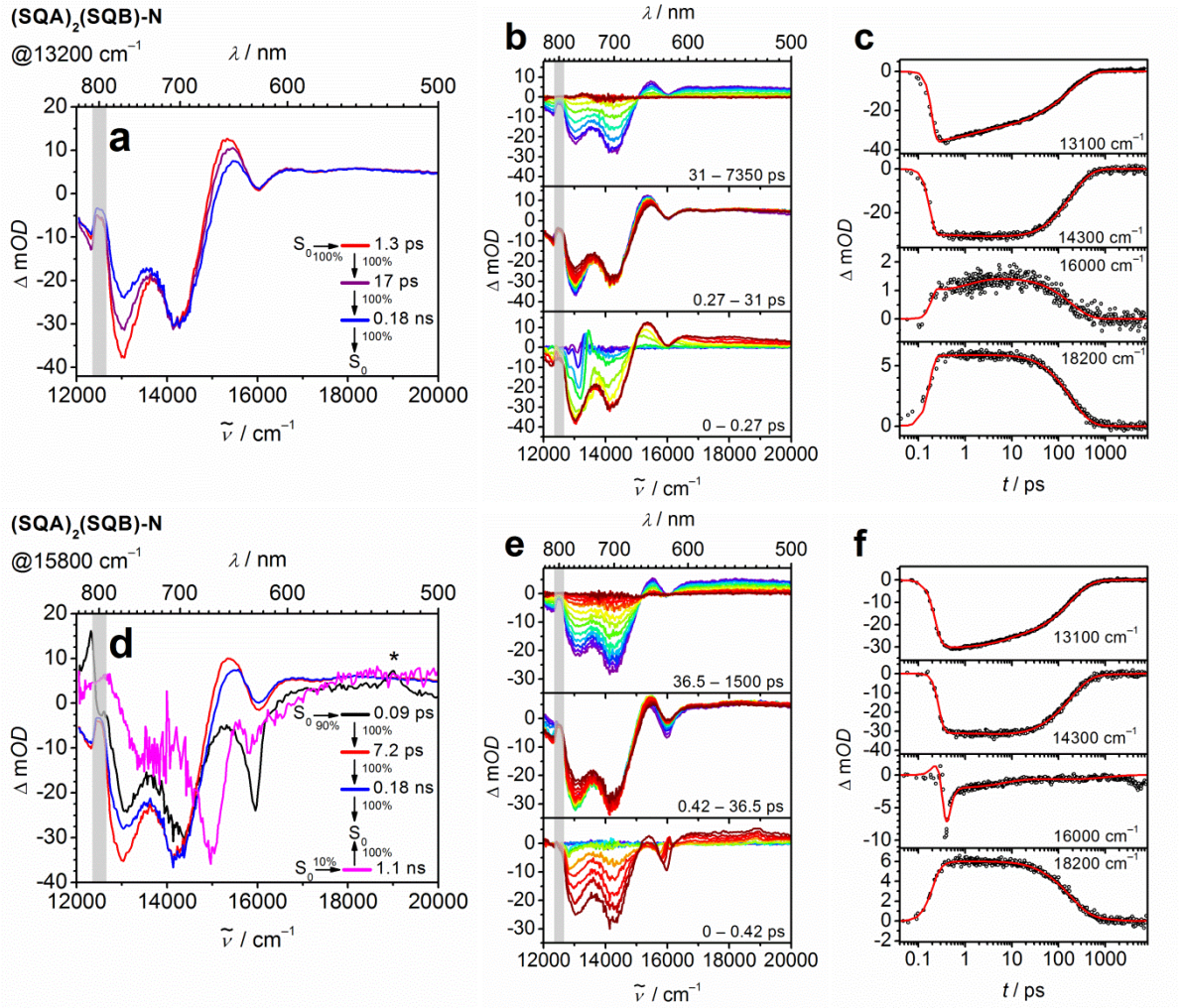

Figure 48 Species associated difference spectra (SADS) of **$(SQA)_2$(SQB)-N** in toluene for excitation at 13200 cm^{-1} (a) and at 15800 cm^{-1} (d) obtained by a heuristic target model (Figure 44). The percentages at the arrows indicate the efficiency for each step. The deviations from 100% are relaxations to the ground state. The spectra at 12500 cm^{-1} ± 200 cm^{-1} (grey bar) are influenced by the laser fundamental and should be taken with caution. The signal indicated with * is caused by the coherent artefact. The colour code of the SADS refers to the dimension of lifetime with exception of the pink SADS which corresponds to localised states. The transient absorption spectra (b, e) and the time scans at selected wavenumbers (c, f) were corrected for chirp and scattered light. Early spectra are given in blue, the later spectra in red.

The global fit of the TA spectra after excitation into the highest exciton band at 15800 cm^{-1} results in four SADS. (Figure 48d) The one with the shortest lifetime (0.09 ps) shows, like the homotrimers, a strong negative signal near the pump energy, resembling the GSB/SE of this state. Alongside with the vanishing of this signal due to interband relaxation the other two negative peaks at 14200 cm^{-1} and 13000 cm^{-1} gain intensity due to higher SE from these states. Then the band at 13000 cm^{-1} loses intensity while the intermediate peak at 14200 cm^{-1} remains unchanged (Figure 48e and f). Additional to the two processes with similar lifetimes (7.2 ps and 0.18 ns), as in the experiment with less pump energy (17 ps and 0.18 ns), there is another SADS with a quite long lifetime of 1.1 ns and a low amplitude. This spectrum shows no resemblance whatsoever with the other three. As reasoned earlier the steady state and time-resolved emission spectra strongly suggest that monomer-like states are populated upon excitation into the high energy exciton manifold. This is possible because the vibronic progression of these states extends to the excitation energy (Figure 44). The comparison of the long lived SADS with the combined normalised absorption and emission spectra of **SQA-NHAc** (Figure 49) shows great similarities supporting the population of a localised state in this case. Therefore this state was included in the target fit as a species that is excited in parallel with an initial population of 10% in order to yield a SADS with comparable intensity as the other SADS.

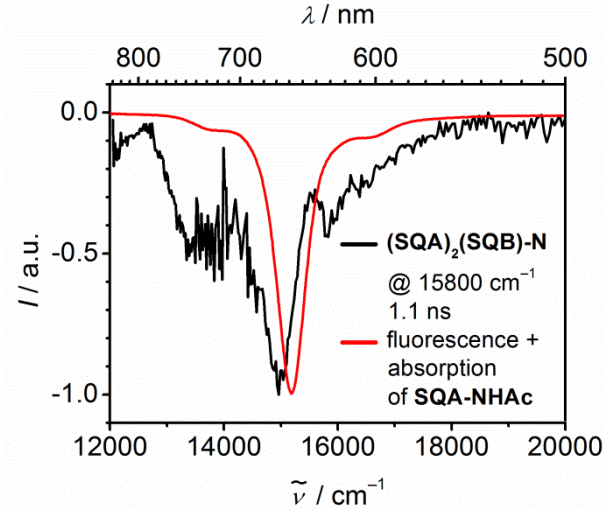

Figure 49 Normalised species associated difference spectrum of the localised state of **$(SQA)_2$(SQB)-N** (black) and negative sum of the normalised fluorescence and absorption spectra of **SQA-NHAc** (red) in toluene.

The TA spectra of **(SQA)$(SQB)_2$-N** after excitation at 13100 cm^{-1} show one broad negative signal at 13000 cm^{-1} that represents the GSB of the two main absorption peaks and the SE

from the lowest exciton state (Figure 50a). In addition there is an ESA at 15100 cm^{-1}. Similar as in the other heterotrimer there are two exciton states in this spectral region that can be populated by the second photon. Therefore the third GSB/SE at 15500 cm^{-1} is compensated by the ESA and is hardly noticeable (Figure 50b). The global fit of the data results in three SADS. Here the first two with τ = 0.65 ps and 20 ps are related to vibrational relaxations and the third with 0.36 ns to the ground state recovery.

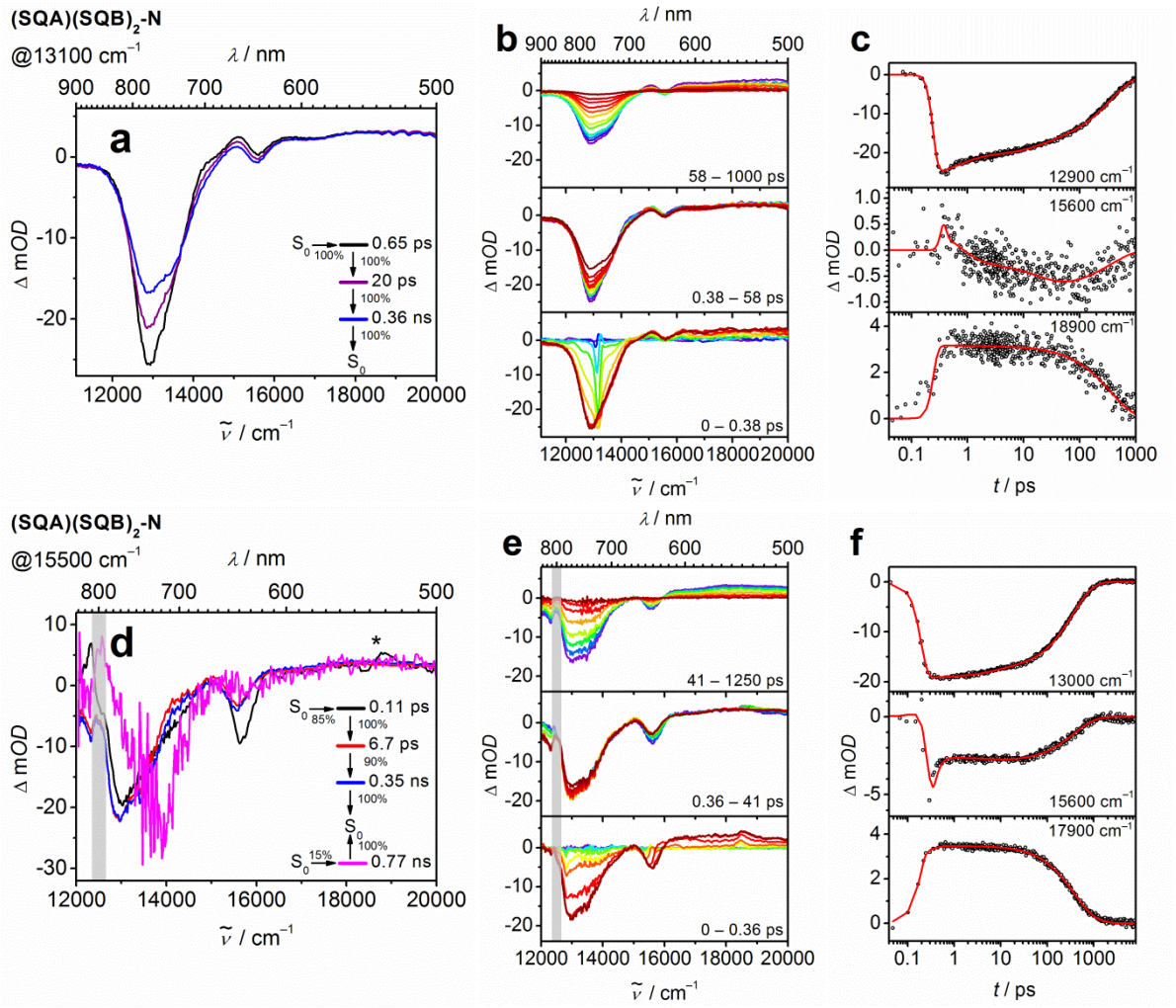

Figure 50 Species associated difference spectra (SADS) of **(SQA)(SQB)$_2$-N** in toluene for excitation at 13100 cm^{-1} (a) and at 15500 cm^{-1} (d) obtained by a heuristic target model (Figure 44). The percentages at the arrows indicate the efficiency for each step. The deviations from 100% are relaxations to the ground state. The spectra at 12500 cm^{-1} ± 200 cm^{-1} (grey bar) are influenced by the laser fundamental and should be taken with caution. The signal indicated with * is caused by the coherent artefact. The colour code of the SADS refers to the dimension of lifetime with exception of the pink SADS which corresponds to localised states. The transient absorption spectra (b, e) and the time scans at selected wavenumbers (c, f) were corrected for chirp and scattered light. Early spectra are given in blue, the later spectra in red.

After excitation at 15500 cm^{-1} there is a pronounced negative peak at 15600 cm^{-1} that subsequently shows intraband relaxation (Figure 50e and f). This is represented by the first SADS with a lifetime of 0.11 ps. In addition to the two SADS with τ = 6.7 ps and 0.35 ns the fit yields a SADS with a lifetime of 0.77 ns (Figure 50d). This spectrum is quite weak and has a bad signal to noise ratio therefore the lifetime has to be taken with caution. In the presented SADS a parallel population of the localised state with 15% intensity was assumed in order to get the same intensity of the ESA at 18000 cm^{-1} as the other SADS. The position of the main peak and the overall structure is very similar to the negative sum of the normalised absorption and emission spectra of **SQB-NHAc** (Figure 51). Hence this SADS is assigned to a localised state although one would expect its lifetime to be in the region of a few ns.

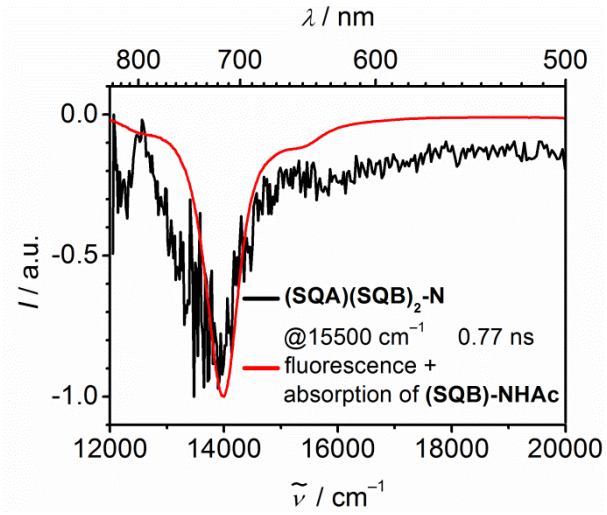

Figure 51 Normalised species associated difference spectrum of the localised state of **(SQA)(SQB)$_2$-N** (black) and negative sum of the normalised fluorescence and absorption spectra of **SQB-NHAc** (red) in toluene.

Upon excitation at 13500 cm^{-1} the heterodimer **(SQA)(SQB)-NH** shows a pronounced GSB/SE at 13400 cm^{-1}. The second GSB/SE at 15400 cm^{-1} is extenuated by the ESA in this region (Figure 53b and c). The global fit gives four SADS that mainly differ in the region around 15000 cm^{-1} (Figure 53a). The first three with lifetimes of 1.4 ps, 8.4 ps and 31 ps are associated with vibrational relaxations while the fourth one (0.33 ns) has the same magnitude of lifetime that was already assigned to the ground state recovery in the heterotrimers.

The spectra of the excitation at 15400 cm^{-1}, the maximum of the second absorption peak, show a larger negative signal at 15500 cm^{-1} that is related to the population of the S'_1 state and a subsequent intraband relaxation (Figure 53e and f). This is also visible in the first SADS with a lifetime of 0.13 ps. The second and third SADS are very similar to the ones acquired for the excitation into the low energy maximum while the fourth one has an unusually long lifetime with 2.2 ns and two negative maxima at 13800 and 14900 cm^{-1}. The position of these peaks is quite similar to the absorption and emission of the monomers **SQA-NHAc** and **SQB-NHAc** (Figure 52). Due to the low signal to noise ratio only one lifetime was observed for the in principle two separate localised states.

The TA experiment upon excitation at 16100 cm^{-1}, which is at the high energy side of the second absorption maximum (Figure 53g, h and i), basically gave the same results as the experiment at 15400 cm^{-1}. However, due to the low intensity of the absorption the long lived state could not be observed, while a stray light component had to be used to get the SADS fits. This measurement was done to exclude a coherent artefact for the time traces of the GSB/SE spectra for the excitation into the maximum of the highest exciton state.

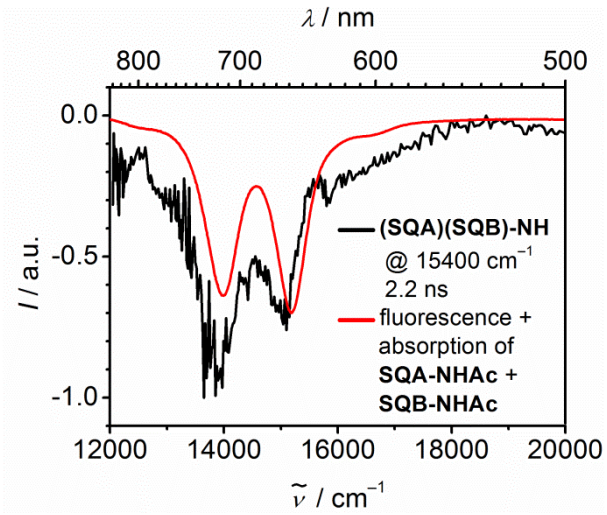

Figure 52 Normalised species associated difference spectrum of the localised state of **(SQA)(SQB)-NH** (black) and negative sum of the normalised fluorescence and absorption spectra of **SQA-NHAc** and **SQB-NHAc** (red) in toluene.

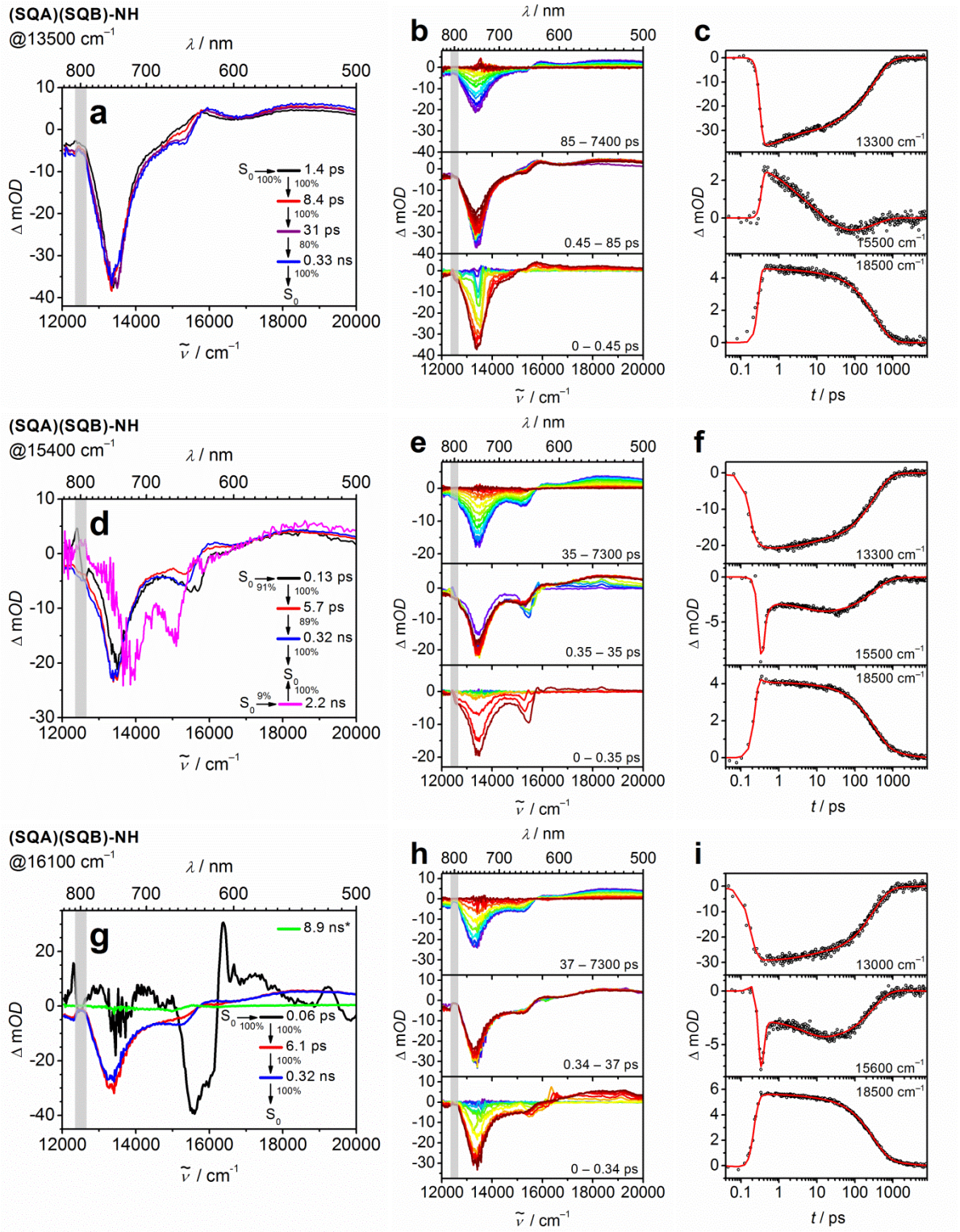

Figure 53 Species associated difference spectra (SADS) of **(SQA)(SQB)-NH** in toluene for excitation at 13500 cm^{-1} (a), at 15400 cm^{-1} (d) and at 16100 cm^{-1} (g, the component with the asterisk (*) green spectrum is caused by stray light) obtained by a heuristic target model (Figure 44). The percentages at the arrows indicate the efficiency for each step. The deviations from 100% are relaxations to the ground state. The spectra at 12500 cm^{-1} ± 200 cm^{-1} (grey bar) are influenced by the laser fundamental and should be taken with caution. The colour code of the SADS refers to the dimension of lifetime with exception of the pink SADS which corresponds to localised states. The transient absorption spectra (b, e, h) and the time scans at selected wavenumbers (c, f, i) were corrected for chirp and scattered light. Early spectra are given in blue, the later spectra in red.

Table 7 Time resolved optical data of the nitrogen substituted squaraine chromophores in toluene at rt.

	τ_f / ns (TCSPC)[a]	τ_i / ps (a_i) (FLUC)[b]	τ_a / ps ($r(t = 0)$) anisotropy (FLUC)[c]	τ / ps (TA)[d] excit. lowest exciton	τ / ps (TA)[d] excit. highest exciton
SQA-NHAc	0.40 (0.04) 1.93 (0.96)				
SQB-NHAc	2.98				
(SQA)(SQB)-NH	0.03 0.06 0.33 1.90			1.4 8.4 31 330 [13500]	0.13 5.7 320 2200 [15400]
$(SQA)_3$-N	0.08 0.13 0.50 1.56	4.2 (0.18) 67 (0.18) 1020 (0.64) [16100/13600]	1530 (0.03) [16100/13600]	3.6 240 1400 [14200]	0.08 4.9 190 1300 [16100]
$(SQA)_2$(SQB)-N	0.15 0.29 1.74 3.07			1.3 17 180 [13200]	0.09 7.2 180 1100 [15800]
(SQA)$(SQB)_2$-N	0.07 0.30 0.51 3.22	16 (-0.10) 350 (0.90) [14400/11100]	880 (0.06) [14400/11100]	0.65 20 360 [13100]	0.11 6.7 350 770 [15500]
$(SQB)_3$-N	0.83			7.3 710 [13100]	0.16 10 730 [14900]

[a] Global deconvolution of fluorescence spectra measured by TCSPC, excitation at 15200 cm^{-1}. The amplitude spectra are shown in Figure 37. For the monomers fluorescence was measured at the maximum only, amplitudes are given in brackets. [b] Isotropic fluorescence lifetime constants (amplitudes) measured by upconversion at the given [pump/fluorescence] wavenumbers. [c] Anisotropy lifetimes (initial amplitudes at $t = 0$) [pump/fluorescence] measured by FLUC. [d] Globally fitted lifetimes of SADS measured by TA [pump wavenumber].

To sum up, the TA experiments upon excitation of the highest exciton state of the hetero superchromophores show to a fractional amount the parallel population of localised SQA* and SQB* states.[1] This population is possible because the vibrational manifold of the S_1 states leads to a significant absorption at the excitation energy (see Figure 44). The existence of such localised SQA* and SQB* states requires an electronical decoupling from the rest of the molecule which in turn can be excited separately. The localised states are observed exclusively in the heterochromophores as SQA* in **(SQA)$_2$(SQB)-N**, as SQB* in **(SQA)(SQB)$_2$-N** and as both SQA* and SQB* in **(SQA)(SQB)-NH**. In theory the population of the SQB* in **(SQA)(SQB)$_2$-N** leaves a fragment containing SQA and SQB in their ground states. These two chromophore branches can then be either excited independently or together, depending on whether they are electronically decoupled or excitonically coupled. In the first case one would expect to see a localised SQA* state as well. The associated signal would be quite small because according to the global fits the decoupling only takes place in 15% of the superchromophore as this is the ratio of (SQA)(SQB)(SQB*)-N upon excitation. However there is no according signal visible in the spectral region around 15200 cm^{-1}. In the case of a coupled SQA/SQB one would expect to see spectral components that are similar to the dimer **(SQA)(SQB)-NH**. Because of the high similarity to the signals of the trimer and their supposed weak intensity, such signals are difficult to detect and were not observed in the measurements. Nevertheless, the analysis of the heterodimer **(SQA)(SQB)-NH** spectra show both localised SQA* and SQB* states. Here once one chromophore is decoupled the other one inevitably has to be decoupled as well and as a result they can be excited separately.

The description of the electronic situation for the homotrimer might bring some light in the questions why the decoupling takes place at all and why it is only observed in the heterochromophores. According to the exciton coupling theory the wavefunctions of the two exciton states in **(SQA)(SQB)-NH** are given by a linear combination of

$$\Psi_+ = \sqrt{\left(\frac{1+s}{2}\right)}\psi_1 + \sqrt{\left(\frac{1-s}{2}\right)}\psi_1 \text{ and } \Psi_- = \sqrt{\left(\frac{1-s}{2}\right)}\psi_1 - \sqrt{\left(\frac{1+s}{2}\right)}\psi_1$$

with $s = 2\Delta E \Big/ \sqrt{4\Delta E^2 + 4J^2}$. If the value of ΔE gets much larger than *J*, the probability of finding the excitation on one chromophore branch $\left(\frac{1+s}{2}\right)$ or the other $\left(\frac{1-s}{2}\right)$ approaches

[1] In this discussion SQA and SQB are used as parts of the superchromophores not as the monomeric squaraines.

either unity or zero. This means that the excitation becomes localised on one branch all the more with increasing energy difference between the branches. Due to small perturbations such as solvent fluctuations or thermal motions the excitation of one branch can be favoured above the other.[140] This is not possible in the homotrimers, because there is no energy difference between the single branches and therefore the probability for the excitation is equal in all of them. Furthermore, the influence of the perturbations under the given conditions is not strong enough to induce a localisation of the excitation.

Of course there is in addition to this explanation the possibility of conformational changes. In comparison to the idealised orientation of the branches and their transition moments (see Figure 54) in solution the chromophores will adopt a propeller-like geometry due to the central triarylamine core.[98] This may result in a few conformers with vanishing electronic exciton coupling. However, if this is the case one would expect that the homotrimers show similar behaviour as the heterochromophores. Given that this is not what we observe, this possibility is highly unlikely.

Nevertheless, the quite high lifetime of the localised SQA* and SQB* states are astonishing. The distance between the localised state (energy donor) and the rest of the molecule (energy acceptor) and the spectral overlap of the moieties fulfil the conditions for a *Förster* dipole-dipole energy transfer, thus resulting in a fast energy transfer into lower lying states. An explanation for the high lifetime might be disadvantageous orientations of the dipole moments. Indeed, one finds perpendicular orientations of one SQA and one SQB branch in the idealised structures of the heterochromophores and their estimated localised transition-dipole moments in Figure 54. This may reduce the dipole-dipole coupling considerably. Given that *Langhals* and *Riedle*[141] showed recently that vibronic coupling can induce very fast energy transfer, even in cases of perfect perpendicular orientation of chromophores, the impact of the orientations of the transition-dipole moments on the lifetimes is questionable.

The SADS with the lifetimes of about 0.1 ps that were observed for all superchromophores upon excitation at the high energy side of the exciton manifold are interpreted as an almost selective population of a higher exciton level. The lifetimes are close to the resolution of the setup and have therefore to be seen more like an upper bound of the real lifetimes. The

subsequent intraband relaxation was although observed in coherent optical 2D experiments with squaraine polymers.[142] Here, the intraband relaxations were in the order of a few 10 fs.

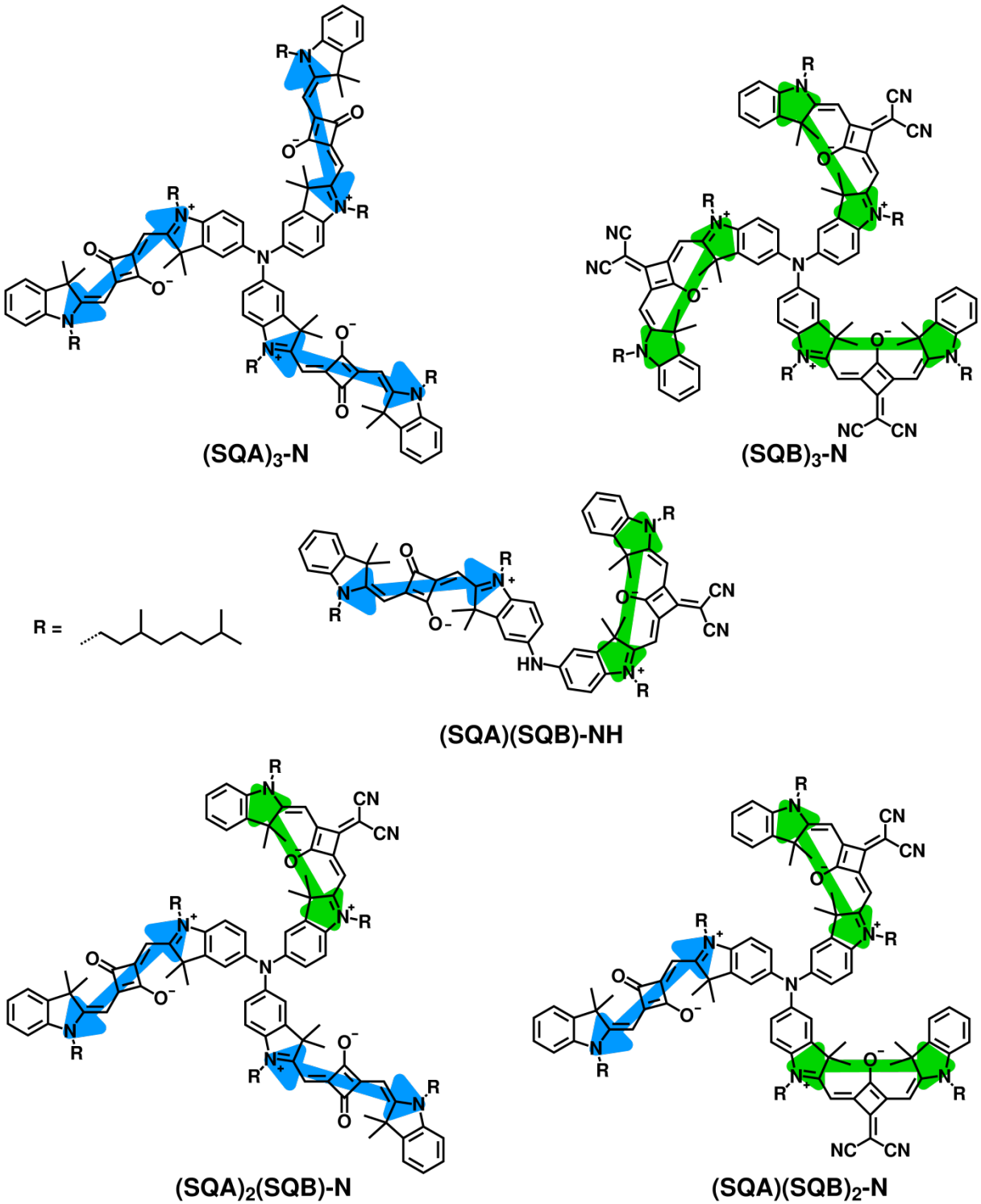

Figure 54 Star-shaped squaraine homo- and heterotrimers and heterodimer along with the respective orientation of transition moments of the lowest energy localised states. The orientation of transition moments are estimated on the basis of CAMB3LYP/ 6-31G* computations of the monomers.[1]

[1] The computations were performed by *Dr. Marco Holzapfel*.

Conclusion

In contrast to the benzothiazole squaraines, transoid and cisoid indolenine squaraines could be trimerised via a *Buchwald-Hartwig* coupling reaction. Due to the reaction conditions not only homotrimers but also heterotrimers could be isolated. In addition the reactions of different chromophores also yielded one heterodimer.

While the homotrimers show a red shift and a broadening of the absorption, the heterotrimers display a broader exciton manifold. This behaviour can be easily explained by exciton coupling theory. The estimated coupling constant of the star-shaped trimer **$(SQB)_3$-N** (600 cm^{-1}) is slightly larger as for a cyclic arrangement of three cisoid squaraines (572 cm^{-1}).[99] Although, due to the allowed transition from the lowest excited state (Figure 25) the star-shaped arrangement should display superior emission efficiency in comparison to the cyclic one, the experiment showed the contrary. While the cyclic arrangement had a quantum yield of 0.14[99] [1] the symmetric star-shaped homotrimer **$(SQB)_3$-N** yielded 0.10. The emission behaviour of the cyclic arrangement is explained by symmetry breaking which transforms the formally forbidden $S_1 \rightarrow S_0$ transition into an allowed one. The smaller band gap of the star-shaped chromophores results in a higher possibility of nonradiative decay in comparison to the monomeric compounds, which might be the reason for their rather low quantum yields.

The emission spectra of the heterochromophores featured next to the typical squaraine fluorescence from the lowest excited state some properties that could be assigned to localised states by transient absorption spectroscopy into the highest excited states. These localised states have a rather long lifetime which is not reduced by energy transfer to lower lying states. Thus, if one wants to design larger somewhat flexible superchromophores for fluorescence applications the strategy to broaden absorption by using different chromophores that are excitonically coupled has its limits if static disorder or fluctuations induce localisation of excitation.

[1] The quantum yield was corrected from a relative quantum yield measurement with the factor of 1.25 to be comparable to the absolute measurements of this work.

3.3.2 Linear Trans Oligomers

Additional to the star-shaped trimers the linear directly linked dimer **dSQA** and trimer **tSQA** were synthesised and characterised.

Synthesis

The palladium catalysed *Suzuki* coupling reaction of a slight excess of the mono brominated *trans*-squaraine **SQA-Br** and the mono boronic ester *trans*-squaraine **SQA-B** with $Pd(PPh_3)_4$ and the base Na_2CO_3 gave the dimer **dSQA** in a good yield of 67 %. In order to not only get the *trans*-trimer **tSQA** but also a functionalised *trans*-dimer **dSQA-B** the reaction of one equivalent of **SQA-B$_2$** and one equivalent of the mono brominated *trans*-squaraine **SQA-Br** was carried out using the same conditions.

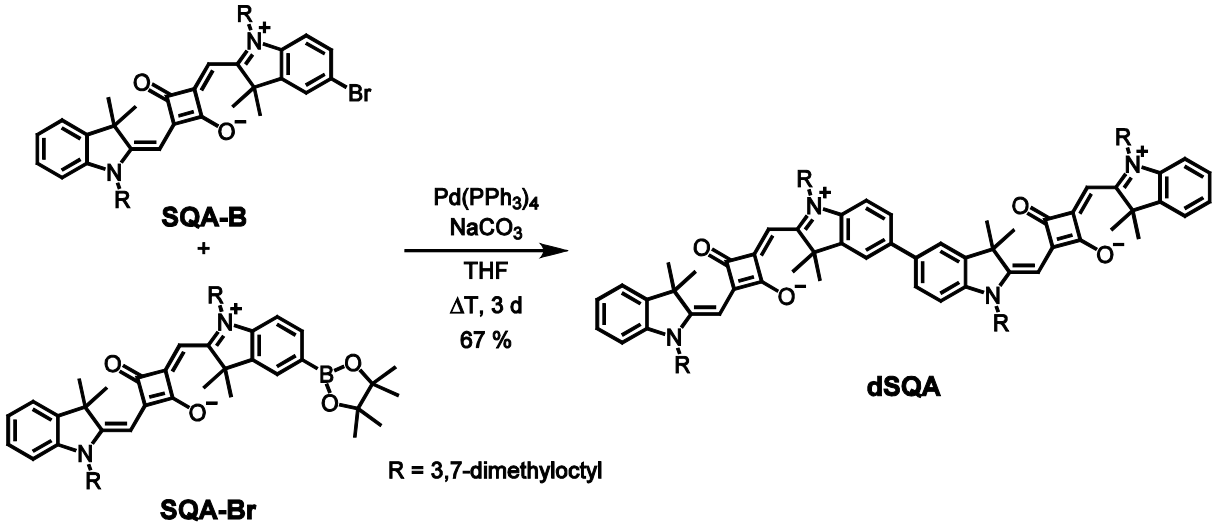

Scheme 41 Synthesis of the *trans*-squaraine dimer **dSQA**.

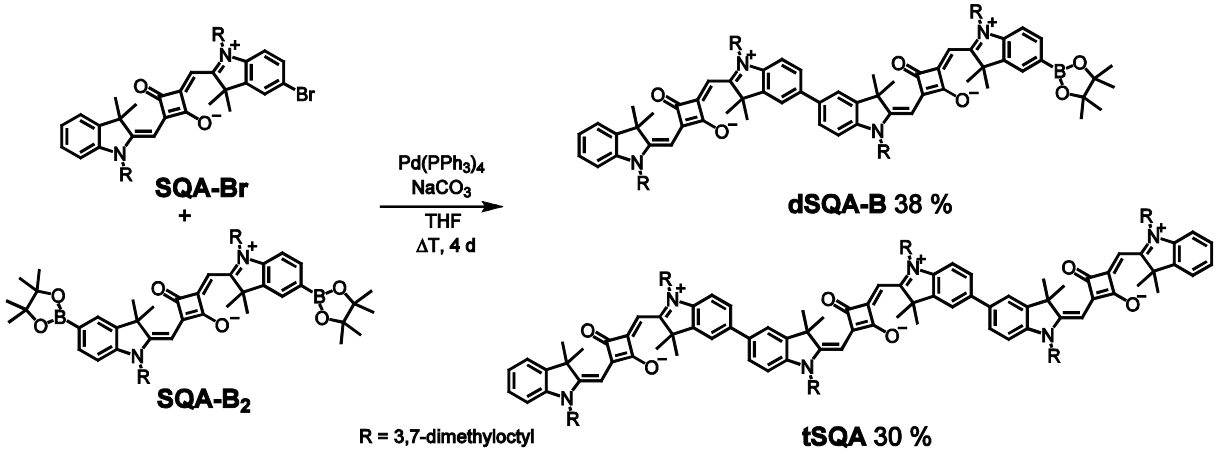

Scheme 42 Synthesis of the *trans*-squaraine trimer **tSQA** and the functionalised dimer **dSQA-B**.

Absorption Spectroscopy

The linear absorption of the *trans*-monomer **SQA**, the dimer **dSQA** and the trimer **tSQA** were measured in toluene (Figure 55), CH_2Cl_2 and $CHCl_3$. All findings are summarised in Table 8. The dimer and trimer showed unusual behaviour in toluene. During the dilution of the samples the intensity of the absorption spectra did not correlate with the concentration while the shape of the spectra remained unchanged. Since aggregation of the molecules could be excluded at the used concentrations, an interaction of the molecules with the glass surface was assumed. Indeed, silylation of the cuvette according to the literature[100, 143] resolved the issue.

The monomeric transoid squaraine **SQA** shows one sharp and intense absorption band at 15500 cm^{-1}, which is typical of squaraine compounds. It represents the HOMO→LUMO transition and has a weak vibronic shoulder at the high energy side.

For the head-to-tail oriented dimer **dSQA** one can consider two idealised structures, a bent and a linear structure both with C_2 symmetry.[94] They can be converted into each other by torsion around the connecting biaryl axis. The exciton coupling interaction of localised transition moments (blue arrows) with their phase relation (direction of the arrows) for both scenarios is depicted in Figure 56. The theory predicts for both orientations two possible electronic transitions into excitonic states that are separated by twice the exciton coupling energy *J*. In the linear alignment only the transition to the lowest exciton state is allowed. In the bent case both transitions are allowed. In solution the angle between the monomers can vary, therefore there are more conformers present. The lowest exciton state (S_1) should be observed as a more intense transition compared to the upper exciton state (S'_1, because it also derives from the S_1 state of the monomer). The absorption spectrum of the dimer (Figure 55) shows an intense transition at 14500 cm^{-1} that is red-shifted by 1000 cm^{-1} in comparison to the monomer. In addition to the vibronic shoulder at the 15800 cm^{-1} region a second weaker band is visible at 16100 cm^{-1}. The difference between the two absorption maxima can be used to estimate the exciton coupling energy *J* which is ca. 800 cm^{-1}.

For the head to tail arrangement of three squaraines as in the trimer **tSQA** the exciton coupling theory becomes more complicated as there are two biaryl axes that can adopt different torsion angles. Therefore many different conformers of the superchromophore are present in solution. Nevertheless, a qualitative solution of the exciton coupling theory should be achieved by the examination of the zig-zag arrangement. This is sketched in Figure 56. For

the trimer exciton coupling theory predicts three exciton states. The lowest one (S_1) is again highly allowed, the highest one (S''_1) is slightly allowed but the intermediate state (S'_1) is forbidden. The separation of the lowest and the highest exciton state is $2\sqrt{2}\,J$. (For the calculation see appendix Table S1) In practice the selection rules should be lifted because of the presence of different conformers. The experiment shows three peak maxima with decreasing intensity from lower to higher energy. The lowest state at 14000 cm^{-1} is again bathochromically shifted by 500 cm^{-1} compared to the lowest state of **dSQA**. From the energy difference of this state and the maximum of the highest energy peak at 16100 cm^{-1} the coupling energy can be estimated as ca. 740 cm^{-1} in good agreement with that of the dimer.

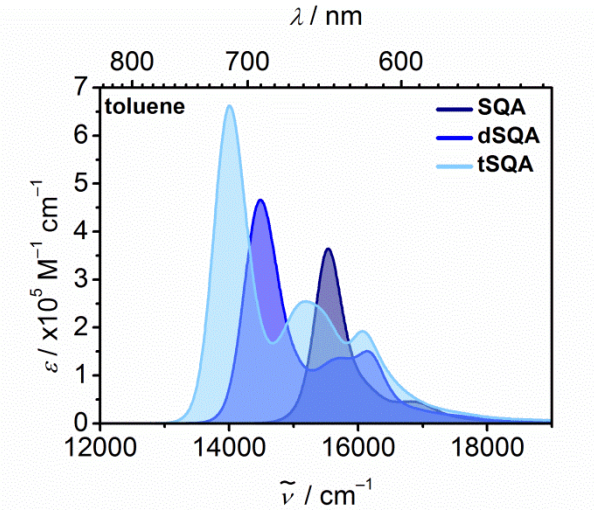

Figure 55 Absorption spectra of the monomer **SQA**, the dimer **dSQA** and the trimer **tSQA** in toluene at rt.

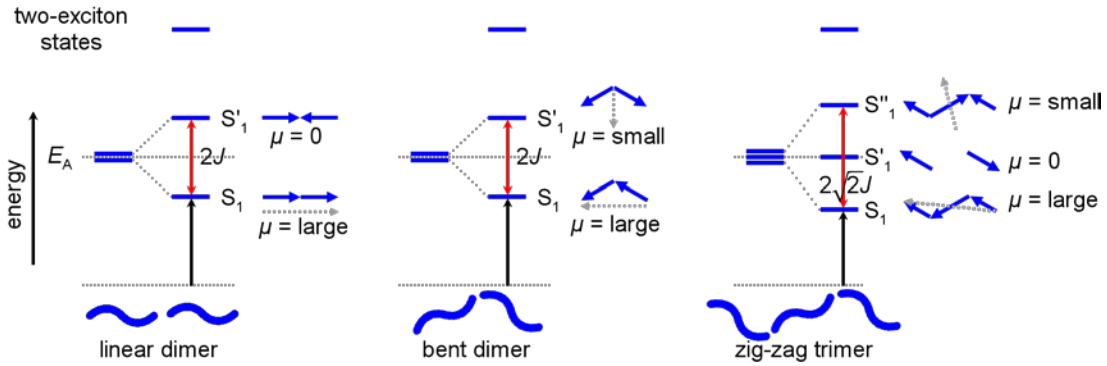

Figure 56 Exciton eigenstates formed by exciton interaction in case of a linear (left) and a bent dimer (middle) and a zig-zag trimer (right). The blue arrows indicate the phase relations of the localised transition moments. Their length is proportional to their magnitude. The grey dashed arrows are the resulting sum of the transition moments. Two-exciton states are formed by interaction of two excited chromophores.

The absorption spectra in the chlorinated solvents are hypsochromic shifted by a few hundred wavenumbers, whereupon the shift becomes less pronounced with increasing chain length. The extinction coefficients are overall somewhat smaller but the spectra are broader. The coupling constants *J* and the squares of the transition-dipole moments are larger than in toluene.

The squared transition moments of the dimer and the trimer show nearly additivity to the monomer and thus follow the *Thomas-Reiche-Kuhn* sum rule.[123] This means, that no other electronic transitions with significant oscillator strength contribute to the exciton manifold. In the superchromophores two-exciton states can be anticipated as the result of the interaction of two excited chromophores.[92, 135] They cannot be excited from the ground state by the absorption of a single photon, but are visible as two consecutive absorption processes from the ground state to the 1PA state and from there to the two-exciton state.

Table 8 Absorption maxima, extinction coefficients, transition moments and coupling constants of the squaraines **SQA**, **dSQA** and **tSQA** in various solvents at rt.

	solvent	$\tilde{\nu}_{abs}$ / cm^{-1} (nm)	ε / $M^{-1}\,cm^{-1}$	μ^2_{abs} / D^2	$\lvert J \rvert$ / cm^{-1}
SQA	CH_2Cl_2	15700 (639)	328000	130	
	$CHCl_3$	15700 (639)	347000	129	
	toluene	15500 (643)	365000	127	
dSQA	CH_2Cl_2	14500 (688)	395000	250	850
	$CHCl_3$	14600 (685)	454000	274	850
	toluene	14500 (690)	466000	248	800
tSQA	CH_2Cl_2	14000 (712)	598000	435	770
	$CHCl_3$	14100 (709)	621000	437	760
	toluene	14000 (714)	663000	410	740

Fluorescence Spectroscopy

The fluorescence spectra and the fluorescence lifetimes of **SQA**, **dSQA** and **tSQA** were measured in $CHCl_3$ and toluene. The data are summarised in Table 9.

Upon excitation into the main absorption band the squaraine monomer **SQA** shows the typical squaraine fluorescence emission. That is the mirror image of the absorption spectrum with a small *Stokes* shift of 200 cm^{-1}. The emission of the dimer and the trimer also resembles the shape of the monomeric compound. The quantum yields in toluene are larger than in $CHCl_3$ and become larger with increasing chain length with the exception of the dimer in $CHCl_3$.

The lifetime measurements were fitted with multiexponential decays and a stretched exponential using *Kohlrausch* equation (56).

$$I = I_0 \exp\left(-\left(t/\bar{\tau}_{fl}\right)^{\beta}\right) \tag{56}$$

The stretching exponents β were close to 1 except for the fits of **dSQA** and **tSQA** in toluene. Therefore a distribution analysis with logarithmically spaced lifetimes was performed (see Table 9 and appendix Figure S2). For the monomer **SQA** in $CHCl_3$ every fit resulted in two lifetimes, therefore the average lifetime was calculated with equation (57) using the amplitudes a_x and the lifetimes τ_x.[144]

$$\bar{\tau} = \frac{a_1\tau_1^2 + a_2\tau_2^2}{a_1\tau_1 + a_2\tau_2} \tag{57}$$

The acquired average lifetimes were used to calculate the transition moments of the fluorescence μ_{fl} by the *Strickler-Berg*[145] equation (58) from the fluorescence quantum yield ϕ_{fl}.

$$k_{fl} = \frac{16\times10^6\pi^3}{3h\varepsilon_0}\frac{n(n^2+2)^2}{9}\left\langle\tilde{\nu}_{fl}^{-3}\right\rangle_{av}^{-1}\mu_{fl}^2 \tag{58}$$

Here $\left\langle\tilde{\nu}_{fl}^{-3}\right\rangle_{av}^{-1} = \int I_{fl}d\tilde{\nu}\Big/\int I_{fl}\,\tilde{\nu}^{-3}d\tilde{\upsilon}$ is the average cubic fluorescence energy and $k_{fl} = \phi_{fl}/\tau_{fl}$ is the radiative rate constant.

The squared fluorescence transition moments of **SQA** are within the experimental uncertainty equal to those of the absorption. For the superchromophores a less than additive behaviour of the relative squared transition moments is observed. The higher values are caused by the superradiance effect, i.e. collective emission from delocalised states.[135, 146-148]

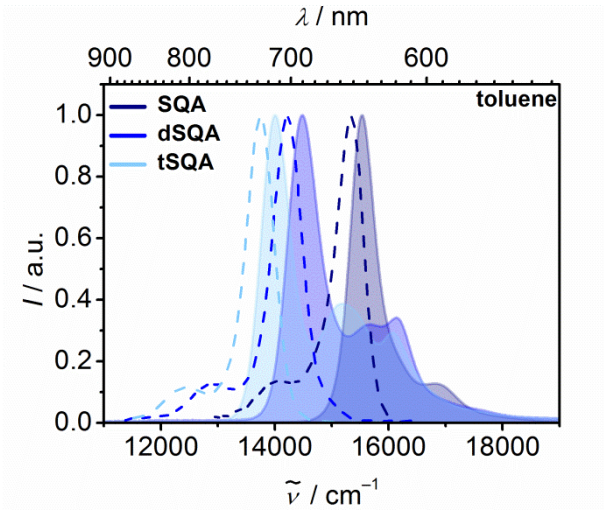

Figure 57 Absorption spectra (shaded areas) and fluorescence spectra (dashed lines) of the monomer **SQA**, the dimer **dSQA** and the trimer **tSQA** in toluene at rt.

Table 9 Fluorescence maxima, quantum yields, lifetimes, squares of the fluorescence and absorption transition dipole moments of the squaraines **SQA**, **dSQA** and **tSQA** in $CHCl_3$ and toluene at rt.

	solvent	$\tilde{\nu}_{fl}$ / cm^{-1}	ϕ_{fl} ($\tilde{\nu}_{fl}$ / cm^{-1})[a]	τ_{fl} / ns (TCSPC)[b]	$\bar{\tau}_{fl}$ / ns [c]	μ_{fl}^2 / D^2	μ_{abs}^2 / D^2
SQA	$CHCl_3$	15500 (645)	0.53±0.014 (16700)	0.26 (0.40) 1.47 (0.60)	1.33[d]	121	129
	toluene	15300 (652)	0.62±0.033 (16700)	0.07 (0.03) 0.20 (0.10) 1.72 (0.87)	1.64 (0.97)	114	127
dSQA	$CHCl_3$	14300 (699)	0.42±0.017 (16700)	0.05 (-0.34) 0.11 (0.13) 0.96 (0.53)	0.94 (0.99)	172	274
	toluene	14200 (702)	0.82±0.033 (16700)	0.15 (-0.31) 0.25 (0.30) 1.82 (0.39)	1.67[e]	172	248
tSQA	$CHCl_3$	13800 (723)	0.58±0.045 (16100)	0.17 (-0.21) 0.66 (0.16) 1.17 (0.63)	1.14 (0.99)	216	437
	toluene	13700 (728)	0.85±0.033 (16100)	0.08 (-0.26) 1.14 (0.42) 1.94 (0.32)	1.57[e]	219	410

[a] Fluorescence quantum yield and excitation wavenumber used for measuring the fluorescence spectra in parentheses. [b] Multiexponential fit of fluorescence decay measured by TSCPC, excitation at 15200 cm^{-1}. Amplitudes are given in brackets. [c] Lifetimes acquired by stretched exponential analysis. Stretching exponent in brackets. [d] Average lifetime calculated with eq. (57). [e] Lifetimes acquired by distribution analysis. The distribution is shown in the appendix in Figure S1.

Two Photon Absorption Induced Fluorescence (2PAF)

The 2PAF spectra of **SQA**, **dSQA** and **tSQA** in toluene are presented in Figure 58 and the cross sections are given in Table 10.

First the 2PA spectrum of the monomeric squaraine **SQA** will be discussed and compared with literature results.[17, 21, 62]

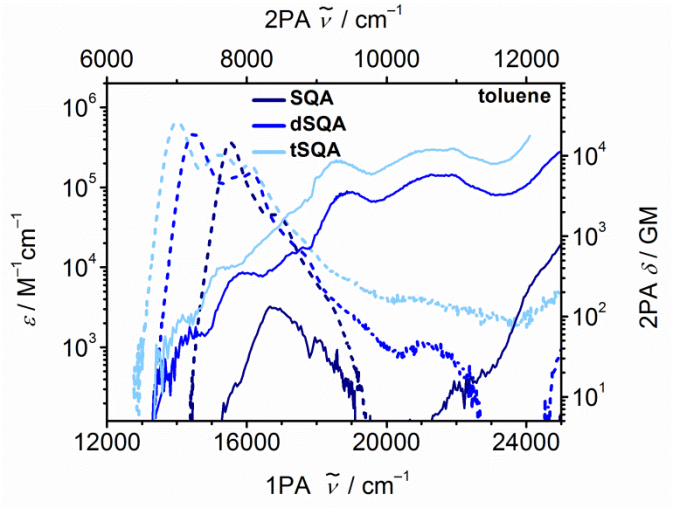

Figure 58 1PA spectra (dashed lines) and 2PA spectra (solid lines) of the monomer **SQA**, the dimer **dSQA** and the trimer **tSQA** in toluene at rt.

The selection rules for the electronic 1PA transition for the centrosymmetric chromophore **SQA** allow transitions from the ground state (A_g) to excited singlet states with u symmetry while transitions to g symmetric states are dipole forbidden.[50] Indeed, TD-DFT computations (see appendix Table S5) assign B_u symmetry to the lowest singlet excited state. The next two transitions are n→π* excitations of the oxygen lone pair electrons into the LUMO which have vanishing oscillator strength due to minimal orbital overlap and are therefore not observed by 1PA and 2PA spectroscopy and disregarded in the following. The next state that has an orbital overlap possesses A_g symmetry and is consequently 1PA forbidden but 2PA allowed. *Scherer et al.*[62] confirmed the symmetry of this state by polarisation dependent 2PAF measurements for **SQA** in $CHCl_3$ with ethyl as the alkyl chain. The state is at 24200 cm^{-1} and is also visible by fluorescence excitation anisotropy (FEA) spectroscopy in viscous media.[17, 21] In addition the 2PA measurement showed a weak transition at 16700 cm^{-1} just a bit above the lowest B_u state at 15700 cm^{-1}. This transition is weakly 2PA allowed because of vibronic coupling to a b_u symmetric vibration (B_u x b_u = A_g).[62] The 2PA spectrum of **SQA** in toluene revealed similar results (Figure 58), with the

exception that the maximum of the 2PA transition at E_2 is not resolved in the measurement but it should be in the immediate vicinity of 25000 cm^{-1}.

The 2PAF spectra of **dSQA** and **tSQA** dramatically differ from the one of **SQA**. The dimer shows in addition to the vibronically allowed 2PA peak at the shoulder of the $S_1 \leftarrow S_0$ transition at 14500 cm^{-1} pronounced maxima at 18800 cm^{-1} (δ_{2PA} = 3430 GM) and at 21800 cm^{-1} (δ_{2PA} = 5780 GM). The comparison of the logarithmically plotted spectra of the 1PA and the 2PA with the FEA spectrum in polyTHF allows a more detailed assignment of the states (see Figure 59).

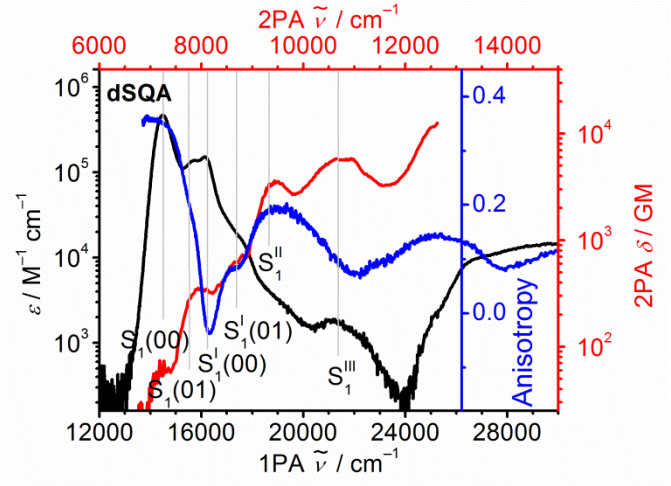

Figure 59 1PA spectrum (black) and 2PA spectrum (red) of the dimer **dSQA** in toluene together with the fluorescence excitation anisotropy spectrum (blue) in polyTHF at 26°C.

The value at the 0-0 peak of the S_1 state of r = 0.36 proves this transition to be polarised parallel to the emission transition moment (ideally r = 0.4 in this case).[144] At the vibronic shoulder (= S_1(0-1) transition) the FEA drops to 0.2. The values at the S'$_1$(0-0) state and its vibronic shoulder S'$_1$(0-1) are -0.03 and 0.09. These low values indicate a pronounced angle between the transition moments of the excitations and the fluorescence ($S_1 \rightarrow S_0$). For the bent case of the dimer the exciton coupling theory predicts a perpendicular orientation of the S'$_1 \leftarrow S_0$ transition moment and therefore ideally an FEA value of r = -0.2 (Figure 56). The two pronounced 2PA peaks at 18800 cm^{-1} and 21800 cm^{-1} show a FEA maximum of 0.2 and a minimum of 0.07 and represent the S''$_1$ and S'''$_1$ states. They are also visible as weak shoulders in the 1PA. These two states cannot be explained by exciton coupling theory. For this reason, an orbital interaction diagram for the linear dimer situation is constructed. The π-HOMO and the π-LUMO of the monomers interact with each other and give in total four

new π-orbitals (Figure 60). With these four orbitals, four excitation configurations can be generated. Due to their orbital symmetry this gives rise to two ground state transitions that are 1PA allowed (g→u) and two that are 1PA forbidden but 2PA allowed (g→g). TD-DFT computations confirm this conclusion (see appendix Table S6). In comparison, the simple excited state exciton interaction theory predicts only two states. It is assumed that the four electronic states that can be observed up to 23000 cm^{-1} are these states and since they all derive from the S_1 of the monomer they are labelled S_1 to S''''_1. Due to energy shifts that can occur because of configuration interaction (CI) mixing, the assignment of the states is intricate. In addition intensity borrowing between states of the same symmetry may change the intensity of the single transitions.[149-151]

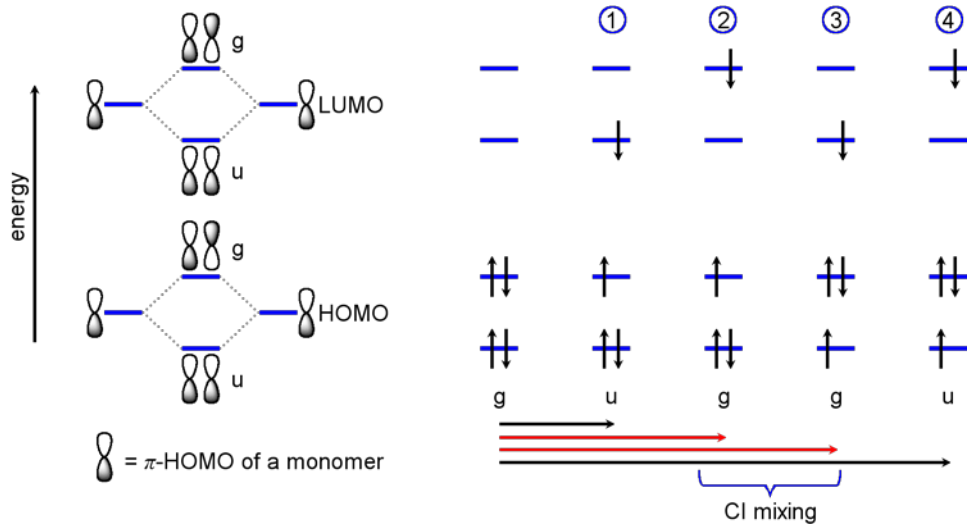

Figure 60 Orbital state diagram for the interaction of two squaraine dyes in a linear (centrosymmetric) arrangement. Configuration 2 and 3 may undergo CI mixing because of similar energy. The black excitations are 1PA allowed; the red excitations are 2PA allowed.

In the trimer **tSQA** the 1PA and the 2PA spectra are shifted slightly to lower energies (see Figure 58 and Table 10). The 2PA cross sections for the S''_1 and the S'''_1 bands of the trimer (E_2 and E_3 in Table 10) are roughly twice the value of the dimer at similar energies. With eq. (6), the ratio between the 2PA cross section of a superchromophore consisting of n monomers $\delta_{2PA}^{(n)}$ and the 2PA cross section of the monomer $\delta_{2PA}^{(1)}$, one can derive a cooperative behaviour of δ_{2PA} in the squaraine oligomers.

In Figure 61 the 2PA spectra of the dimer and the trimer are normalised per squaraine unit. The cooperative behaviour can be observed in all regions except for the vibronic shoulder of the S_0 to S_1 transition (see inlet of Figure 61).

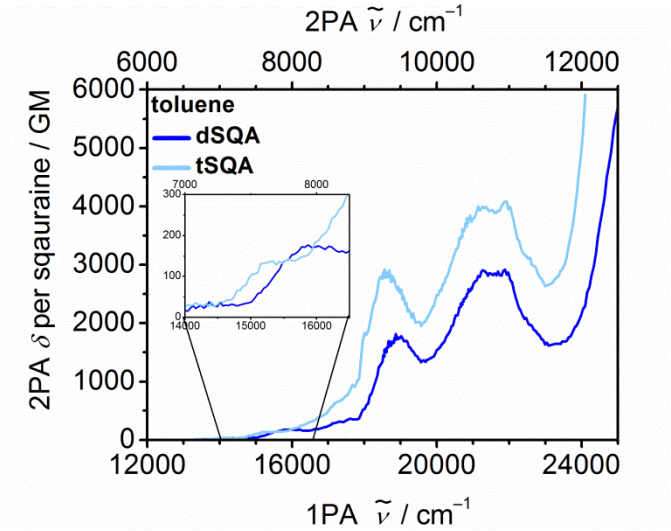

Figure 61 2PA spectra (normalised per squaraine unit) of the dimer **dSQA** and the trimer **tSQA** in toluene at rt.

For all squaraines a strong 2PA at nearly twice the energy of the 1PA is observable because of the double resonance effect of the two exciton state (see Figure 56).

Table 10 One photon cross section at the absorption maximum and 2PA cross sections in the maxima of the squaraines **SQA**, **dSQA** and **tSQA** in toluene at rt.

	σ_{max}^{1PA} /10^{-15} cm^2	E_1 /cm^{-1}	δ_1^{2PA} / GM	E_2 / cm^{-1}	δ_2^{2PA} / GM	E_3 / cm^{-1}	δ_3^{2PA} / GM	E_4 / cm^{-1}	δ_4^{PA} / GM
SQA	1.40	16700	133	25000	800				
dSQA	1.78	15900	340	18800	3430	21800	5780	25000	11400
tSQA	2.54	15400	415	18600	8340	21800	122400	24000	17740

Cyclic Voltammetry

For the transoid squaraines **SQA**, **dSQA** and **tSQA** cyclic voltammetry experiments were carried out in CH_2Cl_2 with $^nBu_4PF_6$ (0.2 M) as electrolyte. The voltammograms are shown in Figure 62, the half wave potentials and the derived HOMO and LUMO energy levels as well as the electrochemical band gap are summarised in Table 11.

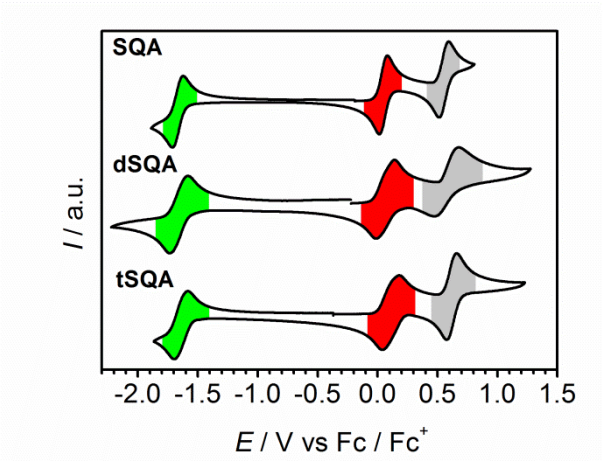

Figure 62 Cyclic voltammograms of **SQA**, **dSQA** and **tSQA** in $CH_2Cl_2/^nBu_4PF_6$ (0.2 M) at a scan rate of 100 mV s^{-1}. All voltammograms are referenced against (Fc/Fc^+), normalised and recorded by first scanning into the oxidative direction.

The monomer **SQA** shows the typical cyclic voltammogram of squaraines with one irreversible reduction at ~1660 mV and two oxidation processes at 50 mV and 550 mV. The first oxidation is a reversible process while the second is irreversible. The irreversibility was determined by measurements at different scan rates (10–4000 mV) and in a thin layer setup. For the dimer the half wave potentials shift to a slightly higher voltage. Differential pulse voltammetry (DPV) reveals that the first oxidation process splits into two one electron processes with a difference of the half wave potentials of 50 mV. In the second oxidation no difference of the half wave potentials is determinable. For the trimer a similar behaviour is observed. A digital fit with Digi Elch, as well as the DPV, shows that this time initially one squaraine is oxidised at 50 mV and then the other two at 75 mV. The second oxidation of each squaraine takes place at 580 mV.

Despite the elongation of the conjugation and the resulting red shift of the absorption no noticeable effect on the HOMO and LUMO energy levels is observed. This means, that in the ground state only a weak electronic interaction takes place and the squaraines behave as nearly independent redox moieties.

Table 11 Redox potentials ($E_{1/2}$), HOMO and LUMO energy levels and band gaps of **SQA**, **dSQA** and **tSQA** in $CH_2Cl_2/^nBu_4PF_6$ (0.2 M) at a scan rate of 100 mV s^{-1} and referenced against (Fc/Fc^+).

	$E^{red}_{1/2}$ / mV	$E^{ox}_{1/2}$ / mV	$E^{ox}_{1/2}$ / mV	$E^{ox}_{1/2}$ / mV	E_{HOMO} / eV	E_{LUMO} / eV	E_{gap} / eV
SQA	-1665[i]	50[r]		555[i]	-5.21	-3.50	1.71
dSQA	-1656[i]	40[r, a]	90[r, a]	585[i]	-5.20	-3.50	1.70
tSQA	-1640[i]	50[r, fit]	75[r, fit]	580[i]	-5.21	-3.52	1.69

[i] irreversible, [r] reversible, [a] potentials extracted from DPV, [fit] fitted with Digi Elch.

Transient Absorption Spectroscopy

The dimer **dSQA** and the trimer **tSQA** were investigated by transient absorption spectroscopy. For both superchromophores the behaviour after excitation at the maximum of the lowest absorption peak and at the maximum of the highest absorption peak of the exciton manifold (Figure 56) was examined. The excited states were probed by white light between 400 – 800 nm. The transient maps were analysed with a sequential model resulting in evolution associated difference spectra (EADS). The estimated state energies of the transoid chromophores are given in Figure 63 together with the lifetimes of the EADS. The transient absorption spectra, the time scans at selected wavenumbers and the EADS of **dSQA** (Figure 64) and **tSQA** (Figure 65) in toluene are shown and discussed in the following.

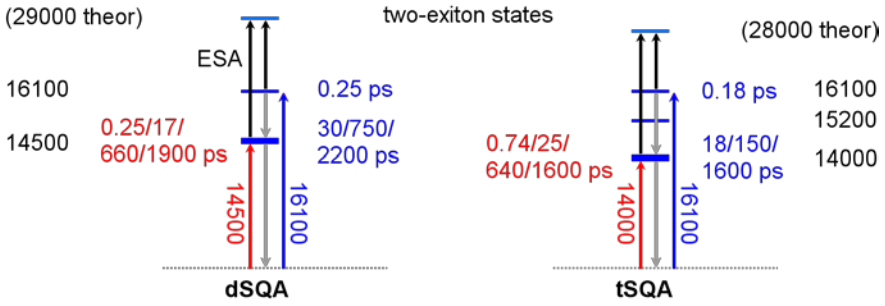

Figure 63 State diagrams of the transient absorption spectra. Lifetimes in red are for excitation into the maximum of the lowest exciton band, those in blue for excitation into the maximum of the the highest exciton band at the given wavenumbers. The state energies were estimated by the peak positions of respective absorption bands. The two-exciton states were estimated (= theor) from the energies of the mono-exciton states. Lifetimes separated by a slash indicate multiexponential decay process from multiple levels with slightly different energy (given as one bold bar). All the energies are not to scale.

The overall behaviour of the linear oligomers is quite similar to the above described **(SQA)(SQB)-NH** (**Figure 53**) and the star-shaped homo- and heterotrimers, therefore the considerations for the shar-shaped trimer with a nitrogen core are applied in the following discussion as well.

The transient maps of **dSQA** show upon excitation into the lowest exciton band at 14500 cm^{-1} a negative intense combined GSB and SE peak at 14400 cm^{-1}. This initial narrow signal forms within instrument response time and broadens after a few 100 fs. The remaining GSB and the ESA to the two-exciton state are both in the region of ~16300 cm^{-1} and therefore almost cancel out. An additional quite weak but broad ESA can be observed above 18000 cm^{-1} (Figure 64b). The sequential model gave four EADS, where the first three

are associated with vibrational relaxations with lifetimes of 0.25 ps, 17 ps and 0.66 ns while the fourth one represents the ground state recovery with a lifetime of 1.9 ns. The later time is very similar to the longest time (1.82 ps) that was acquired by the multiexponential fit of the TSCPC measurement.

After excitation into the highest exciton band at 16100 cm^{-1} the spectra show an additional negative peak at 16300 cm^{-1}. This signal is visible due to the population of the S'_1 state and the resulting shift of the ESA. The peak gets smaller after the S_1 state is populated at the expense of the S'_1 state. This can also be observed in the time scans at 16300 cm^{-1} and 19600 cm^{-1}. However, there is still a discrepancy in the region of the high exciton manifold after 1 ps in the spectra of the two pump energies. The remaining TA map and the lifetimes acquired by the sequential model are very similar to the experiment with lower pump energy. The shortest lifetime of 0.25 ps that is assigned to an intraband relaxation process in the measurement at higher pump energy is in the same region as the first vibrational relaxation upon excitation into the lowest exciton manifold. Hence, there might be two consecutive processes upon excitation at 16100 cm^{-1} but they are too close together and in addition in the proximity of the instrument response to be observed separately.

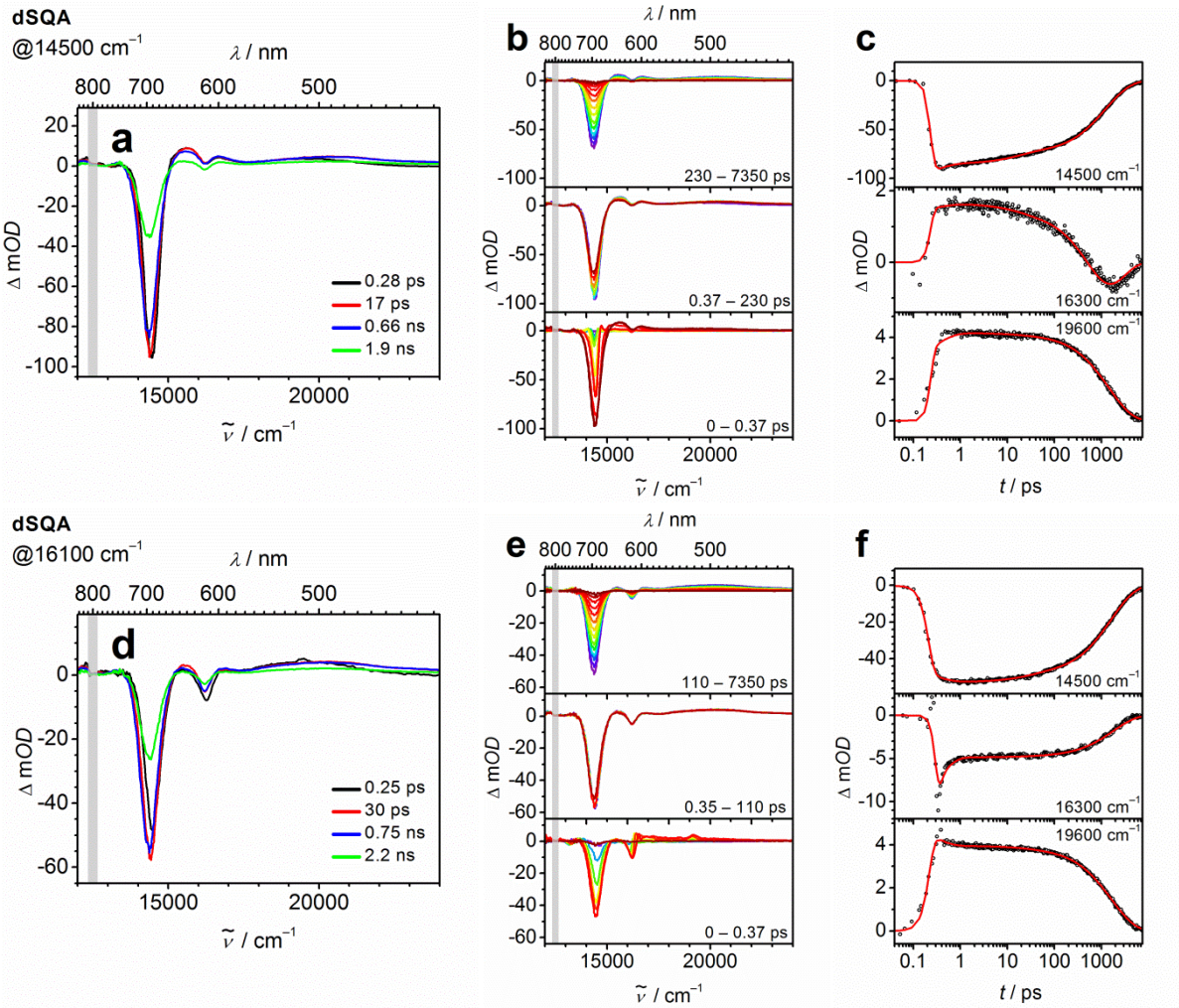

Figure 64 Evolution associated difference spectra (EADS) of **dSQA** in toluene for excitation at 14500 cm^{-1} (a) and at 16100 cm^{-1} (d). The spectra at 12500 cm^{-1} ± 200 cm^{-1} (grey bar) are influenced by the laser fundamental and should be taken with caution. The colour code of the EADS refers to the dimension of lifetime. The transient absorption spectra (b, e) and the time scans at selected wavenumbers (c, f) were corrected for chirp and scattered light. Early spectra are given in blue, the later spectra in red.

In the spectra of the trimer **tSQA** the GSB/SE signal is red-shifted by 500 cm^{-1} in comparison to **dSQA**. Otherwise the spectra and also the sequential fits are very similar to the ones obtained for the dimer. However this time the lifetimes upon excitation at the higher exciton manifold are smaller compared to the lifetimes obtained by the lesser pump energy. The only exception is the longest lifetime, which is unchanged and is assigned to the ground state recovery.

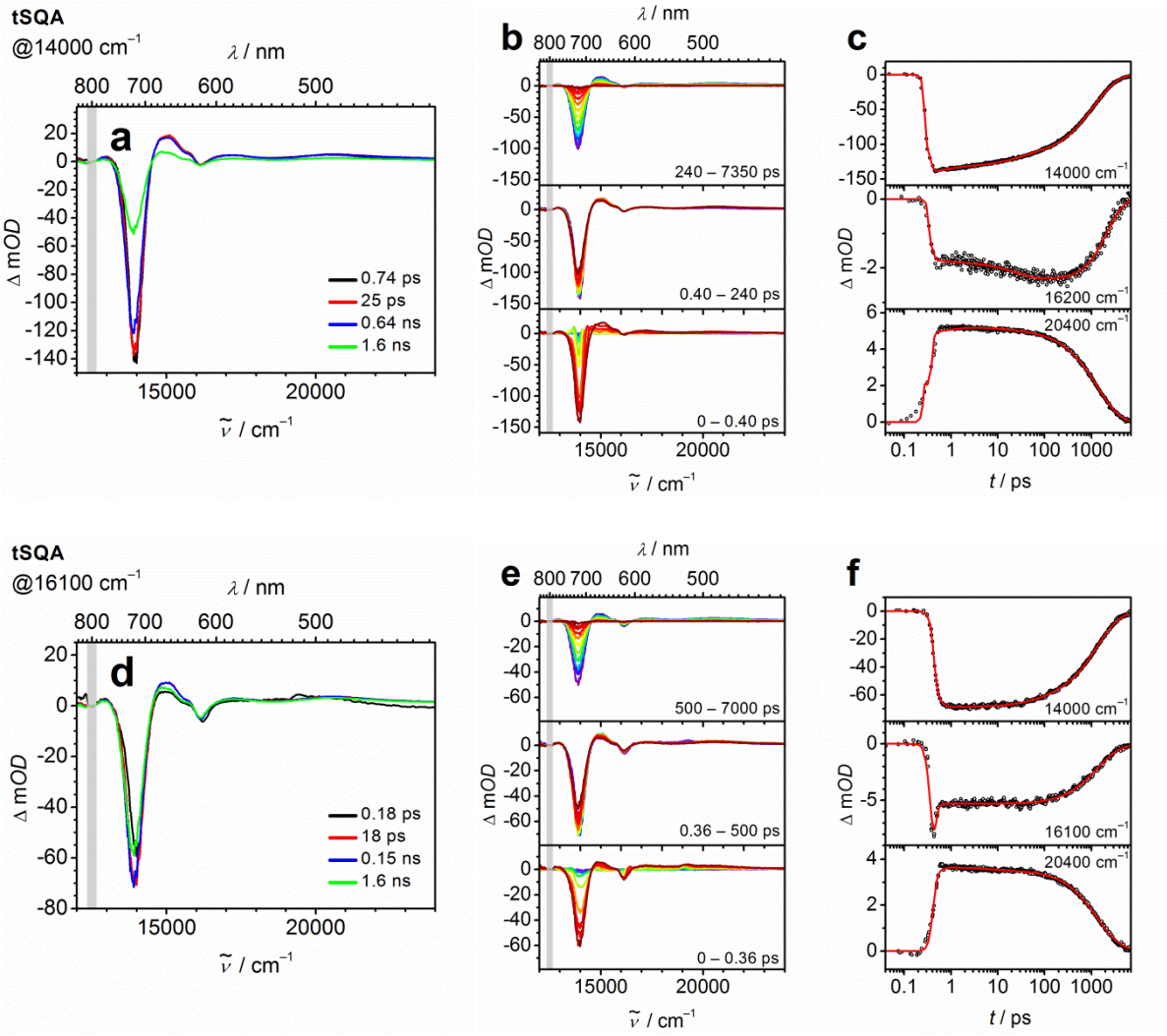

Figure 65 Evolution associated difference spectra (EADS) of **tSQA** in toluene for excitation at 14000 cm^{-1} (a) and at 16100 cm^{-1} (d). The spectra at 12500 cm^{-1} ± 200 cm^{-1} (grey bar) are influenced by the laser fundamental and should be taken with caution. The colour code of the EADS refers to the dimension of lifetime. The transient absorption spectra (b, e) and the time scans at selected wavenumbers (c, f) were corrected for chirp and scattered light. Early spectra are given in blue, the later spectra in red.

Conclusion

The oligomers of the transoid squaraine **SQA** were synthesised by means of palladium catalysed *Suzuki* cross coupling reactions.

The low energy side of the absorption spectra of the dimer **dSQA** and the trimer **tSQA** is red-shifted in comparison to the monomer. This effect is significantly larger for the addition of the first chromophore to the monomer than for the second. In the spectra of the oligomers additional maxima with higher energies are observed. These are caused by exciton coupling

of the single chromophores. The highest exciton state shows a lifetime of a few 100 fs in the fs-pump-probe spectroscopy. In the same experiments the ground state recovery took place in ~2 ns for the dimer and 1.6 ns for the trimer. The elongation of the conjugation had an additive effect on the squares of the transition-dipole moments.

In toluene the fluorescence quantum yield of the chromophores increased with the chain length, despite the smaller optical band-gap due to exciton coupling and the resulting higher possibility of nonradiative decay. The fluorescence spectra of the oligomers represent the mirror images of the absorption of the monomeric **SQA** and have a small *Stokes* shift. Nevertheless, the transition-dipole moments of the oligomers show higher values compared to the monomer. These variations are caused by exciton superradiance. While the multiexponential fits of the time correlated single photon counting measurements typically needed three time constants for an adequate fit, it was also possible to achieve a similar conformity with only one lifetime using either stretched exponential or distribution analysis. The lifetimes of the latter fits correlate with the ground state recovery time of the fs-pump-probe measurements.

The two photon absorption fluorescence experiments of **SQA** in toluene reproduced the literature data in good agreement. The spectra of **dSQA** and **tSQA** differ significantly from the monomer spectra. They show high two photon cross sections in the whole spectral region between 15000 cm^{-1} and 24000 cm^{-1}. The additional bands are a result of symmetry breaking, causing an annulment of the parity rule, and orbital interaction. The two photon transitions of **dSQA** could be assigned to exciton states by a fluorescence excitation anisotropy experiment. The elongation of the dimer by one additional squaraine resulted in an enhancement effect of the two photon absorption cross section.

Despite the red shift of the absorption the electrochemically determined band gap of the chromophores did not change for the superchromophores. This indicates negligible interaction of the chromophores in the ground state.

3.3.3 Star-Shaped Trimers with a Benzene Core

Synthesis

Two star-shaped squaraine trimers with a benzene moiety as the connecting core were synthesised via palladium catalysed *Suzuki* cross coupling reactions. In the reaction of 3.5

equivalents of **SQA-B** with 1,3,5-tribromobenzene, $Pd(PPh_3)_4$ and K_2CO_3/Na_2CO_3 in a mixture of THF/H_2O the trimer **$(SQA)_3$-ben** could be isolated. The reaction of the functionalised dimer **dSQA-B** as reactant using the same conditions resulted in the superchromophore **$(dSQA)_3$-ben** with six monomeric squaraine units. (Scheme 43)

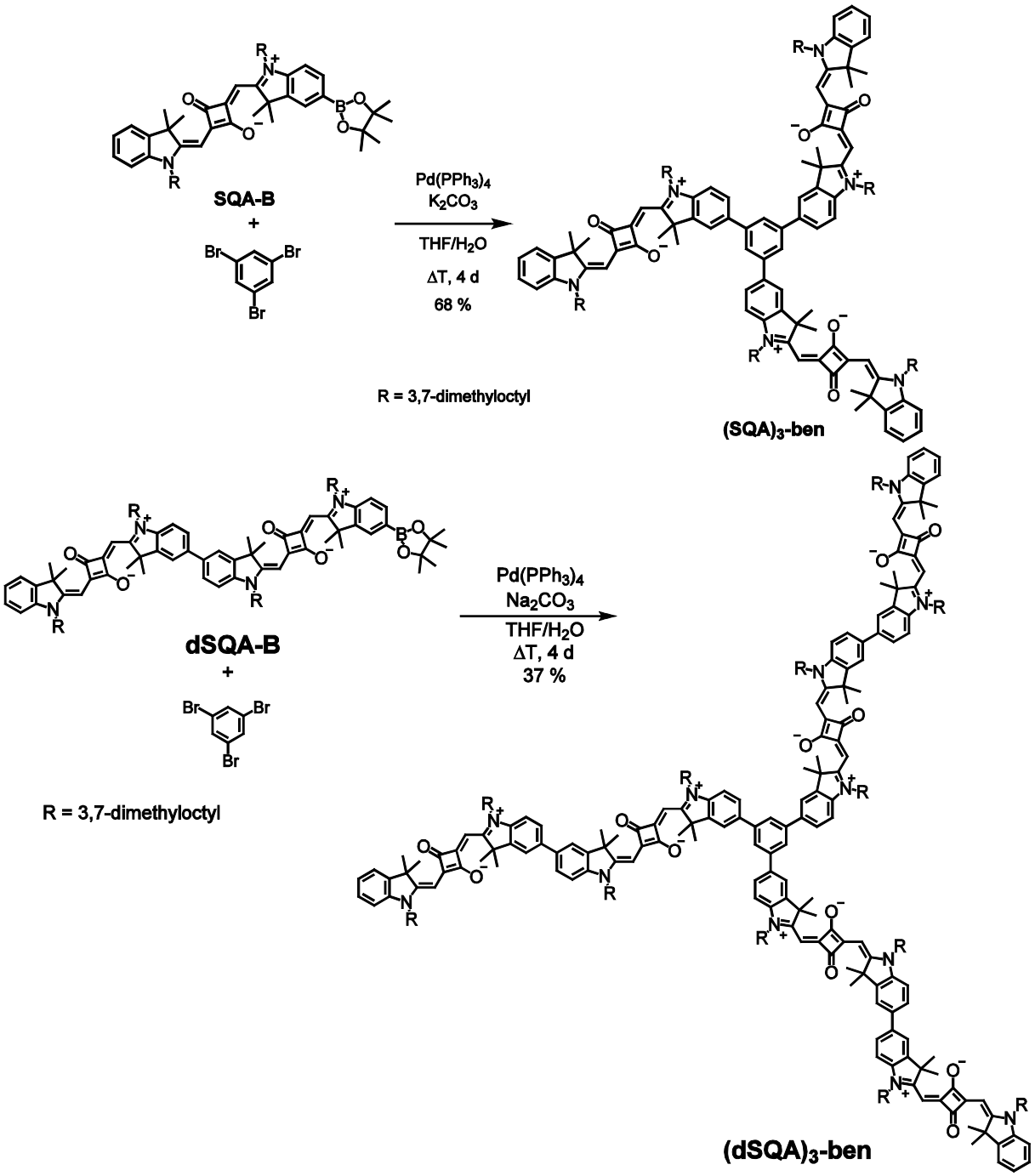

Scheme 43 Synthesis of the star-shaped benzene *trans*-trimer **$(SQA)_3$-ben** and *trans-trans*-trimer **$(dSQA)_3$-ben**.

Absorption Spectroscopy

In toluene the absorption spectrum of the superchromophore **(SQA)$_3$-ben** is red-shifted by 500 cm^{-1} compared to the monomer and displays a small shoulder at the high energy side of the main absorption band. (Figure 66 and Table 12) This additional peak is caused by a weak excitonic coupling. For a truly C_3 symmetric chromophore only a very intense transition into the S_1 state should be visible because the transition into the S'_1 state has no dipole moment as indicated in Figure 67. Due to structural disorder the symmetry breaks and this transition gains intensity. In the larger **(dSQA)$_3$-ben** a similar shoulder is observed. Here the coupling constant can only be roughly estimated because the maximum of the band is hard to determine. In addition there is exciton coupling between the two chromophores of each branch exactly like in the squaraine **dSQA**. The red-shift between the two trimers is with ca. 1000 cm^{-1} the same as in their linear parent chromophores.

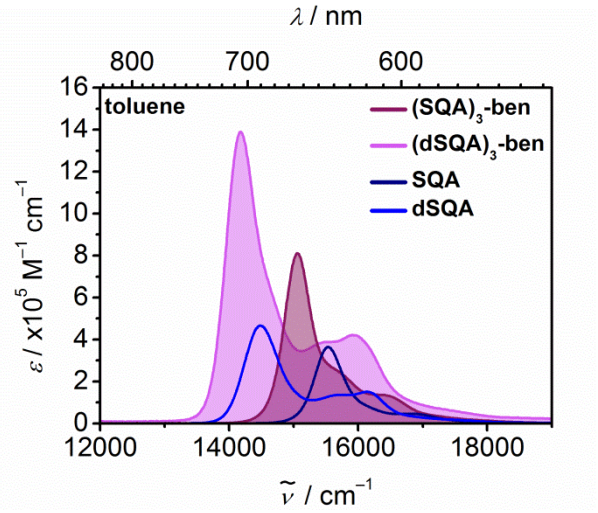

Figure 66 Absorption spectra of the trimers **(SQA)$_3$-ben** and **(dSQA)$_3$-ben** and their parent chromophores **SQA** and **dSQA** in toluene at rt.

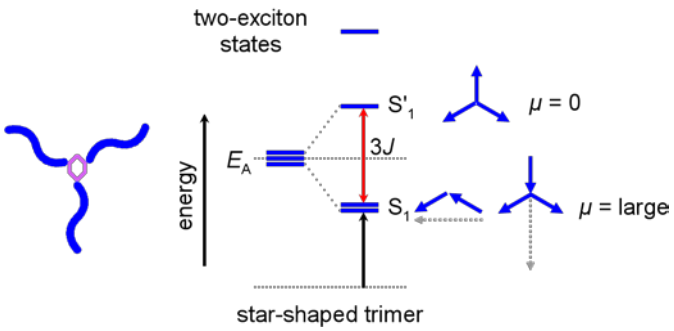

Figure 67 Exciton eigenstates formed by exciton interaction in case of a star-shaped trimer. The blue arrows indicate the phase relations of the localised transition moments. Their length is proportional to their magnitude. The grey dashed arrows are the resulting sum of the transition moments. Two-exciton states are formed by interaction of two excited chromophores.

In $CHCl_3$ the absorption spectra are shifted slightly to the blue and have a higher extinction coefficient. Since the whole spectra are broader the transition-dipole moments and the coupling constants are larger compared to the ones in toluene. In CH_2Cl_2 the chromophores show the same trend but this time the extinction coefficients are unchanged compared to toluene.

The squares of the transition-dipole moments show nearly additivity to their linear analogues, meaning that no other electronic transition with significant oscillator strength contributes to the exciton manifold.

Table 12 Absorption maxima, extinction coefficients, squares of the transition dipole moments, fluorescence maxima, fluorescence quantum yields and coupling constants of the squaraine trimers **$(SQA)_3$-ben** and **$(dSQA)_3$-ben** in various solvents at rt.

	solvent	$\tilde{\nu}_{abs}$ / cm^{-1} (nm)	ε / $M^{-1}\,cm^{-1}$	μ^2 / D^2	$\lvert J \rvert$ / cm^{-1}
(SQA)3-ben	CH_2Cl_2	15100 (660)	811600	361	220
	$CHCl_3$	15200 (658)	912200	386	217
	toluene	15100 (662)	810900	319	215
(dSQA)3-ben	CH_2Cl_2	14200 (704)	1390500	896	170/920
	$CHCl_3$	14300 (699)	1464800	893	180/890
	toluene	14200 (705)	1390200	800	180/880

Fluorescence Spectroscopy

The emission spectra of **$(SQA)_3$-ben** and **$(dSQA)_3$-ben** show the same behaviour as already observed for the oligomers. Their emission is the mirror image of the absorption of the monomer **SQA** with a small *Stokes* shift. (Figure 68) The measured quantum yields in both solvents are comparable to the values that were determined for their linear analogues. (see Table 9 and Table 13)

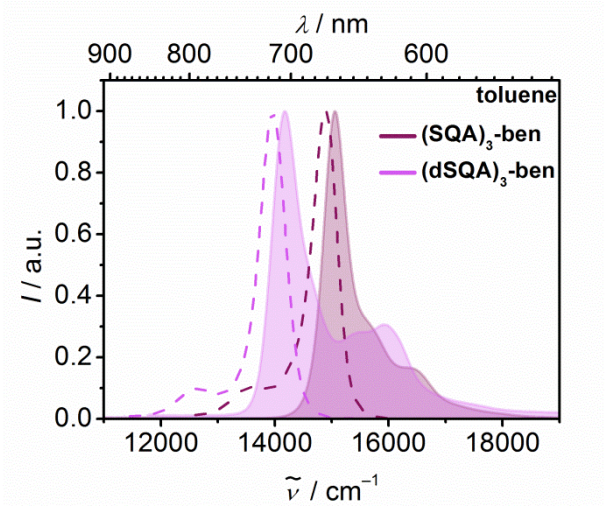

Figure 68 Absorption spectra (shaded areas) and fluorescence spectra (dashed lines) of the trimers **$(SQA)_3$-ben** and **$(dSQA)_3$-ben** in toluene at rt.

The lifetimes that were determined by multiexponential decay and stretched exponential fits using equation (56) are nearly identical to the ones of **SQA** and **dSQA**. The squares of the transition-dipole moments of the fluorescence μ_{fl}, determined with the *Strickler-Berg* equation (58), are smaller than the squares of the transition-dipole moments of the absorption but larger than the values in the parent compounds. This indicates a weak exciton coupling and emission from more localised states.

Table 13 Fluorescence maxima, quantum yields, lifetimes, squares of the fluorescence and absorption transition dipole moments of the squaraines **(SQA)$_3$-ben** and **(dSQA)$_3$-ben** in $CHCl_3$ and toluene at rt.

	solvent	$\tilde{\nu}_{fl}$ / cm^{-1}	ϕ_{fl} ($\tilde{\nu}_{fl}$ / cm^{-1})[a]	τ_{fl} / ns (TCSPC)[b]	$\bar{\tau}_{fl}$ / ns	μ_{fl}^2 /D^2	μ_{abs}^2 / D^2
(SQA)3-ben	$CHCl_3$	15000 (666)	0.64±0.003 (16700)	0.04 (-0.01) 0.54 (0.16) 1.77 (0.83)	1.56 (0.94)[c]	135	386
	toluene	14900 (671)	0.69±0.001 (16700)	0.08 (-0.21) 0.23 (0.17) 1.84 (0.61)	1.71 (0.96)[c]	123	319
(dSQA)3-ben	$CHCl_3$	14100 (711)	0.43±0.029 (16100)	0.09 (-0.21) 0.88 (0.62) 1.21 (0.17)	0.95 (0.98)[c]	182	893
	toluene	14000 (716)	0.80±0.015 (16700)	0.06 (-0.28) 0.98 (0.27) 1.68 (0.45)	1.51[d]	193	800

[a] Fluorescence quantum yield and excitation wavenumber used for measuring the fluorescence spectra in parentheses. [b] Multiexponential fit of fluorescence decay measured by TSCPC, excitation at 15200 cm^{-1}. Amplitudes are given in brackets. [c] Lifetimes acquired by stretched exponential analysis. Stretching exponent in brackets. [d] Lifetime acquired by distribution analysis. The distribution is shown in the appendix in Fig. S2.

Two Photon Absorption Induced Fluorescence

The 2PA spectrum of **(SQA)$_3$-ben** is qualitatively similar to the one of **SQA**, but slightly shifted to lower energies. Therefore the maximum of the first $A_g \leftarrow A_g$ transition could be observed.

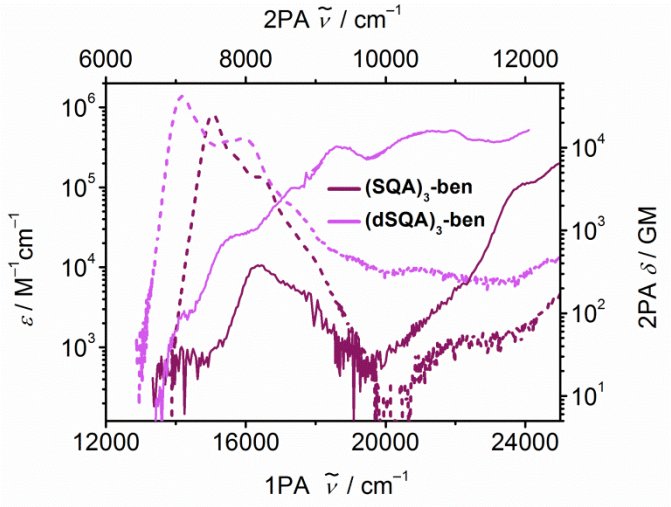

Figure 69 1PA spectra (dashed lines) and 2PA spectra (solid lines) of the trimers **(SQA)$_3$-ben** and **(dSQA)$_3$-ben** in toluene at rt.

In the per squaraine moiety normalised linear 2PA spectrum of the vibronic progression of the S_1 absorption of **SQA** and **$(SQA)_3$-ben** (Figure 70 left) one can see that the relative 2PA cross section has the same size as in the monomer. Unfortunately the maximum of E_2 for **SQA** [17, 21, 62] could not be resolved in our measurement. This would have allowed the evaluation of a true 2PA transition, since the vibronic shoulder showed only additive behaviour in the comparison of **dSQA** and **tSQA** although the other transitions showed cooperative enhancement.

In case of the trimer **$(dSQA)_3$-ben** there are more transitions that can be compared with its parent chromophore. The per squaraine moiety normalised 2PA cross sections at the S''_1 and the S'''_1 bands as well as the band of the vibronic shoulder of the S_1 transition are all equal to the corresponding values of **dSQA,** thus showing additivity (Figure 70 right).

Therefore, it is assumed that in **$(SQA)_3$-ben** the 2PA cross sections of the higher transitions also show additivity. This is in accordance with observations by *Blanchard-Desce et al.*[65] for other superchromophores with a benzene core. Given that the absorption spectra of the star-shaped trimers showed excitonic coupling one would expect more than just additive behaviour. The high oscillator strength of the squaraines should lead to a cooperative behaviour as observed in the linear superchromophores, in spite of the connection by a benzene ring in 1,3,5-position. The merely observed additive behaviour clearly states, that the coupling effect is not so pronounced for the higher excited states. However, the absolute values of the 2PA cross sections for both chromophores have to be taken with care as the determination might possess a systematic error due to surface adsorption effects on the cuvette walls, because the 2PA measurements were performed without silylated cuvettes. This effect especially influences the identification of the exact concentration of the chromophores and consequently also of the fluorescence quantum yield.

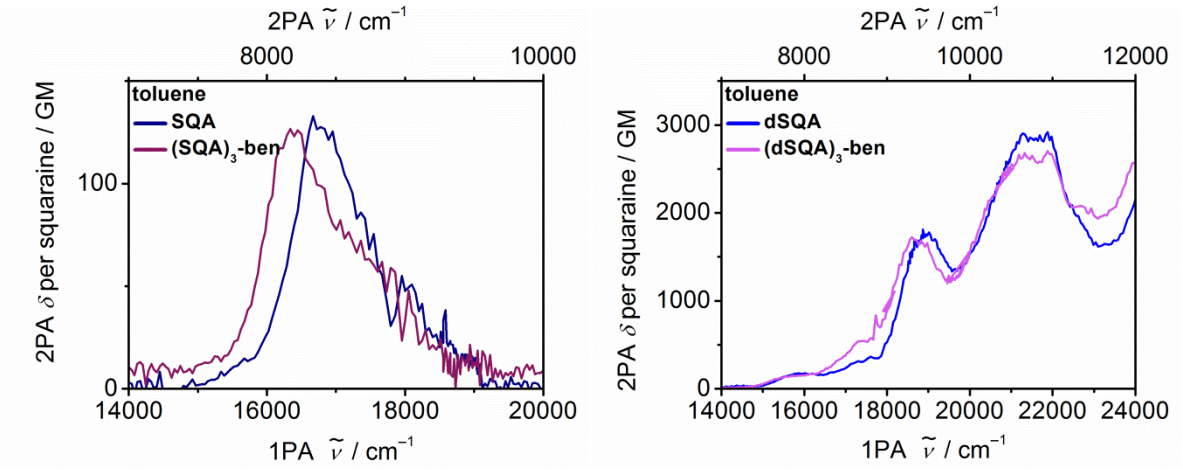

Figure 70 2PA spectra (normalised per squaraine moiety) of **SQA** and **(SQA)$_3$-ben** (left) and the dimer **dSQA** and **(dSQA)$_3$-ben** (right) in toluene at rt.

Table 14 One photon cross section at the absorption maximum and two photon cross sections in the maxima of the squaraines **(SQA)$_3$-ben** and **(dSQA)$_3$-ben** in toluene at rt.

	σ_{max}^{1PA} /10^{-15} cm^2	E_1 /cm^{-1}	δ_1^{2PA} / GM	E_2 /cm^{-1}	δ_2^{2PA} / GM	E_3 /cm^{-1}	δ_3^{2PA} / GM	E_4 /cm^{-1}	δ_4^{2PA} / GM
SQA	1.40	16700	133	25000	800				
(SQA)$_3$-ben	3.10	16400	370	23900	3580				
dSQA	1.78	15900	340	18800	3430	21800	5780	25000	11400
(dSQA)$_3$-ben	5.31	15600	860	18600	10170	21900	16020	24100	16290

Cyclic Voltammetry

The cyclic voltammograms show the same characteristics already observed in the measurements of the parent chromophores. They have one irreversible reduction where all squaraines in the branches get reduced at the same voltage. The same is true for the first oxidation, the sole reversible process, and the second oxidation of **(SQA)$_3$-ben**.

In **(dSQA)$_3$-ben** the first oxidation splits to two separable processes. First each branch gets oxidised once then they get oxidised a second time. The half wave potential at 580 mV covers six electrons in the DPV.

The band gap of the trimers is within the limits of measurement accuracy identical to the band gap of the linear squaraines. This indicates that there is nearly no interaction between the single branches in the ground states.

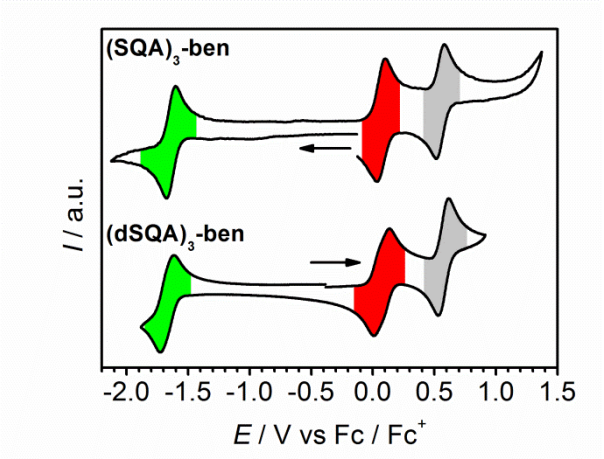

Figure 71 Cyclic voltammograms of **$(SQA)_3$-ben** and **$(dSQA)_3$-ben** in $CH_2Cl_2/^nBu_4PF_6$ (0.2 M) at a scan rate of 100 mV s^{-1}. All voltammograms are referenced against (Fc/Fc^+) and normalised. The scanning direction is indicated by the arrows.

Table 15 Redox potentials ($E_{1/2}$), HOMO and LUMO energy levels and band gaps of **$(SQA)_3$-ben** and **$(dSQA)_3$-ben** in $CH_2Cl_2/ ^nBu_4PF_6$ (0.2 M) at a scan rate of 100 mV s^{-1} and referenced against (Fc/Fc^+).

	$E^{red}_{1/2}$ / mV	$E^{ox}_{1/2}$ / mV	$E^{ox}_{1/2}$ / mV	$E^{ox}_{1/2}$ / mV	E_{HOMO} / eV	E_{LUMO} / eV	E_{gap} / eV
$(SQA)_3$-ben	-1635[i]	70[r]		550[i]	-5.23	-3.52	1.71
$(dSQA)_3$-ben	-1670[i]	50[r,fit]	75[r, fit]	580[i]	-5.21	-3.49	1.72

[i] irreversible, [r] reversible, [fit] fitted with Digi Elch

Transient Absorption Spectroscopy

Both star-shaped trimers **$(SQA)_3$-ben** and **$(dSQA)_3$-ben** were examined by transient absorption spectroscopy. The smaller trimer **$(SQA)_3$-ben** was excited only at the maximum of the absorption spectrum because the higher excitonic state lies within the vibronic shoulder of the S_1 state while **$(dSQA)_3$-ben** was excited both at the lowest and the highest maximum of the exciton manifold. The excited states were probed by white light between 400 – 800 nm. The transient maps were analysed with a sequential model resulting in evolution associated difference spectra (EADS). The estimated state energies of the superchromophores are given in Figure 72 together with the lifetimes of the EADS. The transient absorption spectra, the time scans at selected wavenumbers and the EADS of **$(SQA)_3$-ben** (Figure 73) and **$(dSQA)_3$-ben** (Figure 74) in toluene are shown and discussed in the following.

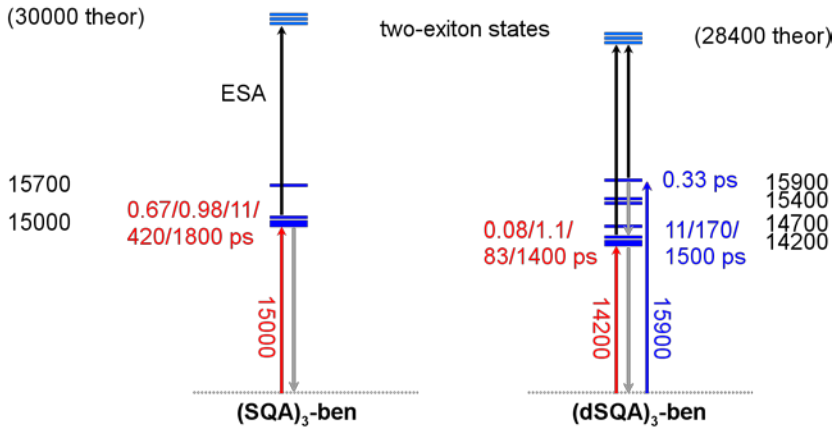

Figure 72 State diagrams of the transient absorption spectra of **$(SQA)_3$-ben** and **$(dSQA)_3$-ben**. Lifetimes in red are for excitation into the maximum of the lowest exciton band, those in blue for excitation into the maximum of the the lowest exciton band at the given wavenumbers. The state energies were estimated by the peak positions of respective absorption bands. The two-exciton states were estimated (= theor) from the energies of the mono-exciton states. Lifetimes separated by a slash indicate multiexponential decay process from multiple levels with slightly different energy (given as one bold bar). All the energies are not to scale.

Upon excitation at 15000 cm^{-1} the transient map of **$(SQA)_3$-ben** shows one intense negative peak at ~15000 cm^{-1} that represents the GSB and SE. The first ESA is only slightly above this region because of the small excitonic coupling between the separate branches. In the region above 16700 cm^{-1} there is an additional broad ESA that becomes even broader within a few 100 ps. The sequential fit of the transient map shows one EADS with a lifetime of 670 fs that shows a few differences to the other four EADS with longer lifetimes. The narrow negative peak at 15100 cm^{-1} is slightly shifted to the blue in comparison to the same feature of the others. In addition the ESA in the high energy region is comparatively small. The time traces of the GSB/SE (15000 cm^{-1}) and the ESA (18500 cm^{-1}) show a local minimum/maximum at ~0.4 ps that is associated with this EADS. The following three EADS with lifetimes of 0.98 ps, 11 ps and 0.42 ns are associated with relaxation processes and the last one (1.8 ns) with ground state recovery. The longer lifetimes are in the same region as the ones acquired by the multiexponential fit of the TCSP (see Table 13).

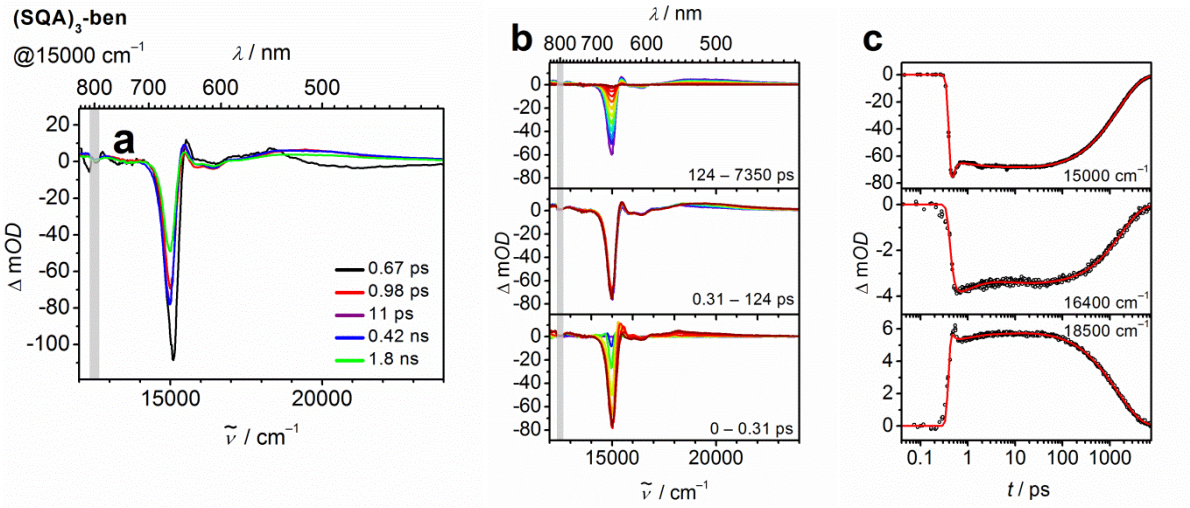

Figure 73 Evolution associated difference spectra (EADS) of **(SQA)$_3$-ben** in toluene for excitation at 15000 cm^{-1} (a). The spectra at 12500 cm^{-1} ± 200 cm^{-1} (grey bar) are influenced by the laser fundamental and should be taken with caution. The colour code of the EADS refers to the dimension of lifetime. The transient absorption spectra (b) and the time scans at selected wavenumbers (c) were corrected for chirp and scattered light. Early spectra are given in blue, the later spectra in red.

The larger trimer **(dSQA)$_3$-ben** displays a similar behaviour upon excitation at the lowest maximum of the exciton manifold. Again the most prominent peak of the EADS with the shortest lifetime (80 fs) is blue shifted by 100 cm^{-1} in comparison to the consecutive EADS. However, this time the local minimum of the GSB/SE (14100 cm^{-1}) is barely discernible, while one can clearly observe a local maximum of the ESA (16600 cm^{-1}). The lifetime of the ground state recovery is with 1.4 ns slightly shorter than the one obtained by the distribution analysis of the TCSPS measurement (1.51 ns).

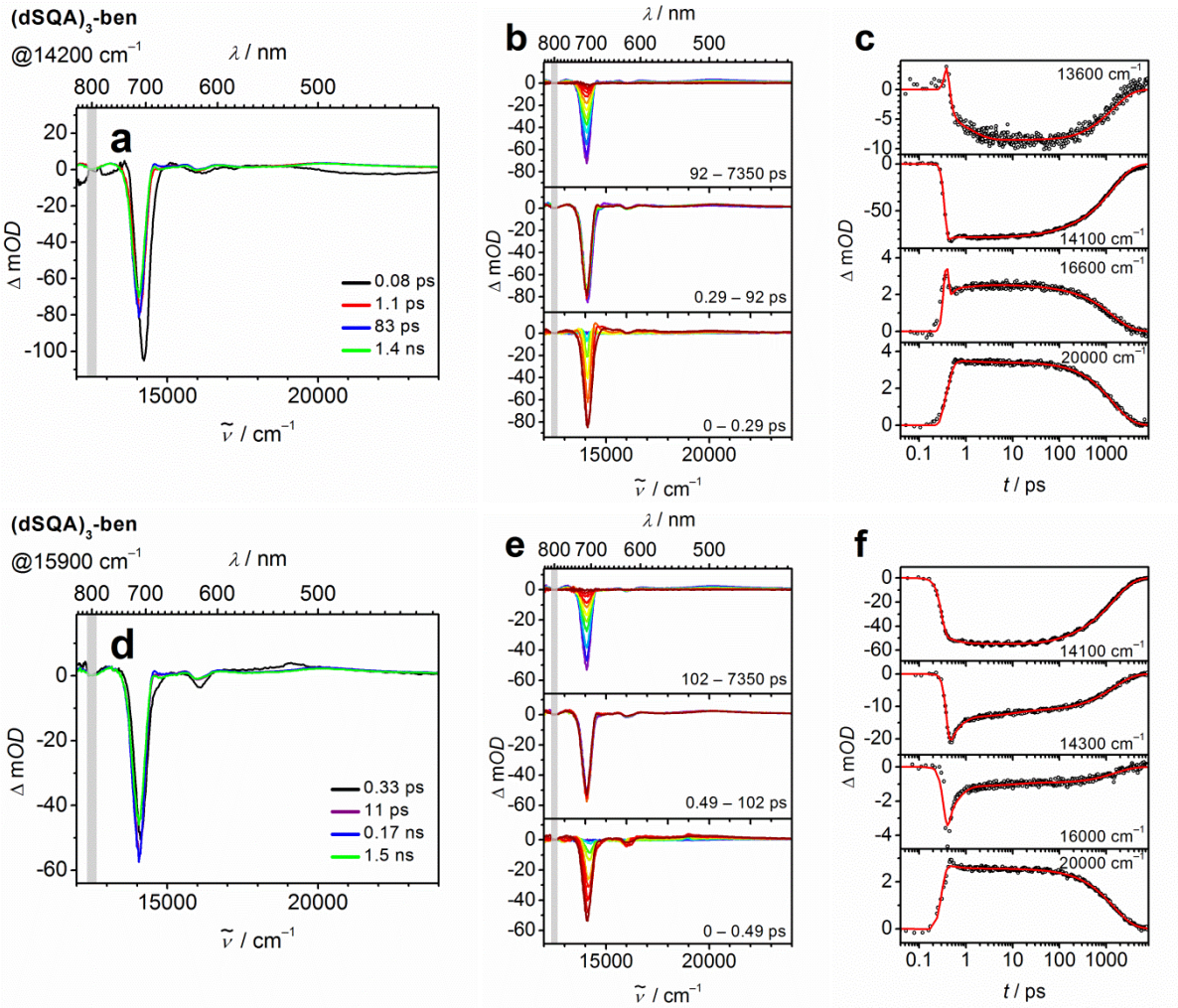

Figure 74 Evolution associated difference spectra (EADS) of **(dSQA)$_3$-ben** in toluene for excitation at 14200 cm^{-1} (a) and at 15900 cm^{-1} (d). The spectra at 12500 cm^{-1} ± 200 cm^{-1} (grey bar) are influenced by the laser fundamental and should be taken with caution. The colour code of the EADS refers to the dimension of lifetime. The transient absorption spectra (b, e) and the time scans at selected wavenumbers (c, f) were corrected for chirp and scattered light. Early spectra are given in blue, the later spectra in red.

The transient map upon excitation at 15900 cm^{-1} looks a bit different. Here initially the highest state of the exciton manifold is populated. This is indicated by the negative peak at 16000 cm^{-1} and by the minimum in the respective time trace. At the high energy side of the absorption a very similar time trace can be observed (14300 cm^{-1}) while the local minimum at ~0.3 ps is absent in the time traces at 14100 cm^{-1}. This behaviour was already established as an intraband relaxation process from the higher exciton level to S_1 in the linear superchromophores **dSQA** and **tSQA**. The sequential fit of the maps results in four EADS. The first one with a lifetime of 0.33 ps is associated to the highest state of the exciton manifold and is in the same dimension as the correspondent EADS of **dSQA** (0.25 ns, Figure 64d). The

other three EADS correspond to relaxation processes (11 ps, 0.17 ns) and ground state recovery (1.5 ns).

The peculiar features within the first picosecond of the transient measurements upon excitation at the lowest energy maximum of the exciton manifold and their possible reasons are discussed exemplarily for **(dSQA)$_3$-ben** in the following.

First of all one has to notice that the multiple processes that can cause this short lived component are hard to discern given the short timescale, therefore only the possibility of the different reasons is discussed. For a more detailed analysis the time resolution of the measurement has to be optimised by *e.g.* the usage of cuvettes with smaller glass walls and/or broader and therefore shorter laser pulses.

The signal (black component in Figure 74a) might be caused by a coherent artefact, since a similar behaviour is also visible in other star-shaped superchromophores after excitation into the lowest exciton band. Indeed such an artefact was observed in pure toluene and is intensity depended on the pump power. If one has a closer look at all transient measurements after excitation into the lower exciton manifold one can always see a small coherent artefact. The signal is quite small in the star-shaped trimers with a nitrogen-core and larger in the other star-shaped trimers. In the transient spectra of **(SQA)$_3$-bor** the signal is still visible at ~4 ps (Figure 92). Hence, it is assumed that the pronounced signals are not only caused by a coherent artefact but also by some additional effect.

One of these effects is transient hole-burning of the ground state population.[127-133] As already discussed for the star-shaped trimers with a nitrogen core there is doubt whether this effect can really be discerned from coherent artefacts when pump and probe pulse overlap in time.[134] Therefore, hole-burning cannot be excluded as a possible reason for the observed signal.

Another of these effects might be that one single superchromophore absorbs not one but two pump photons simultaneously in a nonlinear optical process. In this case the molecule would be excited into the two-exciton state with an estimated state energy of two times the energy of S_1 (Figure 72). The observed probe signal should consist of the GSB, that is unaffected by the energy of the excited chromophores, and of the SE and the ESA of the two-exciton state. The molecule would relax very fast to a state that is formally derived from the S_1 state of a single squaraine. From this state an excitation to the two exciton state

should be possible, accordingly there should be an ESA signal in close proximity of the lower energy maximum of the exciton manifold. In comparison of the normed first and second EADS of **(dSQA)$_3$-ben** one can see that the negative peak is shifted to lower wavenumbers during the measurement (Figure 75). This shift is smaller on the low energy side than on the high energy side. The shift on the low energy side would be associated with the change of the SE, the shift on the high energy side to the ESA to the two exciton state.

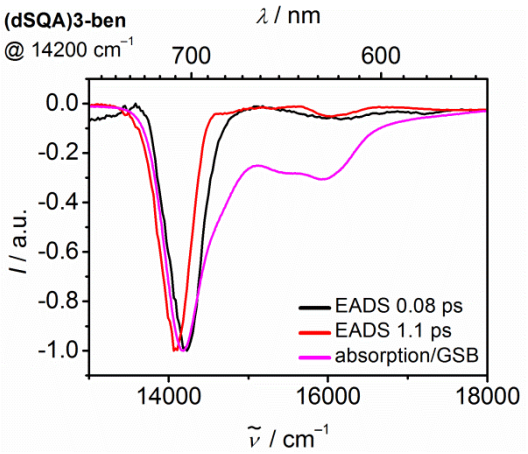

Figure 75 The normed first and second EADS of **(dSQA)$_3$-ben** in toluene for excitation at 14200 cm^{-1} together with the negative normed absorption spectrum of **(dSQA)$_3$-ben** representing the GSB.

The probability to excite one chromophore is determined by the number of photons per area and its one photon absorption cross section. Naturally, for a two photon process the two photon absorption cross section, which in turn depends on the two photon absorption cross section, has to be taken into account. For such a nonlinear process the intensity of the light after its propagation through a sample with the thickness *x* can be calculated by eq. (59)[152]

$$I_{out} = I_{in} \frac{(1-R)^2 e^{-\alpha x}}{1+\frac{\beta}{\alpha} I_{in}(1-R)(1-e^{-\alpha x})} \tag{59}$$

with I_{in} as the light intensity before the sample, *R* as the reflectivity of the sample, *α* as the linear absorption coefficient and *β* as the coefficient responsible for the two photon absorption. If the reflectance by the sample and its linear absorbance are neglected, the formula for the output intensity in case of pure 2PA can be simplified to eq. (60)[152]

$$I_{out} \approx \frac{I_{in}}{1+\beta x I_{in}} \tag{60}$$

The molecular absorption coefficient for 2PA is defined as:

$$\alpha_2 = -\frac{I_{out}}{N\, I_{in}^2} \tag{61}$$

with, *N* as the number of molecules per unit volume.[42]

Therefore, if the observed signal is indeed caused by 2PA one would expect that its intensity scales quadratically with the pump energy. Consequently, the TA measurement was repeated with gradient laser power (Figure 66). For an easier comparability the relevant time traces were divided by their respective pump power. In the traces at 14200 cm^{-1} the relative intensity of the minimum at ~0.3 ps remained nearly unchanged while at 16600 cm^{-1} the signal is not visible at low intensities but gains intensity at higher ones. Given that the signals at 10 nJ and 20 nJ have a very bad signal to noise ratio due to the very small spectral change, a reliable interpretation is not possible. However, the dependency of the signal seems not to be quadratic. The difference in intensity is therefore assigned to the coherent artefact that is pump energy dependent as observed in the measurements of the pure solvent.

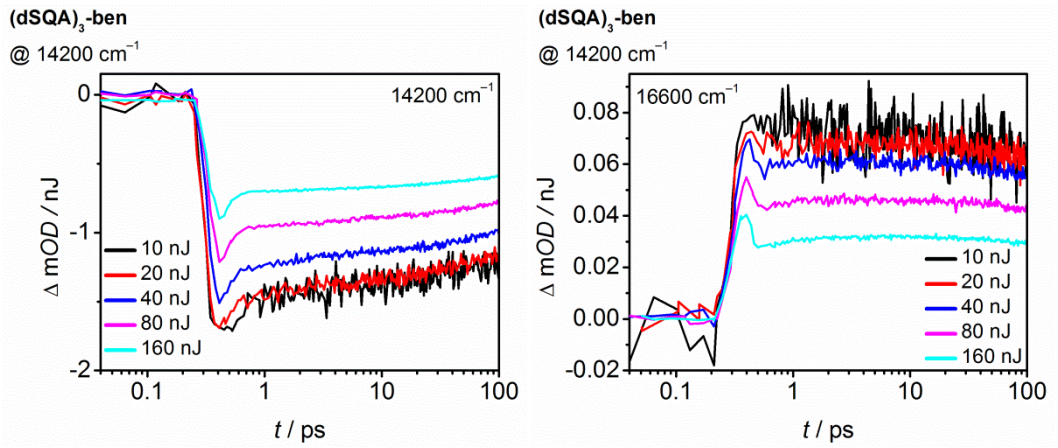

Figure 76 Time traces of the transient absorption of **(dSQA)$_3$-ben** in toluene for excitation at 14200 cm^{-1} divided by the pump energies per pulse.

Nevertheless the transient measurements at gradient intensities show another peculiar behaviour. The probability *P* for the excitation of one chromophore can be calculated by eq. (62)

$$P = 1 - \exp\left(- \frac{E}{(hc/\lambda)\pi (D/2)^2} \frac{\ln(10)1000\varepsilon}{N_{Av}} \right) \tag{62}$$

with the energy per pulse *E*, the wavelength of the pulse λ, the diameter of the laser beam *D*, Planck´s constant *h*, the speed of light *c*, the molar extinction coefficient ε and Avogadro´s constant N_{Av}.[152] Since the energy per pulse is the only variable throughout the measurement and 2PA was already excluded, one would expect to observe a linear dependency in this energy region. However, the relative intensity of the signal decreases with rising pump energy. This means, that in the measurements an additional effect occurs, that cannot be explained. In addition the absolute values have a certain error because after the measurements it was determined that the power of the pulses was indeed higher than first assumed. Therefore, the depicted values have to be taken as the lower threshold and as a result the relative spectra of the higher energies would be even lower in intensity.

The principle assumptions that were made for the 2PA could be used for another explanation for the signals. One or two branches of the superchromophores could be distorted. This deviation of the idealised C_3 symmetry of the chromophores (Figure 67) leads to a decrease of the interaction of the transition-dipole moments of the single branches, which in turn results in a weakening of the excitonic coupling and ultimately, causes a relative blue shift of the absorption. These distorted molecules might be excited preferentially. The red shift between the first and the second EADS would be the result of structural reorientation. This procedure is quite unlikely because of the small timescale with only a few 100 fs. In addition one would expect a longer lifetime for the first EADS in the case of the larger **(dSQA)$_3$-ben** in comparison to the smaller **(SQA)$_3$-ben**. A more likely explanation is that due to the structural distortion the degenerated eigenstates at the lowest exciton manifold split (Figure 67). As a result the chromophores could be excited to the upper one of these two states. The lifetime of the first EADS would then be associated with an intraband relaxation to the lowest state. This process is accompanied by a spectral shift of both the SE and the ESA. The structural reorientation of the superchromophores happens on a longer timescale than the lifetime of the excited state and is therefore not observed. A clearly visible confirmation for the deviation of the idealised C_3 symmetry is the absorption

peak for S'_1, as the transition-dipole moment of this state would be zero in a symmetrical molecule.

This would also explain why this behaviour is not observed in the linear squaraines, as there are no degenerated eigenstates.

Conclusion

Two star-shaped squaraine trimers with a benzene core were synthesised via palladium catalysed *Suzuki* cross coupling reactions. In **$(SQA)_3$-ben** each of the three branches consists of one transoid squaraine and in **$(dSQA)_3$-ben** each branch consist of two directly coupled transoid squaraines, hence, the linear squaraines **SQA** and **dSQA** are used as their reference compounds. In comparison the absorption spectra of the trimers are red-shifted by 400 – 500 cm^{-1} and show one additional peak in the exciton manifold. This peak is caused by excitonic coupling of the three branches via the benzene core. In comparison the squares of the transition-dipole moments show nearly additivity.

The transient spectra of **$(dSQA)_3$-ben** with fs time resolution and pump pulse at the highest maximum of the absorption spectrum show the same behaviour as the spectra of the linear dimer. The initially excited highest state of the exciton manifold is depopulated in 0.33 ps and the ground state recovery is slightly faster with 1.4 ns. In contrast the spectra for both star-shaped trimers display upon excitation at the lowest maximum of the exciton manifold a prominent feature below 1 ps that is not observed in this magnitude for the linear compounds. Admittedly a small portion of this signal is caused by a coherent artefact as it is also observed in the pure solvent but the bigger part has to have another origin. The most likely cause is a splitting of the formally degenerated S_1 states in the superchromophores. Accordingly, the signal is caused by the initial population of the upper one of these states followed by intraband relaxation to the lower one. The most obvious proof that the superchromophores do not adopt ideal C_3 symmetry is the observation of the maximum for the highest exciton state, as its transition-dipole moment would be zero in the symmetrical case.

The star-shaped coupling of three squaraines has nearly no influence on the emissive behaviour of the chromophores besides a red-shift. The only other noticeable deviation is the magnitude of the transition-dipole moments of the fluorescence. They are not additive

but larger than in the monomer, indicating a small excitonic coupling and emission from more localised states.

The two photon absorption spectra of the star-shaped trimers correlate with the spectra of their linear reference chromophores with a slight red shift. The per squaraine moiety normalised spectra clearly show merely additive behaviour for the superchromophores. Therefore, it is assumed that the exciton coupling does not have the expected influence on the higher excited states.

The trimerisation had no influence on the electrochemical characteristics of the chromophores, meaning that there is nearly no interaction between the single branches.

3.3.4 Star-Shaped Trimers with a Triarylamine Core

Synthesis

The *Suzuki*-coupling reaction of 3.5 equivalents of the mono brominated *trans*-squaraine **SQA-Br** with one equivalent of tris(4-(4, 4, 5, 5-tetramethyl-1,3,2-dioxaborolan-2-yl)phenyl)amine (**31**) yielded 18 % of the trimer **$(SQA)_3$-TAA**. The reaction of the mixed squaraine **SQC-Br** with the same conditions resulted in 8 % of the trimer **$(SQC)_3$-TAA**. It was not possible to isolate the trimer **$(SQD)_3$-TAA** from the reaction mixture of the other mixed squaraine **SQD-Br** due to its instability (Scheme 44).

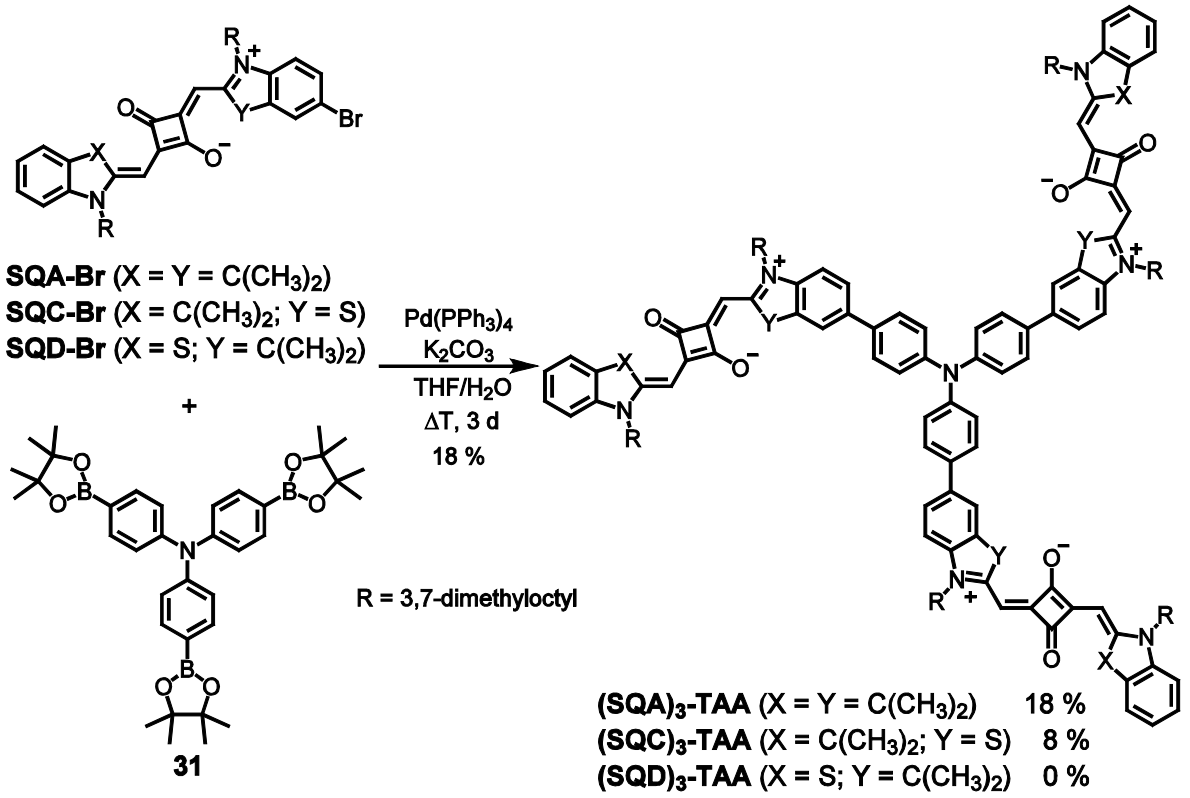

Scheme 44 Synthesis of the star-shaped *trans*-trimers $(SQA)_3$-TAA and $(SQC)_3$-TAA.

The trimer **$(SQB)_3$-TAA** was isolated in a yield of 8 % from the analogue reaction of squaraine **SQB-Br** with the triarylamine core.

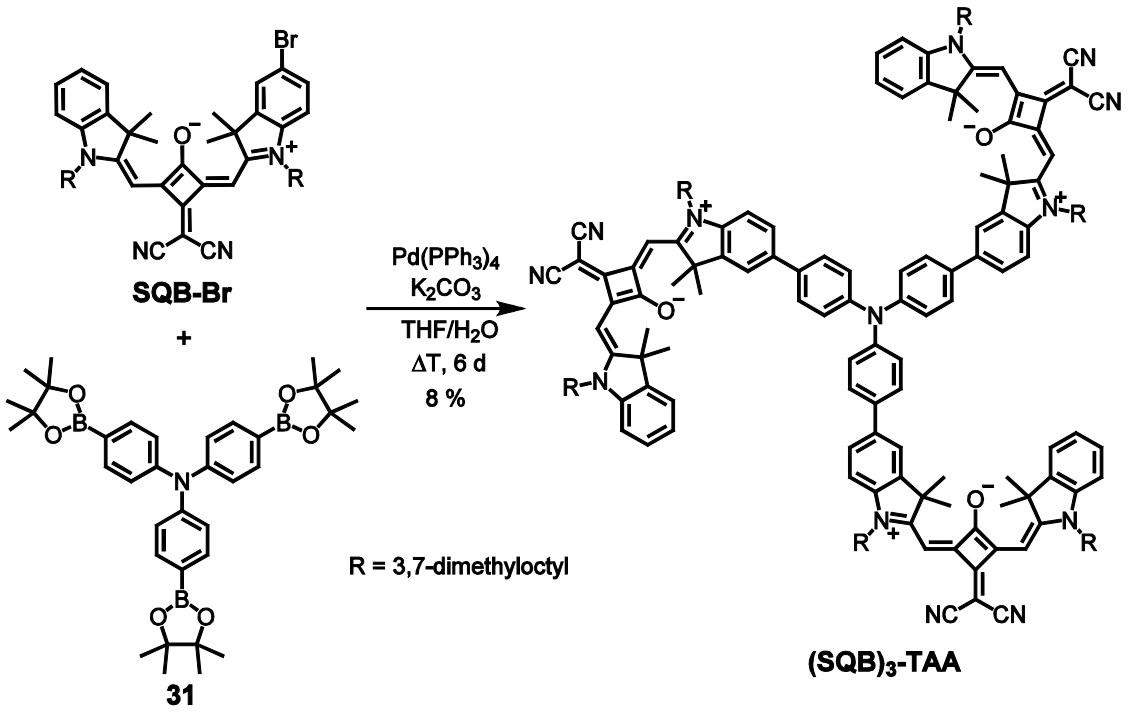

Scheme 45 Synthesis of the star-shaped *cis*-trimer $(SQB)_3$-TAA.

Absorption Spectroscopy

First the absorption spectra of the monomers **SQA**, **SQB**, **SQC-Br** and **SQD-Br** (Figure 77 and Table 16) are discussed before the results of the trimers are presented.

In the squaraine **SQB** one oxygen atom of the central cyclobutadiene ring is replaced by a dicyanomethylene group. This leads to an increased electron acceptor strength and a lowering of the LUMO energy resulting in a red-shift of the main absorption band by ca. 1100 cm^{-1}.[15] Due to its steric demand the dicyanomethylene group forces the chromophore into a cisoid configuration. Therefore the squaraine is no longer centrosymmetric but belongs to the C_{2v} symmetry group. The extinction coefficient and the square of the transition-dipole moment are smaller compared to the transoid **SQA**.

The absorption maxima and the extinction coefficients of the mixed compounds **SQC-Br** and **SQD-Br** are in between the transoid and the cisoid pure indolenine chromophore. The addition of two bromine groups to unsubstituted indolenine squaraines leads to a red-shift of the absorption by roughly 200 cm^{-1}.[15, 24] Therefore one can assume a shift of ca. 100 cm^{-1} if only one bromine group is attached.[98] The extinction coefficient of the transoid squaraine gets smaller by 10 % due to the substitution with the two halogens while in the cisoid compound the maximum has a 10 % higher value.

Taking this into account the absorption of **SQC** = **SQD** in toluene should be at ~15200 cm^{-1} with an extinction coefficient of 300000 M^{-1} cm^{-1}. Hence, the effect of the substitution is slightly stronger if the bromine is located at the benzothiazole as it is the case in **SQC-Br**.

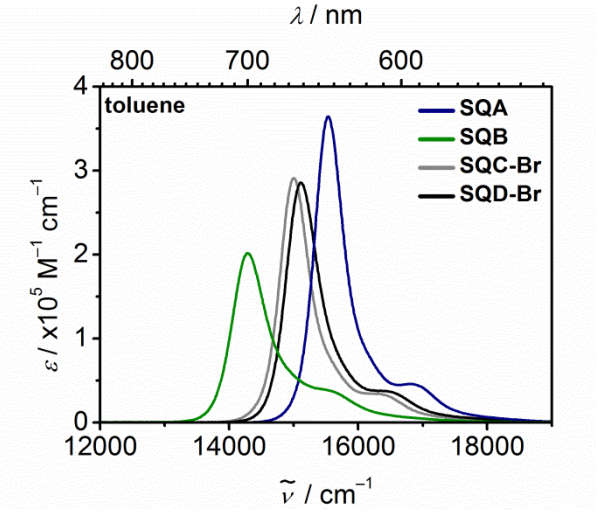

Figure 77 Absorption spectra of the squaraines **SQA**, **SQB**, **SQC-Br** and **SQD-Br** in toluene at rt.

Table 16 Absorption maxima, extinction coefficients and squares of the transition dipole moments of the squaraines **SQA**, **SQB**, **SQC-Br** and **SQD-Br** in various solvents at rt.

	solvent	$\tilde{\nu}_{abs}$ / cm^{-1} (nm)	ε / M^{-1} cm^{-1}	μ^2 / D^2
SQA	CH_2Cl_2	15700 (639)	328000	130
	$CHCl_3$	15700 (639)	347000	129
	toluene	15500 (643)	365000	127
SQB	CH_2Cl_2	14600 (685)	195700	102
	$CHCl_3$	14600 (687)	193700	98.6
	toluene	14300 (700)	202000	92.7
SQC-Br	CH_2Cl_2	15200 (660)	287400	121
	$CHCl_3$	15200 (657)	300000	119
	toluene	15000 (667)	290700	107
SQD-Br	CH_2Cl_2	15300 (654)	259700	123
	$CHCl_3$	15300 (653)	275100	119
	toluene	15100 (662)	285500	112

The star-shaped trimers **$(SQA)_3$-TAA**, **$(SQB)_3$-TAA** and **$(SQC)_3$-TAA** with triarylamine as the connecting core unit show a broadening of the lowest energy absorption band (Figure 78). This is indicative of a weak exciton coupling effect. The bathochromic shift of about 400 – 500 cm^{-1} is due to the addition of the propeller-like triarylamine donor to the quadrupole dyes, thereby breaking the symmetry of the squaraine moieties.[24, 98] The squares of the transition-dipole moments roughly triple upon the trimerisation following the *Thomas-Reiche-Kuhn* sum rule.[123]

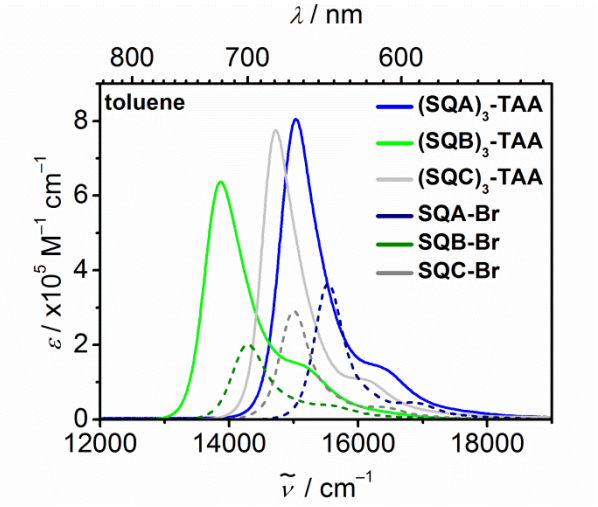

Figure 78 Absorption spectra of the trimers **$(SQA)_3$-TAA**, **$(SQB)_3$-TAA** and **$(SQC)_3$-TAA** and their parent chromophores **SQA-Br**, **SQB-Br** and **SQC-Br** (dashed lines) in toluene at rt.

Table 17 Absorption maxima, extinction coefficients, squares of the transition dipole moments, fluorescence maxima, fluorescence quantum yields and coupling constants of the squaraine trimers **(SQA)$_3$-TAA**, **(SQB)$_3$-TAA** and **(SQC)$_3$-TAA** in various solvents at rt.

	solvent	$\tilde{\nu}_{abs}$ / cm^{-1} (nm)	ε / M^{-1} cm^{-1}	μ^2 / D^2
(SQA)$_3$-TAA	CH_2Cl_2	15100 (661)	830400	435
	$CHCl_3$	15100 (661)	860300	438
	toluene	15000 (665)	804900	363
(SQB)$_3$-TAA	CH_2Cl_2	14100 (708)	615500	384
	$CHCl_3$	14100 (709)	597500	361
	toluene	13900 (721)	636800	332
(SQC)$_3$-TAA	CH_2Cl_2	14900 (672)	740300	363
	$CHCl_3$	14900 (670)	759100	354
	toluene	14700 (679)	774600	324

Fluorescence Spectroscopy

The star-shaped trimers show the typical emission behaviour of squaraines. The fluorescence spectra are the mirror images of the lowest energy absorption band of the monomers with a *Stokes* shift of 200 – 300 cm^{-1}. The change of the solvent from toluene to $CHCl_3$ has a slight effect on the mixed superchromophore **(SQC)$_3$-TAA**, while the cisoid **(SQB)$_3$-TAA** has a significantly smaller quantum yield and less than half of the lifetime. The squares of the fluorescence transition dipole moments indicate that in the star-shaped superchromophores a week excitonic coupling takes place and the emission arises from more localised states.

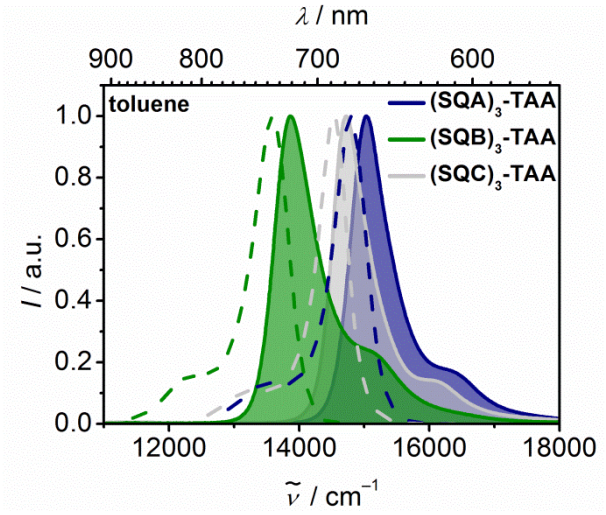

Figure 79 Absorption spectra (shaded areas) and fluorescence spectra (dashed lines) of the trimers **(SQA)$_3$-TAA**, **(SQB)$_3$-TAA** and **(SQC)$_3$-TAA** in toluene at rt.

Table 18 Fluorescence maxima, quantum yields, lifetimes, squares of the fluorescence and absorption transition dipole moments of the squaraines **$(SQA)_3$-TAA**, **$(SQB)_3$-TAA** and **$(SQC)_3$-TAA** in $CHCl_3$ and toluene at rt.

	solvent	$\tilde{\nu}_{fl}$ / cm^{-1}	$\phi_{fl}(\tilde{\nu}_{fl}$ / $cm^{-1})$[a]	τ_{fl} / ns (TCSPC)[b]	$\bar{\tau}_{fl}$ / ns	μ_{fl}^2 / D^2	μ_{abs}^2 / D^2
$(SQA)_3$-TAA	$CHCl_3$	14800 (675)	0.54±0.013 (16700)	0.25 (-0.16) 0.36 (0.25) 1.48 (0.59)	1.32 (0.95)[c]	142	438
	toluene	14800 (676)	0.71±0.009 (16700)	0.05 (-0.13) 0.48 (0.12) 1.96 (0.75)	1.79 (0.96)[c]	125	363
$(SQB)_3$-TAA	$CHCl_3$	13800 (727)	0.30±0.013 (15200)	1.41	1.32 (0.95)[c]	100	361
	toluene	13600 (735)	0.75±0.020 (15200)	3.06	3.02 (0.99)[c]	102	332
$(SQC)_3$-TAA	$CHCl_3$	14700 (680)	0.63±0.016 (16100)	0.25 (-0.29) 0.30 (0.31) 2.19 (0.40)	2.04 (0.96)[c]	108	354
	toluene	14600 (687)	0.66±0.007 (16700)	0.11 (-0.12) 0.46 (0.08) 2.34 (0.80)	2.22 (0.98)[c]	84.6	324

[a] Fluorescence quantum yield and excitation wavenumber used for measuring the fluorescence spectra in parentheses. [b] Multiexponential fit of fluorescence decay measured by TSCPC, excitation at 15200 cm^{-1}. Amplitudes are given in brackets. [c] Lifetimes acquired by stretched exponential analysis. Stretching exponent in brackets.

Two Photon Absorption Induced Fluorescence

Before the 2PAF of the star-shaped trimers **$(SQA)_3$-TAA** and **$(SQB)_3$-TAA** are discussed the findings for the cisoid **SQB** are presented.

The 2PAF spectrum of **SQB** is depicted in Figure 80 together with the 1PA and the fluorescence excitation anisotropy spectrum. In theory the parity selection rules that apply to **SQA** should not hold true for **SQB** because of its C_{2v} symmetry. Consequently all 1PA states should also be 2PA allowed. In practice the 2PAF spectrum of **SQB** is very similar to the one of **SQA** only red-shifted by the same 1100 cm^{-1} like the 1PA and with smaller intensities. There is one weak 2PA cross section at the vibronic shoulder of the S_1 absorption and a higher δ_{2PA} at the S_2 transition at ca. 22800 cm^{-1}. According to TD-DFT computations (see Appendix Table S7) both states have B_2 symmetry and are polarised along the long axis

of the molecule. The S_3 state at ~25000 cm^{-1} is an A_1 state and polarised along the molecular C_2 axis. This state is out of reach of the 2PAF experiment because the quadratic dependence of the fluorescence intensity and the laser power is no longer achieved near the 1PA. The theoretical calculations are in good agreement with the fluorescence excitation anisotropy measurements.

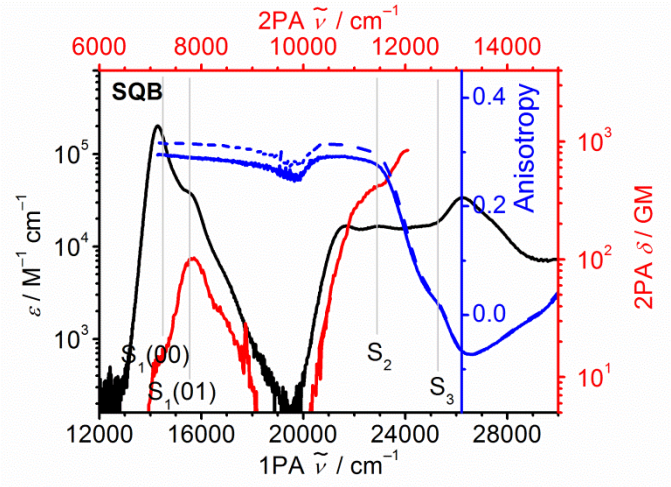

Figure 80 1PA spectrum (black) and 2PA spectrum (red) of **SQB** in toluene together with the fluorescence excitation anisotropy spectrum in polyTHF at 26°C (blue) and at 20°C (dashed blue).

The star-shaped superchromophore **$(SQA)_3$-TAA** displays a similar 2PA spectrum as its parent compound. In the comparison of the per squaraine normalised spectra of **SQA** and **$(SQA)_3$-TAA** (Figure 81 left) the vibronic progression at 17000 cm^{-1} has slightly more intensity in the trimer. The second maximum at E_2 cannot be compared, as the maximum of the S_0 to S_2 transition of **SQA** is not observed in the 2PA measurement. Therefore, the spectrum of **$(SQA)_3$-ben** is also depicted. If one assumes that the star-shaped trimer with the benzene core only displays additive behaviour this comparison clearly shows that **$(SQA)_3$-TAA** presents cooperative behaviour.

The spectrum of the trimer **$(SQB)_3$-TAA** resembles the one of the monomer as well (Figure 81 right). In this case the vibronic progression of the per squaraine normalised spectrum of the trimer has roughly 50 % more intensity than the 2PA of the parent squaraine. The transition at E_2 is even more enhanced.

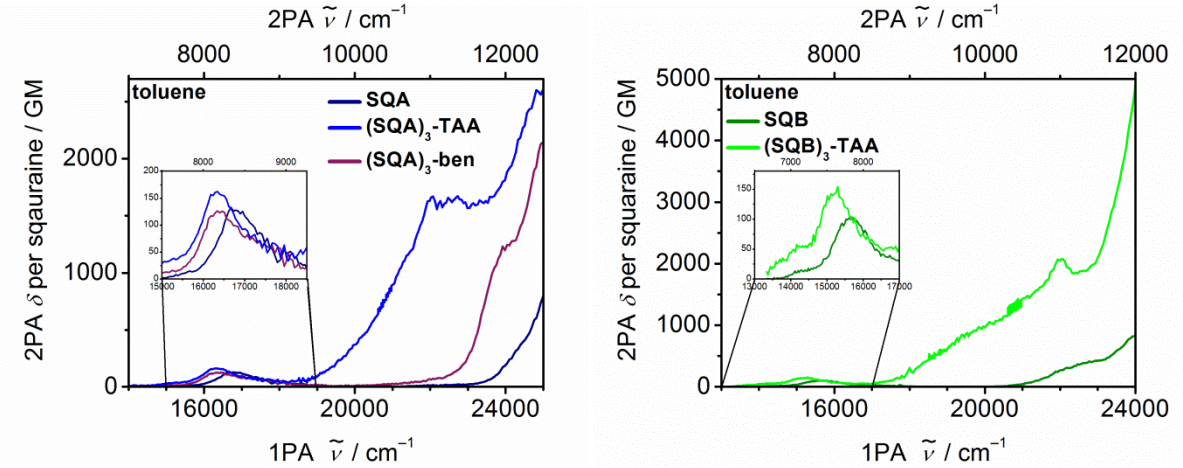

Figure 81 2PA spectra (normalised per squaraine) of **SQA**, **(SQA)$_3$-TAA** and **(SQA)$_3$-ben** (left) and **SQB** and **(SQB)$_3$-TAA** (right) in toluene at rt.

Comparing the 2PA spectra of the trimers in Figure 82 one notices that they are red-shifted by a similar value as the 1PA spectra. Although the extinction coefficients of the one photon absorption of the cisoid squaraines are smaller than the ones of the transoid chromophores the nonlinear absorption has a very similar intensity in both compounds. Consequently, there seems to be a cooperative enhancement effect in both trimers.

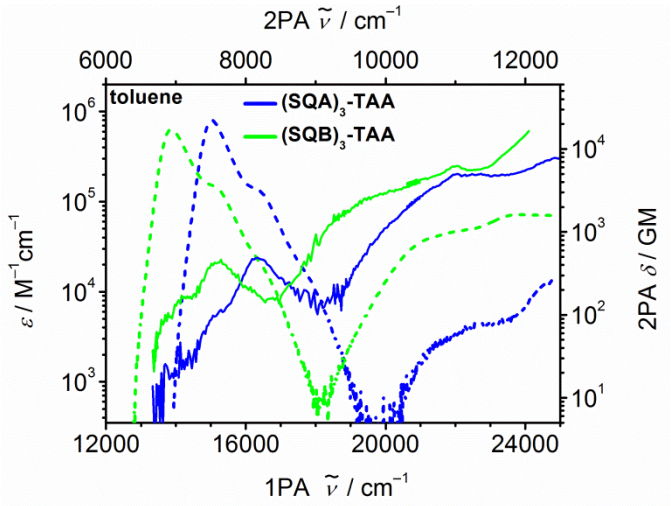

Figure 82 1PA spectra (dashed lines) and 2PA spectra (solid lines) of the trimers **(SQA)$_3$-TAA** and **(SQB)$_3$-TAA** in toluene at rt.

Table 19 One photon cross section at the absorption maximum and two photon cross sections in the maxima of the squaraines **(SQA)$_3$-TAA** and **(SQB)$_3$-TAA** in toluene at rt.

	σ_{max}^{1PA} /10^{-15} cm^2	E_1 /cm^{-1}	δ_1^{2PA} / GM	E_2 /cm^{-1}	δ_2^{2PA} / GM	E_3 /cm^{-1}	δ_3^{2PA} / GM
SQA	1.40	16700	133	25000	800		
(SQA)$_3$-TAA	3.10	16500	470	22100	4890		
SQB	0.903	15600	100	22800	400		
(SQB)$_3$-TAA	2.44	15300	465	22000	6220	24100	16470

Cyclic Voltammetry

The cyclovoltammograms of the trimers show the typical processes of squaraines. There is one irreversible reduction and two oxidation processes. The first one is reversible the second one is irreversible. The oxidation of the central triarylamine core takes place after the second squaraine oxidation (purple area in Figure 83). In the DPV this process has roughly 1/3 intensity of the other processes which proves that in every other process each branch gets oxidised or reduced.

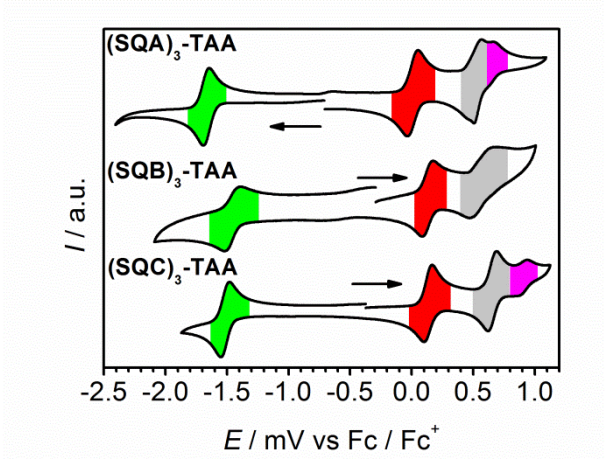

Figure 83 Cyclic voltammograms of **(SQA)$_3$-TAA**, **(SQB)$_3$-TAA** and **(SQC)$_3$-TAA** in CH_2Cl_2/$^nBu_4PF_6$ (0.2 M) at a scan rate of 100 mV s^{-1}. All voltammograms are referenced against (Fc/Fc^+) and normalised. The scanning direction is indicated by the arrows.

In the cisoid star-shaped squaraine the reduction is shifted by ca. 200 mV and the first oxidation by 100 mV compared to the transoid trimer. Therefore the band gap becomes a bit smaller. In the mixed squaraine trimer the whole voltammogram is moved to higher voltages by ~150 mV. Noticeable is the strong shift of the oxidation of the triarylamine by 300 mV.

Table 20 Redox potentials ($E_{1/2}$), HOMO and LUMO energy levels and band gaps of **$(SQA)_3$-TAA**, **$(SQB)_3$-TAA** and **$(SQC)_3$-TAA** in $CH_2Cl_2/^nBu_4PF_6$ (0.2 M) at a scan rate of 100 mV s^{-1} and referenced against (Fc/Fc^+).

	$E^{red}_{1/2}$ / mV	$E^{ox}_{1/2}$ / mV	$E^{ox}_{1/2}$ / mV	$E^{ox}_{1/2}$ / mV	E_{HOMO} / eV	E_{LUMO} / eV	E_{gap} / eV
$(SQA)_3$-TAA	-1670[i]	8[r]	503[i]	584[i]	-5.17	-3.49	1.68
$(SQB)_3$-TAA	-1455[i]	130[r]	[i, x]	[i, x]	-5.29	-3.71	1.58
$(SQC)_3$-TAA	-1513[i]	134[r]	657[i]	903[i]	-5.29	-3.65	1.64

[i] irreversible, [r] reversible, [x] combination of the 2nd oxidation of the squaraines and the oxidation of the triarylamine, therefore the half wave potentials were not determinable

Transient Absorption Spectroscopy

For the star-shaped trimers **$(SQA)_3$-TAA** (Figure 85), **$(SQB)_3$-TAA** (Figure 86) and **$(SQC)_3$-TAA** (Figure 88) the transient measurements were only performed in toluene for the excitation into the lowest excitonic state because the higher excitonic state lies within the vibronic shoulder of the S_1 state. The fit of the transient maps with a sequential model resulted in four or five EADS. The estimated state energies of the superchromophores are given in Figure 84 together with the lifetimes of the EADS.

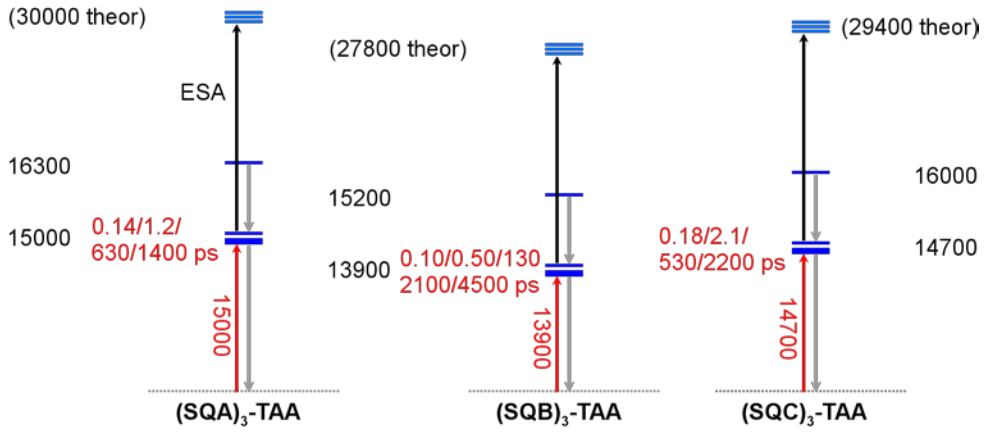

Figure 84 State diagrams of the transient absorption spectra of **$(SQA)_3$-TAA**, **$(SQB)_3$-TAA** and **$(SQC)_3$-TAA**. The red lifetimes are for excitation into the maximum of the lowest exciton band at the given wavenumbers. The state energies were estimated by the peak positions of respective absorption bands. The two-exciton states were estimated (= theor) from the energies of the mono-exciton states. Lifetimes separated by a slash indicate multiexponential decay processes from multiple levels with slightly different energy (given as one bold bar). All the energies are not to scale.

$(SQA)_3$-TAA shows a very similar behaviour upon excitation as the above discussed star-shaped superchromophores with a benzene core. The initially narrow negative peak at

15000 cm^{-1} that forms within the instrument response time is red-shifted within a few 100 ps. As already exemplified for **$(dSQA)_3$-ben** this signal can be caused by diverse processes. In brief, a small part of it is caused by a coherent artefact and the main part is most likely the result of a distortion of the molecule that leads to a splitting of the formally degenerated S_1 states. The signal appears as a local minimum in the time traces of the SE (13600 cm^{-1}) and the combined GSB/SE (14900 cm^{-1}) and as a local maximum in the time trace of the ESA (18500 cm^{-1}). In the time trace at 13600 cm^{-1} where only SE should matter this minimum is not as pronounced but also visible. The sequential fit assigns a lifetime of 140 fs to this process. The following two EADS (1.2 ps and 0.63 ns) are related to relaxation processes and the one with the longest lifetime (1.9 ns) with ground state recovery.

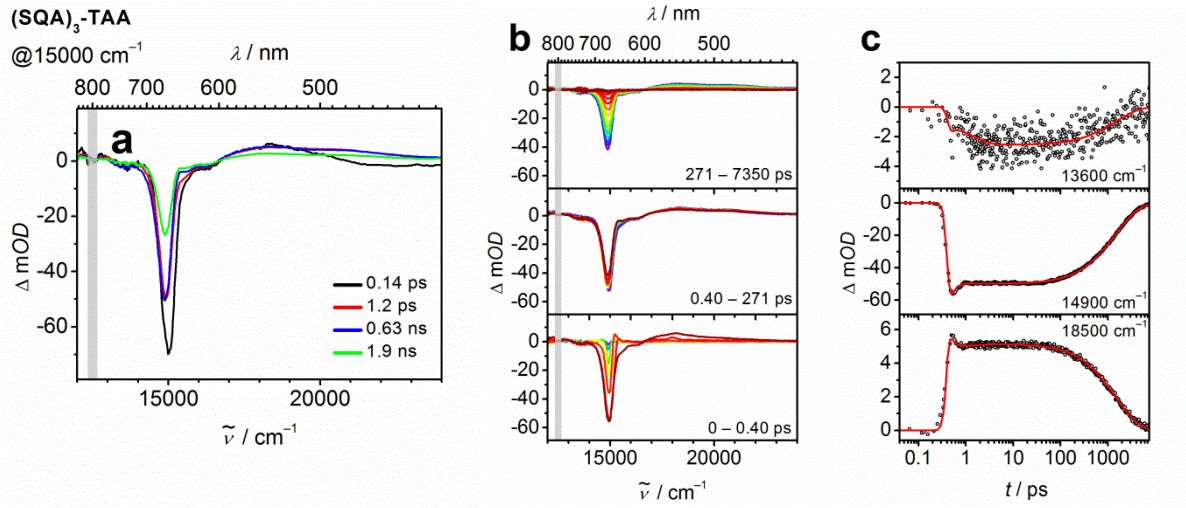

Figure 85 Evolution associated difference spectra (EADS) of **$(SQA)_3$-TAA** in toluene for excitation at 15000 cm^{-1} (a). The spectra at 12500 cm^{-1} ± 200 cm^{-1} (grey bar) are influenced by the laser fundamental and should be taken with caution. The colour code of the EADS refers to the dimension of lifetime. The transient absorption spectra (b) and the time scans at selected wavenumbers (c) were corrected for chirp and scattered light. Early spectra are given in blue, the later spectra in red.

The transient map of the star-shaped trimer of the cisoid chromophores **$(SQB)_3$-TAA** displays a slight difference to the ones of the transoid superchromophore. The EADS with the shortest lifetime technically shows the same features like the one for **$(SQA)_3$-TAA** with the exception of the negative peak at 13700 cm^{-1}. Certainly, the shape of the signal in this region has to be taken with caution due to scattered light and the short timescale that causes problems in the deconvolution process with GLOTARAN. The time traces at 14000 cm^{-1} and 18700 cm^{-1} show a similar local minimum/maximum like in the other star-shaped trimers. In the second EADS the shape of the high energy region has already changed but the GSB/SE

signal at 13700 cm^{-1} is slightly blue shifted in comparison to the consecutive EADS. Hence, the combination of these two spectra shows the same features as the first EADS in the other star-shaped trimers. The last two EADS are also quite unusual. In the multiexponential fit of the TCSPC measurements only one lifetime of 3.06 ns was acquired (Table 18).

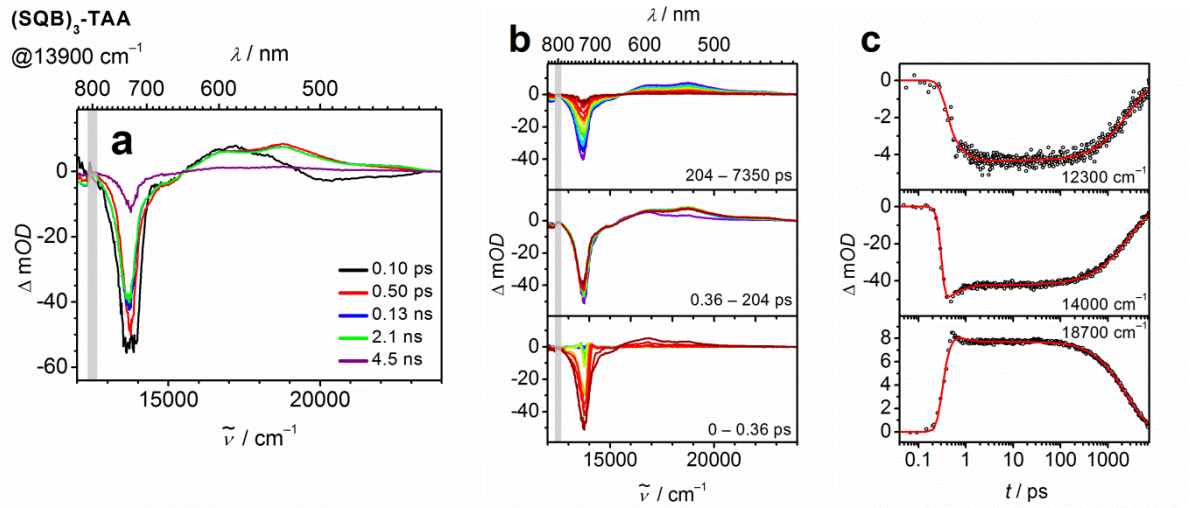

Figure 86 Evolution associated difference spectra (EADS) of **$(SQB)_3$-TAA** in toluene for excitation at 13900 cm^{-1} (a). The spectra at 12500 cm^{-1} ± 200 cm^{-1} (grey bar) are influenced by the laser fundamental and should be taken with caution. The colour code of the EADS refers to the dimension of lifetime. The transient absorption spectra (b) and the time scans at selected wavenumbers (c) were corrected for chirp and scattered light. Early spectra are given in blue, the later spectra in red.

The TCSPC measurements of both the cisoid dimer **dSQB** and the trimer **tSQB** (Figure 87) show two lifetimes if a multiexponential fit is used and only one lifetime if a stretched exponential analysis is applied. The sequential fits of the transient measurements of these compounds again result in two lifetimes in the region of a few ns.[153] Therefore, it is possible that these two lifetimes are associated with the ground state recovery of two slightly different conformations.

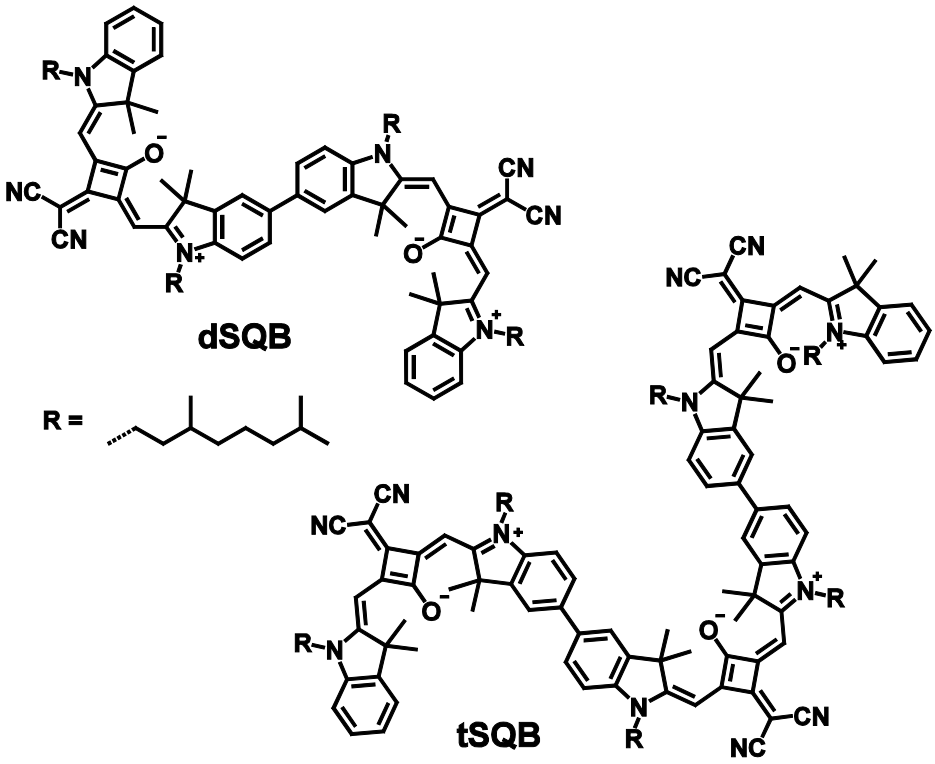

Figure 87 Cisoid squaraine dimer dSQB and trimer tSQB.

The transient maps of the star-shaped trimer **(SQC)$_3$-TAA** show the same features as the ones of **(SQA)$_3$-TAA** just red-shifted by ~300 cm^{-1}. But, in accordance with the results of the multiexponential fits of the TCSPC measurements the EADS show slightly longer lifetimes.

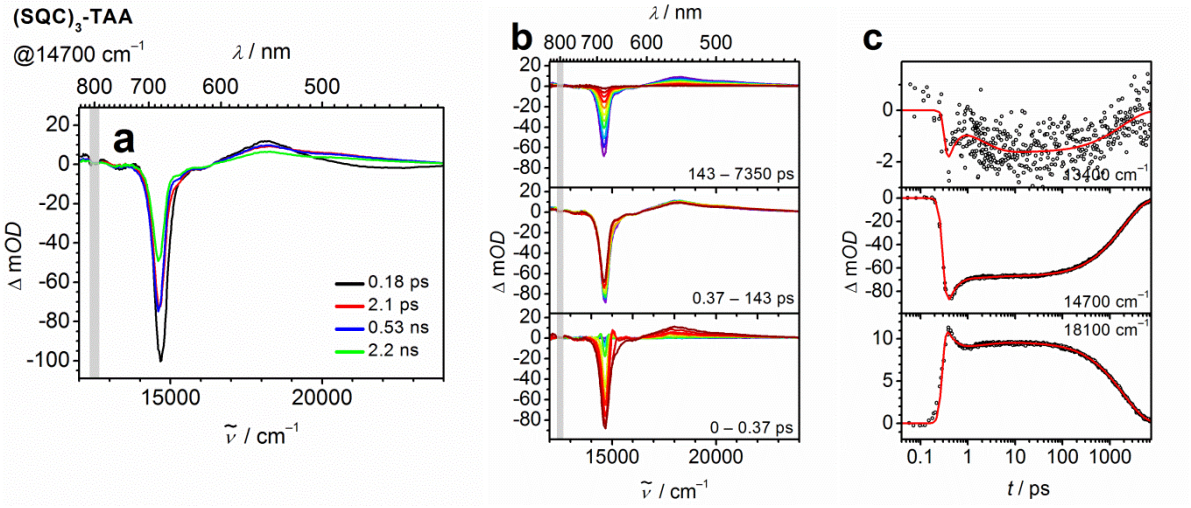

Figure 88 Evolution associated difference spectra (EADS) of **(SQC)$_3$-TAA** in toluene for excitation at 14700 cm^{-1} (a). The spectra at 12500 cm^{-1} ± 200 cm^{-1} (grey bar) are influenced by the laser fundamental and should be taken with caution. The colour code of the EADS refers to the dimension of lifetime. The transient absorption spectra (b) and the time scans at selected wavenumbers (c) were corrected for chirp and scattered light. Early spectra are given in blue, the later spectra in red.

Conclusion

The synthesis of star-shaped trimers with a triarylamine core was successful for the transoid and the cisoid indolenine squaraines **SQA** and **SQB** as well as for the mixed benzothiazole-indolenine squaraine **SQC**. For the reversed mixed squaraine **SQD** where the benzothiazole moiety would be localised at the outer end of the single branches the isolation of the trimerised product was not possible due to its instability.

The absorption spectra of the trimers display a red-shift due to the addition of the propeller like triarylamine core. Not only the optical band gap is influenced but also the electrical band gap is reduced due to the donor character of the core. In addition the absorption spectra show a small broadening of the main absorption band that is symptomatic for a weak excitonic coupling. This effect can also be observed in the fluorescence and the transient absorption measurements. Similar to the superchromophores that are trimerised via a benzene core, **$(SQA)_3$-TAA**, **$(SQB)_3$-TAA** and **$(SQC)_3$-TAA** show a short lived state that is populated initially after the excitation at the lowest maximum of the exciton manifold. This state is most likely formed by a splitting of the formally degenerated S_1 states due to a distortion of the idealised symmetric structure.

In contrast to the superchromophores with a benzene core the trimers **$(SQA)_3$-TAA** and **$(SQB)_3$-TAA** display an enhancement effect of the two photon absorption cross sections. This might be caused by an increase of the density of states because of the enlargement of the π-system. Another reason might be that there are states with charge-transfer character.

3.3.5 Star-Shaped Trimer with an Acceptor Core

Synthesis

The triarylborane squaraine **$(SQA)_3$-bor** was synthesised using the standard *Suzuki*-coupling conditions. Here the central boron centre is protected by six methyl groups and the core unit acts as an acceptor that connects the three donor-acceptor-donor branches.

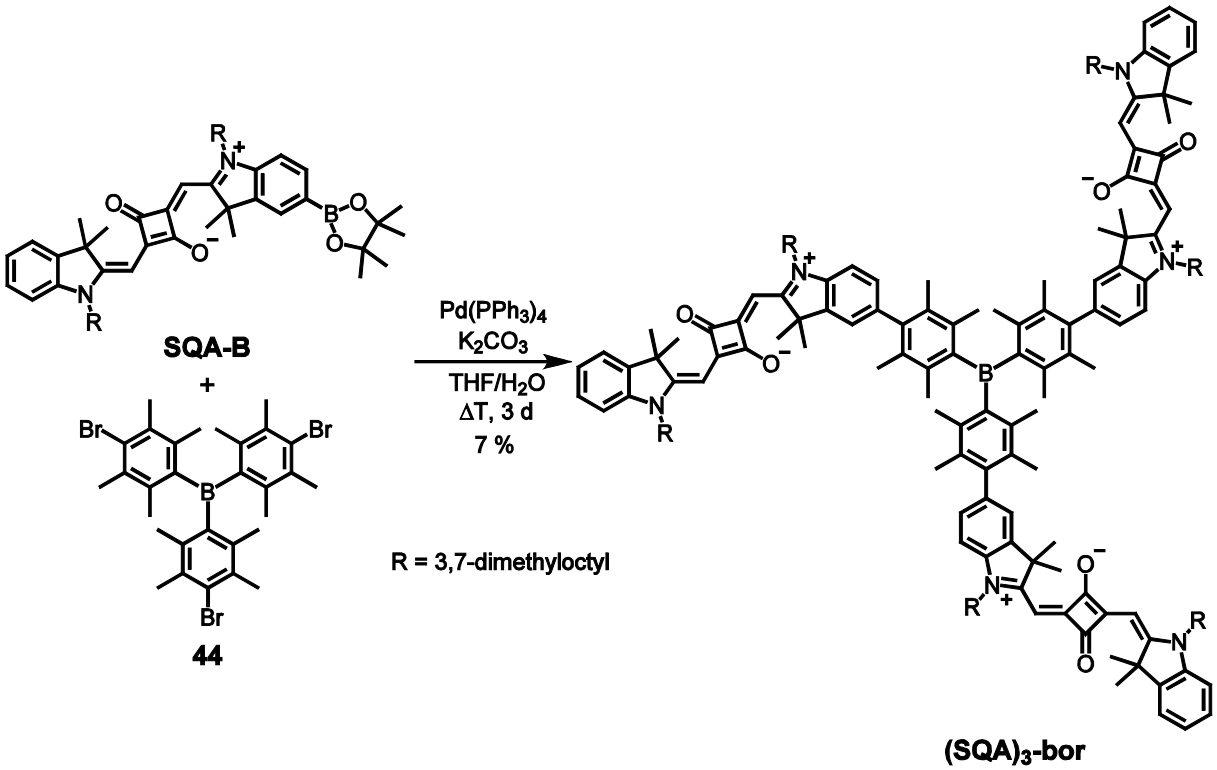

Scheme 46 Synthesis of the star-shaped tris-duryl-boryl trimer **$(SQA)_3$-bor**.

Absorption Spectroscopy

In contrast to the other star-shaped trimers the absorption spectra of the tris-duryl-boryl trimer **$(SQA)_3$-bor** show nearly no broadening of the typical squaraine absorption band at 15300 cm^{-1} in all three investigated solvents. Only when comparing the normalised and shifted main absorption bands of the trimer and its parent chromophore a small coupling effect is visible (Figure 89). Given that the squares of the transition-dipole moments are ca. 3 times as large as in **SQA**, the extinction coefficients of the main absorption are with roughly 1000000 M^{-1} cm^{-1} by far the largest one that were measured for the superchromophores with three squaraine moieties. The absorption maximum is red-shifted by 200 – 300 cm^{-1} in

comparison to the parent chromophore. A small absorption band at ca. 30000 cm^{-1} can be attributed to the tris-duryl-boryl core.

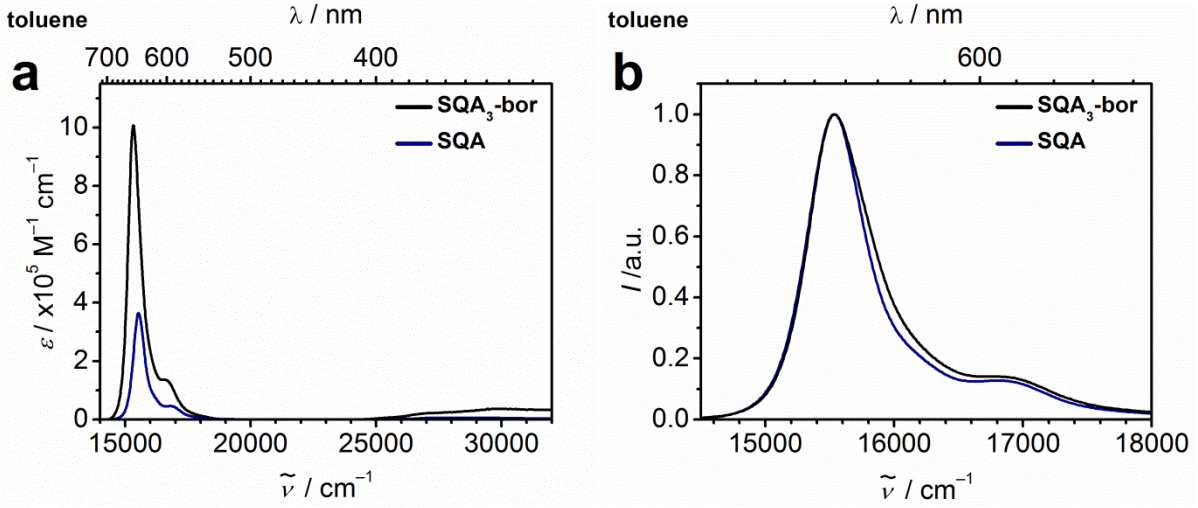

Figure 89 a) Absorption spectra of the trimer **(SQA)$_3$-bor** and its parent compound **SQA** in toluene at rt. b) Normed spectra of **(SQA)$_3$-bor** and **SQA**. The spectrum of the trimer is blue shifted, that both maxima are at the same wavenumber.

Table 21 Absorption maxima, extinction coefficients, square of the transition dipole moment, fluorescence maxima, fluorescence quantum yields and coupling constants of the squaraine trimer (SQA)3-bor in various solvents at rt.

	solvent	$\tilde{\nu}_{abs}$ / cm^{-1} (nm)	ε / M^{-1} cm^{-1}	μ^2 / D^2
(SQA)$_3$-bor	CH_2Cl_2	15400 (649)	1004600	430
	$CHCl_3$	15400 (648)	980900	409
	toluene	15300 (654)	1008000	372

Although formally the tris-duryl-boryl core is a π-electron acceptor due to its free p_z orbital, the lower electronegativity of the boron in comparison to carbon allows it to act as a σ-donor resulting in a shift of the absorption maximum to lower energies.[154] In addition the sterically demanding duryl bridges will most likely assume a propeller like arrangement and thus prohibit an efficient π-overlap.

Fluorescence Spectroscopy

The fluorescence is a mirror image of the main absorption band with a *Stokes* shift of 100 cm^{-1}. The quantum yields are with 60 % in toluene and 55 % in $CHCl_3$ very similar to the values of the monomer. The same holds true for the lifetimes. The squares of the transition-

dipole moments of the fluorescence are slightly smaller than one-third of the squares of the transition-dipole moments of the absorption but higher than in the monomer. This indicates a small coupling between the three branches of the trimer.

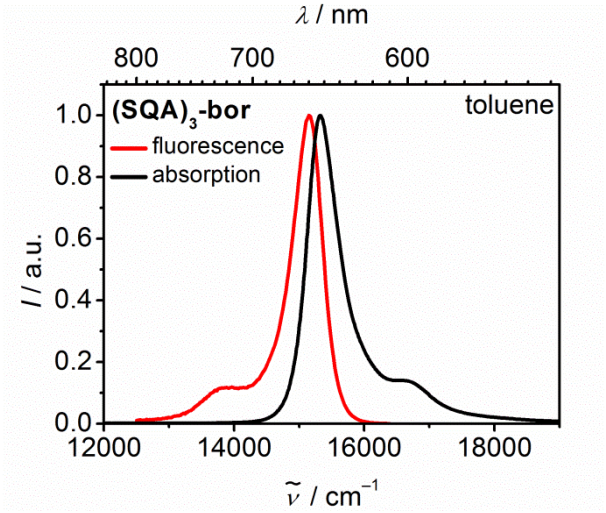

Figure 90 Fluorescence spectrum of the trimer **(SQA)$_3$-bor** in toluene at rt.

Table 22 Fluorescence maxima, quantum yields, lifetimes and fluorescence dipole moments of the squaraine **(SQA)$_3$-bor** in $CHCl_3$ and toluene at rt.

	solvent	$\tilde{\nu}_{fl}$ / cm^{-1}	ϕ_{fl} ($\tilde{\nu}_{fl}$ / cm^{-1})[a]	τ_{fl} / ns (TCSPC)[b]	$\bar{\tau}_{fl}$ / ns	μ^2_{fl} /D^2	μ^2_{abs} / D^2
(SQA)$_3$-bor	$CHCl_3$	15300 (655)	0.55±0.002 (16700)	0.05 (0.05) 0.43 (0.23) 1.59 (0.72)	1.26 (0.89)[c]	137	409
	toluene	15200 (659)	0.60±0.026 (16700)	0.06 (-0,03) 0.34 (0.18) 1.76 (0.79)	1.62 (0.96)[c]	119	372

[a] Fluorescence quantum yield and excitation wavenumber used for measuring the fluorescence spectra in parentheses. [b] Multiexponential fit of fluorescence decay measured by TSCPC, excitation at 15200 cm^{-1}. Amplitudes are given in brackets. [c] Lifetimes acquired by stretched exponential analysis. Stretching exponent in brackets.

Cyclic Voltammetry

The cyclovoltammogram of **(SQA)$_3$-bor** resembles the voltammogram of the parent chromophore in structure and position of the half wave potentials. It has one irreversible reduction at –1670 mV and two oxidation processes. The 1st oxidation process at ~60 mV is reversible and the 2nd at ~570 mV is irreversible.

Völker et al.[98] determined the reduction processes of a transoid squaraine that was substituted with two triarylboranes in THF with $^{n}Bu_4PF_6$ as the electrolyte. They noticed that the borane moieties had no influence on the position of the reduction and oxidation processes of the squaraine. In addition they were able to measure the second reduction of the squaraine at –2500 mV and the first reduction of the boranes at –2650 mV.

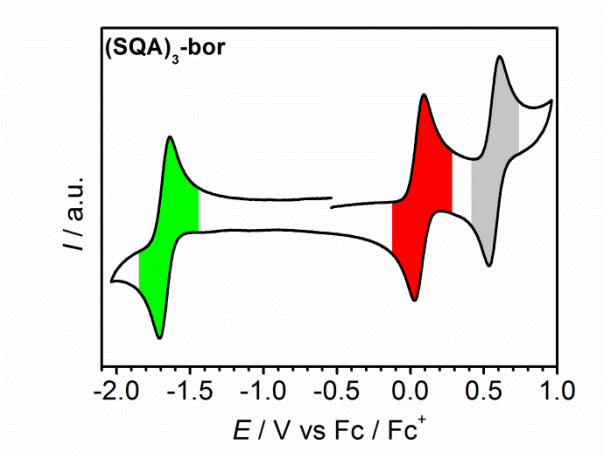

Figure 91 Cyclic voltammogram of **(SQA)$_3$-bor** in $CH_2Cl_2/^{n}Bu_4PF_6$ (0.2 M) at a scan rate of 100 mV s^{-1}. The voltammogram is referenced against (Fc/Fc^+), normalised recorded by first scanning into the oxidative direction.

Table 23 Redox potentials ($E_{1/2}$), HOMO and LUMO energy levels and band gaps of **(SQA)$_3$-bor** in $CH_2Cl_2/^{n}Bu_4PF_6$ (0.2 M) at a scan rate of 100 mV s^{-1} and referenced against (Fc/Fc^+).

	$E^{red}_{1/2}$ / mV	$E^{ox}_{1/2}$ / mV	$E^{ox}_{1/2}$ / mV	E_{HOMO} / eV	E_{LUMO} / eV	E_{gap} / eV
(SQA)$_3$-bor	-1675[i]	60[r]	570[i]	-5.22	-3.49	1.73

[i] irreversible, [r] reversible

Transient Absorption Spectroscopy

The transient spectra of **(SQA)$_3$-bor** in toluene show a behaviour that is quite similar to the spectra of the trimers with a benzene and with a triarylamine core. The most obvious difference is that in the beginning of the measurement two broad peaks are visible at 18400 cm^{-1} and 20200 cm^{-1}. In the other trimers the broad peak at the higher energy develops only with time. The minimum/maximum of the time traces at 15300 cm^{-1} and 19200 cm^{-1} is with ~4 ps significantly broader than in the other star-shaped trimers. The sequential fit of the transient map results in four EADS. The spectral shift between the

minima of the first and the second EADS is with 30 cm^{-1} significantly smaller than in the other superchromophores.

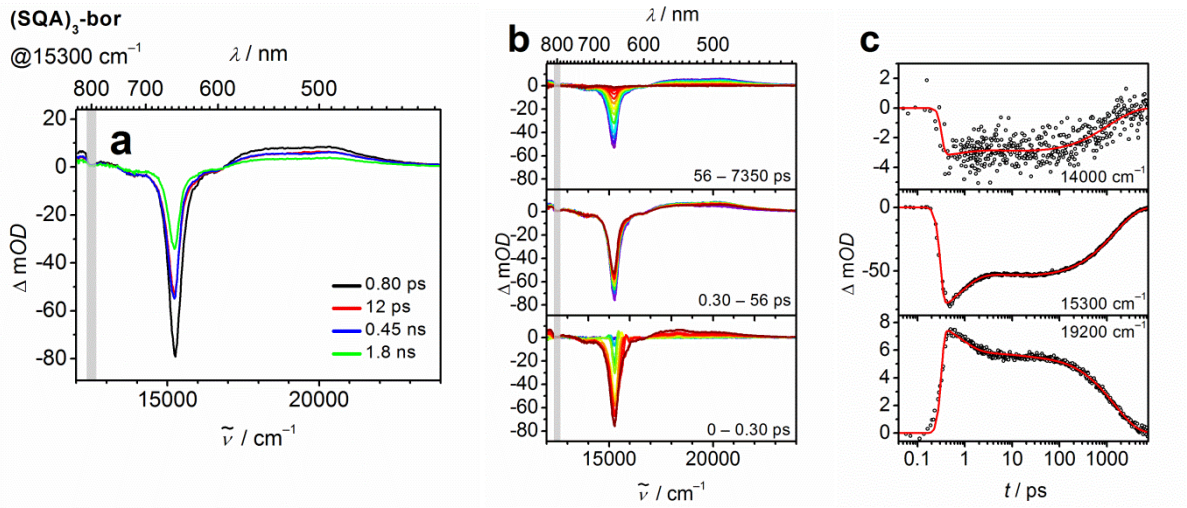

Figure 92 Evolution associated difference spectra (EADS) of **$(SQC)_3$-bor** in toluene for excitation at 15300 cm^{-1} (a). The spectra at 12500 cm^{-1} ± 200 cm^{-1} (grey bar) are influenced by the laser fundamental and should be taken with caution. The colour code of the EADS refers to the dimension of lifetime. The transient absorption spectra (b) and the time scans at selected wavenumbers (c) were corrected for chirp and scattered light. Early spectra are given in blue, the later spectra in red.

Conclusion

The star-shaped trimer **$(SQA)_3$-bor** that has formally a π-electron acceptor core shows a similar spectroscopic behaviour as the trimeric superchromophores with donor cores. This is caused by the sterically demanding duryl bridges that prohibit an effective π-overlap and therefore make the σ-donor capabilities of the boron dominant. The red-shift of the absorption maximum and the excitonic coupling are marginal in this superchromophore, but the lifetime of the initially populated state in the transient measurements is significantly larger than in the other trimers. The electrical properties are nearly unchanged by the trimerisation.

4 Summary

In this work the successful synthesis, the linear and nonlinear spectroscopic properties as well as the electrochemical behaviour of some linear and star-shaped squaraine superchromophores that are based on indolenine derivatives were presented. The attempt to synthesise similar chromophores which contained only benzothiazole squaraines failed unfortunately. However, one trimer that contained mixed benzothiazole indolenine squaraines could be synthesised and investigated as well.

The linear spectroscopic properties, like red-shift and broadening of the absorption, of all superchromophores could be explained by exciton coupling theory. The heterochromophores **(SQA)$_2$(SQB)-N**, **(SQA)(SQB)$_2$-N** and **(SQA)(SQB)-NH** displayed additional to the typical squaraine fluorescence from the lowest excited state some properties that could be assigned to localised states. While the chromophores with **N**-core showed very small emission quantum yields, the chromophores with the other cores and the linear oligomers display an enhancement compared to the monomers.

Transient absorption spectroscopy experiments of the star-shaped superchromophores showed, that their formally degenerated S_1 states are split due to a deviation of the ideal C_3 symmetry. This is also the reason for the observation of an absorption band for the highest exciton state, which is derived from the S_1-state of the monomers, as its transition-dipole moment would be zero in the symmetrical case.

The linear oligomers and the star-shaped superchromophores with a benzene or triarylamine core showed at least additive, sometimes even weak cooperative, behaviour in the two-photon absorption experiments. Additional to higher two-photon absorption cross sections the chromophores showed a pronounced broadening of the nonlinear absorption, due to symmetry breaking and a higher density of states.

Unfortunately it was not possible to solve the problem of the equilibrium of the cisoid and the transoid structure of donor substituted azulene squaraines, due to either instability of the squaraines or steric hindrance.

5 Experimental Section[1]

5.1 Materials and Methods

5.1.1 Steady-State Absorption Spectroscopy

- JASCO V670 UV/Vis/NIR-Spectrophotometer (software SpectraManager v. 2.08.04)
- Agilent Technologies Cary 5000 UV-Vis-NIR spectrophotometer (software Agilent Cary WinUV Analysis and Bio v.4.2)

All solvents were of spectroscopic grade and were used without further purification. Absorption spectra were recorded in 1 cm quartz cuvettes from Starna (Pfungstadt, Germany) at rt. The neat solvent was used as reference. The temperature dependent measurements were performed using a cryostat RUL 80 (MGW-Lauda). Aggregation of the samples could be excluded by a concentration independent behaviour (10^{-7}–10^{-5} M). In order to prohibit interaction with the glass surface the measurements in toluene were performed using a silylated quartz cuvette and in some cases even silylated volumetric flasks.[100, 143]

5.1.2 Steady-State Emission Spectroscopy

- Edinburgh Instruments FLS980 fluorescence lifetime spectrometer (software F980 version 1.2.2)
    - 450 W Xenon lamp / PMT (R928P)
- Edinburgh Instruments FLS920 fluorescence lifetime spectrometer (software F900 version 7.2.1)
    - 450 W Xenon lamp / PMT (R5509-42)

Steady state emission spectra at room temperature were recorded in silylated 1 cm quartz cells from Starna (Pfungstadt, Germany).[100, 143] All solvents were of spectroscopic grade and were used without further purification. In order to exclude self-absorption, the emission spectra were measured with strongly diluted samples (< 0.05 OD). The dissolved samples were purged with argon for 15 min.

[1] Reproduced or adapted in part with permission from: a) H. Ceymann, M. Balkenhohl, A. Schmiedel, M. Holzapfel and C. Lambert, *Phys. Chem. Chem. Phys.*, 2016, **18**, 2646-2657. b) H. Ceymann, A. Rosspeintner, M. H. Schreck, C. Mützel, A. Stoy, E. Vauthey and C. Lambert, Phys. Chem. Chem. Phys., DOI: 10.1039/C6CP02312F.

The quantum yields were determined using optical dense samples in an integrating sphere and eq. (63).

$$\Phi_{obs} = \frac{\int F_{sample}}{\int E_{solvent} - \int E_{sample}} \tag{63}$$

where Φ_{obs} is the observed quantum yield, F_{sample} is the luminescence emission spectrum of the sample, E_{sample} is the spectrum of the light used to excite the sample and $E_{solvent}$ is the spectrum of the light used for excitation with only the solvent in the sphere. The self-absorption of the molecule was taken in account by using eq. (64)

$$1 - a = \frac{\int_0^\infty F_{fl}(\lambda) d\lambda}{\int_0^\infty F_{emission}(\lambda) d\lambda} \tag{64}$$

where the fluorescence spectra of the dilute sample F_{fl} is compared with that of an optical dense sample $F_{emission}$. Finally eq. (65) can be used to determine the quantum efficiency Φ_{fl} of the sample.[155]

$$\Phi_{fl} = \frac{\Phi_{obs}}{1 - a + a \times \Phi_{obs}} \tag{65}$$

Excitation spectra were recorded with the same set-up as was used for the emission spectroscopy. The only difference was the fixed wavelength of the emission whereas the wavelength of the excitation was successively varied.

5.1.3 Time Dependent Fluorescence-Emission

- Edinburgh Instruments FLS980 fluorescence lifetime spectrometer (software F980 version 1.2.2)
    - 15250 cm^{-1} (656 nm) pulsed Laser Diode / PMT (H10720)

The samples were prepared similar to the steady state emission experiments and measured under magic angle conditions. The instrument response function was determined by using a scatterer solution consisting of colloidal silicon in deionised water. Lifetimes were determined by deconvolution of the experimental decay with the instrument response function and by fitting the decay curves with an exponential decay function using the FAST software (version 3.4.2).

5.1.4 Polarised Steady-State Fluorescence Excitation Spectroscopy

- Edinburgh Instruments FLS980 fluorescence lifetime spectrometer (software F980 version 1.2.2)

For the fluorescence anisotropy measurements the fluorimeter was equipped with two polarisation filters. The compounds were dissolved in polyTHF (Mn ~ 650, CAS 25190-06-1, Sigma Aldrich) in silylated 1 cm quartz cells from Starna (Pfungstadt, Germany)[100, 143] and measured at 26 °C and 20 °C using a cryostat FS 2 P (HAAKE).

5.1.5 Femtosecond Spectroscopy[1]

- Newport-Spectra-Physics Solstice one box amplified ultrafast Ti:Sapphire laser system with a fundamental wavenumber of 12500 cm^{-1} (800 nm), a pulse length of 100 fs and a repetition rate of 1 kHz
- Newport-Spectra-Physics TOPAS-C optical parametric amplifier as the source for the pump pulses with a pulse length of 140 fs
- Ultrafast Systems Helios transient absorption spectrometer with a CMOS sensor (1.5 nm intrinsic resolution, 350 – 800 nm sensitivity range) and an InGaAs sensor (3.5 nm intrinsic resolution, 800 – 1600 nm sensitivity range)

All experiments were performed in quartz cuvettes from Spectrocell (Oreland, PA) with an optical path length of 2 mm equipped with a micro-stirrer to allow stirring during the measurement at rt. All samples were dissolved in toluene (Uvasol from Merck), filtered and degassed for 30 min. The optical density was adjusted to ca. 0.3 at the corresponding excitation wavenumber.

5.1.5.1 Femtosecond Transient Absorption Spectroscopy

The output beam from the Solstice amplifier was split into two parts. A small part was focused onto a vertically oscillating CaF_2 crystal to generate a white light continuum between 11800 cm^{-1} (850 nm) and 28600 cm^{-1} (350 nm) which was polarised horizontally (the polarisation was adjusted by using a wire grid (Thorlabs)). The pulse was restricted with filters and used as the probe pulse. The main part was used to pump an optical parametric

[1] The femtosecond spectroscopy measurements were performed by *Alexander Schmiedel* and *Dr. Henning Marciniak* and the analysis was carried out by *Dr. Marco Holzapfel*.

amplifier (TOPAS-C) from Light Conversion to generate the pump pulse with a pulse length of 140 fs at the corresponding excitation wavenumbers. By means of a wire grid (Moxtek) the polarisation axis of the pump pulse was set to magic angle relative to that of the probe beam. The pump pulse (50 nJ, Ø ca. 0.1 mm) and probe pulse (Ø ca. 0.5 mm) met at ca. 6° vertical angle in the sample cuvette. The probe light was measured by a spectrograph equipped with a CMOS sensor (Ultrafast Systems, Helios) in the range between 11900 cm^{-1} (840 nm) and 25000 cm^{-1} (400 nm) with an intrinsic resolution of 1.5 nm. Every second pump pulse was blocked by a mechanical chopper (working at 500 Hz) to measure I and I_0. In order to compensate intensity fluctuations, a reference beam was split off and also detected with an identical spectrograph.

In order to cover the spectral range from 11000 cm^{-1} (910 nm) down to 22000 cm^{-1} (455 nm) accurately without interference around 12500 ± 200 cm^{-1} (800 ± 10 nm) with the fundamental, in one TA experiment a small portion of the light coming from the TOPAS (6500 cm^{-1} / 1530 nm) was used which was frequency doubled. The 13100 cm^{-1} (765 nm) and 6500 cm^{-1} (1530 nm) beams were separated. The 13100 cm^{-1} beam was used as the pump pulse and the 6500 cm^{-1} beam to generate white light in a CaF_2 crystal. Because of larger temporal white light fluctuation, the signal-to-noise ratio is much worse than in all other TA experiments. However, these TA spectra show the accurate spectral shape of GSB/SE band in the 11100 – 14300 cm^{-1} (900 – 700 nm) region.

By means of a computer-controlled linear stage (retro reflector in double pass setup) the relative temporal delay between pump and probe pulse was varied in 20 fs steps from 0 fs to 4 ps and from 4 ps to 8 ns in logarithmic steps with a maximum step size of 200 ps. Steady state absorption spectra were recorded before and after the transient absorption experiment to exclude degradation of the sample. The raw data were corrected for stray light prior to data analysis of the difference spectra map (time × wavelength).

The maps recorded under magic angle conditions were analysed with GLOTARAN[156, 157] including the correction for the white light dispersion (chirp) and modelling the instrument response function and the coherent artefact.

5.1.5.2 Femtosecond Fluorescence-Upconversion Spectroscopy

We used a commercial fluorescence upconversion setup (Halcyone from Ultrafast Systems). The laser system was the same as for the fs-TA-experiments. The output beam was again divided into two parts. One part seeded the optical parametric amplifier (TOPAS-C from Newport Spectra Physics) to generate the pump pulse with a pulse length of 140 fs. The other part of the output beam was used as the gate pulse (12500 cm^{-1}, 800 nm) which was delayed over a maximum of 3 ns in 20 fs steps from 0 fs to 4 ps and in logarithmic steps from 4 ps to 3 ns with a maximum step size of 80 ps with a computer-controlled linear stage. The pump pulse was focused onto the cuvette and the fluorescence light was collected and focused on a 0.5 mm BBO type II crystal for frequency upconversion with the gate beam. All lenses in the setup had a focal length of 100 mm and a thickness of 1.85 mm. The upconverted light was focused on the entrance slit of a double monochromator and measured by a PMT detector. For polarisation dependent measurements the pump beam was set to 45° by a $\lambda/2$ plate relative to the horizontally oriented gate beam. The polarisation of both beams was purified by wire grids (Moxtek). In front of the cuvette, the pump beam was finally adjusted to parallel, perpendicular and magic angle relative to the gate beam with a wire grid. The anisotropic data were analysed by a simultaneous deconvolution fit of the parallel, perpendicular and magic angle traces at selected wavelengths with a self-written implementation in MatLab. A detailed description of this procedure can be found in the literature.[158] Briefly, the measured signal intensity *I* is the convolution of the instrument response function (taken as Gaussian shaped) with the product of the population decay function *S* and respective anisotropy function which depends on *r*.

$$\begin{bmatrix} I_{\parallel}(t) \\ I_{\perp}(t) \\ I_{MA}(t) \end{bmatrix} = \left(S(t) \begin{bmatrix} 1+2r(t) \\ 1-r(t) \\ 1 \end{bmatrix} \right) \otimes IRF$$

5.1.6 Two-Photon-Absorption Spectroscopy[1]

Two-photon cross sections were determined via two-photon excitation spectra using a set-up similar to the one described in the literature.[72] In detail, the output of a TOPAS-Prime in combination with a NirUVis frequency mixer (both from Light Conversion) was used as excitation source. The excitation intensity is adjusted using a combination of a broadband zero-order $\lambda/2$ plate and a Glan-Taylor polariser, and the polarisation was set to vertical. The beam is slightly focused by a (f = 20 cm) lens, which was placed 10 cm before the sample. The pump power was monitored using a powermeter (Thorlabs PM100A) equipped with a thermal sensor (Thorlabs S302C) behind the sample. The fluorescence was focused onto the entrance slit of a monochromator (0.25m Cornerstone, Oriel, grating 74166 Newport) equipped with a multi-pixel photon-counter avalanche photodiode detector (Hamamatsu S-10362-11-050U) using a spherical mirror (Ø= 75 mm, f = 150 mm). The output signal is preamplified (SR240, Stanford Research Systems), processed with a gated boxcar-integrator and averager module (SR250, SRS), digitised (SR245, SRS) and recorded on a computer.

The two photon cross section at a given wavenumber, $\delta_2^{(s)}(\tilde{\nu})$, was calculated as follows[72]

$$\delta_2^{(s)}(\tilde{\nu}) = \frac{F_2^{(s)}(\tilde{\nu}, \lambda_{obs})\phi^{(r)}(\lambda_{obs})C^{(r)}}{F_2^{(r)}(\tilde{\nu}, \lambda_{obs})\phi^{(s)}(\lambda_{obs})C^{(s)}} \delta_2^{(r)}(\nu) \tag{66}$$

Here $F_2^{(x)}(\tilde{\nu}, \lambda_{obs})$ is the (two-photon induced) fluorescence intensity at excitation wavenumber $\tilde{\nu}$ and observation wavelength λ_{obs} for either sample or reference $(x \in \{s,r\})$. c^x and $\phi^x(\lambda_{obs})$ are the concentration and differential fluorescence quantum yield (at the observation wavelength) of sample and reference. LDS698 and Styryl 9M in chloroform were used as reference.[72, 73]

5.1.7 Electrochemistry

All electrochemical measurements were performed in CH_2Cl_2 with tetrabutylammonium hexafluorophosphate $^nBu_4NPF_6$ (0.2 M) as supporting electrolyte. CH_2Cl_2 was first dried over calcium chloride, distilled from calcium hydride and stored over activated alumina prior to use. $^nBu_4NPF_6$ was synthesised according to literature,[159] recrystallised from ethanol/water and dried under high vacuum.

[1] The Two-Photon-Absorption Spectroscopy measurements were performed by *Dr. Arnulf Rosspeintner* in Geneva.

5.1.7.1 Cyclic Voltammetry (CV), Differential Pulse Voltammetry (DPV)

- BAS CV-50 W electrochemical workstation including corresponding software (v. 2.31) or Gamry Instruments Reference 600 Potentiostat/Galvanostat/ZRA (v. 6.2.2, Warminster, PA, USA)

Cyclic voltammograms were measured under an argon atmosphere. The concentration of the solute was 1 – 3 mM. A conventional three electrode set-up consisting of a platinum disc working electrode (Ø = 1 mm), a Ag/AgCl ´LEAK FREE´ reference electrode (Warner Instruments, Hamden, CT, USA) and a platinum wire counter electrode was used. The measurement cell was dried in an oven and flushed with argon prior to use.

The reference electrode was measured against decamethylferoccene/decamethyl-feroccenium and then referenced against the ferrocene/ferrocenium (Fc/Fc^+) redox couple.[160] The measurements were performed at scan rates of 100 mV s^{-1} for the CV and 20 mV s^{-1} for the DPV. Chemical and electrochemical reversability of the redox processes was checked by multi thin layer experiments and measurements at different scan rates (from 10 – 1000 mV s^{-1}), respectively.

If necessary, voltammograms were analysed and fitted with DigiElch Software (Gamry, version 6.F, build 3.005) to have access to potential values of superimposed signals.

The HOMO and LUMO energy levels ($E_{\mathrm{HOMO/LUMO}}$) were obtained from the half-wave potential of the cyclic voltammetry measurements. The potential of the ferrocene/ferrocenium (Fc/Fc^+) redox couple in $CH_2Cl_2/{}^nBu_4NPF_6$ is 0.46 eV vs. the saturated calomel electrode (SEC).[161] Furthermore, the potential of SCE is 0.244 V vs. the normal hydrogen electrode (NHE)[162] which has an absolute potential of 4.46 eV vs vacuum.[163] Accordingly the energy levels in CH_2Cl_2 are

$$E_{\mathrm{HOMO/LUMO}} = -5.16\,eV - E_{1/2}^{\mathrm{ox1/red1}}$$

and the electrochemically derived band gap $E_{\mathrm{gap}} = E_{\mathrm{LUMO}} - E_{\mathrm{HOMO}}$.

5.1.7.2 Spectroelectrochemistry (SEC)

UV/Vis/NIR-spectroelectrochemistry was performed at rt in a custom built three electrode quartz-cell sample compartment implemented in a Jasco V-670 spectrometer (*vide supra*). The cell consists of a platinum disc working electrode (Ø = 6 mm), a gold covered stainless steel (V2A) plate as counter electrode and an AgCl-covered silver wire as pseudo-reference

electrode and the cell volume was flushed with argon before use.[164] All experiments were measured in reflexion with a path length of 100 µm. The working electrode potential was controlled by a Princeton Applied Research Model 283 potentiostat (20 or 50 mV steps). The concentrations of the solutes were 10^{-4} – 10^{-3} M.

5.1.8 NMR Spectroscopy

- Avance III HD 400 FT-Spectrometer (^{1}H: 400.13 MHz, ^{13}C: 100.61 MHz) with a Bruker Ultrashield magnet
- Avance III HD 400 FT-Spectrometer (^{1}H: 400.03 MHz, ^{13}C: 100.59 MHz) with a Bruker Ascend magnet
- Avance III HD 600 FT-Spectrometer (^{1}H: 600.13 MHz, ^{13}C: 150.90 MHz) with an Oxford Instruments magnet
- Avance III HD 600 FT-Spectrometer (^{1}H: 600.43 MHz, ^{13}C: 150.98 MHz) with a Bruker Ascend magnet

^{1}H and ^{13}C NMR spectra were acquired on one of the aforementioned NMR spectrometers in deuterated solvents as indicated (e. g. acetone-d_6, $CDCl_3$, CD_2Cl_2, dimethylsulfoxide-d_6). The 400 MHz spectrometers run at 300 K and the two 600 MHz spectrometers have different temperatures for each solvent, *e. g.*, 303.6 K for $CDCl_3$ or 293.5 K for CD_2Cl_2. Samples were filtered and placed in frequency-matched 5 mm glass sample tubes. Chemical shifts are given in ppm relative to residual nondeuterated solvent signal (^{1}H: $CHCl_3$: δ 7.26 ppm, acetone: δ 2.05 ppm; CH_2Cl_2: δ 5.32 ppm; dimethylsulfoxide: δ 2.50 ppm; ^{13}C: δ $CHCl_3$: δ 77.16 ppm, acetone: δ 29.84 ppm, CH_2Cl_2: δ 53.84 ppm).[165] Deuterated solvents were used as received.
The abbreviations used for declaration of the spin multiplicities and C-atom depictions are: s = singlet, d = doublet, t = triplet, q = quartet, m = multiplet, dd = doublet of doublet. ddd = doublet of doublet of doublet; prim. = primary, sec. = secondary, tert. = tertiary, quart. = quaternary. Multiplet signals or overlapping multiplet signals in proton NMR spectra that could not be assigned to first order couplings are given as (-). The coupling constants are quoted in Hertz (Hz).
Order of declaration for proton spectra: chemical shift (spin multiplicity, coupling constant, number of protons, assignment).

5.1.9 Mass Spectrometry

- Bruker Daltonics microTOF focus (ESI)
- Bruker Daltonics autoflex II (MALDI)

Mass spectra were recorded with a Bruker Daltonics autoflex II (MALDI) in positive mode (POS) using a DCTB (*trans*-2-[3-(4-*tert*-butylphenyl)-2-methyl-2-propenyl-idene]malononitrile) matrix or with a Bruker Daltonic microTOF focus (ESI). All mass spectrometry peaks are reported as m/z. For calculation of the respective mass values of the isotopic distribution, the software module “Bruker Daltonics IsotopePattern” from the software Compass 1.1 from Bruker Daltonics GmbH, Bremen was used. Calculated (calc.) and measured (found) peak values always correspond to the most intense peak of the isotopic distribution.

5.1.10 Microwave Oven

- *µCHEMIST microPREP Microwave Digestion System ATC-FO 300* from MLS (Leutkirch, Germany)

Microwave reactions were performed in a microwave oven with a fibre optical thermometer sensor (ATC-FO, 0–270°C), which controls the reaction temperature by regulation of the output power (0–1200 W) of the microwave oven. The reaction mixture was placed in a pressure quartz vessel (max. 12 bar).

5.1.11 Recycling Gel Permeation Chromatography (GPC)

- Shimadzu recycling Gel Permeation Chromatography System
  - card type system controller (CBM-20Alite)
  - prominence liquid chromatograph (LC-20AD)
  - prominence degassing unit (DGU-20A3R)
  - shimadzu valve unit (FCV-20AH_2)
  - prominence photodiode array detector 190–800 nm (SPD-M20A)
  - shimadzu fraction collector (FRC-10A)
  - software LCsolution (v. 1.25)

Gel permeation chromatography (GPC) was done using two or three preparative GPC columns (styrene-divinylbenzene-copolymer, 50 Å, 100 Å and 500 Å, 600 x 20.8 mm) from PSS. $CHCl_3$ (HPLC grade) was used as eluent with a flow rate of 4 ml min^{-1}.

5.1.12 Flash Chromatography

- Interchim PF 450 Flash-chromatography-system
  - photodiode array UV-vis-detector 175–840 nm
  - fraction collector

Flash Chromatography was done using pre packed Reveleris HP Silica 24 g cartriges from GRACE.

5.2 Synthesis

The reactions were performed in standard glass ware and chemicals that were obtained from commercial suppliers were used without further purification if not stated elsewise. For reactions under nitrogen atmosphere, the nitrogen was dried with Sicapent® from Merck, oxygen was removed with a cupric oxide catalyst R3-11 from BASF and standard Schlenk techniques were used.[166] Solvent for oxygen and/or moisture sensitive reactions were freshly distilled under nitrogen from the appropriate dehydrating agent (sodium/benzophenone "ketyl blue" for THF and dioxane, sodium for toluene and CaH_2 for CH_2Cl_2) and sparged with dry nitrogen before use. Flash chromatography[167] was performed on silica gel (Macherey-Nagel "Silica 60 M", 40 – 63 µm) wet-packed in glass columns.

5.2.1 Reagents

The precursors azulene[168] (**1**), 1-bromoazulene[100, 103] (**2**), 9-(3,7-dimethyloctyl)-3-(4,4,5,5-tetramethyl-1,3,2-dioxaborolan-2-yl)-9H-carbazole[98] (**4**), 9-(3,7-dimethyloctyl)-2-(4,4,5,5-tetramethyl-1,3,2-dioxaborolan-2-yl)-9H-carbazole[98] (**6**), 6-nitro-2-methylbenzothiazole[110] (**8**), 6-amino-2-methylbenzothiazole[110] (**9**), 6-acetamido-2-methylbenzothiazole[111] (**10**), 3,7-dimethyloctyl tosylate[114] (**13**), 3,7-dimethyloctyl bromide[115] (**14**), 1-iodo-3,7-dimethyloctane[116] (**15**), 1,3,5-tris(4, 4, 5, 5-tetramethyl-1,3,2-dioxaborolan-2-yl)benzene[169] (**30**), tris(4-(4, 4, 5, 5-tetramethyl-1,3,2-dioxaborolan-2-yl)phenyl)amine[170] (**31**), 5-bromo-2,3,3-trimethyl-3H-indolenine[118] (**33**) and compound **Az**[101] were synthesised according to the given literature procedures.

Tri(4-bromo-2,3,5,6-tetramethylphenyl)borane (**44**) was provided by *Dr. S. Völker* (Universität Würzburg) and **SQB** by M. H. Schreck (Universität Würzburg).

5.2.2 General Procedures

General Procedure for the Alkylation of Benzothiazole/Indolenine Derivatives according to ref.[24, 29, 62, 97] (GP I)

A benzothiazole/indolenine (1.0 eq.) derivative was diluted/dissolved in/with nitromethane. An excess of the iodoalkane (1.2-3.0 eq.) was added and the solution was refluxed for 15 – 120 h. After cooling the solution was concentrated *in vacuo*. Et_2O was added to the residue and the mixture was left at -30 °C for 2 h. The resulting precipitate was filtered, washed with Et_2O and dried under high vacuum.

General Procedure for the Synthesis of Semisquaraine Esters according to ref.[98, 171] (GP II)

A quaternary benzothiazole/indolenine salt (1.0 eq.) was dissolved in an alcohol. The ester of the squaric acid (1.0 eq.) was added and the solution was heated to 70 °C. Triethylamine (> 2.0 eq.) was added and the solution was stirred for 2 h at 70 °C. The solvent was removed *in vacuo* and the residue was purified by flash column chromatography.

General Procedure for the Saponification of the Semisquaraine Esters according to ref.[171] (GP III)

A semisquaraine ester (1.0 eq.) was dissolved in EtOH and heated to 70 °C. A large excess of a solution of sodium hydroxide (10 N) was added and the solution stirred for 15 min at 70 °C. The mixture was cooled and acidified with hydrochloric acid (2 N). The solvent was removed and the residue dissolved in water (50 ml) and CH_2Cl_2 (50 ml). The organic layer was separated and the aqueous layer extracted with CH_2Cl_2 (2 x 50 ml). The combined organic layers were dried over $MgSO_4$. The solvent was removed *in vacuo* and the residue was purified by flash column chromatography.

General Procedure for the Synthesis of the Unsymmetrical Squaraines according to ref.[98] (GP IV)

A semisquaric acid (1.0 eq.) and quaternary benzothiazole/indolenine salt (1.0 eq.) were dissolved in a 6/4 mixture of *n*-butanol/toluene. Pyridine was added and the solution was refluxed for 18 h using a *Dean-Stark* trap. The solvent was removed *in vacuo* and the residue was purified by flash column chromatography. Finally the crude product was dissolved in a small amount of CH_2Cl_2 and dropped into an excess of *n*-hexane. The resulting precipitate was filtered off and dried under high vacuum.

5.2.3 Precursors

Synthesis of 9-(azulene-1-yl)-9H-carbazole (3)

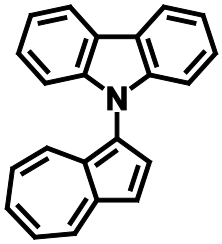

CA: [–]

Under a nitrogen atmosphere 9H-carbazole (200 mg, 1.20 mmol), NaO*t*-Bu (287 mg, 2.99 mmol) and P(*t*-Bu)$_3$ (47.8 µl, 1.00 M in toluene, 47.8 µmol) and freshly prepared 1-bromoazulene (**2**) (248 mg, 1.20 mmol) were dissolved in dry toluene (10 ml). The solution was degassed for 10 min. Then $Pd_2(dba)_3 \cdot CHCl_3$ (61.9 mg, 59.8 µmol) was added and the blue solution was stirred at 80 °C under exclusion of light for 16 h. The solution was cooled to rt and the solvent was evaporated *in vacuo*. The residue was dissolved in CH_2Cl_2 (20 ml) and water (20 ml). The organic layer was separated and the aqueous layer was extracted with CH_2Cl_2 (2 x 20 ml). The combined organic layers were dried over Na_2SO_4 and the solvent was evaporated. The blue residue was purified by flash column chromatography (eluent: petrol ether : CH_2Cl_2 = 19 : 1).

Yield: 102 mg (348 µmol, **29 %**) of a dark blue oil

$C_{22}H_{15}N$ [293.36]

^{1}H-NMR (400 MHz, acetone-d_6, 300 K):

δ [ppm] = 8.59 (dd, $^{3}J_{HH}$ = 9.6 Hz, $^{4}J_{HH}$ = 0.8 Hz, 1H, -C<u>H</u>-), 8.28 – 8.22 (-, 2H, 2x -C<u>H</u>-), 8.06 (d, $^{3}J_{HH}$ = 4.0 Hz, 1H, -C<u>H</u>-), 7.83 (d, $^{3}J_{HH}$ = 10.0 Hz, 1H, -C<u>H</u>-), 7.80 – 7.74 (m, 1H, -C<u>H</u>-), 7.64 (d, $^{3}J_{HH}$ = 4.0 Hz, 1H, -C<u>H</u>-), 7.44 – 7.37 (m, 1H, -C<u>H</u>-), 7.37 – 7.32 (-, 2H, 2x -C<u>H</u>-), 7.30 – 7.25 (-, 2H, 2x -C<u>H</u>-), 7.19 – 7.12 (m, 1H, -C<u>H</u>-), 7.05 – 7.01 (-, 2H, 2x -C<u>H</u>-).

^{13}C-NMR (100 MHz, acetone-d_6, 300 K):

δ [ppm] = 143.6 (2x quart.), 140.5 (quart.), 140.2 (tert.), 139.7 (tert.), 135.8 (tert.), 134.7 (tert.), 134.1 (quart.), 127.0 (2x tert.), 125.5 (tert.), 124.7 (quart.), 124.5 (tert.), 124.2 (2x quart.), 121.3 (2x tert.), 120.8 (2x tert.), 117.4 (tert.), 111.0 (2x tert.).

MALDI-MS (pos.): m/z calc. for $C_{22}H_{15}N$ [$M^{\bullet+}$] 293.120, found: 293.110

Synthesis of 3-(azulene-1-yl)-9-(3,7-dimethyloctyl)-9H-carbazole (5)

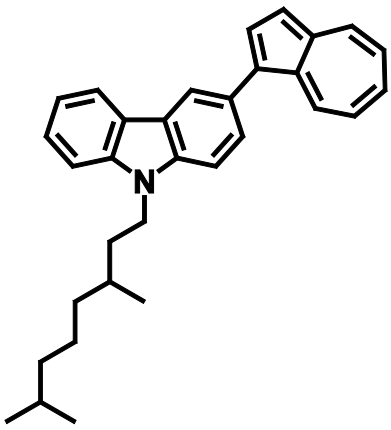

CA: [–]

Under a nitrogen atmosphere 9-(3,7-dimethyloctyl)-3-(4,4,5,5-tetramethyl-1,3,2-dioxaborolan-2-yl)-9H-carbazole (**4**) (563 mg, 1.30 mmol), K_3PO_4 (1.10 g, 5.18 mmol) and P(*t*-Bu)$_3$ (130 µl, 1.00 M in toluene, 130 µmol) and freshly prepared 1-bromoazulene (**2**) (323 mg, 1.56 mmol) were dissolved in dry toluene (15 ml). The solution was degassed for 10 min. Then $Pd_2(dba)_3 \cdot CHCl_3$ (67.3 mg, 65.0 µmol) was added and the blue solution was stirred at 90 °C under exclusion of light for 16 h. The solution was cooled to rt and the solvent was evaporated *in vacuo*. The residue was dissolved in CH_2Cl_2 (20 ml) and water (20 ml). The organic layer was separated and the aqueous layer was extracted with CH_2Cl_2 (2 x 20 ml). The combined organic layers were dried over Na_2SO_4 and the solvent was

evaporated. The blue residue was purified by flash column chromatography (eluent: petrol ether : CH_2Cl_2 = 3 : 1).

Yield: 157 mg (362 µmol, **28 %**) of a green solid

$C_{32}H_{35}N$ [433.63]

^{1}H-NMR (400 MHz, $CDCl_3$, 300 K):

δ [ppm] = 8.62 (d, $^3J_{HH}$ = 9.6 Hz, 1H, -CH-), 8.36 (d, $^3J_{HH}$ = 9.6 Hz, 1H, -CH-), 8.31 (d, $^3J_{HH}$ = 9.6 Hz, 1H, -CH-), 8.32 – 8.30 (m, 1H, -CH-), 8.16 – 8.13 (m, 1H, -CH-), 8.11 (d, $^3J_{HH}$ = 4.0 Hz, 1H, -CH-), 7.73 (dd, $^3J_{HH}$ = 8.4 Hz, $^4J_{HH}$ = 1.6 Hz, 1H, -CH-), 7.61 – 7.55 (m, 1H, -CH-), 7.54 – 7.42 (-, 4H, 4x -CH-), 7.24 (ddd, $^3J_{HH}$ = 8.0 Hz, $^3J_{HH}$ = 6.8 Hz, $^4J_{HH}$ = 1.2 Hz, 1H, -CH-), 7.13 (ddd, $^3J_{HH}$ = 9.6 Hz, $^3J_{HH}$ = 9.6 Hz, $^4J_{HH}$ = 1.2 Hz, 1H, -CH-), 4.45 – 4.29 (m, 2H, -NCH_2-), 1.99 – 1.88 (m, 1H, -NCH_2CH_2-), 1.78 – 1.67 (m, 1H, -NCH_2CH_2-), 1.67 – 1.10 (-, 8H, -$CH(CH_3)$-, -$CH(CH_3)_2$, -$CH_2CH_2CH_2$-), 1.08 (d, $^3J_{HH}$ = 6.4 Hz, 3H, -$CHCH_3$-), 0.87 (d, $^3J_{HH}$ = 6.8 Hz, 6H, -$CH(CH_3)_2$).

^{13}C-NMR (100 MHz, $CDCl_3$, 300 K):

δ [ppm] = 141.6 (quart.), 140.9 (quart.), 139.4 (quart.), 138.2 (tert.), 137.6 (tert.), 137.2 (tert.), 136.0 (tert.), 135.5 (quart.), 132.7 (quart.), 128.4 (quart.), 128.0 (tert.), 125.9 (tert.), 123.5 (quart.), 123.1 (quart.), 123.0 (tert.), 122.8 (tert.), 121.5 (tert.), 120.6 (tert.), 118.9 (tert.), 117.4 (tert.), 108.9 (tert.), 108.8 (tert.), 41.5 (sek.), 39.4 (sek.), 37.3 (sek.), 35.8 (sek.), 31.1 (tert.), 28.1 (tert.), 24.8 (sek.), 22.83 (prim.), 22.75 (prim.), 20.0 (prim.).

Synthesis of 2-(azulene-1-yl)-9-(3,7-dimethyloctyl)-9H-carbazole (7)

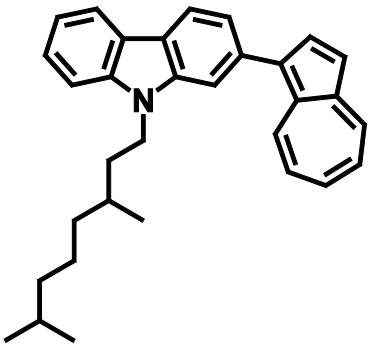

CA: [–]

Under a nitrogen atmosphere 9-(3,7-dimethyloctyl)-2-(4,4,5,5-tetramethyl-1,3,2-dioxaborolan-2-yl)-9H-carbazole (**6**) (350 mg, 808 µmol), K_3PO_4 (686 mg, 3.23 mmol) and P(*t*-Bu)$_3$ (81.0 µl, 1.00 M in toluene, 81.0 µmol) and freshly prepared 1-bromoazulene (**2**) (201 mg, 971 µmol) were dissolved in dry toluene (15 ml). The solution was degassed for 10 min. Then $Pd_2(dba)_3 \cdot CHCl_3$ (41.8 mg, 40.4 µmol) was added and the blue solution was stirred at 90 °C under exclusion of light for 24 h. The solution was cooled to rt and the solvent was evaporated *in vacuo*. The residue was dissolved in CH_2Cl_2 (20 ml) and water (20 ml). The organic layer was separated and the aqueous layer was extracted with CH_2Cl_2 (2x 20 ml). The combined organic layers were dried over Na_2SO_4 and the solvent was evaporated. The blue residue was purified by flash column chromatography (eluent: petrol ether : CH_2Cl_2 = 9 : 1).

Yield: 190 mg (438 µmol, **54 %**) of a blue solid

$C_{32}H_{35}N$ [433.63]

^{1}H-NMR (400 MHz, $CDCl_3$, 300 K):

δ [ppm] = 8.70 (d, $^3J_{HH}$ = 10.0 Hz, 1H, -CH-), 8.39 (d, $^3J_{HH}$ = 9.2 Hz, 1H, -CH-), 8.20 (dd, $^3J_{HH}$ = 8.0 Hz, $^4J_{HH}$ = 0.8 Hz, 1H, -CH-), 8.16 – 8.13 (-, 2H, 2x -CH-), 7.64 – 7.58 (-, 2H, 2x -CH-), 7.53 – 7.41 (-, 4H, 4x -CH-), 7.26 (ddd, $^3J_{HH}$ = 6.8 Hz, $^3J_{HH}$ = 6.8 Hz, $^4J_{HH}$ = 1.2 Hz, 1H, -CH-), 7.16 (ddd, $^3J_{HH}$ = 9.6 Hz, $^3J_{HH}$ = 9.6 Hz, $^4J_{HH}$ = 1.8 Hz, 2H, 2x -CH-), 4.44 – 4.30 (m, 2H, -NCH$_2$-), 1.99 – 1.88 (m, 1H, -NCH$_2$CH$_2$-), 1.77 – 1.66 (m, 1H, -NCH$_2$CH$_2$-), 1.65 – 1.08 (-, 8H, -CH(CH$_3$)-, -CH(CH$_3$)$_2$, -CH$_2$CH$_2$CH$_2$-), 1.05 (d, $^3J_{HH}$ = 6.8 Hz, 3H, -CHCH$_3$-), 0.83 (d, $^3J_{HH}$ = 6.4 Hz, 6H, -CH(CH$_3$)$_2$).

^{13}C-NMR (100 MHz, $CDCl_3$, 300 K):

δ [ppm] = 141.9 (quart.), 141.0 (quart.), 140.9 (quart.), 138.4 (tert.), 137.6 (tert.), 137.4 (tert.), 136.1 (tert.), 135.6 (quart.), 135.3 (quart.), 132.6 (quart.), 125.6 (tert.), 123.4 (tert.), 123.14 (tert.), 123.09 (quart.), 121.6 (quart.), 121.3 (tert.), 120.6 (tert.), 120.5 (tert.), 119.0 (tert.), 117.6 (tert.), 109.7 (tert.), 108.7 (tert.), 41.4 (sek.), 39.4 (sek.), 37.4 (sek.), 35.8 (sek.), 31.1 (tert.), 28.1 (tert.), 24.8 (sek.), 22.8 (prim.), 22.7 (prim.), 19.9 (prim.).

Synthesis of 1,3-dibromo-1,3,5-triazine-2,4,6(1*H*,3*H*,5*H*)-trione (11)

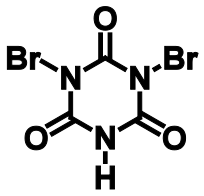

CA: [15114-43-9]

Synthesis according to lit.[112]

To a solution of lithium hydroxide monohydrate (25.2 g, 601 mmol) in water (2.5 l) 1,3,5-triazine-2,4,6-triol (38.8 g, 301 mmol) was added in portions. The mixture was stirred at rt until the solids dissolved. Then bromine (192 g, 1.20 mol) was added. After a short time a pale yellow solid precipitated. The mixture was stirred at rt for 3 h and was then stored for 12 h at 6 °C. The precipitated solid was filtered off and dried in the exsiccator.

Yield: 69.9 g (244 mmol, **81 %**) of a pale yellow solid

$C_3HBr_2N_3O_3$ [286.87]

Synthesis of 6-bromo-2-methylbenzothiazole (12)

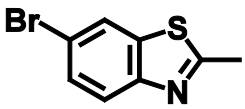

CA: [5304-21-2]

Synthesis according to lit.[96]

To a solution of 2-methylbenzothiazole (11.7 g, 78.4 mmol) in conc. sulfuric acid (250 ml) a solution of dibromoisocyanuric acid (**11**) (11.3 g, 39.4 mmol) in conc. sulfuric acid (300 ml) was added over a period of 2.5 h at rt. After the amber solution was stirred for another 18 h at rt, it was poured on ice and neutralised with a sodium hydroxide solution (10 N). The precipitate was removed and the filtrate extracted with Et_2O (3 x 200 ml). The combined organic layers were dried over Na_2SO_4 and the solvent was removed. The residual clear solution was stored over night at rt. The precipitate was separated and washed with *n*-hexane. The product was dried under high vacuum.

Yield: 5.61 g (24.6 mmol, **31 %**) of colourless crystals

C_8H_6BrNS [228.11]

^{1}H-NMR (400 MHz, $CDCl_3$, 300 K):

δ [ppm] = 7.95 (dd, $^4J_{HH}$ = 2.0 Hz, $^5J_{HH}$ = 0.4 Hz, 1H, -C<u>H</u>-), 7.79 (d, $^3J_{HH}$ = 8.8 Hz, 1H, -C<u>H</u>-), 7.54 (dd, $^3J_{HH}$ = 8.8 Hz, $^4J_{HH}$ = 2.0 Hz, 1H, -C<u>H</u>-), 2.81 (s, 3H, -CC<u>H$_3$</u>).

Synthesis of 3-(3,7-dimethyloctyl)-2-methylbenzothiazol-3-ium iodide (16)

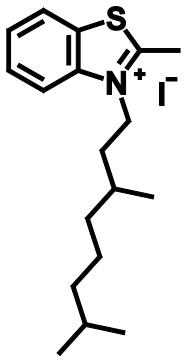

CA: [–]

Synthesis according to GP I:

2-methylbenzothiazole (5.87 g, 39.3 mmol), 1-iodo-3,7-dimethyloctane (**15**) (12.7 g, 47.7 mmol), nitromethane (20 ml); refluxed for 15 h.

Yield: 5.93 g (14.2 mmol, **36 %**) of a colourless solid

$C_{18}H_{28}SN^+I^-$ [417.39]

^{1}H-NMR (400 MHz, $CDCl_3$, 300 K):

δ [ppm] = 8.11 (ddd, $^3J_{HH}$ = 8.0 Hz, $^4J_{HH}$ = 1.2 Hz, $^5J_{HH}$ = 0.4 Hz, 1H, -C<u>H</u>-), 7.86 (d, $^3J_{HH}$ = 8.4 Hz, 1H, -C<u>H</u>-), 7.80 (ddd, $^3J_{HH}$ = 7.2 Hz, $^3J_{HH}$ = 7.2 Hz, $^4J_{HH}$ = 1.2 Hz, 1H, -C<u>H</u>-), 7.69 (ddd, $^3J_{HH}$ = 7.6 Hz, $^3J_{HH}$ = 7.6 Hz, $^4J_{HH}$ = 0.8 Hz, 1H, -C<u>H</u>-), 4.91 – 4.78 (m, 2H, -NC<u>H$_2$</u>-), 3.35 (s, 3H, ,-CC<u>H$_3$</u>), 1.89 – 1.80 (m, 1H, -NCH$_2$C<u>H$_2$</u>-), 1.69 – 1.61 (-, 2H, -NCH$_2$C<u>H$_2$</u>-, -C<u>H</u>(CH$_3$)-), 1.56 – 1.46 (m, 1H, -C<u>H</u>(CH$_3$)$_2$), 1.35 – 1.12 (-, 6H, -C<u>H$_2$</u>C<u>H$_2$</u>C<u>H$_2$</u>-), 1.16 (d, $^3J_{HH}$ = 6.4 Hz, 3H, -CHC<u>H$_3$</u>-), 0.86 (d, $^3J_{HH}$ = 6.8 Hz, 6H, -CH(C<u>H$_3$</u>)$_2$).

Synthesis of 3-hexadecyl-2-methylbenzothiazol-3-ium iodide (17)

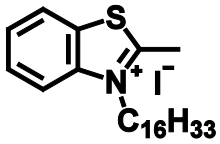

CA: [79916-26-0]

Synthesis according to GP I:

2-methylbenzothiazole (4.69 g, 31.4 mmol), 1-iodohexadecane (13.3 g, 37.7 mmol), nitromethane (20 ml); refluxed for 20 h.

Yield: 9.32 g (18.6 mmol, **59 %**) of a pale grey solid

$C_{24}H_{40}SN^{+}I^{-}$ [501.56]

^{1}H-NMR (400 MHz, $CDCl_3$, 300 K):

δ [ppm] = 8.29 (ddd, $^{3}J_{HH}$ = 8.0 Hz, $^{4}J_{HH}$ = 1.2 Hz, $^{5}J_{HH}$ = 0.8 Hz, 1H, -C<u>H</u>-), 7.97 (d, $^{3}J_{HH}$ = 8.8 Hz, 1H, -C<u>H</u>-), 7.83 (ddd, $^{3}J_{HH}$ = 8.0 Hz, $^{3}J_{HH}$ = 8.0 Hz, $^{4}J_{HH}$ = 1.2 Hz, 1H, -C<u>H</u>-), 7.73 (ddd, $^{3}J_{HH}$ = 7.6 Hz, $^{3}J_{HH}$ = 7.6 Hz, $^{4}J_{HH}$ = 0.8 Hz, 1H, -C<u>H</u>-), 4.85 (t, $^{3}J_{HH}$ = 7.6 Hz, 2H, -NC<u>H$_2$</u>-), 3.46 (s, 3H, ,-CC<u>H$_3$</u>), 2.00 – 1.92 (m, 2H, -NCH$_2$C<u>H$_2$</u>-), 1.53 – 1.46 (m, 2H, -NCH$_2$CH$_2$C<u>H$_2$</u>-), 1.39 – 1.25 (-, 24H, -NCH$_2$CH$_2$CH$_2$C<u>H$_2$</u>C<u>H$_2$</u>C<u>H$_2$</u>C<u>H$_2$</u>C<u>H$_2$</u>C<u>H$_2$</u>C<u>H$_2$</u>C<u>H$_2$</u>C<u>H$_2$</u>C<u>H$_2$</u>C<u>H$_2$</u>CH$_3$), 0.88 (t, $^{3}J_{HH}$ = 6.0 Hz, 3H, -CH$_2$C<u>H$_3$</u>).

Synthesis of 3-hexyl-2-methylbenzothiazol-3-ium iodide (18)

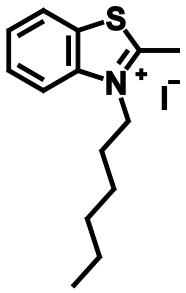

CA: [149690-59-5]

Synthesis according to GP I:

2-methylbenzothiazole (5.87 g, 39.3 mmol), 1-iodohexane (12.5 g, 58.9 mmol), nitromethane (10 ml); refluxed for 16 h.

Yield: 13.0 g (36.0 mmol, **92 %**) of a pale brown solid

$C_{14}H_{20}SN^{+}I^{-}$ [361.29]

^{1}H-NMR (400 MHz, $CDCl_3$, 300 K):

δ [ppm] = 8.24 (ddd, $^{3}J_{HH}$ = 8.4 Hz, $^{4}J_{HH}$ = 1.2 Hz, $^{5}J_{HH}$ = 0.8 Hz, 1H, -C<u>H</u>-), 7.97 (d, $^{3}J_{HH}$ = 8.4 Hz, 1H, -C<u>H</u>-), 7.85 (ddd, $^{3}J_{HH}$ = 8.4 Hz, $^{3}J_{HH}$ = 8.4 Hz, $^{4}J_{HH}$ = 1.2 Hz, 1H, -C<u>H</u>-), 7.75 (ddd, $^{3}J_{HH}$ = 8.0 Hz, $^{3}J_{HH}$ = 8.0 Hz, $^{4}J_{HH}$ = 0.8 Hz, 1H, -C<u>H</u>-), 4.87 (t, $^{3}J_{HH}$ = 8.0 Hz, 2H, -NC<u>H$_2$</u>-), 3.47 (s, 3H, ,-CC<u>H$_3$</u>), 2.01 – 1.93 (m, 2H, -NCH$_2$C<u>H$_2$</u>-), 1.57 – 1.48 (m, 2H, -NCH$_2$CH$_2$C<u>H$_2$</u>-), 1.42 – 1.25 (-, 4H, -NCH$_2$CH$_2$CH$_2$C<u>H$_2$</u>C<u>H$_2$</u>CH$_3$), 0.90 (t, $^{3}J_{HH}$ = 6.8 Hz, 3H, -CH$_2$C<u>H$_3$</u>).

Synthesis of 6-bromo-3-(3,7-dimethyloctyl)-2-methylbenzothiazol-3-ium iodide (19)

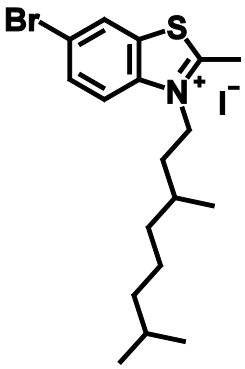

CA: [–]

Synthesis according to GP I:

6-bromo-2-methylbenzothiazole (**5**) (2.20 g, 9.64 mmol), 1-iodo-3,7-dimethyloctane (**15**) (7.76 g, 28.9 mmol), nitromethane (10 ml); refluxed for 5 d.

Yield: 1.55 g (3.12 mmol, **32 %**) of a pale grey solid

$C_{18}H_{27}BrSN^+I^-$ [496.29]

^{1}H-NMR (400 MHz, dimethylsulfoxide-d_6, 300 K):

δ [ppm] = 8.72 (d, $^4J_{HH}$ = 2.0 Hz, 1H, -CH-), 8.22 (d, $^3J_{HH}$ = 9.2 Hz, 1H, -CH-), 8.07 (dd, $^3J_{HH}$ = 8.8 Hz, $^4J_{HH}$ = 2.0 Hz, 1H, -CH-), 4.75 – 4.63 (m, 2H, -NCH_2-), 3.21 (s, 3H, -CCH_3), 1.84 – 1.77 (m, 1H, -NCH_2CH_2-), 1.72 – 1.59 (-, 2H, -NCH_2CH_2-, -$CH(CH_3)$-), 1.56 – 1.46 (m, 1H, -$CH(CH_3)_2$-), 1.39 – 1.11 (-, 6H, -$CH_2CH_2CH_2$-), 1.00 (d, $^3J_{HH}$ = 6.0 Hz, 3H, -$CHCH_3$-), 0.85 (d, $^3J_{HH}$ = 6.8 Hz, 6H, -$CH(CH_3)_2$).

Synthesis of 6-bromo-3-hexadecyl-2-methylbenzothiazol-3-ium iodide (20)

CA: [–]

Synthesis according to GP I:

6-bromo-2-methylbenzothiazole (**5**) (2.00 g, 8.77 mmol), 1-iodohexadecane (9.27 g, 26.3 mmol), nitromethane (10 ml); refluxed for 5 d.

Yield: 1.49 g (2.57 mmol, **29 %**) of a pale brown solid

$C_{24}H_{39}BrSN^+I^-$ [580.45]

^{1}H-NMR (400 MHz, dimethylsulfoxide-d_6, 300 K):

δ [ppm] = 8.70 (d, $^4J_{HH}$ = 2.0 Hz, 1H, -CH-), 8.29 (d, $^3J_{HH}$ = 9.2 Hz, 1H, -CH-), 8.06 (dd, $^3J_{HH}$ = 9.2 Hz, $^4J_{HH}$ = 2.0 Hz, 1H, -CH-), 4.68 (t, $^3J_{HH}$ = 7.6 Hz, 2H, -NCH_2-), 3.19 (s, 3H, ,-CCH_3), 1.84 – 1.77 (m, 2H, -NCH_2CH_2-), 1.45 – 1.37 (m, 2H, -$NCH_2CH_2CH_2$-), 1.35 – 1.23 (-, 24H, -$NCH_2CH_2CH_2CH_2CH_2CH_2CH_2CH_2CH_2$-$CH_2CH_2CH_2CH_2CH_2CH_2CH_3$), 0.85 (t, $^3J_{HH}$ = 6.8 Hz, 3H, -CH_2CH_3).

Synthesis of 6-bromo-3-hexyl-2-methylbenzothiazol-3-ium iodide (21)

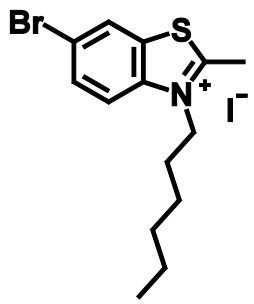

CA: [–]

Synthesis according to GP I:

6-bromo-2-methylbenzothiazole (**5**) (1.49 g, 6.53 mmol), 1-iodohexane (4.14 g, 19.5 mmol), nitromethane (10 ml); refluxed for 7 d.

Yield: 2.30 g (5.23 mmol, **80 %**) of a pale yellow solid

$C_{14}H_{19}BrSN^+I^-$ [440.18]

^{1}H-NMR (400 MHz, dimethylsulfoxide-d_6, 300 K):

δ [ppm] = 8.70 (d, $^4J_{HH}$ = 2.0 Hz, 1H, -CH-), 8.30 (d, $^3J_{HH}$ = 9.2 Hz, 1H, -CH-), 8.07 (dd, $^3J_{HH}$ = 9.2 Hz, $^4J_{HH}$ = 2.0 Hz, 1H, -CH-), 4.68 (t, $^3J_{HH}$ = 8.4 Hz, 2H, -NCH_2-), 3.20 (s, 3H, ,-CCH_3), 1.87 – 1.75 (m, 2H, -NCH_2CH_2-), 1.47 – 1.37 (m, 2H, -$NCH_2CH_2CH_2$-), 1.35 – 1.23 (-, 4H, -$NCH_2CH_2CH_2CH_2CH_2CH_3$), 0.87 (t, $^3J_{HH}$ = 7.6 Hz, 3H, -CH_2CH_3).

Synthesis of 6-acetamido-3-hexyl-2-methylbenzothiazol-3-ium iodide (22)

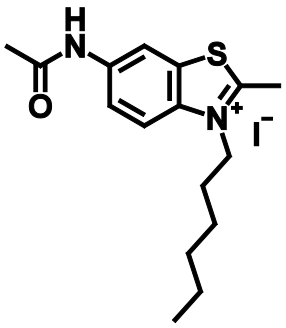

CA: [–]

Synthesis according to GP I:

6-acetamido-2-methylbenzothiazole (**3**) (3.14 g, 15.2 mmol), 1-Iodohexane (3.87 g, 18.2 mmol), nitromethane (10 ml); refluxed for 4 d.

Yield: 5.48 g (13.1 mmol; **86 %**) of a pale grey solid

$C_{16}H_{23}NOSN^{+}I^{-}$ [418.34]

^{1}H-NMR (400 MHz, dimethylsulfoxide-d_6, 300 K):

δ [ppm] = 10.49 (s, 1H, -NH-), 8.83 (d, $^{4}J_{HH}$ = 2.0 Hz, 1H, -CH-), 8.24 (d, $^{3}J_{HH}$ = 9.2 Hz, 1H, -CH-), 7.81 (dd, $^{3}J_{HH}$ = 9.2 Hz, $^{4}J_{HH}$ = 2.0 Hz, 1H, -CH-), 4.63 (t, $^{3}J_{HH}$ = 8.0 Hz, 2H, -NCH_2-), 3.15 (s, 3H, -$COCH_3$), 2.13 (s, 3H, -CCH_3), 1.86 – 1.78 (m, 2H, -NCH_2CH_2-), 1.45 – 1.39 (m, 2H, -$NCH_2CH_2CH_2$-), 1.35 – 1.24 (-, 4H, -$NCH_2CH_2CH_2CH_2CH_2CH_3$), 0.87 (t, $^{3}J_{HH}$ = 6.8 Hz, 3H, -CH_2CH_3).

Synthesis of semisquaraine ester 23

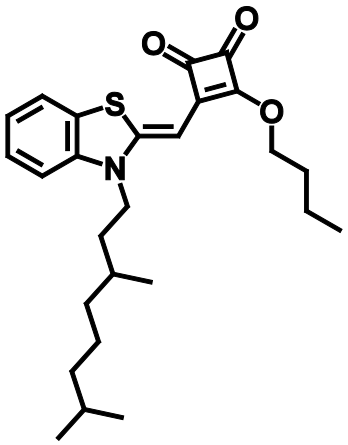

CA: [–]

Synthesis according to GP II:

3-(3,7-dimethyloctyl)-2-methylbenzothiazol-3-ium iodide (**16**) (1.00 g, 2.40 mmol), 3,4-dibutoxycyclobut-3-ene-1,2-dione (542 mg, 2.40 mmol), triethylamine (1.5 ml), *n*-butanol (20 ml); flash column chromatography (eluent: petrol ether : ethyl acetate = 5 : 1).

Yield: 715 mg (1.62 mmol; **68 %**) of an orange powder

$C_{26}H_{35}NO_3S$ [441.63]

^{1}H-NMR (400 MHz, $CDCl_3$, 300 K):

δ [ppm] = 7.48 (dd, $^3J_{HH}$ = 8.0 Hz, $^4J_{HH}$ = 0.8 Hz, 1H, -C<u>H</u>-), 7.34 (ddd, $^3J_{HH}$ = 8.0 Hz, $^3J_{HH}$ = 7.6 Hz, $^4J_{HH}$ = 1.2 Hz, 1H, -C<u>H</u>-), 7.16 (ddd, $^3J_{HH}$ = 7.6 Hz, $^3J_{HH}$ = 7.6 Hz, $^4J_{HH}$ = 1.2 Hz, 1H, -C<u>H</u>-), 7.04 (d, $^3J_{HH}$ = 8.4 Hz, 1H, -C<u>H</u>-), 5.44 (s, 1H, -CC<u>H</u>C-), 4.81 (t, $^3J_{HH}$ = 6.4 Hz, 2H, -C<u>H$_2$</u>$CH_2CH_2CH_3$), 4.05 – 3.91 (m, 2H, -NC<u>H$_2$</u>-), 1.89 – 1.82 (-, 2H, -CH_2C<u>H$_2$</u>CH_2CH_3), 1.80 – 1.14 (-, 12H, -NCH_2C<u>H$_2$</u>-, -C<u>H</u>CH_3-, -C<u>H</u>$(CH_3)_2$, -C<u>H$_2$</u>C<u>H$_2$</u>C<u>H$_2$</u>-, -CH_2CH_2C<u>H$_2$</u>CH_3), 1.05 (d, $^3J_{HH}$ = 6.4 Hz, 3H, -CHC<u>H$_3$</u>), 1.00 (t, $^3J_{HH}$ = 7.6 Hz, 3H, -$CH_2CH_2CH_2$C<u>H$_3$</u>), 0.88 (d, $^3J_{HH}$ = 6.8 Hz, 6H, -CH(C<u>H$_3$</u>$)_2$).

MALDI-MS (pos.): m/z calc. for $C_{26}H_{35}NO_3S$ [$M^{\bullet+}$] 441.233, found: 441.223

Synthesis of semisquaraine ester 24

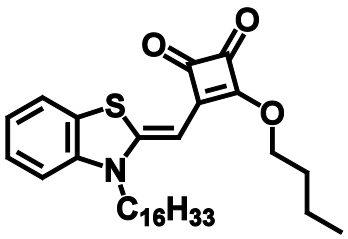

CA: [–]

Synthesis according to GP II:

3-hexadecyl-2-methylbenzothiazol-3-ium iodide (**17**) (2.00 g, 3.88 mmol), 3,4-dibutoxycyclobut-3-ene-1,2-dione (902 mg, 3.99 mmol), triethylamine (1.5 ml), *n*-butanol (20 ml); flash column chromatography (eluent: petrol ether : ethyl acetate = 3 : 1).

Yield: 1.25 g (2.38 mmol; **61 %**) of an orange powder

$C_{32}H_{47}NO_3S$ [525.79]

^{1}H-NMR (400 MHz, $CDCl_3$, 300 K):

δ [ppm] = 7.49 (dd, $^3J_{HH}$ = 8.0 Hz, $^4J_{HH}$ = 0.8 Hz, 1H, -C<u>H</u>-), 7.34 (ddd, $^3J_{HH}$ = 8.0 Hz, $^3J_{HH}$ = 7.6 Hz, $^4J_{HH}$ = 1.2 Hz, 1H, -C<u>H</u>-), 7.16 (ddd, $^3J_{HH}$ = 7.6 Hz, $^3J_{HH}$ = 7.6 Hz, $^4J_{HH}$ = 1.2 Hz, 1H, -C<u>H</u>-), 7.05 (d, $^3J_{HH}$ = 8.4 Hz, 1H, -C<u>H</u>-), 5.46 (s, 1H, -CC<u>H</u>C-), 4.82 (t, $^3J_{HH}$ = 6.4 Hz, 2H, -C<u>H$_2$</u>CH$_2$CH$_2$CH$_3$), 3.97 (t, $^3J_{HH}$ = 7.2 Hz, 2H, -NC<u>H$_2$</u>-), 1.90 – 1.75 (-, 4H, -CH$_2$C<u>H$_2$</u>CH$_2$CH$_3$, -NCH$_2$C<u>H$_2$</u>-), 1.57 – 1.49 (m, 2H, -CH$_2$CH$_2$C<u>H$_2$</u>CH$_3$), 1.47 – 1.26 (-, 26H, -NCH$_2$CH$_2$C<u>H$_2$</u>C<u>H$_2$</u>C<u>H$_2$</u>C<u>H$_2$</u>C<u>H$_2$</u>C<u>H$_2$</u>C<u>H$_2$</u>-C<u>H$_2$</u>C<u>H$_2$</u>C<u>H$_2$</u>C<u>H$_2$</u>C<u>H$_2$</u>C<u>H$_2$</u>CH$_3$), 1.00 (t, $^3J_{HH}$ = 7.6 Hz, 3H, -CH$_2$CH$_2$CH$_2$C<u>H$_3$</u>), 0.85 (t, $^3J_{HH}$ = 6.8 Hz, 3H, -CH$_2$C<u>H$_3$</u>).

MALDI-MS (pos.): m/z calc. for $C_{32}H_{47}NO_3S$ [$M^{\bullet+}$] 525.327, found: 525.327

Synthesis of semisquaraine ester 25

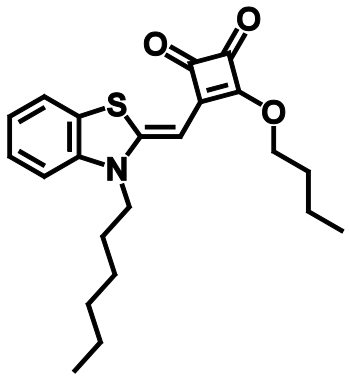

CA: [–]

Synthesis according to GP II:

3-hexyl-2-methylbenzothiazol-3-ium iodide (**18**) (2.00 g, 5.54 mmol), 3,4-dibutoxycyclobut-3-ene-1,2-dione (1.25 g, 5.52 mmol), triethylamine (2 ml), *n*-butanol (20 ml); flash column chromatography (eluent: petrol ether : ethyl acetate = 2 : 1).

Yield: 1.10 g (2.85 mmol; **52 %**) of an orange powder

$C_{22}H_{27}NO_3S$ [385.52]

^{1}H-NMR (400 MHz, $CDCl_3$, 300 K):

δ [ppm] = 7.49 (dd, $^3J_{HH}$ = 8.0 Hz, $^4J_{HH}$ = 0.8 Hz, 1H, -C<u>H</u>-), 7.34 (ddd, $^3J_{HH}$ = 8.4 Hz, $^3J_{HH}$ = 7.6 Hz, $^4J_{HH}$ = 1.2 Hz, 1H, -C<u>H</u>-), 7.16 (ddd, $^3J_{HH}$ = 7.6 Hz, $^3J_{HH}$ = 7.6 Hz, $^4J_{HH}$ = 0.8 Hz, 1H, -C<u>H</u>-), 7.05 (d, $^3J_{HH}$ = 8.4 Hz, 1H, -C<u>H</u>-), 5.47 (s, 1H, -CC<u>H</u>C-), 4.82 (t, $^3J_{HH}$ = 6.8 Hz, 2H, -C<u>H$_2$</u>$CH_2CH_2CH_3$), 3.97 (t, $^3J_{HH}$ = 7.6 Hz, 2H, -NC<u>H$_2$</u>-), 1.90 – 1.75 (-, 4H, -NCH_2C<u>H$_2$</u>-, -CH_2C<u>H$_2$</u>CH_2CH_3), 1.57 – 1.49 (m, 2H, -CH_2CH_2C<u>H$_2$</u>CH_3), 1.47 – 1.29 (-, 6H, -NCH_2CH_2C<u>H$_2$</u>-C<u>H$_2$</u>-C<u>H$_2$</u>CH_3), 1.00 (t, $^3J_{HH}$ = 7.6 Hz, 3H, -$CH_2CH_2CH_2C$<u>H$_3$</u>), 0.91 (t, $^3J_{HH}$ = 7.2 Hz, 3H, -CH_2C<u>H$_3$</u>).

MALDI-MS (pos.): m/z calc. for $C_{22}H_{27}NO_3S$ [$M^{\bullet+}$] 385.171, found: 385.173

Synthesis of semisquaraine acid 26

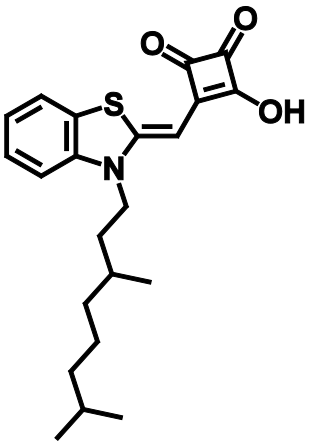

CA: [–]

Synthesis according to GP II:

Compound **23** (1.37 g, 3.10 mmol), solution of sodium hydroxide (10 N, 2.0 ml), ethanol (20 ml); flash column chromatography (eluent: petrol ether : ethyl acetate = 1 : 1).

Yield: 1.10 g (2.85 mmol; **92 %**) of an orange powder

$C_{22}H_{27}NO_3S$ [385.52]

^{1}H-NMR (400 MHz, acetone-d_6, 300 K):

δ [ppm] = 7.50 (dd, $^3J_{HH}$ = 7.6 Hz, $^4J_{HH}$ = 0.8 Hz, 1H, -C<u>H</u>-), 7.18 (ddd, $^3J_{HH}$ = 8.0 Hz, $^3J_{HH}$ = 8.0 Hz, $^4J_{HH}$ = 1.2 Hz, 1H, -C<u>H</u>-), 6.97 (d, $^3J_{HH}$ = 8.0 Hz, 1H, -C<u>H</u>-), 6.92 (ddd, $^3J_{HH}$ = 7.6 Hz, $^3J_{HH}$ = 7.6 Hz, $^4J_{HH}$ = 1.2 Hz, 1H, -C<u>H</u>-), 5.39 (s, 1H, -CC<u>H</u>C-), 3.95 – 3.79 (-, 2H, -NC<u>H$_2$</u>-), 1.67 – 1.17 (-, 10H, -C<u>H</u>CH$_3$-, -NCH$_2$C<u>H$_2$</u>-, -C<u>H</u>(CH$_3$)$_2$, -C<u>H$_2$</u>C<u>H$_2$</u>C<u>H$_2$</u>-), 0.98 (d, $^3J_{HH}$ = 6.4 Hz, 3H, -CHC<u>H$_3$</u>), 0.84 (d, $^3J_{HH}$ = 6.8 Hz, 6H, -CH(C<u>H$_3$</u>)$_2$).

The signal for the -O<u>H</u> is missing.

Synthesis of semisquaraine acid 27

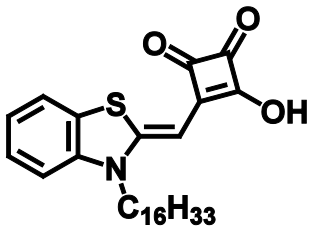

CA: [–]

Synthesis according to GP III:

Compound **24** (250 mg, 457 µmol), solution of sodium hydroxide (10 N, 0.5 ml), ethanol (10 ml); flash column chromatography (eluent: CH_2Cl_2 : MeOH = 9 : 1).

Yield: 201 mg (428 µmol; **94 %**) of an orange powder

$C_{28}H_{39}NO_3S$ [469.68]

^{1}H-NMR (400 MHz, dimethylsulfoxide-d_6, 300 K):

δ [ppm] = 7.44 (dd, $^3J_{HH}$ = 7.6 Hz, $^4J_{HH}$ = 1.2 Hz, 1H, -C<u>H</u>-), 7.17 (ddd, $^3J_{HH}$ = 8.0 Hz, $^3J_{HH}$ = 7.6 Hz, $^4J_{HH}$ = 1.2 Hz, 1H, -C<u>H</u>-), 7.02 (d, $^3J_{HH}$ = 7.6 Hz, 1H, -C<u>H</u>-), 6.91 (dd, $^3J_{HH}$ = 7.6 Hz, $^4J_{HH}$ = 0.8 Hz, 1H, -C<u>H</u>-), 5.40 (s, 1H, -CC<u>H</u>C-), 3.83 (t, $^3J_{HH}$ = 7.2 Hz, 2H, -NC<u>H$_2$</u>-), 1.65 – 1.58 (m, 2H, -NCH$_2$C<u>H$_2$</u>-), 1.39 – 1.23 (-, 26H, -NCH$_2$CH$_2$C<u>H$_2$</u>C<u>H$_2$</u>C<u>H$_2$</u>C<u>H$_2$</u>C<u>H$_2$</u>C<u>H$_2$</u>C<u>H$_2$</u>C<u>H$_2$</u>C<u>H$_2$</u>C<u>H$_2$</u>C<u>H$_2$</u>C<u>H$_2$</u>CH$_3$), 0.85 (t, $^3J_{HH}$ = 6.8 Hz, 3H, -CH$_2$C<u>H$_3$</u>).

The signal for the -O<u>H</u> is missing.

Synthesis of semisquaraine acid 28

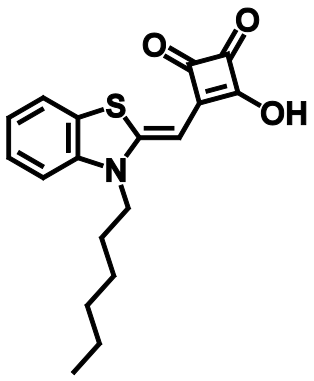

CA: [–]

Synthesis according to GP III:

Compound **25** (586 mg, 1.52 mmol), solution of sodium hydroxide (10 N, 0.5 ml), ethanol (20 ml); flash column chromatography (eluent: CH_2Cl_2 : ethyl acetate = 9 : 1).

Yield: 480 mg (1.46 mmol; **96 %**) of an orange powder

$C_{18}H_{19}NO_3S$ [329.42]

^{1}H-NMR (400 MHz, dimethylsulfoxide-d_6, 300 K):

δ [ppm] = 7.44 (dd, $^3J_{HH}$ = 7.6 Hz, $^4J_{HH}$ = 0.8 Hz, 1H, -CH-), 7.17 (ddd, $^3J_{HH}$ = 8.0 Hz, $^3J_{HH}$ = 7.6 Hz, $^4J_{HH}$ = 1.2 Hz, 1H, -CH-), 7.02 (d, $^3J_{HH}$ = 8.4 Hz, 1H, -CH-), 6.91 (ddd, $^3J_{HH}$ = 7.6 Hz, $^3J_{HH}$ = 7.6 Hz, $^4J_{HH}$ = 0.8 Hz, 1H, -CH-), 5.39 (s, 1H, -CCHC-), 3.84 (t, $^3J_{HH}$ = 8.0 Hz, 2H, -NCH_2-), 1.66 – 1.58 (m, 2H, -NCH_2CH_2-), 1.41 – 1.28 (-, 6H, -$NCH_2CH_2CH_2CH_2CH_2CH_3$), 0.86 (t, $^3J_{HH}$ = 7.2 Hz, 3H, -CH_2CH_3).

The signal for the -OH is missing.

Synthesis of tris(2-methylbenzothiazol-6-yl)amine 29

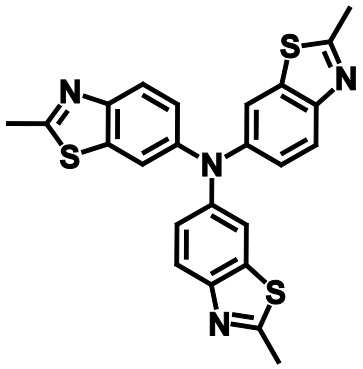

CA: [–]

Under a nitrogen atmosphere 6-amine-2-methylbenzothiazole (**9**) (100 mg, 609 µmol), 6-bromo-2-methylbenzothiazole (**12**) (306 mg, 1.34 mmol), NaO*t*-Bu (146 mg, 1.52 mmol) and P(*t*-Bu)$_3$ (24.4 µl, 1.00 M in toluene, 24.4 µmol) were dissolved in dry toluene (10 ml). The solution was degassed for 10 min. Then $Pd_2(dba)_3 \cdot CHCl_3$ (31.5 mg, 30.4 µmol) was added and the blue solution was stirred at 80 °C under exclusion of light for 3 d. The solution was cooled to rt and the solvent was evaporated *in vacuo*. The blue residue was dissolved in CH_2Cl_2 (100 ml) and water (100 ml). The organic layer was separated and the aqueous layer was extracted with CH_2Cl_2 (2 x 100 ml). The combined organic layers were dried over Na_2SO_4 and the solvent was evaporated. The blue residue was purified by flash column chromatography (eluent: CH_2Cl_2).Yield: 140 mg (305 µmol, **50 %**) of an orange oil.

$C_{24}H_{18}N_4S_3$ [458.63]

^{1}H-NMR (400 MHz, $CDCl_3$, 300 K):

δ [ppm] = 7.81 (d, $^3J_{HH}$ = 8.4 Hz, 3H, 3 x -C<u>H</u>-), 7.49 (d, $^4J_{HH}$ = 2.4 Hz, 3H, 3x -C<u>H</u>-), 7.22 (dd, $^3J_{HH}$ = 8.0 Hz, $^4J_{HH}$ = 2.4 Hz, 3H, 3 x -C<u>H</u>-), 2.79 (s, 9H, 3 x -CH_3).

MALDI-MS (pos.): m/z calc. for $C_{24}H_{18}N_4S_3$ [$M^{\bullet+}$] 458.069, found: 458.021

Synthesis of 1-(3,7-dimethyloctyl)-2,3,3-trimethyl-3H-indol-1-ium iodide (32)

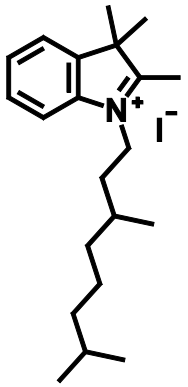

CA: [–]

Synthesis according to GP I:

2,3,3-trimethyl-3H-indole (3.00 g, 18.8 mmol), 1-iodo-3,7-dimethyloctane (**15**) (6.06 g, 22.6 mmol), nitromethane (10 ml); refluxed for 18 h.

<u>Yield</u>: 6.70 g (15.7 mmol; **84 %**) of a pale brown solid

$C_{21}H_{34}N^+I^-$ [427.41]

^{1}H-NMR (400 MHz, $CDCl_3$, 300 K):

δ [ppm] = 7.59 – 7.54 (-, 4H, 4x -C<u>H</u>-), 4.70 – 4.57 (m, 2H, -NC<u>H_2</u>-), 3.11 (s, 3H, -CC<u>H_3</u>), 1.91 – 1.82 (m, 1H, -NCH_2C<u>H_2</u>-), 1.75 – 1.63 (-, 8H, -C(C<u>H_3</u>)<u>$_2$</u>, -NCH_2C<u>H_2</u>-, -C<u>H</u>(CH_3)-), 1.56 – 1.46 (m, 1H, -C<u>H</u>(CH_3)<u>$_2$</u>-), 1.41 – 1.11 (-, 6H, -C<u>H_2</u>C<u>H_2</u>C<u>H_2</u>-), 1.07 (d, $^3J_{HH}$ = 6.0 Hz, 3H, -CHC<u>H_3</u>-), 0.85 (d, $^3J_{HH}$ = 6.0 Hz, 6H, 2x -CH(C<u>H_3</u>)<u>$_2$</u>).

Synthesis of 5-bromo-1-(3,7-dimethyloctyl)-2,3,3-trimethyl-3H-indol-1-ium iodide (34)

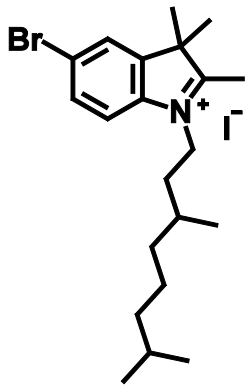

CA: [–]

Synthesis according to GP I:

5-bromo-2,3,3-trimethhyl-3H-indolenine (**33**) (20.7 g, 86.9 mmol), 1-iodo-3,7-dimethyloctane (**15**) (46.0 g, 172 mmol), nitromethane (40 ml); refluxed for 44 h.

Yield: 27.7 g (54.7 mmol; **63 %**) of a pale brown solid

$C_{21}H_{33}BrN^+I^-$ [506.30]

^{1}H-NMR (400 MHz, $CDCl_3$, 300 K):

δ [ppm] = 7.74 – 7.67 (-, 2H, 2x -C<u>H</u>-), 7.49 (d, $^3J_{HH}$ = 8.4 Hz, 1H, -C<u>H</u>-), 4.70 – 4.55 (m, 2H, -NC<u>H$_2$</u>-), 3.07 (s, 3H, -CC<u>H$_3$</u>), 1.90 – 1.77 (m, 1H, -NCH$_2$C<u>H$_2$</u>-), 1.75 – 1.61 (-, 8H, -C(C<u>H$_3$</u>)$_2$, -NCH$_2$C<u>H$_2$</u>-, -C<u>H</u>(CH$_3$)-), 1.57 – 1.45 (m, 1H, -C<u>H</u>(CH$_3$)$_2$-), 1.42 – 1.10 (-, 6H, -C<u>H$_2$</u>C<u>H$_2$</u>C<u>H$_2$</u>-), 1.06 (d, $^3J_{HH}$ = 6.0 Hz, 3H, -CHC<u>H$_3$</u>-), 0.86 (d, $^3J_{HH}$ = 6.0 Hz, 6H, 2x -CH(C<u>H$_3$</u>)$_2$).

Synthesis of 5-nitro-2,3,3-trimethyl-3H-indole (35)

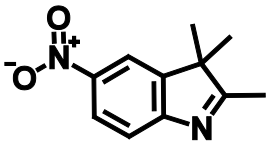

CA: [3484-22-8]

Synthesis according to lit.[119]

To a solution of 2,3,3-trimethylindole (12.0 g, 75.4 mmol) in sulfuric acid (50 ml) that was cooled down to 0 °C a solution of sodium nitrate (6.41 g, 75.4 mmol) in sulfuric acid (100 ml) was added without exceeding 5 °C. After stirring for 1 h the solution was diluted with water (600 ml) and neutralised by the addition of solid sodium hydroxide. The resulting precipitate

was filtered off, solubilised in ethyl acetate (200 ml) and washed with water (2x 200 ml). Then the organic layer was dried over $MgSO_4$. The solvent was removed and the product dried under high vacuum.

Yield: 14.9 g (73.0 mmol; **97 %**) of a brown solid

$C_{11}H_{12}N_2O_2$ [204.23]

^{1}H-NMR (400 MHz, $CDCl_3$, 300 K):

δ [ppm] = 8.23 (dd, $^3J_{HH}$ = 8.4 Hz, $^4J_{HH}$ = 2.4 Hz, 1H, -CH-), 8.14 (dd, $^4J_{HH}$ = 2.4 Hz, $^5J_{HH}$ = 0.4 Hz, 1H, -CH-), 7.60 (d, $^3J_{HH}$ = 8.4 Hz, 1H -CH-), 2.34 (s, 3H, -CCH_3), 1.36 (s, 6H, -$C(CH_3)_2$).

Synthesis of 5-amino-2,3,3-trimethyl-3H-indole (36)

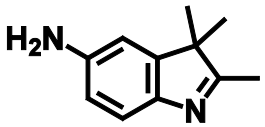

CA: [773-63-7]

Synthesis according to lit.[119]

5-Nitro-2,3,3-trimethylindole (**35**) (11.1 g, 54.4 mmol) and tin(II) chloride dihydrate (73.6 g, 326 mmol) were suspended in hydrochloric acid (2N, 250 ml) and refluxed for 2 h. After cooling to rt and filtration the solution was neutralised with sodium sulfate (20 %). The resulting precipitate was filtered off and dried under high vacuum.

Yield: 9.37 g (53.8 mmol; **99 %**) of a brown solid

$C_{11}H_{14}N_2$ [174.24]

^{1}H-NMR (400 MHz, $CDCl_3$, 300 K):

δ [ppm] = 7.30 (d, $^3J_{HH}$ = 8.0 Hz, 1H, -CH-), 6.62 (dd, $^4J_{HH}$ = 2.0 Hz, $^5J_{HH}$ = 0.4 Hz, 1H -CH-), 6.59 (dd, $^3J_{HH}$ = 8.0 Hz, $^4J_{HH}$ = 2.0 Hz, 1H, -CH-), 3.61 (s, 2H, -NH_2), 2.21 (s, 3H, -CCH_3), 1.26 (s, 6H, -$C(CH_3)_2$).

Synthesis of 5-acetamido-2,3,3-trimethyl-3H-indole (37)

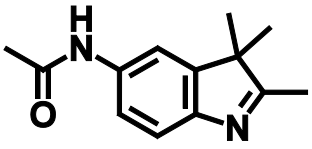

CA: [231632-87-4]

5-Amino-2,3,3-trimethylindole (**36**) (1.00 g, 5.74 mmol) was dissolved in dry CH_2Cl_2 (20 ml). Acetic anhydride (514 µl, 5.45 mmol) and N,N,N-triethylamine (756 µl, 5.45 mmol) were added and the mixture stirred for 30 min at rt. The solvent was removed and the residue purified by flash column chromatography (eluent: ethyl acetate).

Yield: 1.17 g (5.41 mmol; **99 %**) of a brown solid

$C_{13}H_{16}N_2O$ [216.28]

^{1}H-NMR (400 MHz, $CDCl_3$, 300 K):

δ [ppm] = 7.75 (d, $^4J_{HH}$ = 2.0 Hz, 1H, -CH-), 7.44 (d, $^3J_{HH}$ = 8.0 Hz, 1H, -CH-), 7.35 (s, 1H -NH-), 7.15 (dd, $^3J_{HH}$ = 8.4 Hz, $^4J_{HH}$ = 2.0 Hz, 1H, -CH-), 2.26 (s, 3H, -COCH$_3$), 2.18 (s, 3H, -CCH$_3$), 1.29 (s, 6H, -C(CH$_3$)$_2$).

Synthesis of 5-acetamido-1-(3,7-dimethyloctyl)-2,3,3-trimethyl-3H-indol-1-ium iodide (38)

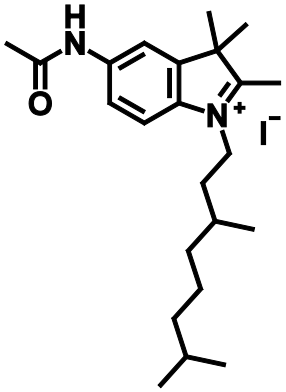

CA: [1865677-82-2]

Synthesis according to GP I:

5-Acetamido-2,3,3-trimethyl-3H-indole (**37**) (5.73 g, 26.5 mmol), 1-iodo-3,7-dimethyloctane (**8**) (8.53 g, 31.8 mmol), nitromethane (30 ml); refluxed for 18 h, precipitation in Et_2O and acetone (20:1).

Yield: 8.03 g (16.6 mmol; **63 %**) of a yellow green solid

$C_{23}H_{37}NON^{+}I^{-}$ [484.46]

^{1}H-NMR (400 MHz, dimethylsulfoxide-d_6, 300 K):

δ [ppm] = 10.32 (s, 1H, -NH-), 8.05 (d, $^{4}J_{HH}$ = 0.8 Hz, 1H, -CH-), 7.83 (d, $^{3}J_{HH}$ = 8.8 Hz, 1H, -CH-), 7.66 (dd, $^{3}J_{HH}$ = 8.8 Hz, $^{4}J_{HH}$ = 2.0 Hz, 1H, -CH-), 4.43 – 4.34 (-, 2H, -NCH_2-), 3.38 (s, 3H, -$COCH_3$), 2.79 (s, 3H, -CCH_3), 1.88 – 1.76 (m, 1H, -NCH_2CH_2-), 1.70 – 1.57 (-, 2H, -NCH_2CH_2-, -$CH(CH_3)$-), 1.50 (s, 6H, -$C(CH_3)_2$), 1.56 – 1.44 (m, 1H, -$CH(CH_3)_2$-), 1.40 – 1.06 (-, 6H, -$CH_2CH_2CH_2$-), 1.05 (d, $^{3}J_{HH}$ = 6.0 Hz, 3H, -$CHCH_3$-), 0.848 (d, $^{3}J_{HH}$ = 6.6 Hz, 3H, -$CH(CH_3)_2$), 0.846 (d, $^{3}J_{HH}$ = 6.6 Hz, 3H, -$CH(CH_3)_2$).

Synthesis of semisquaraine ester 39

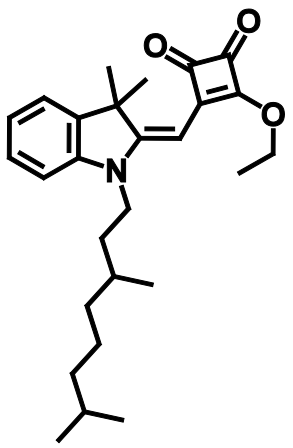

CA: [–]

Synthesis according to GP II:

1-(3,7-Dimethyloctyl)-2,3,3-trimethyl-3H-indol-1-ium iodide (**32**) (5.37 g, 12.6 mmol), 3,4-diethoxycyclobut-3-ene-1,2-dione (1.78 g, 10.5 mmol), triethylamine (5 ml), EtOH (130 ml); flash column chromatography (eluent: petrol ether : ethyl acetate = 9 : 1).

Yield: 1.78 g (4.20 mmol; **40 %**) of an orange powder

$C_{27}H_{37}NO_3$ [423.59]

^{1}H-NMR (400 MHz, acetone-d_6, 300 K):

δ [ppm] = 7.41 (ddd, $^{3}J_{HH}$ = 7.4 Hz, $^{3}J_{HH}$ = 7.4 Hz, $^{4}J_{HH}$ = 1.2 Hz, 1H, -CH-), 7.30 (ddd, $^{3}J_{HH}$ = 8.0 Hz, $^{3}J_{HH}$ = 7.5 Hz, ^{4}J = 1.2 Hz, 1H, -CH-), 7.11 – 7.06 (-, 2H, 2x -CH-), 5.45 (s, 1H, -CCHC-), 4.87 (q, $^{3}J_{HH}$ = 7.2 Hz, 2H, -CH_2CH_3), 4.03 – 3.91 (m, 2H,

-NC<u>H</u>$_2$-), 1.81 – 1.72 (m, 1H, -NCH$_2$C<u>H</u>$_2$-), 1.68 – 1.14 (-, 9H, -NCH$_2$C<u>H</u>$_2$-, -C<u>H</u>CH$_3$-, -C<u>H</u>(CH$_3$)$_2$, -C<u>H</u>$_2$C<u>H</u>$_2$C<u>H</u>$_2$-), 1.62 (s, 3H, -C(C<u>H</u>$_3$)$_2$), 1.61 (s, 3H, -C(C<u>H</u>$_3$)$_2$), 1.51 (t, $^3J_{HH}$ = 7.2 Hz, 3H, -CH$_2$C<u>H</u>$_3$), 1.06 (d, $^3J_{HH}$ = 6.4 Hz, 3H, -CHC<u>H</u>$_3$), 0.86 (d, $^3J_{HH}$ = 6.6 Hz, 6H, -CH(C<u>H</u>$_3$)$_2$).

Synthesis of the semisquaraine ester 40

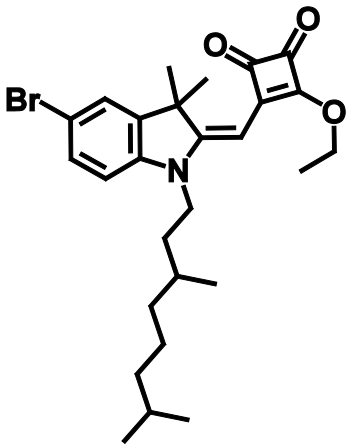

CA: [–]

Synthesis according to GP II:

5-bromo-1-(3,7-dimethyloctyl)-2,3,3-trimethyl-3H-indol-1-ium iodide (**34**) (3.72 g, 7.35 mmol), 3,4-diethoxycyclobut-3-ene-1,2-dione (1.00 g, 5.88 mmol), triethylamine (3 ml), EtOH (20 ml); flash column chromatography (eluent: petrol ether : ethyl acetate = 9 : 1).

<u>Yield:</u> 927 mg (1.84 mmol; **31 %**) of an orange powder

$C_{27}H_{36}BrNO_3$ [502.48]

^{1}H-NMR (400 MHz, acetone-d$_6$, 300 K):

δ [ppm] = 7.56 (d, $^4J_{HH}$ = 2.0 Hz, 1H, -C<u>H</u>-), 7.44 (dd, $^3J_{HH}$ = 8.4 Hz, $^4J_{HH}$ = 2.0 Hz, 1H, -C<u>H</u>-), 7.05 (d, $^3J_{HH}$ = 8.4 Hz, 1H, -C<u>H</u>-), 5.46 (s, 1H, -CC<u>H</u>C-), 4.88 (q, $^3J_{HH}$ = 7.2 Hz, 2H, -C<u>H</u>$_2$CH$_3$), 3.99 – 3.92 (m, 2H, -NC<u>H</u>$_2$-), 1.82 – 1.71 (m, 1H, -NCH$_2$C<u>H</u>$_2$-), 1.68 – 1.47 (-, 3H, -NCH$_2$C<u>H</u>$_2$-, -C<u>H</u>CH$_3$-, -C<u>H</u>(CH$_3$)$_2$), 1.64 (s, 3H, -C(C<u>H</u>$_3$)$_2$), 1.63 (s, 3H, -C(C<u>H</u>$_3$)$_2$), 1.51 (t, $^3J_{HH}$ = 7.2 Hz, 3H, -CH$_2$C<u>H</u>$_3$), 1.46 – 1.13 (-, 6H, -C<u>H</u>$_2$C<u>H</u>$_2$C<u>H</u>$_2$-), 1.05 (d, $^3J_{HH}$ = 7.2 Hz, 3H, -CHC<u>H</u>$_3$), 0.86 (d, $^3J_{HH}$ = 6.8 Hz, 6H, -CH(C<u>H</u>$_3$)$_2$).

Synthesis of the semisquaraine acid 41

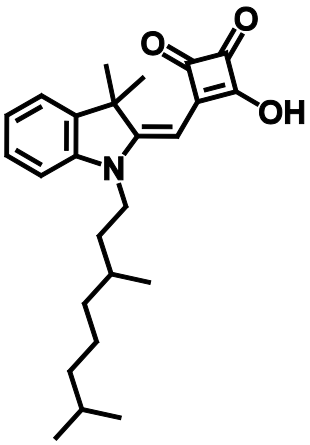

CA: [1865677-83-3]

Synthesis according to GP III:

39 (3.10 g, 7.32 mmol), solution of sodium hydroxide (10 N, 3.0 ml), EtOH (30 ml).

Yield: 2.62 g (6.62 mmol; **90 %**) of an orange powder

$C_{25}H_{33}NO_3$ [395.54]

^{1}H-NMR (400 MHz, acetone-d_6, 300 K):

δ [ppm] = 7.37 (dd, $^3J_{HH}$ = 8.0 Hz, $^4J_{HH}$ = 1.2 Hz, 1H, -C<u>H</u>-), 7.27 (ddd, $^3J_{HH}$ = 8.0 Hz, $^3J_{HH}$ = 8.0 Hz, $^4J_{HH}$ = 1.2 Hz, 1H, -C<u>H</u>-), 7.05 – 7.01 (-, 2H, 2x -C<u>H</u>-), 5.64 (s, 1H, -CC<u>H</u>C-), 4.03 – 3.96 (m, 2H, -NC<u>H$_2$</u>-), 1.83 – 1.73 (m, 1H, -NCH$_2$C<u>H$_2$</u>-), 1.64 (s, 6H, -C(C<u>H$_3$</u>)<u>$_2$</u>), 1.58 – 1.12 (-, 9H, -C<u>H</u>CH$_3$-, -NCH$_2$C<u>H$_2$</u>-, -C<u>H</u>(CH$_3$)$_2$, -C<u>H$_2$</u>C<u>H$_2$</u>C<u>H$_2$</u>-), 1.04 (d, $^3J_{HH}$ = 6.4 Hz, 3H, -CHC<u>H$_3$</u>), 0.84 (d, $^3J_{HH}$ = 6.4 Hz, 6H, -CH(C<u>H$_3$</u>)<u>$_2$</u>).

The signal for the -O<u>H</u> is missing.

Synthesis of 42

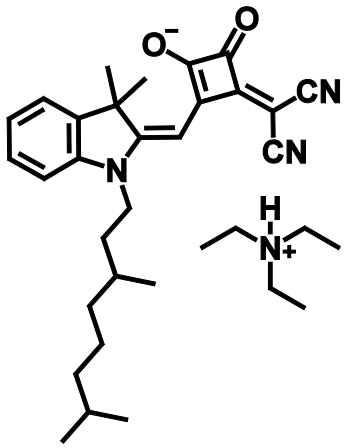

CA: [1865677-84-4]

Synthesis according to lit.[172]

Compound **39** (860 mg, 2.03 mmol) and malononitrile (268 mg, 4.06 mmol) were dissolved in EtOH (30 ml). Triethylamine (1 ml) was added dropwise and the solution was stirred for 1 h at rt. The solvent was removed *in vacuo* and the residue was purified by flash column chromatography (eluent: CH_2Cl_2/MeOH 95:5).

Yield: 1.04 g (1.91 mmol; **94 %**) of an orange solid

$C_{28}H_{32}N_3O_2^- C_6H_{16}N^+$ [544.77]

^{1}H-NMR (400 MHz, acetone-d_6, 300 K):

δ [ppm] = 8.83 (bs, 1H, -NH), 7.31 (dd, $^3J_{HH}$ = 7.2 Hz, $^4J_{HH}$ = 0.8 Hz, 1H, -CH-), 7.20 (ddd, $^3J_{HH}$ = 7.6 Hz, $^3J_{HH}$ = 7.6 Hz, $^4J_{HH}$ = 1.2 Hz, 1H, -CH-), 6.96 – 6.88 (-, 2H, 2x -CH-), 5.89 (s, 1H, -CCHC-), 3.80 – 3.68 (m, 2H, -NCH_2-), 3.09 (q, $^3J_{HH}$ = 7.2 Hz, 6H, -N(CH_2CH_3)$_3$), 1.65 – 1.59 (m, 1H, -NCH_2CH_2-), 1.56 (s, 6H, -C(CH_3)$_2$), 1.52 – 1.05 (-, 9H, -$CHCH_3$-, -NCH_2CH_2-, -CH(CH_3)$_2$, -$CH_2CH_2CH_2$-), 1.17 (t, $^3J_{HH}$ = 7.6 Hz, 9H, -N(CH_2CH_3)$_3$), 0.92 (d, $^3J_{HH}$ = 6.4 Hz, 3H, -$CHCH_3$), 0.81 (d, $^3J_{HH}$ = 6.4 Hz, 6H, -CH(CH_3)$_2$).

Synthesis of 43

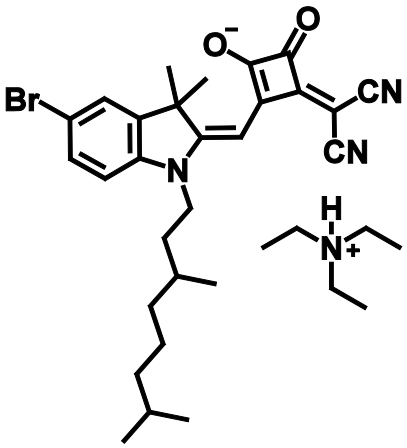

CA: [–]

Synthesis according to lit.[172]

Compound **40** (860 mg, 1.71 mmol) and malononitrile (226 mg, 3.42 mmol) were dissolved in EtOH (30 ml). Triethylamine (1 ml) was added dropwise and the solution was stirred for 1 h at rt. The solvent was removed *in vacuo* and the residue was purified by flash column chromatography (eluent: CH_2Cl_2/MeOH 95:5).

Yield: 1.04 g (1.67 mmol; **98 %**) of an orange solid

$C_{28}H_{31}BrN_3O_2^- C_6H_{16}N^+$ [623.67]

^{1}H-NMR (400 MHz, dimethylsulfoxide-d_6, 300 K):

δ [ppm] = 8.84 (bs, 1H, -NH), 7.53 (d, $^4J_{HH}$ = 2.0 Hz, 1H, -CH-), 7.36 (dd, $^3J_{HH}$ = 8.4 Hz, $^4J_{HH}$ = 2.0 Hz, 1H, -CH-), 6.87 (d, $^3J_{HH}$ = 8.4 Hz, 1H, -CH-), 5.88 (s, 1H, -CCHC-), 3.78 – 3.66 (m, 2H, -NCH_2-), 3.10 (q, $^3J_{HH}$ = 7.2 Hz, 6H, -N(C$H_2$$CH_3$)$_3$), 1.64 – 1.51 (m, 1H, -CHCH$_3$), 1.56 (s, 6H, -C(CH_3)$_2$), 1.50 – 1.05 (-, 9H, -CH(CH_3)$_2$, -NCH$_2$CH_2-, -CH_2CH_2CH_2-), 1.17 (t, $^3J_{HH}$ = 7.2 Hz, 9H, -N(CH$_2$CH_3)$_3$), 0.92 (d, $^3J_{HH}$ = 6.4 Hz, 3H, -CHCH_3), 0.81 (d, $^3J_{HH}$ = 6.4 Hz, 6H, -CH(CH_3)$_2$).

5.2.4 Squaraines

Synthesis of Az1

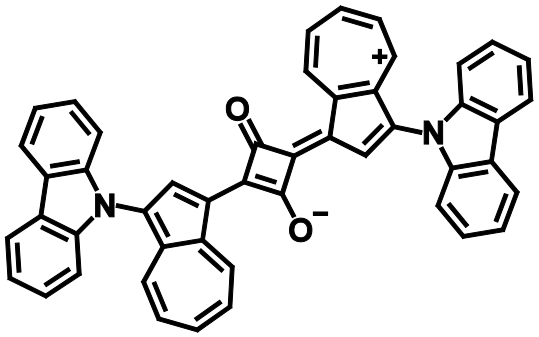

CA: [–]

Synthesis according to lit.[101]

9-(Azulene-1-yl)-9H-carbazole **(3)** (92.0 mg, 314 µmol) and 3,4-dihydroxycyclobut-3-ene-1,2-dione (17.9 mg, 157 µmol) were dissolved in a 6/4 mixture of *n*-butanol/toluene (100 ml). The mixture was refluxed for 5 h using a *Dean-Stark* trap. The solvent was removed *in vacuo* and the residue was purified by flash column chromatography (eluent: petrol ether : CH_2Cl_2 = 1 : 1 → CH_2Cl_2).

Yield: 75.0 mg (113 µmol; **36 %**) of a dark blue solid

$C_{48}H_{28}N_2O_2$ [664.75]

^{1}H-NMR (400 MHz, $CDCl_3$, 300 K):

δ [ppm] = 10.71 (d, $^3J_{HH}$ = 9.6 Hz, 2H, 2x -CH-), 9.22 (s, 2H, 2x -CH-), 8.21 (d, $^3J_{HH}$ = 7.2 Hz, 4H, 4x -CH-), 8.03 – 7.88 (-, 6H, 6x -CH-), 7.52 – 7.31 (-, 10H, 10x -CH-), 7.22 – 7.14 (-, 4H, 4x -CH-).

Synthesis of Az2

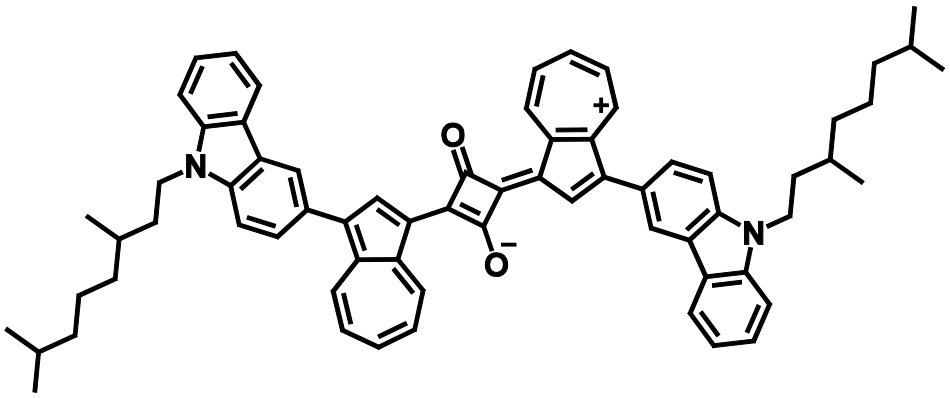

CA: [–]

Synthesis according to lit.[101]

3-(Azulene-1-yl)-9-(3,7-dimethyloctyl)-9H-carbazole **(5)** (150 mg, 346 µmol) and 3,4-dihydroxycyclobut-3-ene-1,2-dione (19.7 mg, 173 µmol) were dissolved in a 6/4 mixture of *n*-butanol/toluene (100 ml). The mixture was refluxed for 5 h using a *Dean-Stark* trap. The solvent was removed *in vacuo* and the residue was purified by flash column chromatography (eluent: CH_2Cl_2 → ethyl acetate).

Yield: 140 mg (148 µmol; **86 %**) of a black solid

$C_{68}H_{68}N_2O_2$ [945.28]

^{1}H-NMR (400 MHz, $CDCl_3$, 300 K):

δ [ppm] = 10.61 (d, $^3J_{HH}$ = 10.0 Hz, 2H, 2x -CH-), 9.18 (s, 2H, 2x -CH-), 8.71 (d, $^3J_{HH}$ = 10.0 Hz, 2H, 2x -CH-), 8.34 (s, 2H, 2x -CH-), 8.16 (d, $^3J_{HH}$ = 7.2 Hz, 2H, 2x -CH-), 7.90 – 7.71 (-, 6H, 6x -CH-), 7.57 – 7.42 (-, 8H, 8x -CH-), 7.31 – 7.24 (-, 2H, 2x -CH-), 4.46 – 4.31 (m, 4H, 2x -NCH_2-), 2.00 – 1.89 (m, 2H, 2x -NCH_2CH_2-), 1.80 – 1.68 (m, 2H, 2x -NCH_2CH_2-), 1.68 – 1.12 (-, 16H, 2x -$CH(CH_3)$-, 2x -$CH(CH_3)_2$, 2x -$CH_2CH_2CH_2$-), 1.09 (d, $^3J_{HH}$ = 6.4 Hz, 6H, 2x -$CHCH_3$-), 0.88 (d, $^3J_{HH}$ = 6.8 Hz, 12H, 2x -$CH(CH_3)_2$).

MALDI-MS (pos.): m/z calc. for $C_{68}H_{68}N_2O_2$ [$M^{\bullet+}$] 944.527, found: 944.509

Synthesis of Az3

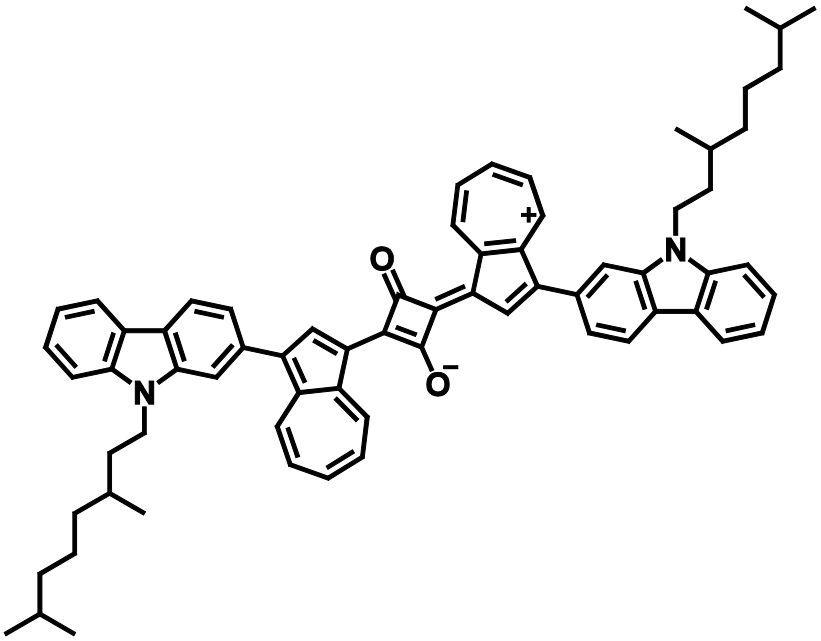

CA: [–]

Synthesis according to lit.[101]

2-(Azulene-1-yl)-9-(3,7-dimethyloctyl)-9H-carbazole **(7)** (122 mg, 281 µmol) and 3,4-dihydroxycyclobut-3-ene-1,2-dione (16.0 mg, 140 µmol) were dissolved in a 6/4 mixture of *n*-butanol/toluene (100 ml). The mixture was refluxed for 5 h using a *Dean-Stark* trap. The solvent was removed *in vacuo* and the residue was purified by flash column chromatography (eluent: CH_2Cl_2 → ethyl acetate).

Yield: 72.0 mg (76.2 µmol; **54 %**) of a black solid

$C_{68}H_{68}N_2O_2$ [945.28]

^{1}H-NMR (400 MHz, $CDCl_3$, 300 K):

δ [ppm] = 10.65 (d, $^3J_{HH}$ = 9.6 Hz, 2H, 2x -CH-), 9.21 (s, 2H, 2x -CH-), 8.74 (d, $^3J_{HH}$ = 10.0 Hz, 2H, 2x -CH-), 8.23 (d, $^3J_{HH}$ = 8.0 Hz, 2H, 2x -CH-), 8.16 (d, $^3J_{HH}$ = 8.0 Hz, 2H, 2x -CH-), 7.89 (-, 2H, 2x -CH-), 7.80 (-, 2H, 2x -CH-), 7.64 (s, 2H, 2x -CH-), 7.59 – 7.43 (-, 8H, 8x -CH-), 7.31 – 7.24 (-, 2H, 2x -CH-), 4.48 – 4.32 (m, 4H, 2x -NCH_2-), 1.98 – 1.87 (m, 2H, 2x -NCH_2CH_2-), 1.84 – 1.07 (-, 18H, 2x -NCH_2CH_2-, 2x -$CH(CH_3)$-, 2x -$CH(CH_3)_2$, 2x -$CH_2CH_2CH_2$-), 1.05 (d, $^3J_{HH}$ = 6.4 Hz, 6H, 2x -$CHCH_3$-), 0.79 (d, $^3J_{HH}$ = 6.8 Hz, 12H, 2x -$CH(CH_3)_2$).

MALDI-MS (pos.): m/z calc. for $C_{68}H_{68}N_2O_2$ [$M^{\bullet+}$] 944.527, found: 944.502

Synthesis of B1

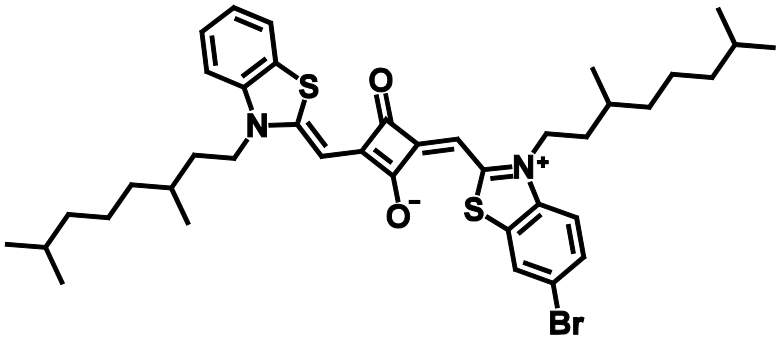

CA: [–]

Synthesis according to GP IV:

Compound **26** (643 mg, 1.67 mmol), 6-bromo-3-(3,7-dimethyloctyl)-2-methylbenzothiazol-3-ium iodide (**19**) (828 mg, 1.67 mmol), pyridine (1 ml), 6/4 mixture of *n*-butanol/toluene (100 ml); flash column chromatography (eluent: CH_2Cl_2 : MeOH = 99 : 1).

Yield: 508 mg (690 µmol; **41 %**) of a blue powder

$C_{40}H_{51}BrN_2O_2S_2$ [735.88]

^{1}H-NMR (400 MHz, $CDCl_3$, 300 K):

δ [ppm] = 7.61 – 7.54 (-, 2H, 2x -CH-), 7.46 – 7.36 (-, 2H, 2x -CH-), 7.22 (ddd, $^3J_{HH}$ = 7.2 Hz, $^3J_{HH}$ = 7.2 Hz, $^4J_{HH}$ = 0.8 Hz, 1H, -CH-), 7.13 (d, $^3J_{HH}$ = 8.4 Hz, 1H, -CH-), 6.88 (d, $^3J_{HH}$ = 8.8 Hz, 1H, -CH-), 5.90 (s, 1H, -CCHC-), 5.81 (s, 1H, -CCHC-), 4.16 – 3.93 (-, 4H, 4x -NCH_2-), 1.83 – 1.10 (-, 20H, 2x -$CHCH_3$-, 2x -NCH_2CH_2-, 2x -$CH(CH_3)_2$, 2x -$CH_2CH_2CH_2$-), 1.05 (d, $^3J_{HH}$ = 6.0 Hz, 3H, -$CHCH_3$), 1.03 (d, $^3J_{HH}$ = 6.0 Hz, 3H, -$CHCH_3$), 0.88 (-, 12H, 2x -$CH(CH_3)_2$).

Synthesis of B2

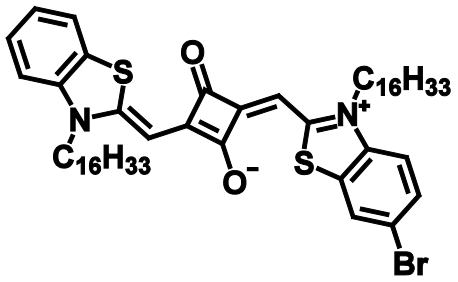

CA: [–]

Synthesis according to GP IV:

Compound **27** (198 mg, 422 µmol), 6-bromo-3-hexadecyl-2-methylbenzothiazol-3-ium iodide (**20**) (245 mg, 422 µmol), pyridine (0.5 ml), 6/4 mixture of *n*-butanol/toluene (100 ml); flash column chromatography (eluent: CH_2Cl_2 : MeOH = 9 : 1).

Yield: 187 mg (207 µmol; **49 %**) of a blue powder

$C_{52}H_{75}BrN_2O_2S_2$ [904.20]

^{1}H-NMR (400 MHz, $CDCl_3$, 300 K):

δ [ppm] = 7.62 – 7.54 (-, 2H, 2x -CH-), 7.44 – 7.35 (-, 2H, 2x -CH-), 7.22 (ddd, $^3J_{HH}$ = 8.0 Hz, $^3J_{HH}$ = 8.0 Hz, $^4J_{HH}$ = 0.8 Hz, 1H, -CH-), 7.15 (d, $^3J_{HH}$ = 8.4 Hz, 1H, -CH-), 6.89 (d, $^3J_{HH}$ = 8.8 Hz, 1H, -CH-), 5.90 (s, 1H, -CCHC-), 5.81 (s, 1H, -CCHC-), 4.07 (t, $^3J_{HH}$ = 7.6 Hz, 2H, 2x -NCH_2-), 3.97 (t, $^3J_{HH}$ = 7.6 Hz, 2H, 2x -NCH_2-), 1.87 – 1.68 (-, 4H, 2x -NCH_2CH_2-), 1.49 – 1.18 (-, 52H, 2x -$NCH_2CH_2CH_2CH_2CH_2CH_2$-$CH_2CH_2CH_2CH_2$-$CH_2CH_2CH_2CH_2CH_2CH_3$), 0.89 – 0.85 (-, 6H, 2x -CH_2CH_3).

MALDI-MS (pos.): m/z calc. for $C_{52}H_{75}BrN_2O_2S_2$ [$M^{\bullet+}$] 904.444, found: 904.443

Synthesis of B3

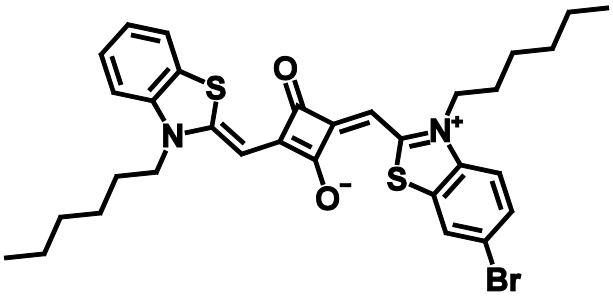

CA: [–]

Synthesis according to GP IV:

Compound **28** (298 mg, 905 µmol), 6-bromo-3-hexyl-2-methylbenzothiazol-3-ium iodide (**21**) (398 mg, 904 µmol), pyridine (1 ml), 6/4 mixture of *n*-butanol/toluene (100 ml); flash column chromatography (eluent: CH_2Cl_2 : MeOH = 9 : 1).

Yield: 268 mg (430 µmol; **48 %**) of a blue powder

$C_{32}H_{35}BrN_2O_2S_2$ [623.67]

^{1}H-NMR (400 MHz, $CDCl_3$, 300 K):

δ [ppm] = 7.58 – 7.55 (-, 2H, 2x -CH-), 7.45 – 7.36 (-, 2H, 2x -CH-), 7.23 (ddd, ^3J = 7.6 Hz, ^3J = 7.6 Hz, ^4J = 1.2 Hz, 1H, -CH-), 7.16 (d, ^3J = 8.4 Hz, 1H, -CH-), 6.90 (d, ^3J = 8.8 Hz, 1H, -CH-), 5.92 (s, 1H, -CCHC-), 5.83 (s, 1H, -CCHC-), 4.09 (t, ^3J = 8.0 Hz, 2H, -NCH_2-), 3.98 (t, ^3J = 8.0 Hz, 2H, -NCH_2-), 1.87 – 1.71 (-, 4H, 2x -NCH_2CH_2-), 1.49 – 1.26 (-, 12H, -$NCH_2CH_2CH_2CH_2CH_2CH_3$), 0.91 (t, $^3J_{HH}$ = 6.0 Hz, 3H, -CH_2CH_3), 0.90 (t, $^3J_{HH}$ = 6.0 Hz, 3H, -CH_2CH_3).

MALDI-MS (pos.): m/z calc. for $C_{32}H_{35}BrN_2O_2S_2$ [$M^{\bullet+}$] 624.130, found: 624.135

Synthesis of B4

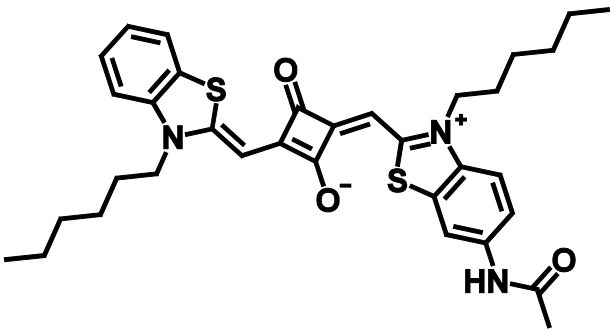

CA: [–]

Synthesis according to GP IV:

Compound **28** (706 mg, 2.14 mmol), 6-acetamido-3-hexyl-2-methylbenzothiazol-3-ium iodide (**22**) (897 mg, 2.14 mmol), pyridine (1 ml), 6/4 mixture of *n*-butanol/toluene (100 ml); flash column chromatography (eluent: CH_2Cl_2 : MeOH = 98 : 2).

Yield: 260 mg (432 µmol; **20 %**) of a blue powder

$C_{34}H_{39}N_3O_3S_2$ [601.83]

^{1}H-NMR (400 MHz, $CDCl_3$, 300 K):

δ [ppm] = 7.71 (s, 1H, -NH-), 7.65 (d, $^3J_{HH}$ = 8.8 Hz, 1H, -CH-), 7.52 (s, 1H, -CH-), 7.52 (d, $^3J_{HH}$ = 8.0 Hz, 1H, -CH-), 7.34 (ddd, $^3J_{HH}$ = 7.2 Hz, $^3J_{HH}$ = 7.2 Hz, $^4J_{HH}$ = 0.8 Hz, 1H, -CH-), 7.19 (ddd, $^3J_{HH}$ = 7.6 Hz, $^3J_{HH}$ = 7.6 Hz, $^4J_{HH}$ = 0.8 Hz, 1H, -CH-), 7.10 (d, $^3J_{HH}$ = 8.4 Hz, 1H, -CH-), 7.04 (d, $^3J_{HH}$ = 8.8 Hz, 1H, -CH-), 5.85 (s, 1H, -CCHC-), 5.84 (s, 1H, -CCHC-), 4.09 – 3.97 (-, 4H, 2x -NCH_2-), 2.19 (s, 3H, -$NHCCH_3$), 1.90 – 1.71 (-, 4H, 2x -NCH_2CH_2-), 1.49 – 1.24 (-, 12H, 2x -$NCH_2CH_2CH_2CH_2CH_2CH_3$), 0.903 (t, $^3J_{HH}$ = 7.2 Hz, 3H, -CH_2CH_3), 0.898 (t, $^3J_{HH}$ = 7.2 Hz, 3H, -CH_2CH_3).

MALDI-MS (pos.): m/z calc. for $C_{34}H_{39}N_3O_3S_2$ [$M^{\bullet+}$] 601.243, found: 601.259

Synthesis of B5

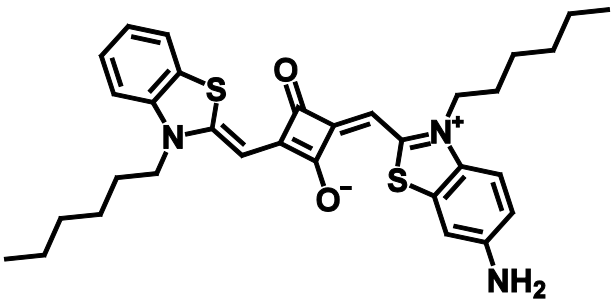

CA: [–]

Compound **B4** (86.0 mg, 143 µmol) was dissolved in EtOH (40 ml). Hydrochloric acid (5 ml 2N) was added and the solution was heated to 85 °C under exclusion of light. After 2 h the reaction mixture was allowed to cool to rt, neutralised with a solution of potassium carbonate (10 %) and extracted with CH_2Cl_2 (3x 50 ml). The solvent was removed *in vacuo* and the residue was purified by flash column chromatography (eluent: CH_2Cl_2 /MeOH 98:2).

Yield: 29.0 mg (51.8 µmol; **36 %**) of a blue solid

$C_{32}H_{37}N_3O_2S_2$ [559.79]

^{1}H-NMR (400 MHz, $CDCl_3$, 300 K):

δ [ppm] = 7.47 (dd, $^3J_{HH}$ = 8.0 Hz, $^4J_{HH}$ = 0.8 Hz, 1H, -CH-), 7.31 (ddd, $^3J_{HH}$ = 7.8 Hz, $^3J_{HH}$ = 7.8 Hz, $^4J_{HH}$ = 1.2 Hz, 1H, -CH-), 7.13 (dd, $^3J_{HH}$ = 8.0 Hz, $^3J_{HH}$ = 8.0 Hz, 1H, -CH-), 7.03 (d, $^3J_{HH}$ = 8.0 Hz, 1H, -CH-), 6.95 (d, $^3J_{HH}$ = 8.8 Hz, 1H, -CH-), 6.85 (d, $^4J_{HH}$ = 2.4 Hz, 1H, -CH-), 6.70 (dd, $^3J_{HH}$ = 8.4 Hz, $^4J_{HH}$ = 2.0 Hz, 1H, -CH-), 5.84 (s, 1H, -CCHC-), 5.79 (s, 1H, -CCHC-), 4.06 – 3.95 (-, 4H, 2x -NCH_2-), 3.87 – 3.74 (-, 2H, -NH_2), 1.84 – 1.73 (-, 4H, 2x -NCH_2CH_2-), 1.47 – 1.22 (-, 12H, 2x -$NCH_2CH_2CH_2CH_2CH_3$), 0.902 (t, $^3J_{HH}$ = 6.8 Hz, 3H, -CH_2CH_3), 0.899 (t, $^3J_{HH}$ = 6.8 Hz, 3H, -CH_2CH_3).

MALDI-MS (pos.): m/z calc. for $C_{32}H_{37}N_3O_2S_2$ [$M^{\bullet+}$] 559.232, found: 559.232

Synthesis of SQA-Br

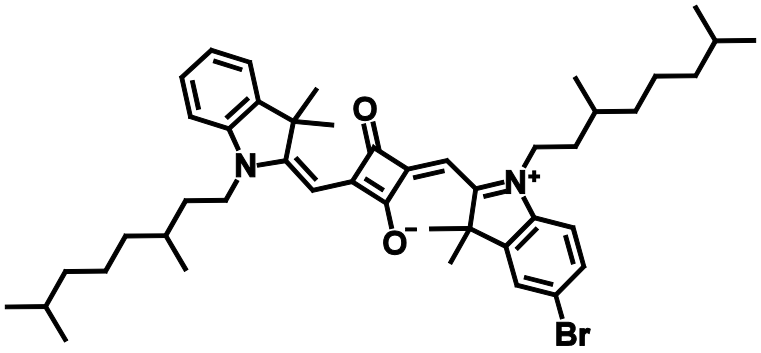

CA: [1865677-87-7]

Synthesis according to GP IV:

Compound **41** (941 mg, 2.38 mmol), 5-bromo-1-(3,7-dimethyloctyl)-2,3,3-trimethyl-3H-indol-1-ium iodide (**34**) (1.21 g, 2.39 mmol), pyridine (7 ml), 6/4 mixture of *n*-butanol/toluene (100 ml); flash column chromatography (eluent: CH_2Cl_2).

Yield: 1.11 g (1.47 mmol; **62 %**) of a blue powder

$C_{46}H_{63}BrN_2O_2$ [755.91]

^{1}H-NMR (400 MHz, $CDCl_3$, 300 K):

δ [ppm] = 7.44 – 7.38 (-, 2H, 2x -C<u>H</u>-), 7.37 (dd, $^3J_{HH}$ = 7.2 Hz, $^4J_{HH}$ = 1.0 Hz, 1H, -C<u>H</u>-), 7.32 (ddd, $^3J_{HH}$ = 7.7 Hz, $^3J_{HH}$ = 7.7 Hz, $^4J_{HH}$ = 1.2 Hz, 1H, -C<u>H</u>-), 7.17 (ddd, $^3J_{HH}$ = 7.5 Hz, $^3J_{HH}$ = 7.5 Hz, $^4J_{HH}$ = 0.8 Hz, 1H, -C<u>H</u>-), 6.99 (d, $^3J_{HH}$ = 8.0 Hz, 1H, -C<u>H</u>-), 6.78 (d, $^3J_{HH}$ = 8.4 Hz, 1H, -C<u>H</u>-), 6.00 (s, 1H, -CC<u>H</u>C-), 5.92 (s, 1H, -CC<u>H</u>C-), 4.10 – 3.84 (-, 4H, 2x -NC<u>H$_2$</u>-), 1.79 (s, 6H, 2x -CC<u>H$_3$</u>), 1.78 (s, 6H, 2x -CC<u>H$_3$</u>), 1.67 – 1.48 (-, 8H, 2x -NCH$_2$C<u>H$_2$</u>-, 2x -C<u>H</u>CH$_3$-, 2x -C<u>H</u>(CH$_3$)$_2$), 1.44 – 1.12 (-, 12H, 2x -C<u>H$_2$</u>C<u>H$_2$</u>C<u>H$_2$</u>-), 1.05 (d, $^3J_{HH}$ = 6.4 Hz, 3H, -CHC<u>H$_3$</u>), 1.03 (d, $^3J_{HH}$ = 6.4 Hz, 3H, -CHC<u>H$_3$</u>), 0.88 – 0.85 (-, 12H, 2x -CH(C<u>H$_3$</u>)$_2$).

Synthesis of SQA-Br_2

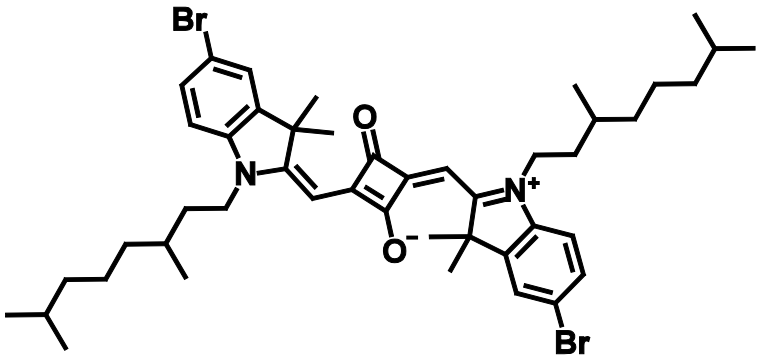

CA:[–]

Synthesis according to lit.[98]

5-Bromo-1-(3,7-dimethyloctyl)-2,3,3-trimethyl-3H-indol-1-ium iodide (**34**) (2.50 g, 4.94 mmol) and 3,4-dihydroxycyclobut-3-ene-1,2-dione (282 mg, 2.47 mmol) were dissolved in a 6/4 mixture of *n*-butanol/toluene (100 ml). Pyridine (5 ml) was added and the mixture was refluxed for 19 h using a *Dean-Stark* trap. The solvent was removed *in vacuo* and the residue was purified by flash column chromatography (eluent: CH_2Cl_2). Finally the crude product was dissolved in a small amount of CH_2Cl_2 and dropped into an excess of *n*-hexane. The resulting precipitate was filtered off and dried under high vacuum.

Yield: 1.40 g (1.68 mmol; **68 %**) of a blue powder

$C_{46}H_{62}Br_2N_2O_2$ [834.81]

^{1}H-NMR (400 MHz, $CDCl_3$, 300 K):

δ [ppm] = 7.45 – 7.40 (-, 4H, 4x -C<u>H</u>-), 6.82 (d, $^3J_{HH}$ = 8.4 Hz, 2H, 2x -C<u>H</u>-), 5.95 (s, 2H, 2x -CC<u>H</u>C-), 4.06 – 3.86 (m, 4H, 2x -NC<u>H$_2$</u>-), 1.83 – 1.45 (-, 8H, 2x -NCH$_2$C<u>H$_2$</u>-, 2x -C<u>H</u>CH$_3$-, 2x -C<u>H</u>(CH$_3$)$_2$), 1.77 (s, 12H, 2x –C(C<u>H$_3$</u>)$_2$), 1.44 – 1.10 (-, 12H, 2x -C<u>H$_2$</u>C<u>H$_2$</u>C<u>H$_2$</u>-), 1.03 (d, $^3J_{HH}$ = 6.0 Hz, 6H, 2x -CHC<u>H$_3$</u>), 0.87 (d, $^3J_{HH}$ = 6.8 Hz, 12H, 2x -CH(C<u>H$_3$</u>)$_2$).

Synthesis of SQA-B

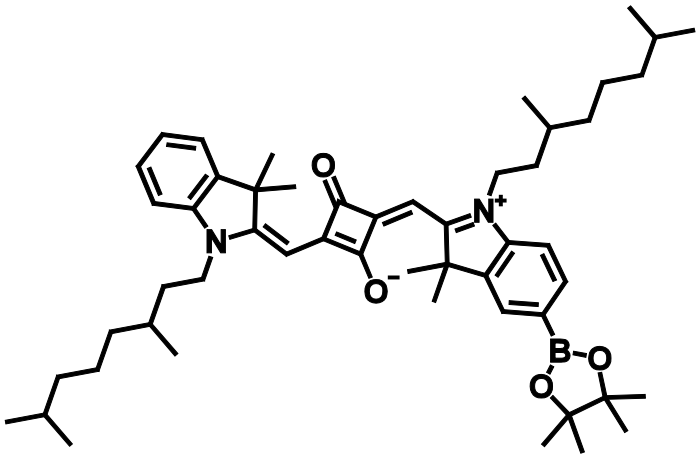

CA: [–]

Under nitrogen atmosphere **SQA-Br** (500 mg, 661 µmol), 4,4,4',4',5,5,5',5'-octamethyl-2,2'-bi(1,3,2-dioxaborolane) (168 mg, 662 µmol) and KOAc (64.9 mg, 661 µmol) were dissolved in dry 1,4-dioxane (10 ml). The solution was degassed for 10 min. Then $Pd(PhCN)_2Cl_2$ (12.7 mg, 33.1 µmol) and 1,1'-bis(diphenylphosphino)ferrocene (18.3 mg, 33.0 µmol) were added and the blue solution was refluxed for 18 h under exclusion of light. The solvent was removed *in vacuo* and the blue residue was purified by flash column chromatography (eluent: petrol ether : ethyl acetate = 1 : 1 → CH_2Cl_2 : ethyl acetate = 1 : 1). Finally the crude product was dissolved in a small amount of CH_2Cl_2 and dropped into an excess of *n*-hexane. The resulting precipitate was filtered off and dried under high vacuum.

Yield: 377 mg (470 µmol; **71 %**) of a blue powder

$C_{52}H_{75}BN_2O_4$ [802.98]

^{1}H-NMR (400 MHz, $CDCl_3$, 300 K):

δ [ppm] = 7.78 (dd, $^3J_{HH}$ = 8.0 Hz, $^4J_{HH}$ = 1.2 Hz, 1H, -CH-), 7.76 – 7.73 (m, 1H, -CH-), 7.36 (dd, $^3J_{HH}$ = 7.7 Hz, $^4J_{HH}$ = 0.9 Hz, 1H, -CH-), 7.31 (ddd, $^3J_{HH}$ = 7.7 Hz, $^3J_{HH}$ = 7.7 Hz, $^4J_{HH}$ = 1.0 Hz, 1H, -CH-), 7.15 (ddd, $^3J_{HH}$ = 7.5 Hz, $^3J_{HH}$ = 7.5 Hz, $^4J_{HH}$ = 0.7 Hz, 1H, -CH-), 6.97 (d, $^3J_{HH}$ = 8.3 Hz, 1H, -CH-), 6.93 (d, $^3J_{HH}$ = 8.3 Hz, 1H, -CH-), 5.98 (s, 1H, -CCHC-), 5.96 (s, 1H, -CCHC-), 4.07 – 3.92 (-, 4H, 2x -NCH_2-), 2.08 – 1.89 (-, 2H, 2x -NCH_2CH_2-), 1.85 – 1.46 (-, 18H, 2x -NCH_2CH_2-, 2x -$CHCH_3$, 2x -$CH(CH_3)_2$, 2x -$C(CH_3)_2$), 1.36 (s, 12H, 2x –$OC(CH_3)_2$), 1.42 – 1.10 (-, 12H, 2x -$CH_2CH_2CH_2$-), 1.05 (d, $^3J_{HH}$ = 5.7 Hz, 3H, -$CHCH_3$), 1.03 (d, $^3J_{HH}$ = 5.7 Hz, 3H, -$CHCH_3$), 0.87 (d, $^3J_{HH}$ = 6.4 Hz, 6H, -$CH(CH_3)_2$), 0.86 (d, $^3J_{HH}$ = 6.4 Hz, 6H, -$CH(CH_3)_2$).

Synthesis of SQA-B_2

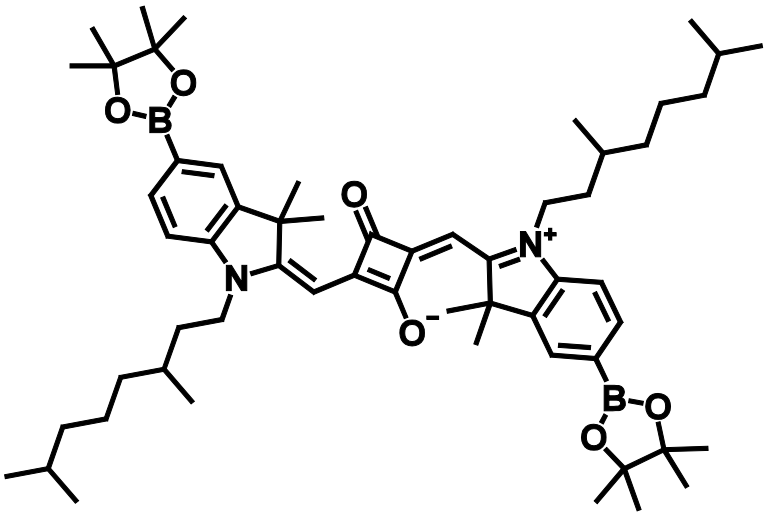

CA: [–]

Under a nitrogen atmosphere **SQA-Br_2** (1.40 g, 1.68 mmol), 4,4,4',4',5,5,5',5'-octamethyl-2,2'-bi(1,3,2-dioxaborolane) (1.07 g, 4.21 mmol) and KOAc (494 mg, 5.03 mmol) were dissolved in dry 1,4-dioxane (15 ml). The solution was degassed for 10 min. Then $Pd(PhCN)_2Cl_2$ (51.0 mg, 133 µmol) and 1,1'-bis(diphenylphosphino)ferrocene (74.0 mg, 133 µmol) were added and the blue solution was refluxed for 18 h under exclusion of light. The solvent was removed *in vacuo* and the blue residue was purified by flash column chromatography (eluent: petrol ether : ethyl acetate = 1 : 1 → CH_2Cl_2 : ethyl acetate = 1 : 1). Finally the crude product was dissolved in a small amount of CH_2Cl_2 and dropped into an excess of *n*-hexane. The resulting precipitate was filtered off and dried under high vacuum.

Yield: 805 mg (867 µmol; **52 %**) of a blue powder

$C_{58}H_{86}B_2N_2O_6$ [928.94]

^{1}H-NMR (400 MHz, $CDCl_3$, 300 K):

δ [ppm] = 7.78 (dd, $^3J_{HH}$ = 8.0 Hz, $^4J_{HH}$ = 1.2 Hz, 2H, 2x -CH-), 7.76 (s, 2H, 2x -CH-), 6.95 (d, $^3J_{HH}$ = 8.0 Hz, 2H, 2x -CH-), 5.98 (s, 2H, 2x -CCHC-), 4.10 – 3.89 (m, 4H, 2x -NCH_2-), 1.85 – 1.71 (m, 2H, 2x -NCH_2CH_2-), 1.79 (s, 12H, 2x -$C(CH_3)_2$), 1.65 – 1.45 (-, 6H, 2x -NCH_2CH_2-, 2x -$CHCH_3$, 2x -$CH(CH_3)_2$), 1.36 (s, 24H, 4x –$OC(CH_3)_2$), 1.40 – 1.10 (-, 12H, 2x -$CH_2CH_2CH_2$-), 1.03 (d, $^3J_{HH}$ = 6.0 Hz, 6H, 2x -$CHCH_3$), 0.86 (d, $^3J_{HH}$ = 6.8 Hz, 12H, 2x -$CH(CH_3)_2$).

Synthesis of SQA-NHAc

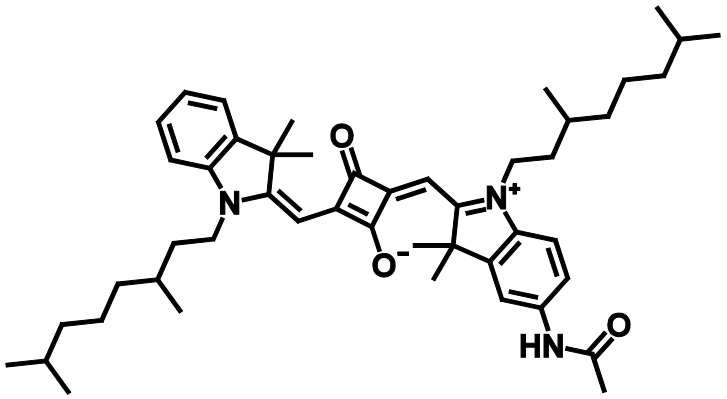

CA: [1865677-85-5]

Synthesis according to GP IV:

Compound **41** (156 mg, 394 µmol), 5-acetamido-1-(3,7-dimethyloctyl)-2,3,3-trimethyl-3H-indol-1-ium iodide (**38**) (191 mg, 394 µmol), pyridine (3 ml), 6/4 mixture of *n*-butanol/toluene (100 ml); flash column chromatography (eluent: CH_2Cl_2 : MeOH = 99 : 1).

Yield: 240 mg (327 µmol; **83 %**) of a blue powder

$C_{48}H_{67}N_3O_3$ [734.07]

^{1}H-NMR (600 MHz, CD_2Cl_2, 303.6 K):

δ [ppm] = 7.67 (s, 1H, -NH-), 7.54 (d, $^4J_{HH}$ = 2.0 Hz, 1H, -CH-), 7.51 (dd, $^3J_{HH}$ = 8.4 Hz, $^4J_{HH}$ = 2.0 Hz, 1H, -CH-), 7.36 (dd, $^3J_{HH}$ = 7.5 Hz, $^4J_{HH}$ = 0.6 Hz, 1H, -CH-), 7.31 (ddd, $^3J_{HH}$ = 7.7 Hz, $^3J_{HH}$ = 7.7 Hz, $^4J_{HH}$ = 1.2 Hz, 1H, -CH-), 7.13 (ddd, $^3J_{HH}$ = 7.5 Hz, $^3J_{HH}$ = 7.5 Hz, $^4J_{HH}$ = 0.5 Hz, 1H, -CH-), 6.99 (d, $^3J_{HH}$ = 8.0 Hz, 1H, -CH-), 6.93 (d, $^3J_{HH}$ = 8.5 Hz, 1H, -CH-), 5.88 (s, 1H, -CCHC-), 5.87 (s, 1H, -CCHC-), 4.04 – 3.87 (-, 4H, 2x -NCH_2-), 2.15 (s, 3H, -NHCCH_3), 1.82 – 1.77 (-, 2H, 2x -NCH_2CH_2-), 1.76 – 1.74 (-, 12H, 2x -$C(CH_3)_2$), 1.64 – 1.48 (-, 6H, 2x –NCH_2CH_2-, 2x -$CHCH_3$, 2x -$CH(CH_3)_2$), 1.42 – 1.12 (-, 12H, 2x -$CH_2CH_2CH_2$-), 1.04 (d, $^3J_{HH}$ = 6.2 Hz, 3H, -$CHCH_3$), 1.03 (d, $^3J_{HH}$ = 6.0 Hz, 3H, -$CHCH_3$), 0.87 – 0.85 (-, 12H, 2x -$CH(CH_3)_2$).

^{13}C-NMR (151 MHz, CD_2Cl_2, 303.6 K):

δ [ppm] = 182.1 (2x quart.), 180.1 (quart.), 179.8 (quart.), 169.72 (quart.), 169.67 (quart.), 168.5 (quart.), 143.3 (quart.), 142.9 (quart.), 142.5 (quart.),139.0 (quart.), 135.1 (quart.), 128.1 (tert.), 123.8 (tert.), 122.5 (tert.), 119.9 (tert.), 115.0 (tert.),

109.8 (tert.), 109.6 (tert.), 86.7 (tert.), 86.6 (tert.), 49.8 (quart.), 49.5 (quart.), 42.5 (sec.), 42.3 (sec.), 39.5 (2x sec.), 37.4 (2x sec.), 34.1 (sec.), 34.0 (sec.), 31.46 (tert.), 31.45 (tert.), 28.4 (tert.), 28.3 (tert.), 27.09 (2x prim.), 27.07 (2x prim.), 25.06 (sec.), 25.05 (sec.), 24.7 (prim.), 22.8 (2x prim.), 22.7 (2x prim.), 19.73 (prim.), 19.71 (prim.).

Synthesis of SQA-NH_2

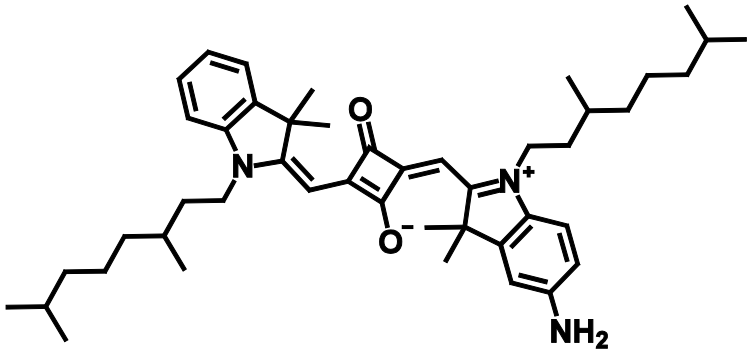

CA: [1865689-91-3]

SQA-NHAc (467 mg, 636 µmol) was dissolved in EtOH (100 ml). hydrochloric acid (20 ml 2N) was added and the solution was heated to 85 °C under exclusion of light. After 2 h the reaction mixture was allowed to cool to rt, neutralised with a 10 % solution of potassium carbonate and extracted with CH_2Cl_2 (3x 50 ml). The solvent was removed *in vacuo* and the residue was purified by flash column chromatography (eluent: CH_2Cl_2 /MeOH 99:1).

Yield: 249 mg (360 µmol; **57 %**) of a blue solid

$C_{46}H_{65}N_3O_2$ [692.03]

^{1}H-NMR (400 MHz, $CDCl_3$, 300 K):

δ [ppm] = 7.32 (d, $^3J_{HH}$ = 7.6 Hz, 1H, -CH-), 7.27 (ddd, $^3J_{HH}$ = 7.7 Hz, $^3J_{HH}$ = 7.7 Hz, $^4J_{HH}$ = 1.2 Hz, 1H, -CH-), 7.08 (ddd, $^3J_{HH}$ = 7.5 Hz, $^3J_{HH}$ = 7.5 Hz, $^4J_{HH}$ = 0.6 Hz, 1H, -CH-), 6.89 (d, $^3J_{HH}$ = 7.9 Hz, 1H, -CH-), 6.78 (d, $^3J_{HH}$ = 8.4 Hz, 1H, -CH-), 6.72 (d, $^4J_{HH}$ = 2.0 Hz, 1H, -CH-), 6.62 (dd, $^3J_{HH}$ = 8.4 Hz, $^4J_{HH}$ = 2.0 Hz, 1H, -CH-), 5.90 (s, 1H, -CCHC-), 5.88 (s, 1H, -CCHC-), 4.04 – 3.85 (-, 4H, 2x -NCH_2-), 3.81 – 3.62 (m, 2H, -NH_2), 1.77 (s, 6H, -$C(CH_3)_2$), 1.76 (s, 6H, -$C(CH_3)_2$), 1.84 – 1.71 (-, 2H, 2x -$NH_2CH_2CH_2$-), 1.65 – 1.45 (-, 6H, 2x -$NH_2CH_2CH_2$-, 2x -$CHCH_3$, 2x -$CH(CH_3)_2$),

1.41 – 1.11 (-, 12H, 2x -C$\underline{H_2}$C$\underline{H_2}$C$\underline{H_2}$-), 1.04 (d, $^3J_{HH}$ = 6.0 Hz, 3H, -CHC$\underline{H_3}$),1.03 (d, $^3J_{HH}$ = 6.0 Hz, 3H, -CHC$\underline{H_3}$), 0.88 – 0.84 (-, 12H, 2x -CH(C$\underline{H_3}$)$\underline{_2}$).

MALDI-MS (pos.): m/z calc. for $C_{46}H_{65}N_3O_2$ [$M^{\bullet+}$] 691.507, found: 691.527

Synthesis of SQA

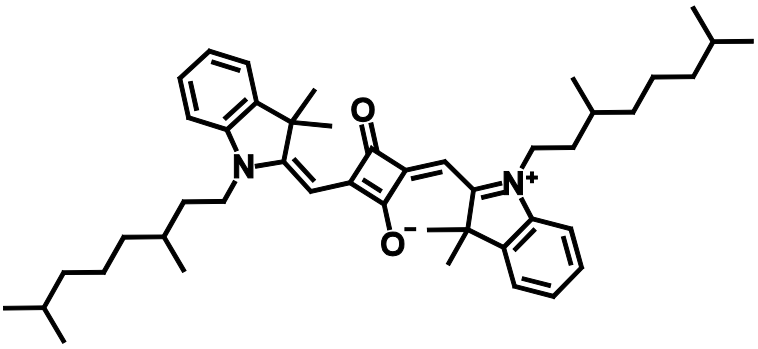

CA:[–]

Synthesis according to lit.[98]

1-(3,7-Dimethyloctyl)-2,3,3-trimethyl-3H-indol-1-ium iodide (**32**) (2.50 g, 5.85 mmol) and 3,4-dihydroxycyclobut-3-ene-1,2-dione (334 mg, 2.93 mmol) were dissolved in a 6/4 mixture of *n*-butanol/toluene (100 ml). Pyridine (5 ml) was added and the mixture was refluxed for 19 h using a *Dean-Stark* trap. The solvent was removed *in vacuo* and the residue was purified by flash column chromatography (eluent: CH_2Cl_2 : MeOH = 99 : 1→98 : 2). Finally the crude product was dissolved in a small amount of CH_2Cl_2 and dropped into an excess of *n*-hexane. The resulting precipitate was filtered off and dried under high vacuum.

Yield: 901 g (1.33 mmol; **45 %**) of a blue powder

$C_{46}H_{64}N_2O_2$ [677.01]

^{1}H-NMR (400 MHz, $CDCl_3$, 300 K):

δ [ppm] = 7.35 (dd, $^3J_{HH}$ = 7.2 Hz, $^4J_{HH}$ = 0.8 Hz, 2H, 2x -C$\underline{H}$-), 7.30 (ddd, $^3J_{HH}$ = 7.6 Hz, $^3J_{HH}$ = 7.6 Hz, $^4J_{HH}$ = 0.8 Hz, 2H, 2x -C$\underline{H}$-), 7.13 (ddd, $^3J_{HH}$ = 7.2 Hz, $^3J_{HH}$ = 7.2 Hz, $^4J_{HH}$ = 0.8 Hz, 2H, 2x -C$\underline{H}$-), 6.95 (d, $^3J_{HH}$ = 8.0 Hz, 2H, 2x -C$\underline{H}$-), 5.96 (s, 2H, 2x -CC$\underline{H}$C-), 4.09 – 3.90 (m, 4H, 2x -NC$\underline{H_2}$-), 1.85 – 1.74 (m, 2H, 2x -NCH$_2$C$\underline{H_2}$-), 1.79 (s, 12H, 2x -C(C$\underline{H_3}$)$\underline{_2}$), 1.66 – 1.57 (-, 4H, 2x -NCH$_2$C$\underline{H_2}$-, 2x -C$\underline{H}$CH$_3$-), 1.56 – 1.47 (m, 2H, 2x -C$\underline{H}$(CH$_3$)$\underline{_2}$), 1.42 – 1.12 (-, 12H, 2x -C$\underline{H_2}$C$\underline{H_2}$C$\underline{H_2}$-), 1.04 (d, $^3J_{HH}$ = 6.0 Hz, 6H, 2x -CHC$\underline{H_3}$), 0.87 (d, $^3J_{HH}$ = 6.8 Hz, 12H, 2x -CH(C$\underline{H_3}$)$\underline{_2}$).

Synthesis of dSQA

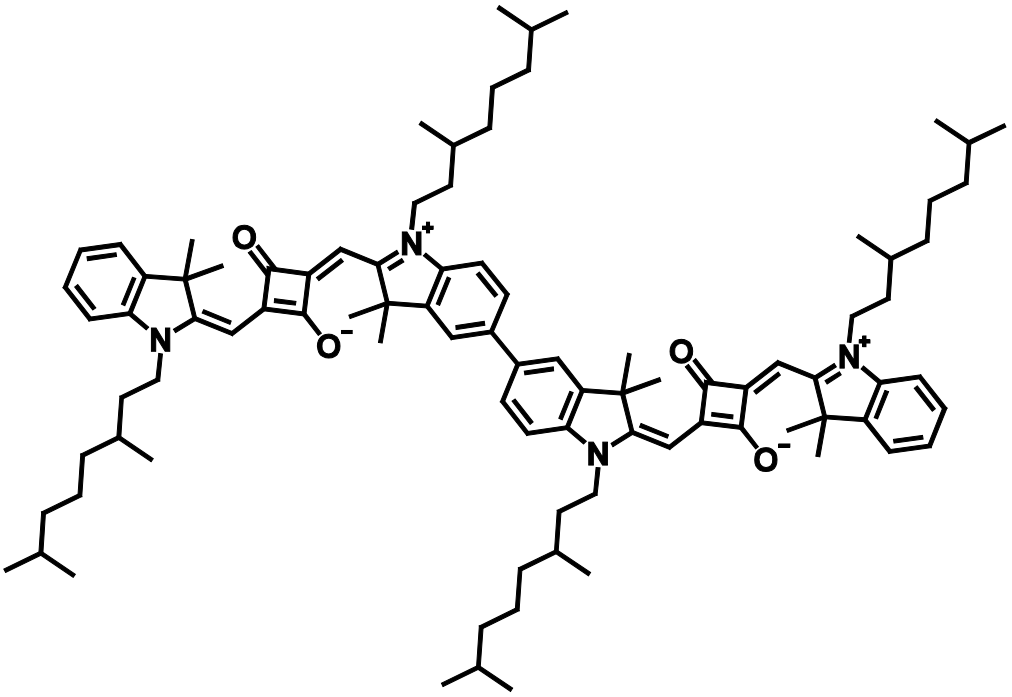

CA: [–]

Under a nitrogen atmosphere **SQA-Br** (37.0 mg, 48.9 µmol) and **SQA-B** (33.0 mg, 41.1 µmol) were dissolved in peroxide free THF (8 ml). A saturated aqueous solution of $NaCO_3$ (2 ml) was added and the solution was degassed for 15 min. Then $Pd(PPh_3)_4$ (4.75 mg, 4.11 µmol) was added and the blue solution was refluxed under exclusion of light for 3 d. The solvent was removed in vacuo and the blue residue was purified by flash column chromatography (eluent: CH_2Cl_2 : MeOH = 99 : 1→98 : 2). The main fraction was purified by GPC ($CHCl_3$). Finally the crude product was dissolved in a small amount of CH_2Cl_2 and dropped into an excess of *n*-hexane. The resulting precipitate was filtered off and dried under high vacuum.

Yield: 37.0 mg (27.4 µmol; **67 %**) of a blue powder

$C_{92}H_{126}N_4O_4$ [1352.01]

^{1}H-NMR (600 MHz, CD_2Cl_2, 293.5 K):

δ[ppm] = 7.55 – 7.50 (-, 4H, 4x -CH-), 7.36 (d, $^3J_{HH}$ = 7.2 Hz, 2H, 2x -CH-), 7.34 – 7.28 (m, 2H, 2x -CH-), 7.15 (dd, $^3J_{HH}$ = 7.2 Hz, $^3J_{HH}$ = 7.2 Hz, 2H, 2x -CH-), 7.02 (d, $^3J_{HH}$ = 8.4 Hz, 2H, 2x -CH-), 6.67 (d, $^3J_{HH}$ = 7.8 Hz, 2H, 2x -CH-), 6.03 – 5.94 (-, 4H, 4x -CH-), 4.17 – 3.88 (-, 8H, 4x -NCH_2-), 1.85 (s, 12H, 2x -$C(CH_3)_2$), 1.80 (s, 12H, 2x -$C(CH_3)_2$), 1.71 – 1.57 (-, 8H, 4x -NCH_2CH_2-, 4x -$CHCH_3$), 1.57 – 1.47 (-, 4H, 4x -NCH_2CH_2-), 1.45 – 1.10 (-, 28H, 4x -$CH_2CH_2CH_2$-, 4x -$CH(CH_3)_2$), 1.07 (d,

$^{3}J_{HH}$ = 6.0 Hz, 6H, 2x -CHC$\underline{H_3}$), 1.05 (d, $^{3}J_{HH}$ = 6.0 Hz, 6H, 2x -CHC$\underline{H_3}$), 0.872 (d, $^{3}J_{HH}$ = 6.6 Hz, 12H, 2x -CH(C$\underline{H_3}$)$\underline{_2}$), 0.868 (d, $^{3}J_{HH}$ = 6.6 Hz, 12H, 2x -CH(C$\underline{H_3}$)$\underline{_2}$).

^{13}C-NMR (151 MHz, CD_2Cl_2, 293.5 K):

δ[ppm] = 182.5 (2x quart.), 180.2 (quart.), 179.3 (quart.), 170.3 (quart.), 169.4 (quart.), 143.3 (quart.), 142.5 (2x quart.), 141.9 (quart.), 136.8 (quart.), 127.9 (tert.), 126.8 (tert.), 123.9 (tert.), 122.5 (tert.), 121.0 (tert.), 109.6 (tert.), 109.4 (tert.), 87.0 (tert.), 86.8 (tert.), 49.5 (quart.), 49.4 (quart.), 42.3 (2x sec.), 39.32 (sec.), 39.31 (sec.), 37.29 (sec.), 37.26 (sec.), 34.0 (2x sec.), 31.4 (2x tert.), 28.1 (2x tert.), 27.4 (2x prim.), 27.1 (2x prim.), 24.83 (sec.), 24.81 (sec.), 22.848 (prim.), 22.836 (prim.), 22.74 (prim.), 22.73 (prim.), 19.78 (prim.), 19.74 (prim.).

ESI-MS (pos., high res.):

m/z calc. for $C_{138}H_{188}N_6O_6$ [$M^{\bullet+}$] 1350.97736, found: 1350.97682

Δ: 0.40 ppm

Synthesis of dSQA-B and tSQA

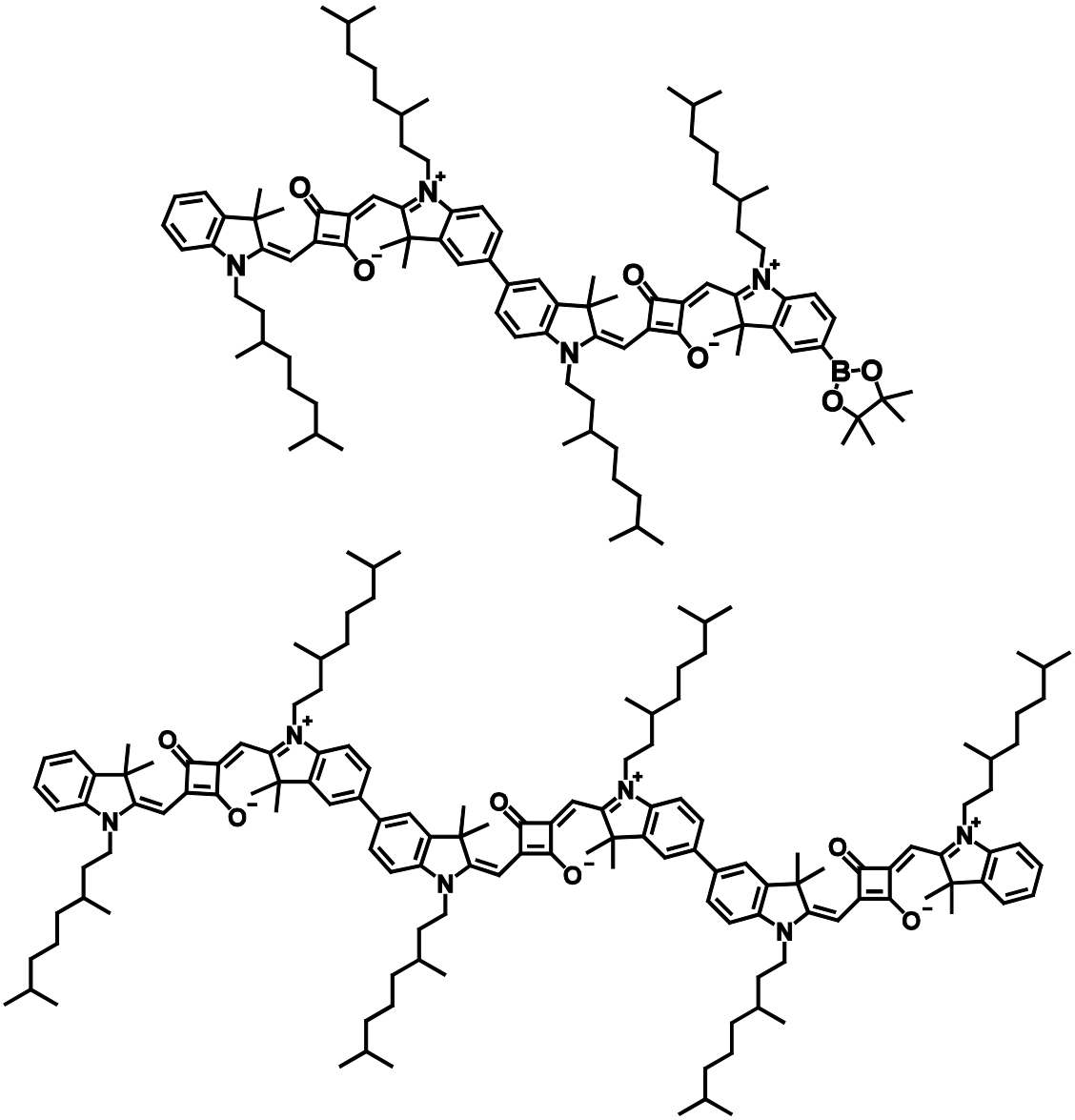

Under a nitrogen atmosphere **SQA-Br** (332 mg, 439 µmol) and **SQA-B$_2$** (462 mg, 462 µmol) were dissolved in peroxide free THF (10 ml). A saturated aqueous solution of $NaCO_3$ (3 ml) was added and the solution was degassed for 15 min. Then $Pd(PPh_3)_4$ (25.4 mg, 22.0 µmol) was added and the blue solution was refluxed under exclusion of light for 4 d. The solvent was removed in vacuo and the blue residue was purified by flash column chromatography (eluent: CH_2Cl_2 : MeOH = 99 : 1→98 : 2). The main fraction was purified by GPC ($CHCl_3$). Finally the crude product was dissolved in a small amount of CH_2Cl_2 and dropped into an excess of *n*-hexane. The resulting precipitate was filtered off and dried under high vacuum.

dSQA-B:

CA: [–]

Yield: 249 mg (168 µmol; **38 %**) of a blue powder

$C_{98}H_{137}BN_4O_6$ [1477.97]

^{1}H-NMR (600 MHz, CD_2Cl_2, 293.5 K):

δ[ppm] = 7.75 – 7.72 (-, 2H, 2x -CH-), 7.59 – 7.56 (-, 4H, 4x -CH-), 7.38 (dd, $^3J_{HH}$ = 7.2 Hz, $^4J_{HH}$ = 0.6 Hz, 1H, -CH-), 7.32 (dd, $^3J_{HH}$ = 7.8 Hz, $^4J_{HH}$ = 1.2 Hz, 1H, -CH-), 7.16 (ddd, $^3J_{HH}$ = 7.8 Hz, $^3J_{HH}$ = 7.8 Hz, $^4J_{HH}$ = 0.6 Hz, 1H, -CH-), 7.10 (d, $^3J_{HH}$ = 8.4 Hz, 1H, -CH-), 7.07 (d, $^3J_{HH}$ = 8.4 Hz, 1H, -CH-), 7.02 (d, $^3J_{HH}$ = 7.8 Hz, 1H, -CH-), 7.00 (d, $^3J_{HH}$ = 8.4 Hz, 1H, -CH-), 5.97 (s, 1H, -CH-), 5.93 (-, 3H, 3x -CH-), 4.15 – 3.92 (-, 8H, 4x -NCH$_2$-), 1.89 – 1.70 (-, 28H, 4x -NCH$_2$CH$_2$-, 4x -C(CH$_3$)$_2$), 1.63 – 1.59 (-, 8H, 4x -NCH$_2$CH$_2$-, 4x -CHCH$_3$), 1.58 – 1.49 (-, 4H, 4x -CH(CH$_3$)$_2$), 1.46 – 1.14 (-, 36H, 4x -CH$_2$CH$_2$CH$_2$-, 2x -OC(CH$_3$)$_2$), 1.084 (d, $^3J_{HH}$ = 6.0 Hz, 3H, -CHCH$_3$), 1.082 (d, $^3J_{HH}$ = 6.0 Hz, 3H, -CHCH$_3$), 1.07 (d, $^3J_{HH}$ = 6.0 Hz, 3H, -CHCH$_3$), 1.06 (d, $^3J_{HH}$ = 6.0 Hz, 3H, -CHCH$_3$), 0.874 (-, 12H, 2x -CH(CH$_3$)$_2$), 0.869 (d, $^3J_{HH}$ = 6.6 Hz, 6H, -CH(CH$_3$)$_2$), 0.866 (d, $^3J_{HH}$ = 6.6 Hz, 6H, -CH(CH$_3$)$_2$).

^{13}C-NMR (151 MHz, CD_2Cl_2, 293.5 K):

δ[ppm] = 182.04 (4x quart.), 181.35 (quart.), 181.0 (quart.), 180.4 (quart.), 180.1 (quart.), 170.2 (quart.), 170.1 (quart.), 169.6 (quart.), 169.4 (quart.), 145.5 (quart.), 143.5 (2x quart.), 142.8 (quart.), 142.6 (quart.), 142.3 (quart.), 142.1 (quart.), 141.8 (quart.), 137.1 (quart.), 136.7 (quart.), 135.3 (tert.), 128.4 (tert.), 128.1 (tert.), 126.9 (2x tert.), 124.1 (quart.), 124.0 (tert.), 122.6 (tert.), 121.1 (2x tert.), 110.1 (tert.), 109.9 (tert.), 109.8 (tert.), 109.0 (tert.), 87.4 (2x tert.), 87.1 (tert.), 86.9 (tert.), 84.2 (quart.), 49.8 (quart.), 49.63 (quart.), 49.57 (quart.), 49.2 (quart.), 42.6 (sec.), 42.5 (sec.), 42.43 (sec.), 42.35 (sec.), 39.5 (4x sec.), 37.48 (sec.), 37.47 (sec.), 34.46 (2x sec.), 34.2 (sec.), 34.12 (sec.), 34.09 (sec.), 34.06 (sec.), 31.5 (4x tert.), 28.37 (2x tert.), 28.36 (2x tert.), 27.28 (prim.), 27.27 (prim.), 27.20 (2x prim.), 27.19 (2x prim.), 27.07 (prim.), 27.06 (prim.), 25.10 (2x sec.), 25.07 (2x sec.), 25.05 (prim.), 22.82 (2x prim.), 22.81 (2x prim.), 22.73 (2x prim.), 22.72 (2x prim.), 19.79 (2x prim.), 19.76 (prim.), 19.75 (prim.).

tSQA:

CA: [–]

Yield: 133 mg (65.6 µmol; **30 %**) of a blue powder

$C_{138}H_{188}N_6O_6$ [2027.01]

^{1}H-NMR (600 MHz, CD_2Cl_2, 293.5 K):

δ[ppm] = 7.60 – 7.57 (-, 6H, 6x -CH-), 7.56 (dd, $^4J_{HH}$ = 1.8 Hz, $^4J_{HH}$ = 1.8 Hz, 2H, 2x -CH-), 7.38 (d, $^3J_{HH}$ = 7.2 Hz, 2H, 2x -CH-), 7.33 (ddd, $^3J_{HH}$ = 7.8 Hz, $^3J_{HH}$ = 7.8 Hz, $^3J_{HH}$ = 7.8 Hz, $^4J_{HH}$ = 0.6 Hz, 2H, 2x -CH-), 7.16 (dd, $^3J_{HH}$ = 7.2 Hz, $^3J_{HH}$ = 7.2 Hz, 2H, 2x -CH-), 7.08 (dd, $^3J_{HH}$ = 7.2 Hz, $^3J_{HH}$ = 7.2 Hz, 4H, 4x -CH-), 7.02 (d, $^3J_{HH}$ = 7.8 Hz, 2H, 2x -CH-), 6.00 – 5.88 (-, 6H, 6x -CH-), 4.14 – 3.94 (-, 12H, 6x -NCH_2-), 1.83 – 1.76 (-, 42H, 6x -NCH_2CH_2-, 6x -$C(CH_3)_2$), 1.70 – 1.59 (-, 12H, 6x -NCH_2CH_2-, 6x -$CHCH_3$), 1.56 – 1.51 (-, 6H, 6x -$CH(CH_3)_2$), 1.47 – 1.12 (-, 36H, 6x -$CH_2CH_2CH_2$-), 1.09 (d, $^3J_{HH}$ = 6.0 Hz, 6H, 2x -$CHCH_3$), 1.08 (d, $^3J_{HH}$ = 6.0 Hz, 6H, 2x -$CHCH_3$), 1.07 (d, $^3J_{HH}$ = 6.0 Hz, 6H, 2x -$CHCH_3$), 0.880 (d, $^3J_{HH}$ = 6.6 Hz, 12H, 2x -$CH(CH_3)_2$), 0.876 (d, $^3J_{HH}$ = 6.6 Hz, 12H, 2x -$CH(CH_3)_2$), 0.87 (d, $^3J_{HH}$ = 6.6 Hz, 12H, 2x -$CH(CH_3)_2$).

^{13}C-NMR (151 MHz, CD_2Cl_2, 293.5 K):

δ[ppm] = 182.1 (3x quart.), 181.0 (quart.), 180.4 (quart.), 180.2 (quart.), 170.2 (quart.), 169.6 (quart.), 169.4 (quart.), 143.5 (2x quart.), 142.8 (quart.), 142.7 (quart.), 142.31 (quart.), 142.26 (quart.), 136.9 (quart.), 136.8 (quart.), 128.1 (tert.), 126.9 (2x tert.), 124.0 (tert.), 122.6 (tert.), 121.1 (2x tert.), 110.04 (tert.), 109.95 (tert.), 109.8 (tert.), 87.3 (tert.), 87.1 (tert.), 86.9 (tert.), 49.68 (quart.), 49.65 (quart.), 49.6 (quart.), 42.52 (2x sec.), 42.45 (sec.), 39.6 (2x sec.), 39.5 (sec.), 37.50 (2x sec.), 37.48 (sec.), 34.19 (sec.), 34.15 (sec.), 34.1 (sec.), 31.5 (3x tert.), 28.39 (2x tert.), 28.38 (tert.), 27.3 (4x prim.), 27.1 (2x prim.), 25.11 (2x sec.), 25.09 (sec.), 22.84 (2x prim.), 22.83 (prim.), 22.75 (2x prim.), 22.74 (prim.), 19.81 (2x prim.), 19.77 (prim.).

ESI-MS (pos., high res.):

m/z calc. for $C_{138}H_{188}N_6O_6$ [$M^{\bullet+}$] 2026.46180, found: 2026.46389

Δ: 1.03 ppm

Synthesis of SQB-Br

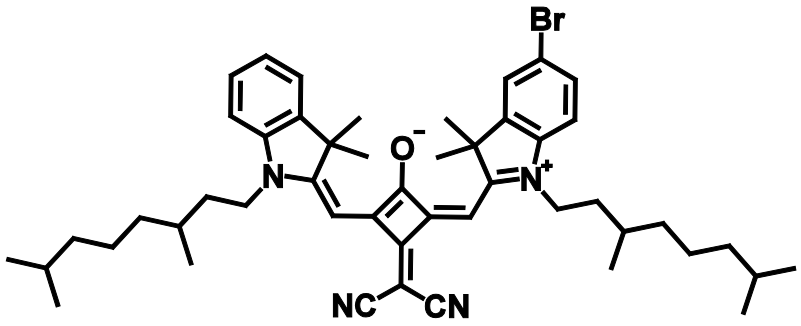

CA: [1865677-89-9]

Synthesis according to GP IV:

43 (1.04 g, 1.67 mmol), 1-(3,7-dimethyloctyl)-2,3,3-trimethyl-3H-indol-1-ium iodide (**32**) (713 mg, 1.67 mmol), pyridine (6 ml), 6/4 mixture of *n*-butanol/toluene (100 ml); flash column chromatography (eluent: CH_2Cl_2).

Yield: 1.02 g (1.27 mmol; **76 %**) of a blue powder

$C_{49}H_{63}BrN_4O$ [803.96]

^{1}H-NMR (400 MHz, $CDCl_3$, 300 K):

δ [ppm] = 7.49 – 7.45 (-, 2H, -2x -CH-), 7.41 (dd, $^3J_{HH}$ = 7.4 Hz, $^4J_{HH}$ = 0.8 Hz, 1H, -CH-), 7.37 (ddd, $^3J_{HH}$ = 7.7 Hz, $^3J_{HH}$ = 7.7 Hz, $^4J_{HH}$ = 1.2 Hz, 1H, -CH-), 7.24 (ddd, $^3J_{HH}$ = 7.5 Hz, $^3J_{HH}$ = 7.5 Hz, $^4J_{HH}$ = 1.0 Hz, 1H, -CH-), 7.11 (d, $^3J_{HH}$ = 7.9 Hz, 1H, -CH-), 6.90 (d, $^3J_{HH}$ = 8.4 Hz, 1H, -CH-), 6.52 (s, 1H, -CCHC-), 6.42 (s, 1H, -CCHC-), 4.14 – 3.91 (-, 4H, 2x -NCH_2-), 1.85 – 1.70 (-, 2H, 2x -NCH_2CH_2-), 1.76 (s, 6H, -$C(CH_3)_2$), 1.74 (s, 6H, -$C(CH_3)_2$), 1.70 – 1.11 (-, 18H, 2x -NCH_2CH_2-, 2x -$CH(CH_3)_2$, 2x -$CHCH_3$-, 2x -$CH_2CH_2CH_2$-), 1.03 (d, $^3J_{HH}$ = 6.3 Hz, 3H, -$CHCH_3$), 1.01 (d, $^3J_{HH}$ = 6.3 Hz, 3H, -$CHCH_3$), 0.88 – 0.84 (-, 12H, 2x -$CH(CH_3)_2$).

MALDI-MS (pos.): m/z calc. for $C_{49}H_{63}BrN_4O$ [$M^{\bullet+}$] 804.417, found: 804.432

Synthesis of SQB-NHAc

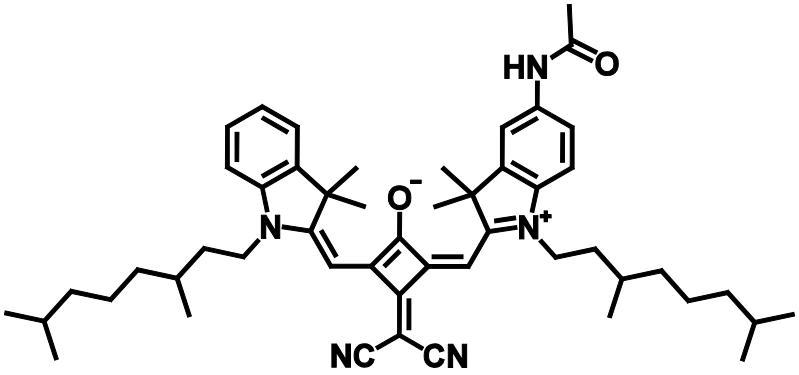

CA: [–]

Synthesis according to GP IV:

42 (700 mg, 1.28 mmol), 5-acetamido-1-(3,7-dimethyloctyl)-2,3,3-trimethyl-3H-indol-1-ium iodide (**38**) (623 mg, 1.29 mmol), pyridine (5 ml), 6/4 mixture of *n*-butanol/toluene (100 ml); flash column chromatography (eluent: CH_2Cl_2 : MeOH = 99 : 1).

Yield: 816 mg (1.04 mmol; **81 %**) of a dark green powder

$C_{51}H_{67}N_5O_2$ [782.11]

^{1}H-NMR (600 MHz, $CDCl_3$, 303.6 K):

δ [ppm] = 7.60 (d, ^4J = 1.8 Hz, 1H, -CH-), 7.44 (dd, ^3J = 9.0 Hz, ^4J = 1.8 Hz, 1H, -CH-), 7.37 – 7.32 (-, 3H, 2x -CH-, -NH-), 7.20 (dd, ^3J = 7.4 Hz, ^3J = 7.4 Hz, 1H, -CH-), 7.02 (d, ^3J = 7.8 Hz, 1H, -CH-), 6.93 (d, ^3J = 8.4 Hz, 1H, -CH-), 6.48 (s, 1H, -CCHC-), 6.45 (s, 1H, -CCHC-), 4.89 – 3.90 (-, 4H, 2x –NCH_2-), 2.21 (s, 3H, -CCH_3), 1.81 – 1.69 (-, 2H, 2x -NCH_2CH_2-), 1.763 (s, 6H, -$C(CH_3)_2$), 1.759 (s, 6H, -$C(CH_3)_2$), 1.68 – 1.56 (-, 4H, 2x -NCH_2CH_2-, 2x -$CHCH_3$-), 1.55 – 1.48 (-, ^3J = 6.6 Hz, 2H, 2x -$CH(CH_3)_2$), 1.41 – 1.11 (-, 12H, 2x -$CH_2CH_2CH_2$-), 1.02 (d, ^3J = 6.6 Hz, 3H, -$CHCH_3$), 1.01 (d, ^3J = 6.6 Hz, 3H, -$CHCH_3$), 0.857 (d, ^3J = 6.6 Hz, 6H, -$CH(CH_3)_2$), 0.856 (d, ^3J = 6.6 Hz, 6H, -$CH(CH_3)_2$).

^{13}C-NMR (151 MHz, $CDCl_3$, 303.6 K):

δ [ppm] = 173.4 (quart.), 171.8 (quart.), 171.5 (quart.), 168.4 (quart.), 167.8 (quart.), 166.5 (quart.), 166.4 (quart.), 143.5 (quart.), 142.6 (quart.), 142.1 (quart.), 138.5 (quart.), 135.2 (quart.), 128.1 (tert.), 124.6 (tert.), 122.4 (tert.), 119.9 (tert.), 119.14 (quart.), 119.07 (quart.), 114.9 (tert.), 110.2 (tert.), 110.1 (tert.),

89.2 (tert.), 89.1 (tert.), 49.8 (quart.), 49.6 (quart.), 43.1 (sec.), 43.0 (sec.), 40.9 (quart.), 39.30 (sec.), 39.29 (sec.), 37.28 (sec.), 37.25 (sec.), 34.21 (sec.), 34.20 (sec.), 31.1 (tert.), 31.0 (tert.), 28.120 (tert.), 28.116 (tert.), 26.76 (prim.), 26.72 (2 x prim.), 26.70 (prim.), 24.76 (sec.), 24.75 (sec.), 24.70 (prim.), 22.84 (prim.), 22.83 (prim.), 22.7 (2 x prim), 19.83 (prim.), 19.80 (prim.).

MALDI-MS (pos.): m/z calc. for $C_{51}H_{67}N_5O_2$ [$M^{\bullet+}$] 781.529, found: 781.496

Synthesis of SQB-NH_2

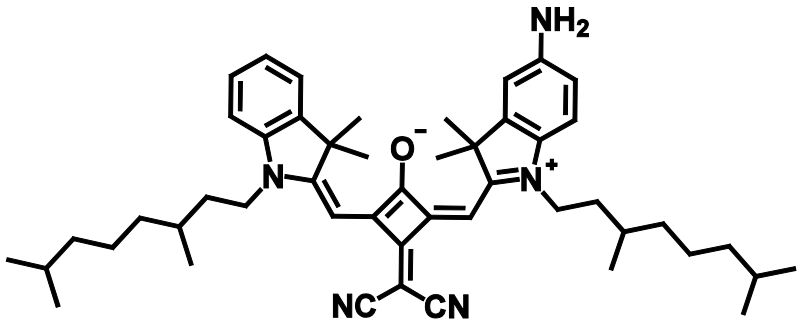

CA: [1865677-86-6]

SQB-NHAc (816 mg, 1.04 mmol) was dissolved in EtOH (100 ml). Hydrochloric acid (2N, 40 ml) was added and the solution was heated to 85 °C under exclusion of light. After 3 h the reaction mixture was allowed to cool to rt, neutralised with a 10 % solution of potassium carbonate and extracted with CH_2Cl_2 (3x 50 ml). The solvent was removed *in vacuo* and the residue was purified by flash column chromatography (eluent: CH_2Cl_2/MeOH 99:1).

Yield: 709 mg (958 µmol; **92 %**) of a green solid

$C_{49}H_{65}N_5O_2$ [740.08]

^{1}H-NMR (400 MHz, $CDCl_3$, 300 K):

δ [ppm] = 7.33 – 7.28 (-, 2H, 2x -CH-), 7.14 (ddd, ^3J = 7.6 Hz, ^3J = 7.6 Hz, ^4J = 0.6 Hz, 1H, -CH-), 6.96 (d, ^3J = 8.0 Hz, 1H, -CH-), 6.87 (d, ^3J = 8.4 Hz, 1H, -CH-), 6.70 (d, ^4J = 2.0 Hz, 1H, -CH-), 6.64 (dd, ^3J = 8.0 Hz, ^4J = 2.0 Hz, 1H, -CH-), 6.46 (s, 1H, -CCHC-), 6.39 (s, 1H, -CCHC-), 4.89 – 3.92 (-, 4H, 2x –NCH_2-), 3.80 (s, 2H, -NH_2), 1.81 – 1.71 (-, 2H, 2x -NCH_2CH_2-), 1.75 (s, 6H, -$C(CH_3)_2$), 1.74 (s, 6H, -$C(CH_3)_2$), 1.69 – 1.10 (-, 18H, 2x -NCH_2CH_2-, 2x -$CHCH_3$-, 2x -$CH(CH_3)_2$, 2x -$CH_2CH_2CH_2$-),

1.02 (d, ^3J = 6.6 Hz, 3H, -CHC<u>H</u>$_3$), 1.01 (d, ^3J = 6.6 Hz, 3H, -CHC<u>H</u>$_3$), 0.88 – 0.84 (-, 12H, 2x -CH(C<u>H</u>$_3$)$_2$).

Synthesis of SQC-Br

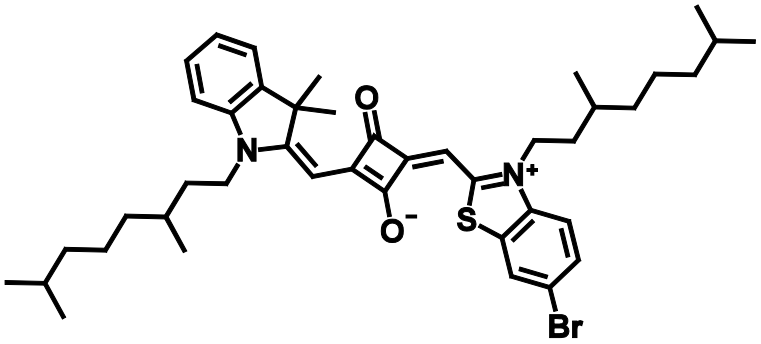

CA: [–]

Synthesis according to GP IV:

41 (300 mg, 758 µmol), 6-bromo-3-(3,7-dimethyloctyl)-2-methylbenzothiazol-3-ium iodide (**19**) (376 mg, 758 µmol), pyridine (3 ml), 6/4 mixture of *n*-butanol/toluene (100 ml); flash column chromatography (eluent: CH_2Cl_2/MeOH 99:1).

<u>Yield:</u> 155 mg (208 µmol; **27 %**) of a blue powder

$C_{43}H_{57}BrN_2O_2S$ [745.90]

^{1}H-NMR (400 MHz, $CDCl_3$, 300 K):

δ [ppm] = 7.71 (d, $^4J_{HH}$ = 1.2 Hz, 1H, -C<u>H</u>-), 7.51 (dd, $^3J_{HH}$ = 8.8 Hz, $^4J_{HH}$ = 2.0 Hz, 1H, -C<u>H</u>-), 7.34 (dd, $^3J_{HH}$ = 7.6 Hz, $^4J_{HH}$ = 0.8 Hz, 1H, -C<u>H</u>-), 7.30 (ddd, $^3J_{HH}$ = 7.6 Hz, $^3J_{HH}$ = 7.6 Hz, $^4J_{HH}$ = 1.2 Hz, 1H, -C<u>H</u>-), 7.12 (dd, $^3J_{HH}$ = 7.2 Hz, $^3J_{HH}$ = 7.2 Hz, 1H, -C<u>H</u>-), 7.03 (d, $^3J_{HH}$ = 8.8 Hz, 1H, -C<u>H</u>-), 6.97 (d, $^3J_{HH}$ = 8.0 Hz, 1H, -C<u>H</u>-), 5.90 (s, 1H, -CC<u>H</u>C-), 5.77 (s, 1H, -CC<u>H</u>C-), 4.20 – 3.88 (-, 4H, 2x -NC<u>H</u>$_2$-), 1.88 – 1.74 (-, 2H, 2x -NCH$_2$C<u>H</u>$_2$-), 1.72 (s, 6H, 2x –C(C<u>H</u>$_3$)$_2$), 1.67 – 1.47 (-, 6H, 2x -NCH$_2$C<u>H</u>$_2$-, 2x -C<u>H</u>CH$_3$-, 2x -C<u>H</u>(CH$_3$)$_2$), 1.43 – 1.13 (-, 12H, 2x -C<u>H</u>$_2$C<u>H</u>$_2$C<u>H</u>$_2$-), 1.05 (d, $^3J_{HH}$ = 6.4 Hz, 3H, -CHC<u>H</u>$_3$), 1.04 (d, $^3J_{HH}$ = 6.4 Hz, 3H, -CHC<u>H</u>$_3$), 0.87 (d, $^3J_{HH}$ = 6.8 Hz, 6H, -CH(C<u>H</u>$_3$)$_2$), 0.86 (d, $^3J_{HH}$ = 6.8 Hz, 6H, -CH(C<u>H</u>$_3$)$_2$).

MALDI-MS (pos.): m/z calc. for $C_{43}H_{57}BrN_2O_2S$ [$M^{\bullet+}$] 746.331, found: 746.367

Synthesis of SQD-Br

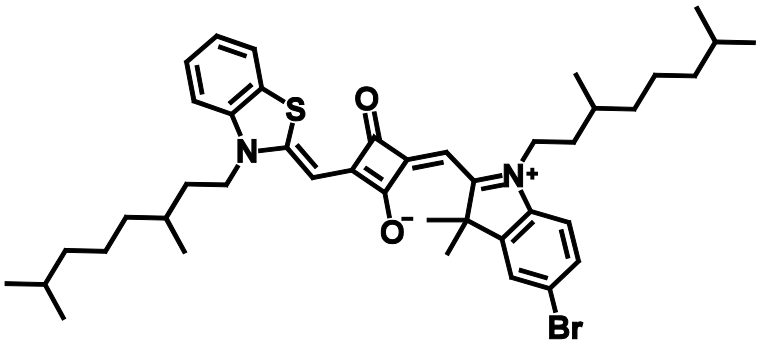

CA: [–]

Synthesis according to GP IV:

26 (340 mg, 882 µmol), 5-bromo-1-(3,7-dimethyloctyl)-2,3,3-trimethyl-3H-indol-1-ium iodide (**34**) (447 mg, 883 µmol), pyridine (3 ml), 6/4 mixture of *n*-butanol/toluene (100 ml); flash column chromatography (eluent: CH_2Cl_2 : MeOH 99 : 1).

Yield: 280 mg (375 µmol; **43 %**) of a blue powder

$C_{43}H_{57}BrN_2O_2S$ [745.90]

^{1}H-NMR (400 MHz, CD_2Cl_2, 300 K):

δ [ppm] = 7.68 (dd, $^3J_{HH}$ = 8.0 Hz, $^4J_{HH}$ = 0.8 Hz, 1H, -C<u>H</u>-), 7.47 (ddd, $^3J_{HH}$ = 7.6 Hz, $^3J_{HH}$ = 7.6 Hz, $^4J_{HH}$ = 1.2 Hz, 1H, -C<u>H</u>-), 7.42 – 7.36 (-, 2H, 2x -C<u>H</u>-), 7.31 (ddd, $^3J_{HH}$ = 7.6 Hz, $^3J_{HH}$ = 7.6 Hz, $^4J_{HH}$ = 0.8 Hz, 1H, -C<u>H</u>-), 7.27 (d, $^3J_{HH}$ = 8.4 Hz, 1H, -C<u>H</u>-), 6.77 (d, $^3J_{HH}$ = 8.8 Hz, 1H, -C<u>H</u>-), 6.00 (s, 1H, -CC<u>H</u>C-), 5.71 (s, 1H, -CC<u>H</u>C-), 4.30 – 4.14 (-, 2H, 2x -NC<u>H</u>$_2$-), 3.95 – 3.79 (-, 2H, 2x -NC<u>H</u>$_2$-), 1.90 – 1.46 (-, 8H, 2x -NCH$_2$C<u>H</u>$_2$-, 2x -C<u>H</u>CH$_3$-, 2x -C<u>H</u>(CH$_3$)$_2$), 1.72 (s, 6H, -C(C<u>H</u>$_3$)$_2$), 1.45 – 1.12 (-, 12H, 2x -C<u>H</u>$_2$C<u>H</u>$_2$C<u>H</u>$_2$-), 1.07 (d, $^3J_{HH}$ = 6.4 Hz, 3H, -CHC<u>H</u>$_3$), 1.03 (d, $^3J_{HH}$ = 6.4 Hz, 3H, -CHC<u>H</u>$_3$), 0.88 (d, $^3J_{HH}$ = 6.8 Hz, 6H, -CH(C<u>H</u>$_3$)$_2$), 0.87 (d, $^3J_{HH}$ = 6.8 Hz, 6H, -CH(C<u>H</u>$_3$)$_2$).

MALDI-MS (pos.): m/z calc. for $C_{43}H_{57}BrN_2O_2S$ [$M^{\bullet+}$] 746.331, found: 746.308

Synthesis of $(SQA)_3$-N

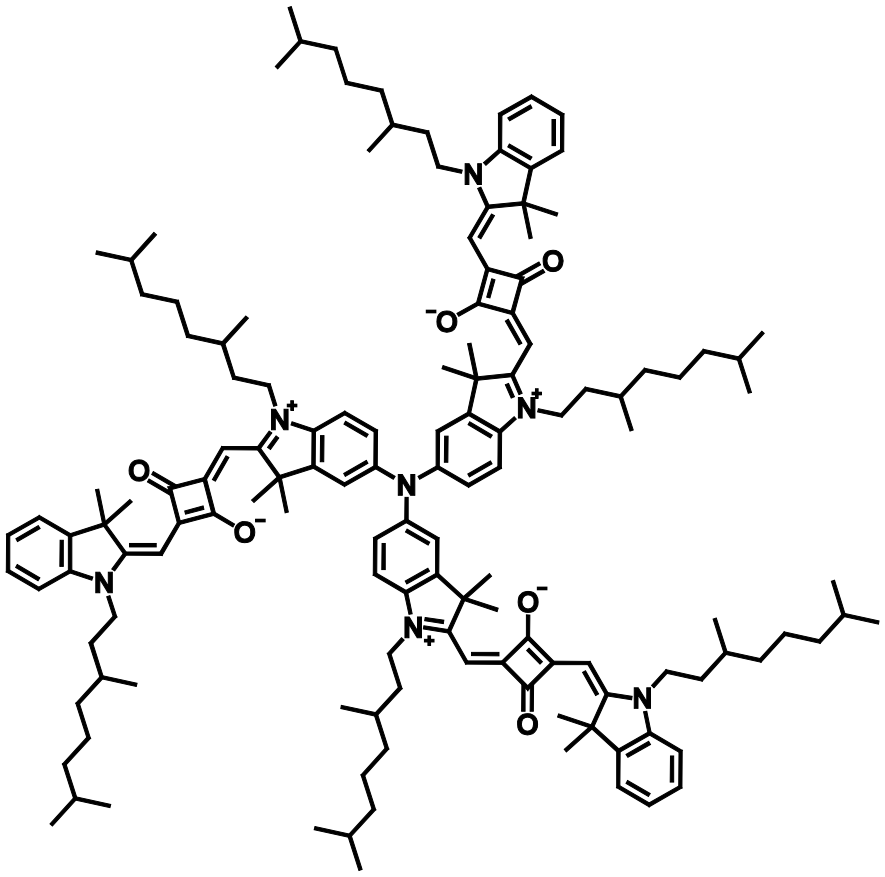

CA: [1865677-88-8]

Under a nitrogen atmosphere **SQA-NH_2** (95.0 mg, 137 µmol), **SQA-Br** (228 mg, 302 µmol), NaO*t*-Bu (33.0 mg, 343 µmol) and P(*t*-Bu)$_3$ (6.86 µl, 1.00 M in toluene, 6.86 µmol) were dissolved in dry toluene (10 ml). The solution was degassed for 10 min. Then $Pd_2(dba)_3 \cdot CHCl_3$ (7.10 mg, 6.86 µmol) was added and the blue solution was stirred at 80 °C under exclusion of light for 3 d. The solution was cooled to rt and the solvent was evaporated *in vacuo*. The blue residue was dissolved in CH_2Cl_2 (100 ml) and water (100 ml). The organic layer was separated and the aqueous layer was extracted with CH_2Cl_2 (2x 100 ml). The combined organic layers were dried over Na_2SO_4 and the solvent was evaporated. The blue residue was purified by flash column chromatography (eluent: CH_2Cl_2/MeOH 99:1). The main fraction contained additional to the desired trimer some dimer. This fraction was purified by another flash column chromatography. The ratio of MeOH in the eluent (CH_2Cl_2) was raised in 0.1‰ steps from 0‰ to 7.0‰. Finally the crude product was dissolved in a small amount of CH_2Cl_2 and dropped into an excess of *n*-hexane. The resulting precipitate was filtered off and dried under high vacuum.

Yield: 9.00 mg (4.41 µmol, **3 %**) of a blue powder

$C_{138}H_{189}N_7O_6$ [2042.03]

^{1}H-NMR (600 MHz, CD_2Cl_2, 293.5 K):

δ [ppm] = 7.35 (dd, $^3J_{HH}$ = 7.5 Hz, $^4J_{HH}$ = 0.7 Hz, 3H, 3x -CH-), 7.30 (ddd, $^3J_{HH}$ = 7.8 Hz, $^3J_{HH}$ = 7.8 Hz, $^4J_{HH}$ = 1.1 Hz, 3H, 3x -CH-), 7.15 (d, $^4J_{HH}$ = 2.0 Hz, 3H, 3x -CH-), 7.12 (ddd, $^3J_{HH}$ = 7.4 Hz, $^3J_{HH}$ = 7.4 Hz, $^4J_{HH}$ = 0.6 Hz, 3H, 3x -CH-), 7.03 – 6.96 (-, 6H, 6x -CH-), 6.89 (d, $^3J_{HH}$ = 8.7 Hz, 3H, 3x -CH-), 5.89 (s, 3H, 3x -CCHC-), 5.86 (s, 3H, 3x -CCHC-), 4.11 – 3.86 (-, 12H, 6x -NCH_2-) 1.85 – 1.76 (-, 6H, 6x -NCH_2CH_2-) 1.74 (s, 18H, 3x -$C(CH_3)_2$), 1.70 (s, 18H, 3x -$C(CH_3)_2$), 1.66 – 1.46 (-, 18H, 6x -NCH_2CH_2-, 6x -$CHCH_3$, 6x -$CH(CH_3)_2$), 1.45 – 1.11 (-, 36H, 6x -$CH_2CH_2CH_2$-), 1.06 (d, $^3J_{HH}$ = 6.4 Hz, 9H, 3x -$CHCH_3$), 1.03 (d, $^3J_{HH}$ = 6.4 Hz, 9H, 3x -$CHCH_3$), 0.87 (d, $^3J_{HH}$ = 6.6 Hz, 18H, 3x -$CH(CH_3)_2$), 0.85 (d, $^3J_{HH}$ = 6.6 Hz, 18H, 3x -$CH(CH_3)_2$).

^{13}C-NMR (151 MHz, CD_2Cl_2, 293.5 K):

δ [ppm] = 182.1 (2x quart.), 180.0 (quart.), 179.4 (quart.), 169.38 (quart.), 169.31 (quart.), 144.7 (quart.), 144.1 (quart.), 142.9 (quart.), 142.5 (quart.), 138.3 (quart.), 128.1 (tert.), 123.7 (tert.), 123.6 (tert.), 122.5 (tert.), 118.6 (tert.), 110.4 (tert.), 109.5 (tert.), 86.8 (tert.), 86.6 (tert.), 49.7 (quart.), 49.4 (quart.), 42.6 (sec.), 42.3 (sec.), 39.51 (sec.), 39.49 (sec.), 37.4 (2x sec.), 34.2 (sec.), 34.0 (sec.), 31.51 (tert.), 31.46 (tert.), 28.37 (tert.), 28.34 (tert.), 27.1 (2x prim.), 27.0 (2x prim.), 25.1 (sec.), 25.0 (sec.), 22.84 (prim.), 22.79 (prim.), 22.74 (prim.), 22.70 (prim.), 19.74 (prim.), 19.73 (prim.).

ESI-MS (pos., high res.):

m/z calc. for $C_{138}H_{189}N_7O_6$ [$M^{\bullet+}$] 2041.47268, found: 2041.47634

Δ: 1.79 ppm

Synthesis of $(SQB)_3$-N

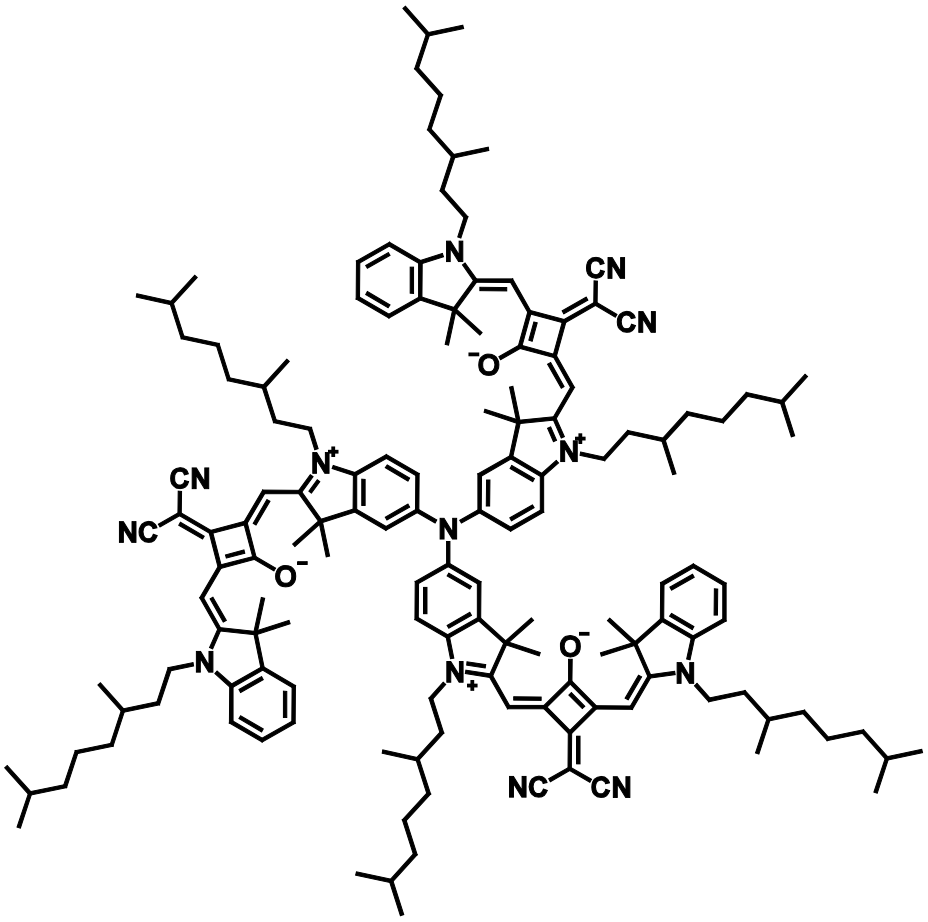

CA: [1865677-90-2]

Under a nitrogen atmosphere **SQB-NH_2** (200 mg, 270 µmol), **SQB-Br** (478 mg, 595 µmol), NaO*t*-Bu (64.9 mg, 675 µmol) and P(*t*-Bu)$_3$ (13.5 µl, 1.00 M in toluene, 13.5 µmol) were dissolved in dry toluene (20 ml). The solution was degassed for 10 min. Then $Pd_2(dba)_3 \cdot CHCl_3$ (14.0 mg, 13.5 µmol) was added and the green solution was stirred at 80 °C under exclusion of light for 3 d. The solution was cooled to rt and the solvent was evaporated *in vacuo*. The green residue was dissolved in CH_2Cl_2 (100 ml) and water (100 ml). The organic layer was separated and the aqueous layer extracted with CH_2Cl_2 (2x 100 ml). The combined organic layers were dried over Na_2SO_4 and the solvent was evaporated. The blue residue was purified by flash column chromatography (eluent: CH_2Cl_2 → CH_2Cl_2/MeOH 99.9:0.1 → 99.5:0.5). The main fraction contained additional to the desired trimer some dimer. This fraction was purified by another flash column chromatography with a gradient of: CH_2Cl_2/MeOH 99.95:0.05 → 99.9:0.1 → 99.8:0.2. Finally the crude product was dissolved in a small amount of CH_2Cl_2 and dropped into an excess of *n*-hexane. The resulting precipitate was filtered off and dried under high vacuum.

Yield: 27.0 mg (12.4 µmol, **5 %**) of a green powder

$C_{147}H_{189}N_{13}O_3$ [2186.17]

^{1}H-NMR (600 MHz, CD_2Cl_2, 293.5 K):

δ [ppm] = 7.37 – 7.32 (-, 6H, 6x -CH-), 7.20 – 7.16 (-, 6H, 6x -CH-), 7.07 – 7.02 (-, 6H, 6x -CH-), 6.97 (d, $^3J_{HH}$ = 8.7 Hz, 3H, 3x -CH-), 6.46 (s, 3H, 3x -CCHC-), 6.44 (s, 3H, 3x -CCHC-), 4.11 – 3.94 (-, 12H, 6x -NCH_2-), 1.84 – 1.75 (-, 6H, 6x -NCH_2CH_2-), 1.71 (s, 18H, 3x -$C(CH_3)_2$), 1.70 (s, 18H, 3x -$C(CH_3)_2$), 1.73 – 1.48 (-, 18H, 6x -NCH_2CH_2-, 6x -$CHCH_3$, 6x -$CH(CH_3)_2$), 1.45 – 1.11 (-, 36H, 6x -$CH_2CH_2CH_2$-), 1.04 (d, $^3J_{HH}$ = 6.4 Hz, 9H, 3x -$CHCH_3$), 1.02 (d, $^3J_{HH}$ = 6.5 Hz, 9H, 3x -$CHCH_3$), 0.87 (d, $^3J_{HH}$ = 6.5 Hz, 18H, 3x -$CH(CH_3)_2$), 0.86 (d, $^3J_{HH}$ = 6.4 Hz, 18H, 3x -$CH(CH_3)_2$).

^{13}C-NMR (151 MHz, CD_2Cl_2, 293.5 K):

δ [ppm] = 173.6 (quart.), 171.6 (quart.), 171.1 (quart.), 167.9 (quart.), 166.07 (quart.), 166.05 (quart.), 145.1 (quart.), 144.5 (quart.), 142.8 (quart.), 142.4 (quart.), 138.0 (quart.), 128.3 (tert.), 124.7 (tert.), 123.9 (tert.), 122.5 (tert.), 119.23 (quart.), 119.15 (quart.), 118.4 (tert.), 111.3 (tert.), 110.4 (tert.), 89.5 (tert.), 89.2 (tert.), 49.8 (quart.), 49.7 (quart.), 43.5 (sec.), 43.2 (sec.), 40.48 (quart.), 39.53 (sec.), 39.52 (sec.), 37.5 (2x sec.), 34.5 (sec.), 34.3 (sec.), 31.33 (tert.), 31.29 (tert.), 28.40 (tert.), 28.38 (tert.), 26.66 (prim.), 26.63 (prim.), 26.60 (prim.), 26.57 (prim.), 25.04 (sec.), 25.01 (sec.), 22.84 (prim.), 22.81 (prim.), 22.75 (prim.), 22.72 (prim.), 19.79 (prim.), 19.77 (prim.).

ESI-MS (pos., high res.):

m/z calc. for $C_{147}H_{189}N_{13}O_3$ [$M^{\bullet+}$] 2185.50630, found: 2185.50695

Δ: 0.30 ppm

Synthesis of (SQA)(SQB)$_2$-N

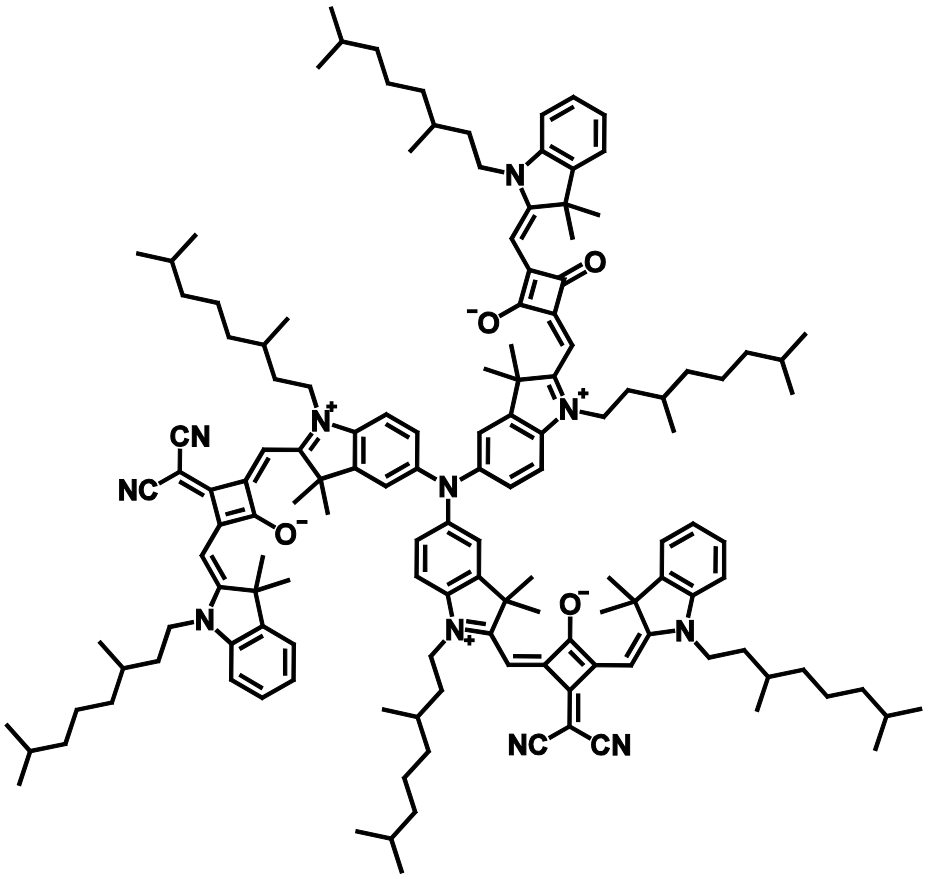

CA: [1865677-91-3]

Under a nitrogen atmosphere **SQA-NH$_2$** (78.0 mg, 113 µmol), **SQB-Br** (199 mg, 248 µmol), NaO*t*-Bu (27.1 mg, 282 µmol) and P(*t*-Bu)$_3$ (5.64 µl, 1.00 M in toluene, 5.64 µmol) were dissolved in dry toluene (10 ml). The solution was degassed for 10 min. Then $Pd_2(dba)_3 \cdot CHCl_3$ (5.83 mg, 5.63 µmol) was added and the blue solution was stirred at 80 °C under exclusion of light for 3 d. The solution was cooled to rt and the solvent was evaporated *in vacuo*. The green residue was dissolved in CH_2Cl_2 (100 ml) and water (100 ml). The organic layer was separated and the aqueous layer extracted with CH_2Cl_2 (2x 100 ml). The combined organic layers were dried over Na_2SO_4 and the solvent was evaporated. The green residue was purified by flash column chromatography (eluent: CH_2Cl_2 → CH_2Cl_2/MeOH 99.9:0.1 → 99.5:0.5). The main fraction was purified by another flash column chromatography. The ratio of MeOH in the eluent (CH_2Cl_2) was raised in 0.1‰ steps from 0‰ to 6.0‰. Finally the crude product was dissolved in a small amount of CH_2Cl_2 and dropped into an excess of *n*-hexane. The resulting precipitate was filtered off and dried under high vacuum.

Yield: 25.7 mg (12.0 µmol, **11 %**) of a green powder

$C_{144}H_{189}N_{11}O_4$ [2138.12]

^{1}H-NMR (600 MHz, CD_2Cl_2, 293.5 K):

δ [ppm] = 7.37 – 7.29 (-, 6H, 6x -CH-), 7.19 – 7.16 (-, 5H, 5x -CH-), 7.14 (dd, $^3J_{HH}$ = 7.5 Hz, $^3J_{HH}$ = 7.5 Hz, $^4J_{HH}$ = 0.5 Hz, 1H, -CH-), 7.06 – 7.01 (-, 5H, 5x -CH-), 6.99 (d, $^3J_{HH}$ = 8.0 Hz, 1H, -CH-), 6.96 (d, $^3J_{HH}$ = 8.6 Hz, 2H, 2x -CH-), 6.91 (d, $^3J_{HH}$ = 8.6 Hz, 1H, -CH-), 6.46 (s, 2H, 2x -CCHC-), 6.43 (s, 2H, 2x -CCHC-), 5.90 (s, 1H, -CCHC-), 5.88 (s, 1H, -CCHC-), 4.10 – 3.92 (-, 12H, 6x -NCH_2-), 1.85 – 1.46 (-, 42H, 6x -NCH_2CH_2-, 6x -$CHCH_3$, 6x -$CH(CH_3)_2$, 3x -$C(CH_3)_2$), 1.74 (s, 6H, -$C(CH_3)_2$), 1.70 (s, 12H, 2x -$C(CH_3)_2$), 1.44 – 1.11 (-, 36H, 6x -$CH_2CH_2CH_2$-), 1.07 (d, $^3J_{HH}$ = 6.3 Hz, 3H, -$CHCH_3$), 1.04 (d, $^3J_{HH}$ = 6.4 Hz, 3H, -$CHCH_3$), 1.03 (d, $^3J_{HH}$ = 6.5 Hz, 6H, 2x -$CHCH_3$), 1.02 (d, $^3J_{HH}$ = 6.5 Hz, 6H, 2x -$CHCH_3$), 0.88 (d, $^3J_{HH}$ = 6.7 Hz, 6H, -$CH(CH_3)_2$), 0.87 (d, $^3J_{HH}$ = 6.0 Hz, 12H, 2x -$CH(CH_3)_2$), 0.86 (d, $^3J_{HH}$ = 6.1 Hz, 12H, 2x -$CH(CH_3)_2$), 0.84 (d, $^3J_{HH}$ = 6.7 Hz, 6H, -$CH(CH_3)_2$).

^{13}C-NMR (151 MHz, CD_2Cl_2, 293.5 K):

δ [ppm] = 182.08 (2x quart.), 179.9 (quart.), 179.7 (quart.), 173.57 (quart.), 171.5 (quart.), 171.2 (quart.), 169.8 (quart.), 169.1 (quart.), 167.8 (quart.), 166.1 (quart.), 165.9 (quart.), 145.4 (quart.), 144.5 (quart.), 144.2 (quart.), 144.1 (quart.), 142.9 (quart.), 142.8 (quart.), 142.6 (quart.), 142.4 (quart.), 138.9 (quart.), 137.7 (quart.), 128.3 (tert.), 128.1 (tert.) 124.6 (tert.), 124.3 (tert.), 123.9 (tert.), 123.5 (tert.), 122.5 (2x tert.), 119.26 (quart.), 119.19 (quart.), 119.14 (tert.), 118.1 (tert.), 111.3 (tert.), 110.4 (tert.), 110.3 (tert.), 109.7 (tert.), 89.5 (tert.), 89.1 (tert.), 86.9 (tert.), 86.7 (tert.), 49.9 (quart.), 49.64 (quart.), 49.57 (quart.), 49.5 (quart.), 43.5 (sec.), 43.2 (sec.), 42.6 (sec.), 42.4 (sec.), 40.4 (quart.), 39.52 (3x sec.), 39.49 (sec.), 37.46 (2x sec.), 37.44 (2x sec.), 34.5 (sec.), 34.3 (sec.), 34.2 (sec.), 34.0 (sec.), 31.52 (tert.), 31.47 (tert.), 31.33 (tert.), 31.29 (tert.), 28.39 (tert.), 28.38 (tert.), 28.37 (tert.), 28.34 (tert.), 27.08 (2x prim.), 27.06 (2x prim.), 26.68 (prim.), 26.65 (prim.), 26.57 (prim.), 26.54 (prim.), 25.09 (sec.), 25.05 (sec.), 25.03 (sec.), 25.01 (sec.), 22.84 (2x prim.), 22.81 (prim.), 22.79 (prim.), 22.75 (2x prim.), 22.72 (prim.), 22.71 (prim.), 19.78 (prim.), 19.77 (prim.), 19.76 (prim.), 19.73 (prim.).

ESI-MS (pos., high res.):

m/z calc. for $C_{144}H_{189}N_{11}O_4$ [$M^{\bullet+}$] 2137.49509, found: 2137.49587

Δ: 0.36 ppm

Synthesis of (SQA)(SQB)-NH

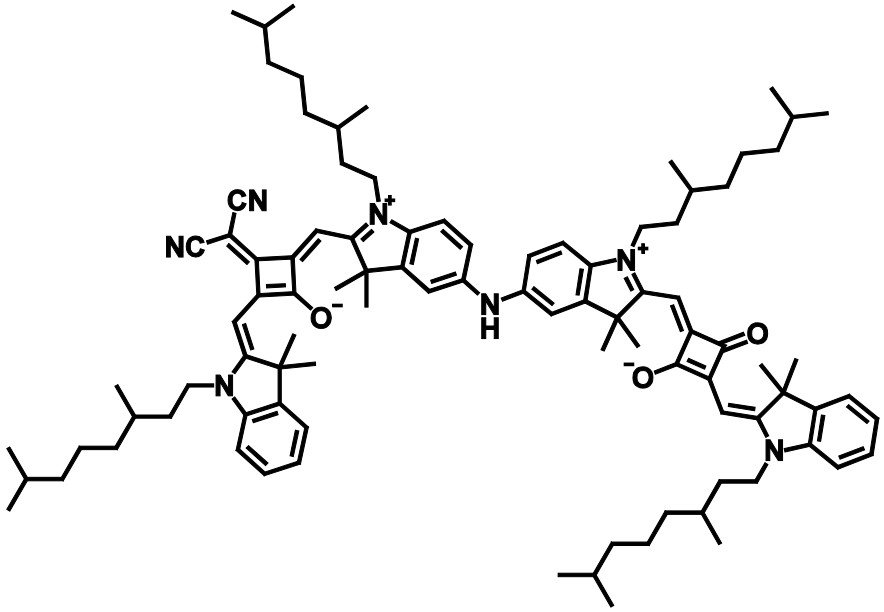

CA: [1865677-92-4]

Under a nitrogen atmosphere **SQB-NH$_2$** (300 mg, 405 µmol), **SQA-Br** (919 mg, 1.22 mmol), NaO*t*-Bu (117 mg, 1.22 mmol) and P(*t*-Bu)$_3$ (20.3 µl, 1.00 M in toluene, 20.3 µmol) were dissolved in dry toluene (20 ml). The solution was degassed for 10 min. Then $Pd_2(dba)_3 \cdot CHCl_3$ (21.0 mg, 20.3 µmol) was added and the blue solution was stirred at 100 °C under exclusion of light for 4 d. The solution was cooled to rt and the solvent was evaporated *in vacuo*. The blue residue was dissolved in CH_2Cl_2 (100 ml) and water (100 ml). The organic layer was separated and the aqueous layer was extracted with CH_2Cl_2 (2x 100 ml). The combined organic layers were dried over Na_2SO_4 and the solvent was evaporated. The blue residue was purified by flash column chromatography (eluent: CH_2Cl_2/MeOH 99:1). Finally the crude product was dissolved in a small amount of CH_2Cl_2 and dropped into an excess of *n*-hexane. The resulting precipitate was filtered off and dried under high vacuum.

Yield: 260 mg (184 µmol, **45 %**) of a blue powder

$C_{95}H_{127}N_7O_3$ [1415.07]

^{1}H-NMR (600 MHz, CD_2Cl_2, 293.5 K):

δ [ppm] = 7.41 – 7.29 (-, 8H, 8x -C<u>H</u>-), 7.20 – 7.12 (-, 2H, 2x -C<u>H</u>-), 7.06 – 6.97 (-, 4H, 4x -C<u>H</u>-), 6.57 – 6.28 (-, 2H, 2x -CC<u>H</u>C-), 6.07 – 5.67 (-, 2H, 2x -CC<u>H</u>C-), 4.43 – 3.64 (-, 8H, 4x -NC<u>H$_2$</u>-), 1.84 – 1.70 (-, 16H, 4x -NCH$_2$C<u>H$_2$</u>-, 2x -C(C<u>H$_3$</u>)$_2$), 1.76 (s, 6H, 2x -C(C<u>H$_3$</u>)$_2$), 1.73 (s, 6H, -C(C<u>H$_3$</u>)$_2$), 1.69 – 1.47 (-, 12H , 4x -NCH$_2$C<u>H$_2$</u>-, 4x -C<u>H</u>CH$_3$, 4x -C<u>H</u>(CH$_3$)$_2$), 1.45 – 1.11 (-, 24H, 4x -C<u>H$_2$</u>C<u>H$_2$</u>C<u>H$_2$</u>-), 1.07 (d, $^{3}J_{HH}$ = 6.5 Hz, 3H, -CHC<u>H$_3$</u>), 1.05 (d, $^{3}J_{HH}$ = 6.5 Hz, 3H, -CHC<u>H$_3$</u>), 1.03 (d, $^{3}J_{HH}$ = 6.6 Hz, 3H, -CHC<u>H$_3$</u>), 1.02 (d, $^{3}J_{HH}$ = 6.6 Hz, 3H, -CHC<u>H$_3$</u>), 0.88 (d, $^{3}J_{HH}$ = 6.7 Hz, 6H, -CH(C<u>H$_3$</u>)$_2$), 0.87 (d, $^{3}J_{HH}$ = 6.8 Hz, 6H, -CH(C<u>H$_3$</u>)$_2$), 0.86 (d, $^{3}J_{HH}$ = 6.7 Hz, 6H, -CH(C<u>H$_3$</u>)$_2$), 0.85 (d, $^{3}J_{HH}$ = 6.7 Hz, 6H, -CH(C<u>H$_3$</u>)$_2$).

The signal for the -CN<u>H</u>C- is missing.

^{13}C-NMR (151 MHz, CD_2Cl_2, 293.5 K):

δ [ppm] = 182.1 (4x quart.), 173.7 (quart.), 170.7 (4x quart.), 167.8 (2x quart.), 165.0 (quart.), 144.5 (2x quart.), 142.7 (8x quart.), 128.2 (4x tert.), 124.3 (2x tert.), 122.5 (4x tert.), 119.3 (2x quart.), 110.1 (4x tert.), 88.9 (2x tert.), 86.9 (tert.), 86.7 (tert.), 50.2 (quart.), 49.8 (quart.), 49.4 (2x quart.), 43.0 (4x sec.), 40.4 (quart.), 39.5 (4x sec.), 37.5 (4x sec.), 34.3 (4x sec.), 31.5 (2x tert.), 31.3 (2x tert.), 28.4 (4x tert.), 27.8 (4x prim), 26.6 (4x prim.), 25.1 (2x sec.), 25.0 (2x sec.), 22.8 (4x prim.), 22.7 (4x prim.), 19.8 (2x prim.), 19.7 (2x prim.).

ESI-MS (pos., high res.):

m/z calc. for $C_{95}H_{127}N_7O_3$ [$M^{\bullet+}$] 1415.00274, found: 1415.00304

Δ: 0.21 ppm

Synthesis of $(SQA)_2$(SQB)-N

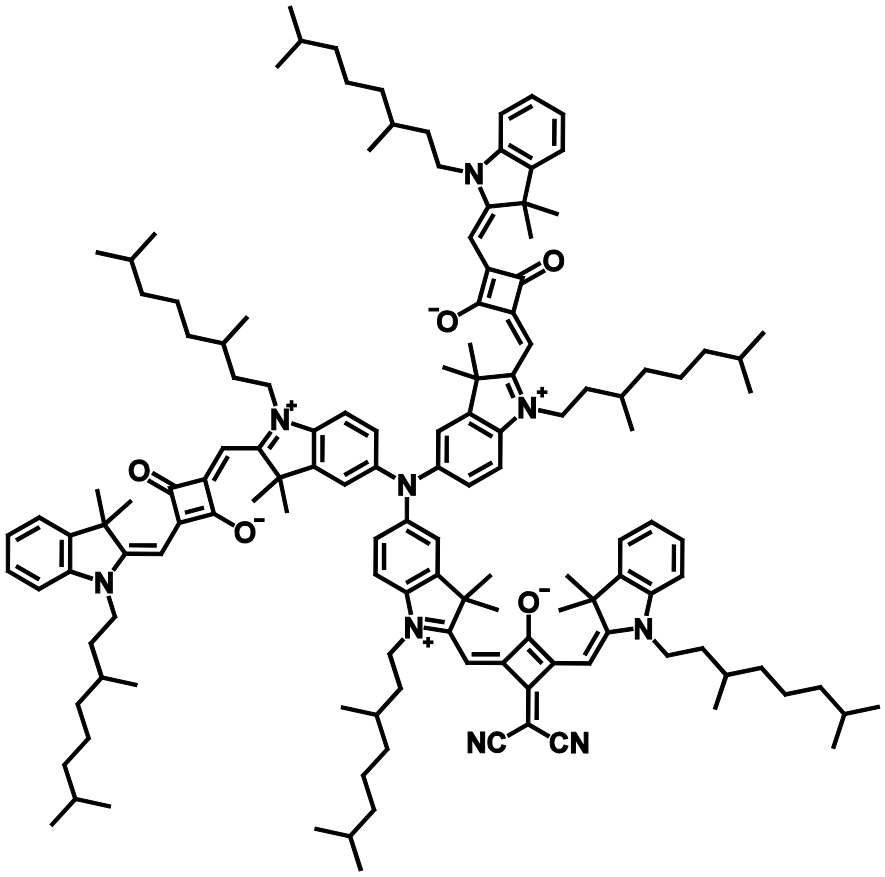

CA: [1865677-93-5]

Under a nitrogen atmosphere **(SQA)SQB)-NH** (260 mg, 184 µmol), **SQA-Br** (167 mg, 221 µmol), NaO*t*-Bu (53.0 mg, 552 µmol) and P(*t*-Bu)$_3$ (9.19 µl, 1.00 M in toluene, 9.19 µmol) were dissolved in dry toluene (20 ml). The solution was degassed for 10 min. Then $Pd_2(dba)_3 \cdot CHCl_3$ (9.51 mg, 9.19 µmol) was added and the blue solution was stirred at 100 °C under exclusion of light for 4 d. The solution was cooled to rt and the solvent was evaporated *in vacuo*. The blue residue was dissolved in CH_2Cl_2 (100 ml) and water (100 ml). The organic layer was separated and the aqueous layer extracted with CH_2Cl_2 (2x 100 ml). The combined organic layers were dried over Na_2SO_4 and the solvent was evaporated. The blue residue was purified by flash column chromatography (eluent: CH_2Cl_2/MeOH 99:1). The main fraction was additionally purified by GPC. Finally the crude product was dissolved in a small amount of CH_2Cl_2 and dropped into an excess of *n*-hexane. The resulting precipitate was filtered off and dried under high vacuum.

Yield: 26.0 mg (11.9 µmol, **6** %) of a blue powder

$C_{141}H_{189}N_9O_5$ [2090.07]

^{1}H-NMR (600 MHz, CD_2Cl_2, 293.5 K):

δ [ppm] = 7.36 – 7.33 (-, 3H, 3x -C<u>H</u>-), 7.33 – 7.29 (-, 3H, 3x -C<u>H</u>-), 7.18 – 7.12 (-, 6H, 6x -C<u>H</u>-), 7.04 – 6.94 (-, 7H 7x -C<u>H</u>-), 6.90 (d, $^{3}J_{HH}$ = 8.9 Hz, 2H, 2x -C<u>H</u>-), 6.46 (s, 1H, -CC<u>H</u>C-), 6.42 (s, 1H, -CC<u>H</u>C-), 5.90 (s, 2H, 2x -CC<u>H</u>C-), 5.87 (s, 2H, 2x-CC<u>H</u>C-), 4.10 – 3.91 (-, 12H, 6x -NC<u>H$_2$</u>-), 1.86 – 1.47 (-, 42H, 3x -C(C<u>H$_3$</u>)<u>$_2$</u>, 6x -NCH$_2$C<u>H$_2$</u>-, 6x -C<u>H</u>CH$_3$, 6x -C<u>H</u>(CH$_3$)$_2$), 1.74 (s, 12H, 2x -C(C<u>H$_3$</u>)<u>$_2$</u>), 1.69 (s, 6H, -C(C<u>H$_3$</u>)<u>$_2$</u>), 1.46 – 1.11 (-, 36H, 6x –C<u>H$_2$</u>C<u>H$_2$</u>C<u>H$_2$</u>-), 1.07 (d, $^{3}J_{HH}$ = 6.2 Hz, 6H, 2x -CHC<u>H$_3$</u>), 1.04 (d, $^{3}J_{HH}$ = 6.2 Hz, 6H, 2x -CHC<u>H$_3$</u>), 1.03 (d, $^{3}J_{HH}$ = 6.5 Hz, 3H, -CHC<u>H$_3$</u>), 1.01 (d, $^{3}J_{HH}$ = 6.6 Hz, 3H, -CHC<u>H$_3$</u>), 0.87 (d, $^{3}J_{HH}$ = 6.7 Hz, 12H, 2x -CH(C<u>H$_3$</u>)<u>$_2$</u>), 0.86 (d, $^{3}J_{HH}$ = 6.8 Hz, 6H, -CH(C<u>H$_3$</u>)<u>$_2$</u>), 0.85 (d, $^{3}J_{HH}$ = 6.6 Hz, 6H, -CH(C<u>H$_3$</u>)<u>$_2$</u>), 0.84 (d, $^{3}J_{HH}$ = 6.7 Hz, 12H, 2x -CH(C<u>H$_3$</u>)<u>$_2$</u>).

^{13}C-NMR (151 MHz, CD_2Cl_2, 293.5 K):

δ [ppm] = 182.0 (2x quart.), 179.9 (quart.), 179.7 (quart.), 173.6 (quart.), 171.3 (2x quart.), 169.6 (quart.), 169.3 (quart.), 167.8 (quart.), 166.2 (quart.), 165.6 (quart.), 145.8 (quart.), 144.5 (quart.), 144.4 (quart.), 144.2 (quart.), 142.9 (quart.), 142.8 (quart.), 142.5 (quart.), 142.4 (quart.), 138.6 (quart.), 137.4 (quart.), 128.3 (tert.), 128.1 (tert.), 124.5 (tert.), 124.0 (tert.), 123.8 (tert.), 123.1 (tert.), 122.5 (2x tert.), 119.3 (quart.), 119.2 (quart.), 118.9 (tert.), 117.7 (tert.), 111.2 (tert.), 110.4 (tert.), 110.2 (tert.), 109.6 (tert.), 89.5 (tert.), 89.0 (tert.), 86.9 (tert.), 86.7 (tert.), 49.9 (quart.), 49.62 (quart.), 49.58 (quart.), 49.5 (quart.), 43.6 (sec.), 43.1 (sec.), 42.6 (sec.), 42.3 (sec.), 40.4 (quart.), 39.52 (3x sec.), 39.49 (sec.), 37.47 (sec.), 37.45 (2x sec.), 37.44 (sec.), 34.5 (sec.), 34.3 (sec.), 34.2 (sec.), 34.0 (sec.), 31.51 (tert.), 31.47 (tert.), 31.33 (tert.), 31.29 (tert.), 28.39 (tert.), 28.38 (tert.), 28.37 (tert.), 28.34 (tert.), 27.1 (2x prim.), 27.0 (2x prim.), 26.71 (prim.), 26.67 (prim.), 26.53 (prim.), 26.50 (prim.), 25.09 (sec.), 25.05 (sec.), 25.02 (sec.), 25.01 (sec.), 22.84 (2x prim.), 22.81 (prim.), 22.80 (prim.), 22.75 (2x prim.), 22.73 (prim.), 22.71 (prim.), 19.78 (2x prim.), 19.75 (prim.), 19.73 (prim.).

ESI-MS (pos., high res.):

m/z calc. for $C_{141}H_{189}N_9O_5$ [$M^{\bullet+}$] 2089.48389, found: 2089.48455

Δ: 0.32 ppm

Synthesis of $(SQA)_3$-ben

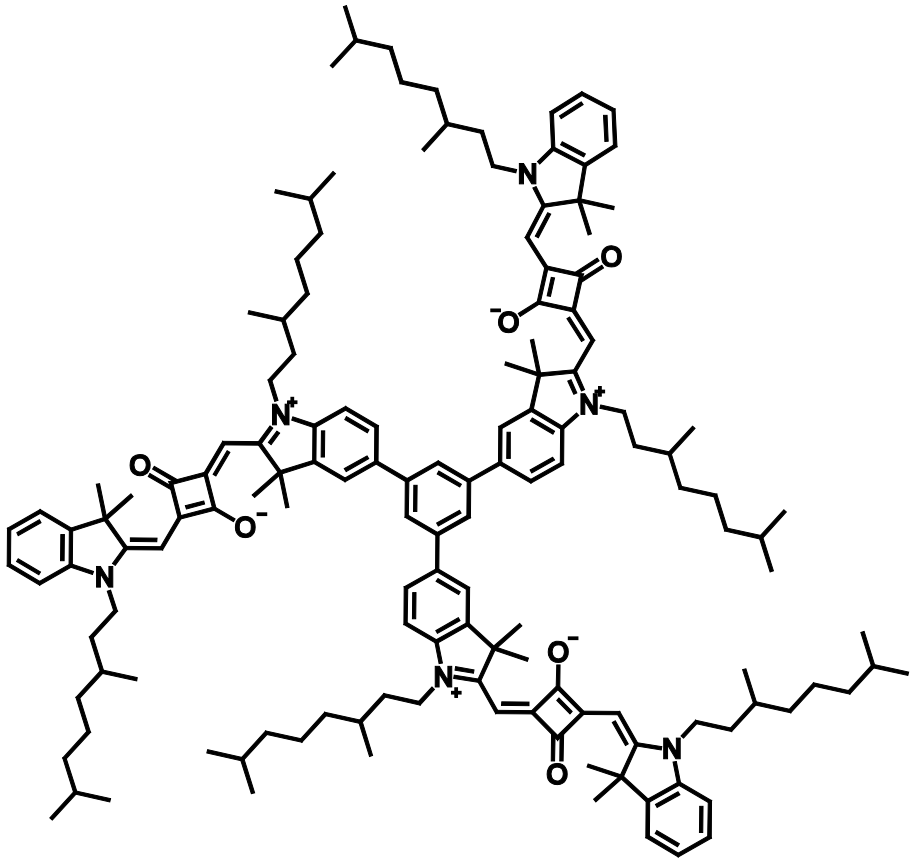

CA: [–]

Under a nitrogen atmosphere **SQA-B** (150 mg, 187 µmol) and 1,3,5-tribromobenzene (17.8 mg, 56.5 µmol) were dissolved in THF (12 ml). A saturated aqueous solution of K_2CO_3 (2 ml) was added and the mixture was degassed for 15 min. Then $Pd(PPh_3)_4$ (3.27 mg, 2.83 µmol) was added and the solution was refluxed under exclusion of light for 4 d. The solvent was removed *in vacuo* and the blue residue was purified by flash column chromatography (eluent: CH_2Cl_2/MeOH 99.5:0.5 → 99:1 → 98:2). Finally the crude product was dissolved in a small amount of CH_2Cl_2 and dropped into an excess of *n*-hexane. The resulting precipitate was filtered off and dried under high vacuum.

Yield: 81.0 mg (38.5 μmol; **68 %**) of a blue powder

$C_{144}H_{192}N_6O_6$ [2103.11]

^{1}H-NMR (600 MHz, $CDCl_3$, 303.6 K):

δ [ppm] = 7.70 (s, 3H, 3x -C<u>H</u>-), 7.65 (dd, $^3J_{HH}$ = 8.1 Hz, $^4J_{HH}$ = 1.6 Hz, 3H, 3x -C<u>H</u>-), 7.63 (d, $^4J_{HH}$ = 1.5 Hz, 3H, 3x -C<u>H</u>-), 7.36 (d, $^3J_{HH}$ = 7.3 Hz, 3H, 3x -C<u>H</u>-), 7.31 (ddd, $^3J_{HH}$ = 8.1 Hz, $^3J_{HH}$ = 8.1 Hz, $^4J_{HH}$ = 1.2 Hz, 3H, 3x -C<u>H</u>-), 7.16 (dd, $^3J_{HH}$ = 7.3 Hz,

$^{3}J_{HH}$ = 7.3 Hz, 3H, 3x -C<u>H</u>-), 7.08 (d, $^{3}J_{HH}$ = 8.1 Hz, 3H, 3x -C<u>H</u>-), 6.97 (d, $^{3}J_{HH}$ = 8.0 Hz, 3H, 3x -C<u>H</u>-), 6.00 (s, 3H, 3x -CC<u>H</u>C-), 5.99 (s, 3H, 3x -CC<u>H</u>C-), 4.16 – 3.91 (-, 12H, 6x -NC<u>H$_2$</u>-), 1.94 – 1.73 (-, 6H, 6x -NCH$_2$C<u>H$_2$</u>-), 1.87 (s, 18H, 3x -C(C<u>H$_3$</u>)<u>$_2$</u>), 1.80 (s, 18H, 3x -C(C<u>H$_3$</u>)<u>$_2$</u>), 1.71 – 1.57 (-, 12H, 6x -NCH$_2$C<u>H$_2$</u>-, 6x -C<u>H</u>CH$_3$), 1.57 – 1.48 (-, 6H, 6x -C<u>H</u>(CH$_3$)$_2$), 1.45 – 1.11 (-, 36H, 6x -C<u>H$_2$</u>C<u>H$_2$</u>C<u>H$_2$</u>), 1.08 (d, $^{3}J_{HH}$ = 6.0 Hz, 9H, 3x -CHC<u>H$_3$</u>), 1.04 (d, $^{3}J_{HH}$ = 6.2 Hz, 9H, 3x -CHC<u>H$_3$</u>), 0.88 (d, $^{3}J_{HH}$ = 6.6 Hz, 18H, 3x -CH(C<u>H$_3$</u>)<u>$_2$</u>), 0.86 (d, $^{3}J_{HH}$ = 6.7 Hz, 18H, 3x -CH(C<u>H$_3$</u>)<u>$_2$</u>).

^{13}C-NMR (151 MHz, $CDCl_3$, 303.6 K):

δ [ppm] = 182.5 (2x quart.), 180.4 (quart.), 179.3 (quart.), 170.4 (quart.), 169.4 (quart.), 143.3 (quart.), 142.6 (2x quart.), 142.44 (quart.), 142.39 (quart.), 137.0 (quart.), 127.9 (tert.), 127.3 (tert.), 125.0 (tert.), 124.0 (tert.), 122.5 (tert.), 121.6 (tert.), 109.6 (tert.), 109.5 (tert.), 87.0 (tert.), 86.8 (tert.), 49.6 (quart.), 49.5 (quart.), 42.3 (2x sec.), 39.32 (sec.), 39.30 (sec.), 37.30 (sec.), 37.26 (sec.), 34.0 (2x sec.), 31.37 (prim.), 31.35 (prim.), 28.12 (prim.), 28.10 (prim.), 27.4 (2x tert.), 27.13 (tert.), 27.12 (tert.), 24.84 (sec.), 24,80 (sec.), 22.87 (prim.), 22.84 (prim.), 22.76 (prim.), 22.74 (prim.), 19.8 (prim.), 19.7 (prim.).

ESI-MS (pos., high res.):

m/z calc. for $C_{144}H_{192}N_6O_6$ [$M^{\bullet+}$] 2102.49310, found: 2102.49663

Δ: 1.68 ppm

Synthesis of $(dSQA)_3$-ben

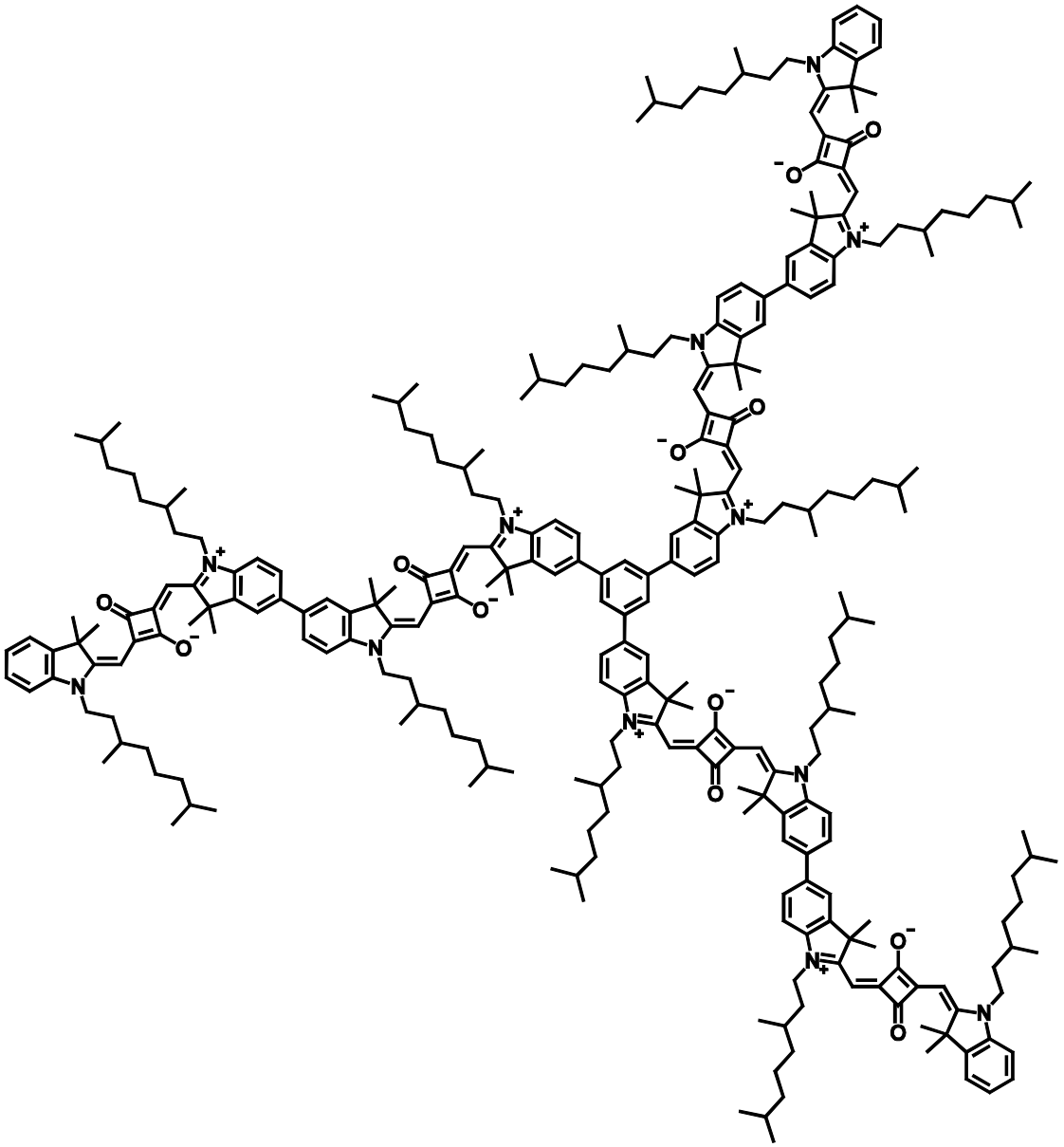

CA: [–]

Under a nitrogen atmosphere **dSQA-B** (150 mg, 101 µmol) and 1,3,5-tribromobenzene (6.26 mg, 19.9 µmol) were dissolved in peroxide free THF (10 ml). A saturated aqueous solution of Na_2CO_3 (2 ml) was added and the solution was degassed for 15 min. Then $Pd(PPh_3)_4$ (3.45 mg, 2.99 µmol) was added and the blue solution was refluxed under exclusion of light for 4 d. The solvent was removed in vacuo and the blue residue was purified by flash column chromatography (eluent: CH_2Cl_2 : MeOH = 99 : 1→98 : 2). The main fraction was purified by GPC ($CHCl_3$). Finally the crude product was dissolved in a small amount of CH_2Cl_2 and dropped into an excess of *n*-hexane. The resulting precipitate was filtered off and dried under high vacuum.

Yield: 30.0 mg (7.27 µmol; **37 %**) of a blue powder

$C_{282}H_{378}N_{12}O_{12}$ [4128.10]

^{1}H-NMR (600 MHz, CD_2Cl_2, 293.5 K):

δ[ppm] = 7.80 (s, 3H, 3x -CH-), 7.74 – 7.71 (-, 6H, 6x -CH-), 7.59 – 7.56 (-, 12H, 12x -CH-), 7.38 (d, $^{3}J_{HH}$ = 7.8 Hz, 3H, 3x -CH-), 7.32 (ddd, $^{3}J_{HH}$ = 7.3 Hz, $^{3}J_{HH}$ = 7.3 Hz, $^{4}J_{HH}$ = 0.6 Hz, 3H, 3x -CH-), 7.18 – 7.14 (-, 6H, 6x -CH-), 7.10 – 7.06 (-, 6H, 6x -CH-), 7.02 (d, $^{3}J_{HH}$ = 7.8 Hz, 3H, 3x -CH-), 6.01 – 5.91 (-, 12H, 12x -CH-), 4.17 – 3.94 (-, 24H, 12x -NCH_2-), 1.94 – 1.73 (-, 84H, 12x -$C(CH_3)_2$, 12x -NCH_2CH_2-), 1.71 – 1.59 (-, 24H, 12x -NCH_2CH_2-, 12x -$CHCH_3$), 1.59 – 1.48 (-, 12H, 12x -$CH(CH_3)_2$), 1.48 – 1.13 (-, 72H, 12x -$CH_2CH_2CH_2$), 1.12 (d, $^{3}J_{HH}$ = 6.0 Hz, 9H, 3x -$CHCH_3$), 1.11 (d, $^{3}J_{HH}$ = 6.0 Hz, 9H, 3x -$CHCH_3$), 1.09 (d, $^{3}J_{HH}$ = 6.0 Hz, 9H, 3x -$CHCH_3$), 1.07 (d, $^{3}J_{HH}$ = 6.0 Hz, 9H, 3x -$CHCH_3$), 0.89 (d, $^{3}J_{HH}$ = 6.6 Hz, 18H, 3x -$CH(CH_3)_2$), 0.873 (-, 36H, 6x -$CH(CH_3)_2$), 0.869 (d, $^{3}J_{HH}$ = 6.6 Hz, 18H, 3x -$CH(CH_3)_2$).

^{13}C-NMR (151 MHz, CD_2Cl_2, 293.5 K):

δ[ppm] = 182.0 (4x quart.), 180.9 (quart.), 180.7 (quart.), 180.3 (quart.), 180.1 (quart.), 170.2 (quart.), 169.8 (quart.), 169.6 (quart.), 169.4 (quart.), 143.5 (3x quart.), 142.8 (quart.), 142.74 (quart.), 142.68 (quart.), 142.6 (quart.), 142.3 (quart.), 142.2 (quart.), 137.00 (quart.), 136.98 (quart.), 136.7 (quart.), 128.1 (tert.), 127.5 (tert.), 126.9 (2x tert.), 124.9 (tert.), 124.0 (tert.), 122.6 (tert.), 121.7 (tert.), 121.1 (2x tert.), 110.1 (tert.), 110.0 (tert.), 109.9 (tert.), 109.8 (tert.), 87.31 (tert.), 87.29 (tert.), 87.1 (tert.), 86.9 (tert.), 49.72 (quart.), 49.68 (quart.), 49.63 (quart.), 49.58 (quart.), 42.59 (sec.), 42.57 (sec.), 42.5 (sec.), 42.4 (sec.), 39.54 (sec.), 39.53 (3x sec.), 37.50 (sec.), 37.48 (2x sec.), 37.46 (sec.), 34.2 (2x sec.), 34.13 (sec.), 34.09 (sec.), 31.53 (prim.), 31.50 (3x prim.), 28.39 (prim.), 28.38 (2x prim.), 28.37 (prim.), 27.31 (2x tert.), 27.28 (tert.), 27.27 (tert.), 27.24 (tert.), 27.23 (tert.), 27.07 (tert.), 27.06 (tert.), 25.12 (sec.), 25.10 (2x sec.), 25.08 (sec.), 22.85 (prim.), 22.83 (2x prim.), 22.82 (prim.), 22.76 (prim.), 22.74 (2x prim.), 22.73 (prim.), 19.82 (prim.), 19.80 (2x prim.), 19.76 (prim.).

ESI-MS (pos., high res.):

m/z calc. for $C_{282}H_{378}N_{12}O_{12}$ [$M^{\bullet+}$] 2063.97126, found: 2063.97001

Δ: 0.61 ppm

Synthesis of $(SQA)_3$-TAA

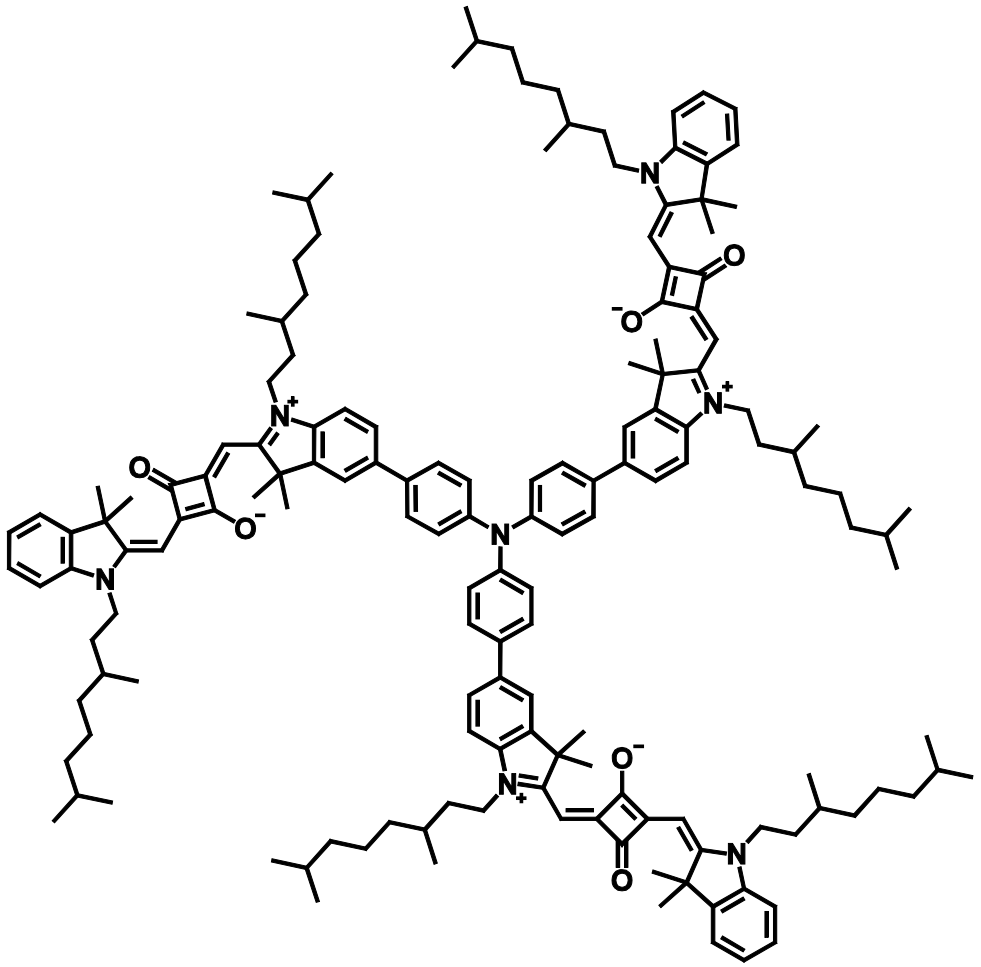

CA: [–]

Under a nitrogen atmosphere **SQA-Br** (340 mg, 450 µmol) and tris(4-(4, 4, 5, 5-tetramethyl-1,3,2-dioxaborolan-2-yl)phenyl)amine (**31**) (80.0 mg, 128 µmol) were dissolved in THF (12 ml). A saturated aqueous solution of K_2CO_3 (2 ml) was added and the mixture was degassed for 15 min. Then $Pd(PPh_3)_4$ (7.42 mg, 6.42 µmol) was added and the blue solution was refluxed under exclusion of light for 3 d. The solvent was removed *in vacuo* and the residue was purified by flash column chromatography (eluent: CH_2Cl_2/MeOH 99.5:0.5 → 99:1 → 98:2). Finally the crude product was dissolved in a small amount of CH_2Cl_2 and dropped into an excess of *n*-hexane. The resulting precipitate was filtered off and dried under high vacuum.

Yield: 51.0 mg (22.5 µmol; **18 %**) of a blue powder

$C_{156}H_{201}N_7O_6$ [2270.31]

^{1}H-NMR (600 MHz, CD_2Cl_2, 293.5 K):

δ [ppm] = 7.60 – 7.57 (-, 12H, 12x -C<u>H</u>-), 7.37 (dd, $^{3}J_{HH}$ = 7.2 Hz, $^{4}J_{HH}$ = 1.1 Hz, 3H, 3x -C<u>H</u>-), 7.32 (ddd, $^{3}J_{HH}$ = 7.8 Hz, $^{3}J_{HH}$ = 7.8 Hz, $^{4}J_{HH}$ = 1.1 Hz, 3H, 3x -C<u>H</u>-), 7.29 – 7.22 (-, 6H, 6x -C<u>H</u>-), 7.15 (ddd, $^{3}J_{HH}$ = 7.5 Hz, $^{3}J_{HH}$ = 7.5 Hz, $^{4}J_{HH}$ = 0.5 Hz, 3H, 3x -C<u>H</u>-), 7.07 (d, $^{3}J_{HH}$ = 8.3 Hz, 3H, 3x -C<u>H</u>-), 7.01 (d, $^{3}J_{HH}$ = 8.0 Hz, 3H, 3x -C<u>H</u>-), 5.93 (s, 3H, 3x -CC<u>H</u>C-), 5.92 (s, 3H, 3x -CC<u>H</u>C-), 4.12 – 3.95 (-, 12H, 6x -NC<u>H$_2$</u>-), 1.88 – 1.73 (-, 6H, 6x -NCH$_2$C<u>H$_2$</u>-), 1.82 (s, 18H, 3x -C(C<u>H$_3$</u>)<u>$_2$</u>), 1.76 (s, 18H, 3x -C(C<u>H$_3$</u>)<u>$_2$</u>), 1.70 – 1.59 (-, 12H, 6x -NCH$_2$C<u>H$_2$</u>-, 6x -C<u>H</u>CH$_3$), 1.58 – 1.48 (-, 6H, 6x -C<u>H</u>(CH$_3$)$_2$), 1.46 – 1.14 (-, 36H, 6x -C<u>H$_2$</u>C<u>H$_2$</u>C<u>H$_2$</u>-), 1.08 (d, $^{3}J_{HH}$ = 6.0 Hz, 9H, 3x -CHC<u>H$_3$</u>), 1.06 (d, $^{3}J_{HH}$ = 6.6 Hz, 9H, 3x -CHC<u>H$_3$</u>), 0.87 (d, $^{3}J_{HH}$ = 6.6 Hz, 18H, 3x -CH(C<u>H$_3$</u>)<u>$_2$</u>), ,0.86 (d, $^{3}J_{HH}$ = 6.6 Hz, 18H, 3x -CH(C<u>H$_3$</u>)<u>$_2$</u>).

^{13}C-NMR (151 MHz, CD_2Cl_2, 293.5 K):

δ [ppm] = 182.0 (2x quart.), 180.6 (quart.), 180.1 (quart.), 170.0 (quart.), 169.5 (quart.), 147.0 (quart.), 143.6 (quart.), 142.8 (quart.), 142.6 (quart.), 142.1 (quart.), 136.6 (quart.), 135.7 (quart.), 128.1 (tert.), 128.0 (2x tert.), 126.6 (tert.), 124.9 (2x tert.), 123.9 (tert.), 122.6 (tert.), 120.9 (tert.), 109.9 (tert.), 109.7 (tert.), 87.0 (tert.), 86.8 (tert.), 49.58 (quart.), 49.58 (quart.), 42.5 (sec.), 42.4 (sec.), 39.52 (sec.), 39.51 (sec.), 37.47 (sec.), 37.45 (sec.), 34.14 (sec.), 34.07 (sec.), 31.50 (prim.), 31.49 (prim.), 28.37 (prim.), 28.36 (prim.), 27.25 (tert.), 27.23 (tert.), 27.08 (tert.), 27.07 (tert.), 25.09 (sec.), 25.07 (sec.), 22.82 (prim.), 22.81 (prim), 22.73 (prim.), 22.72 (prim.), 19.8 (prim.), 19.7 (prim.).

ESI-MS (pos., high res.):

m/z calc. for $C_{156}H_{201}N_7O_6$ [$M^{\bullet+}$] 2269.56659, found: 2269.56774

Δ: 0.51 ppm

Synthesis of $(SQB)_3$-TAA

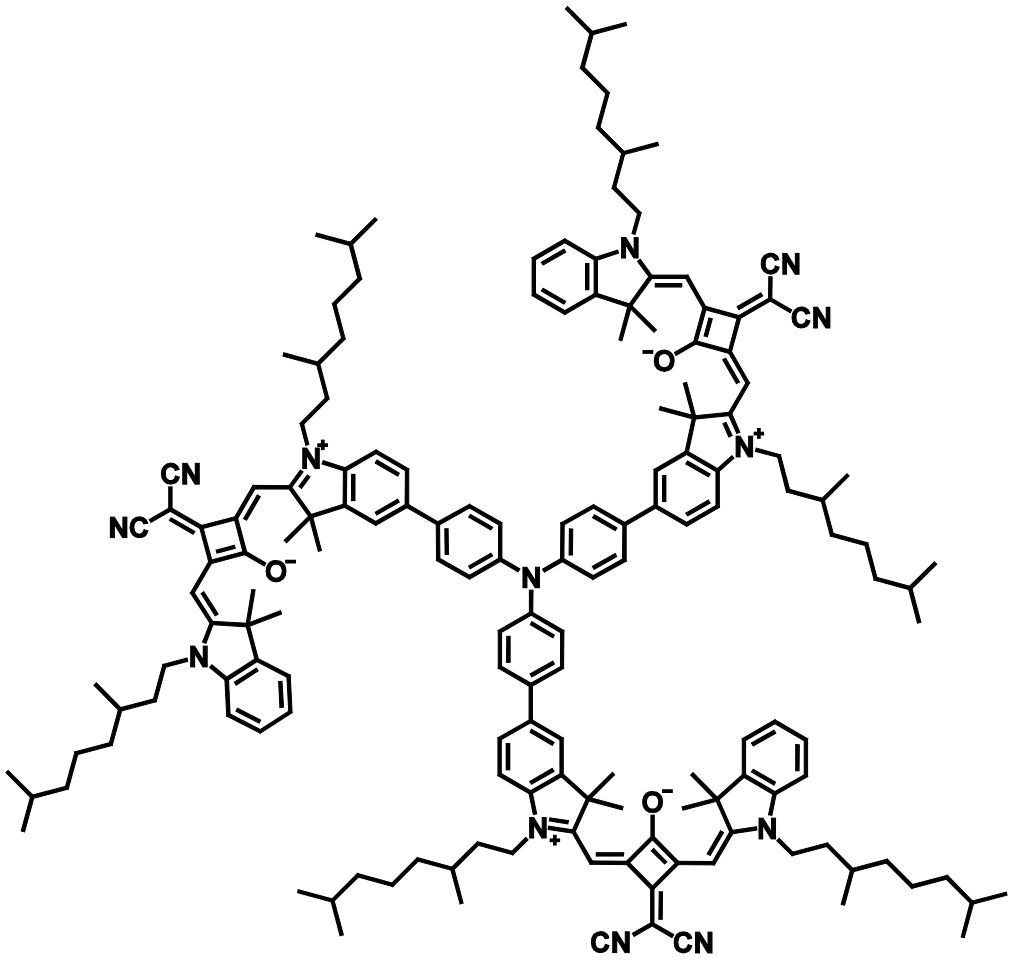

CA: [–]

Under a nitrogen atmosphere **SQB-Br** (226 mg, 281 µmol) and tris(4-(4, 4, 5, 5-tetramethyl-1,3,2-dioxaborolan-2-yl)phenyl)amine (**31**) (50.0 mg, 80.2 µmol) were dissolved in THF (10 ml). A saturated aqueous solution of K_2CO_3 (2 ml) was added and the mixture was degassed for 15 min. Then $Pd(PPh_3)_4$ (4.64 mg, 4.02 µmol) was added and the green solution was refluxed under exclusion of light for 6 d. The solvent was removed *in vacuo* and the residue was purified by flash column chromatography (eluent: CH_2Cl_2 → CH_2Cl_2/MeOH 99:1 → 98:2 → 97:3). The main fraction was purified by GPC. Finally the crude product was dissolved in a small amount of CH_2Cl_2 and dropped into an excess of *n*-hexane. The resulting precipitate was filtered off and dried under high vacuum.

Yield: 16.0 mg (6.63 µmol; **8 %**) of a green powder

$C_{165}H_{201}N_{13}O_3$ [2414.45]

^{1}H-NMR (600 MHz, CD_2Cl_2, .293.5 K):

δ [ppm] = 7.61 – 7.58 (-, 12H, 12x -C<u>H</u>-), 7.40 (d, $^{3}J_{HH}$ = 7.5 Hz, 3H, 3x -C<u>H</u>-), 7.36 (ddd, $^{3}J_{HH}$ = 7.9 Hz, $^{3}J_{HH}$ = 7.9 Hz, $^{4}J_{HH}$ = 0.8 Hz, 3H, 3x -C<u>H</u>-), 7.29 – 7.25 (-, 6H, 6x -C<u>H</u>-), 7.22 (ddd, $^{3}J_{HH}$ = 7.6 Hz, $^{3}J_{HH}$ = 7.6 Hz, $^{4}J_{HH}$ = 0.6 Hz, 3H, 3x -C<u>H</u>-), 7.14 (d, $^{3}J_{HH}$ = 9.0 Hz, 3H, 3x -C<u>H</u>-), 7.08 (d, $^{3}J_{HH}$ = 8.0 Hz, 3H, 3x -C<u>H</u>-), 6.49 (s, 3H, 3x -CC<u>H</u>C-), 6.48 (s, 3H, 3x -CC<u>H</u>C-), 4.14 – 3.98 (-, 12H, 6x -NC<u>H$_2$</u>-), 1.87 – 1.73 (-, 6H, 6x -NCH$_2$C<u>H$_2$</u>-), 1.81 (s, 18H, 3x -C(C<u>H$_3$</u>)<u>$_2$</u>), 1.76 (s, 18H, 3x -C(C<u>H$_3$</u>)<u>$_2$</u>), 1.71 – 1.57 (-, 12H, 6x -NCH$_2$C<u>H$_2$</u>-, 6x -C<u>H</u>CH$_3$), 1.57 – 1.48 (-, 6H, 6x -C<u>H</u>(CH$_3$)$_2$), 1.46 – 1.13 (-, 36H, 6x -C<u>H$_2$</u>C<u>H$_2$</u>C<u>H$_2$</u>-), 1.05 (d, $^{3}J_{HH}$ = 6.4 Hz, 9H, 3x -CHC<u>H$_3$</u>), 1.03 (d, $^{3}J_{HH}$ = 6.5 Hz, 9H, 3x -CHC<u>H$_3$</u>), 0.87 (d, $^{3}J_{HH}$ = 6.6 Hz, 18H, 3x -CH(C<u>H$_3$</u>)<u>$_2$</u>), 0.86 (d, $^{3}J_{HH}$ = 6.6 Hz, 18H, 3x -CH(C<u>H$_3$</u>)<u>$_2$</u>).

^{13}C-NMR (151 MHz, CD_2Cl_2, 303.6 K):

δ [ppm] = 173.5 (quart.), 172.2 (quart.), 171.6 (quart.), 167.9 (quart.), 166.8 (quart.), 166.3 (quart.), 147.1 (quart.), 143.7 (quart.), 142.9 (quart.), 142.3 (quart.), 141.6 (quart.), 137.5 (quart.), 135.5 (quart.), 128.4 (tert.), 128.2 (2x tert.), 126.8 (tert.), 124.9 (3x tert.), 122.6 (tert.), 120.9 (tert.), 119.17 (quart.), 119.14 (quart.), 110.7 (tert.), 110.5 (tert.), 89.5 (tert.), 89.4 (tert.), 49.8 (2x quart.), 43.4 (sec.), 43.3 (sec.), 40.6 (quart.), 39.54 (sec.), 39.52 (sec.), 37.49 (sec.), 37.47 (sec.), 34.42 (sec.), 34.37 (sec.), 31.3 (tert.), 31.0 (tert.), 28.40 (tert.), 28.39 (tert.), 26.9 (prim.), 26.8 (prim.), 26.7 (prim.), 26.6 (prim.), 25.04 (sec.), 25.02 (sec.), 22.83 (prim.), 22.82 (prim.), 22.74 (prim.), 22.73 (prim.), 19.82 (prim.), 19.78 (prim.).

ESI-MS (pos., high res.):

m/z calc. for $C_{165}H_{201}N_{13}O_3$ [$M^{\bullet 2+}$] 1206.79983, found: 1206.80119

Δ: 1.13 ppm

Synthesis of $(SQC)_3$-TAA

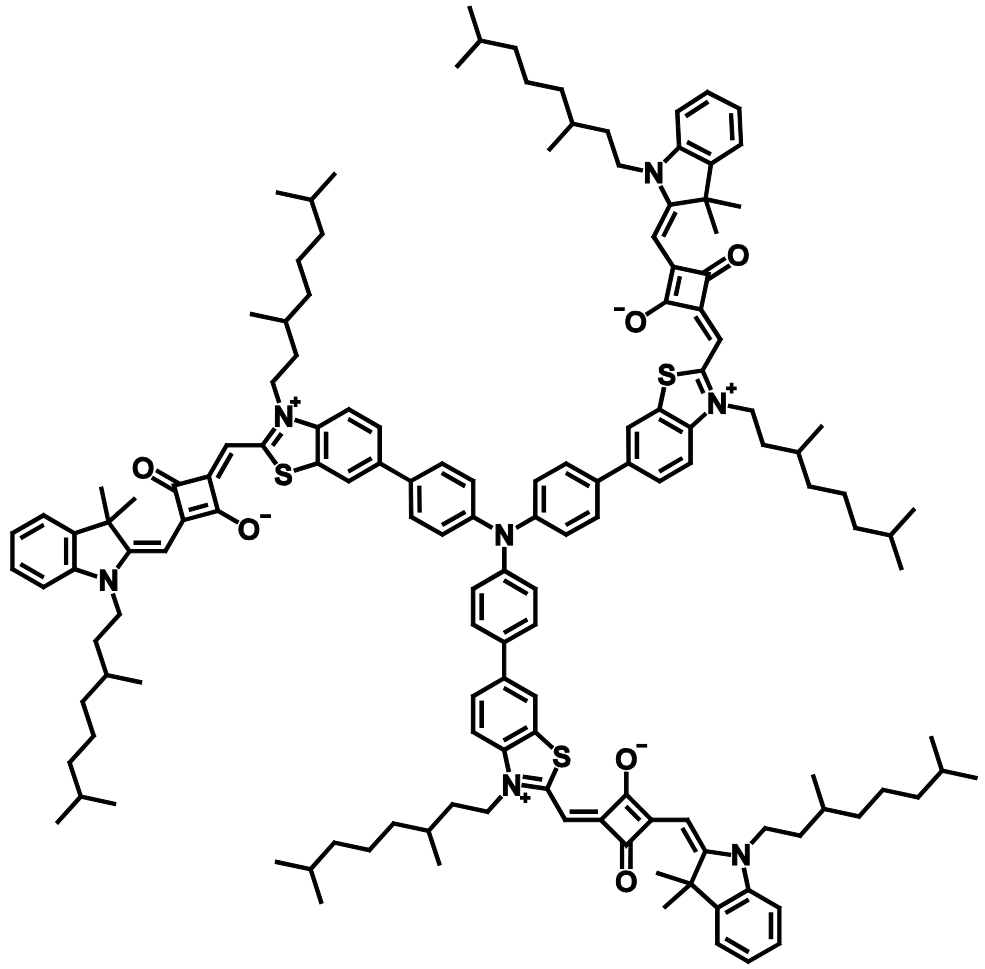

CA: [–]

Under a nitrogen atmosphere **SQC-Br** (467 mg, 626 µmol) and tris(4-(4, 4, 5, 5-tetramethyl-1,3,2-dioxaborolan-2-yl)phenyl)amine (**31**) (111 mg, 178 µmol) were dissolved in THF (20 ml). A saturated aqueous solution of K_2CO_3 (5 ml) was added and the mixture was degassed for 15 min. Then $Pd(PPh_3)_4$ (10.3 mg, 8.91 µmol) was added and the solution was refluxed under exclusion of light for 4 d. The solvent was removed *in vacuo* and the blue residue was purified by flash column chromatography (eluent: CH_2Cl_2/MeOH 99.5:0.5 → 99:1 → 98:2). The raw product was purified by GPC. Finally the crude product was dissolved in a small amount of CH_2Cl_2 and dropped into an excess of *n*-hexane. The resulting precipitate was filtered off and dried under high vacuum.

Yield: 32.0 mg (14.3 µmol; **8 %**) of a blue powder

$C_{147}H_{183}N_7O_6S_3$ [2240.27]

^{1}H-NMR (600 MHz, $CDCl_3$, 303.6 K):

δ [ppm] = 7.84 (d, $^{4}J_{HH}$ = 1.3 Hz, 3H, 3x -C<u>H</u>-), 7.68 (dd, $^{3}J_{HH}$ = 8.5 Hz, $^{4}J_{HH}$ = 1.6 Hz, 3H, 3x -C<u>H</u>-), 7.59 –7.53 (-, 6H, 6x -C<u>H</u>-), 7.33 (d, $^{3}J_{HH}$ = 7.3 Hz, 3H, 3x -C<u>H</u>-), 7.30 – 7.26 (-, 12H, 12x -C<u>H</u>-), 7.08 (dd, $^{3}J_{HH}$ = 7.4 Hz, $^{3}J_{HH}$ = 7.4 Hz, 3H, 3x -C<u>H</u>-), 6.94 (d, $^{3}J_{HH}$ = 7.9 Hz, 3H, 3x -C<u>H</u>-), 5.98 (s, 3H, 3x -CC<u>H</u>C-), 5.75 (s, 3H, 3x -CC<u>H</u>C-), 4.28 – 4.14 (m, 6H, 3x -NC<u>H$_2$</u>-), 4.04 – 3.84 (m, 6H, 3x -NC<u>H$_2$</u>-), 1.91 – 1.84 (m, 3H, 3x -NCH$_2$C<u>H$_2$</u>-), 1.82 – 1.66 (-, 9H, 3x -NCH$_2$C<u>H$_2$</u>-, 6x -C<u>H</u>CH$_3$), 1.73 (s, 18H, 3x C(C<u>H$_3$</u>)<u>$_2$</u>), 1.58 – 1.49 (-, 12H; 6x -NCH$_2$C<u>H$_2$</u>-, 6x -C<u>H</u>(CH$_3$)$_2$), 1.47 – 1.12 (-, 36H, 6x -C<u>H$_2$</u>C<u>H$_2$</u>C<u>H$_2$</u>-), 1.08 (d, $^{3}J_{HH}$ = 6.2 Hz, 9H, 3x -CHC<u>H$_3$</u>), 1.04 (d, $^{3}J_{HH}$ = 6.3 Hz, 9H, 3x -CHC<u>H$_3$</u>), 0.88 (d, $^{3}J_{HH}$ = 6.7 Hz, 18H, 3x -CH(C<u>H$_3$</u>)<u>$_2$</u>), 0.86 (d, $^{3}J_{HH}$ = 6.7 Hz, 18H, 3x -CH(C<u>H$_3$</u>)<u>$_2$</u>).

^{13}C-NMR (151 MHz, $CDCl_3$, 303.6 K):

δ [ppm] = 182.1 (quart.), 181.2 (quart.), 180.0 (quart.), 175.6 (quart.), 167.9 (quart.), 161.1 (quart.), 147.4 (quart.), 143.1 (quart.), 142.3 (quart.), 140.4 (quart.), 137.6 (quart.), 134.5 (quart.), 130.2 (quart.), 128.3 (2x tert.), 128.0 (tert.), 126.5 (tert.), 125.0 (2x tert.), 123.1 (tert.), 122.4 (tert.), 120.3 (tert.), 112.4 (tert.), 109.1 (tert.), 86.3 (2x tert.), 49.0 (quart.), 45.5 (sec.), 42.0 (sec.), 39.53 (sec.), 39.50 (sec.), 37.5 (sec.), 37.4 (sec.), 34.6 (sec.), 33.9 (sec.), 31.5 (prim.), 31.4 (prim.), 28.5 (tert.), 28.4 (tert.), 25.1 (sec.), 25.0 (sec.), 22.8 (2x prim.), 22.73 (prim.), 22.72 (prim.), 19.8 (prim.), 19.6 (prim.).

ESI-MS (pos., high res.):

m/z calc. for $C_{147}H_{183}N_7O_6S_3$ [$M^{\bullet+}$] 2239.34189, found: 2239.34449

Δ: 1.16 ppm

Synthesis of $(SQA)_3$-bor

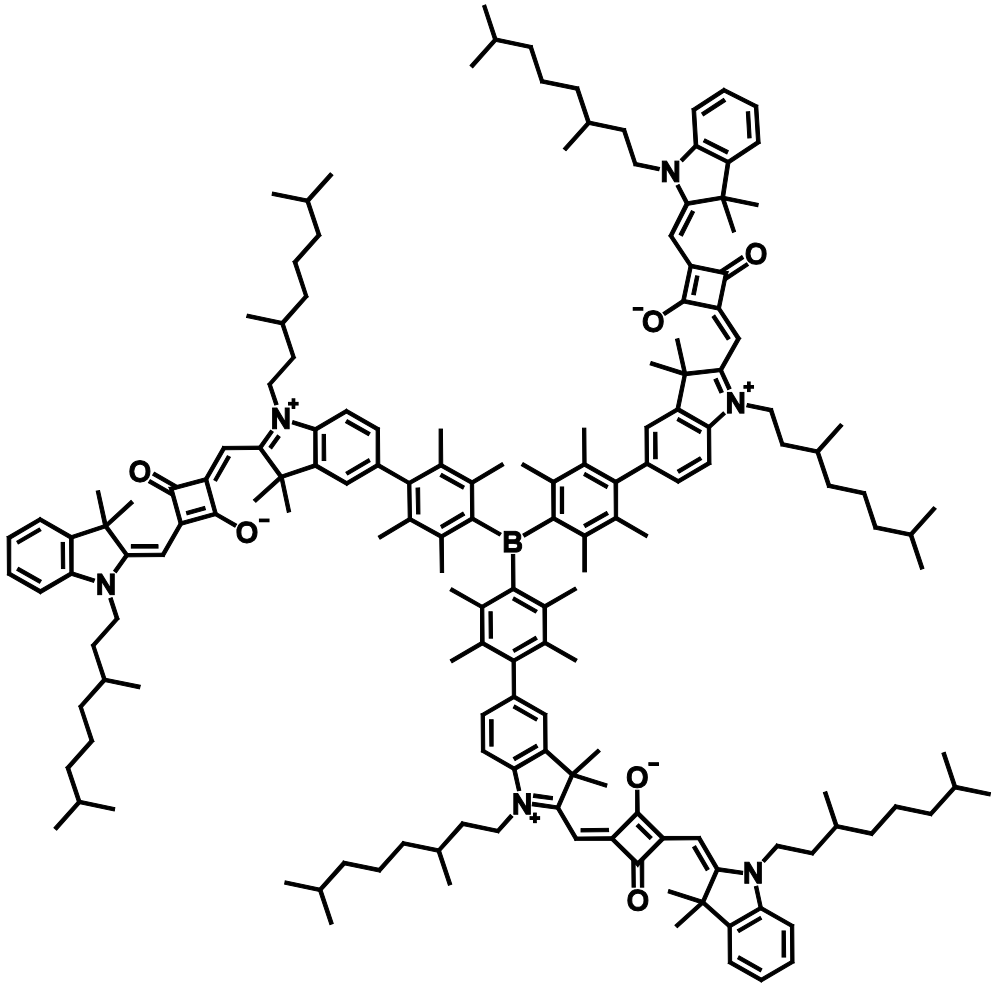

CA: [–]

Under a nitrogen atmosphere **SQA-B** (250 mg, 311 µmol) and tris(4-bromo-2,3,5,6-tetramethylphenyl)borane (**44**) (61.1 mg, 94.4 µmol) were dissolved in THF (10 ml). A saturated aqueous solution of K_2CO_3 (2 ml) was added and the mixture was degassed for 15 min. Then $Pd(PPh_3)_4$ (5.45 mg, 4.72 µmol) was added and the solution was refluxed under exclusion of light for 3 d. The solvent was removed *in vacuo* and the blue residue was purified by flash column chromatography (eluent: CH_2Cl_2/MeOH 99.5:0.5 → 99:1 → 98:2). The raw product was purified by GPC. Finally the crude product was dissolved in a small amount of CH_2Cl_2 and dropped into an excess of *n*-hexane. The resulting precipitate was filtered off and dried under high vacuum.

Yield: 17.0 mg (6.98 µmol; **7 %**) of a blue powder

$C_{168}H_{225}BN_6O_6$ [2435.44]

^{1}H-NMR (600 MHz, CD_2Cl_2, 293.5 K):

δ [ppm] = 7.36 (d, $^{3}J_{HH}$ = 7.5 Hz, 3H, 3x -C<u>H</u>-), 7.31 (dd, $^{3}J_{HH}$ = 7.5 Hz, $^{3}J_{HH}$ = 7.5 Hz, 3H, 3x -C<u>H</u>-), 7.17 – 7.05 (-, 12H, 12x -C<u>H</u>-), 7.00 (d, $^{3}J_{HH}$ = 7.2 Hz, 3H, 3x -C<u>H</u>-), 5.96 (s, 3H, 3x -CC<u>H</u>C-), 5.90 (s, 3H, 3x -CC<u>H</u>C-), 4.25 – 3.82 (-, 12H, 6x -NC<u>H$_2$</u>-), 2.13 (s, 18H, 6x -CC<u>H$_3$</u>), 1.91 (s, 9H, 3x -CC<u>H$_3$</u>), 1.90 (s, 9H, 3x -CC<u>H$_3$</u>), 1.88 – 1.72 (-, 6H, 6x -NCH$_2$C<u>H$_2$</u>-), 1.79 (s, 18H, 3x –C(C<u>H$_3$</u>)<u>$_2$</u>), 1.75 (s, 18H, 3x -CC<u>H$_3$</u>)<u>$_2$</u>), 1.71 – 1.49 (-, 18H, 6x -NCH$_2$C<u>H$_2$</u>-, 6x -C<u>H</u>CH$_3$, 6x -C<u>H</u>(CH$_3$)$_2$), 1.48 – 1.13 (-, 36H, 6x -C<u>H$_2$</u>C<u>H$_2$</u>C<u>H$_2$</u>-), 1.10 (d, $^{3}J_{HH}$ = 6.1 Hz, 9H, 3x -CHC<u>H$_3$</u>), 1.06 (d, $^{3}J_{HH}$ = 6.3 Hz, 9H, 3x -CHC<u>H$_3$</u>), 0.88 (d, $^{3}J_{HH}$ = 6.7 Hz, 18H, 3x -CH(C<u>H$_3$</u>)<u>$_2$</u>), 0.86 (d, $^{3}J_{HH}$ = 6.7 Hz, 18H, 3x -CH(C<u>H$_3$</u>)<u>$_2$</u>).

^{13}C-NMR (151 MHz, CD_2Cl_2, 293.5 K):

δ [ppm] = 182.1 (2x quart.), 180.3 (quart.), 179.7 (quart.), 170.2 (quart.), 169.6 (quart.), 149.4 (quart.), 143.2 (quart.), 142.9 (2x quart.), 142.5 (quart.), 141.2 (quart.), 139.3 (quart.), 136.23 (quart.), 136.16 (quart.), 132.0 (2x quart.), 129.2 (tert.), 128.1 (tert.), 124.0 (tert.), 123.8 (tert.), 122.5 (tert.), 109.6 (tert.), 109.4 (tert.), 86.8 (tert.), 86.7 (tert.), 49.7 (quart.), 49.5 (quart.), 42.6 (sec.), 42.3 (sec.), 39.53 (sec.), 39.51 (sec.), 37.47 (sec.), 37.46 (sec.), 34.2 (sec.), 34.0 (sec.), 31.6 (prim.), 31.5 (prim.), 28.38 (2x tert.), 28.35 (2x tert.), 27.1 (3x prim.), 25.09 (sec.), 25.07 (sec.), 22.82 (prim.), 22.80 (prim.), 22.74 (prim.), 22.71 (prim.), 20.5 (prim.), 19.8 (prim.), 19.7 (prim.), 18.18 (prim.), 18.16 (prim.).

ESI-MS (pos., high res.):

m/z calc. for $C_{168}H_{225}BN_6O_6$ [$M^{\bullet+}$] 2434.76195, found: 2434.76921

Δ: 2.98 ppm

6 Literature

1. A. H. Schmidt, *Synthesis-Stuttgart*, 1980, 961-994.
2. A. H. Schmidt in *Oxocarbons*, ed. R. West, Elsevier Science, 1980, ch. 10, pp. 185-231.
3. A. Treibs and K. Jacob, *Angew. Chem. Int. Ed.*, 1965, **4**, 694.
4. A. Treibs and K. Jacob, *Liebigs Ann. Chem.*, 1966, **699**, 153-167.
5. H. E. Sprenger and W. Ziegenbein, *Angew. Chem. Int. Ed.*, 1967, **6**, 553-554.
6. H. E. Sprenger and W. Ziegenbein, *Angew. Chem. Int. Ed.*, 1968, **7**, 530-535.
7. S. Cohen and S. G. Cohen, *J. Am. Chem. Soc.*, 1966, **88**, 1533-1536.
8. D. Keil and H. Hartmann, *Dyes and Pigments*, 2001, **49**, 161-179.
9. K. Jyothish, K. T. Arun and D. Ramaiah, *Org. Lett.*, 2004, **6**, 3965-3968.
10. K.-Y. Law and F. C. Bailey, *J. Chem. Soc., Chem. Commun.*, 1990, 863-865.
11. K. Y. Law and F. C. Bailey, *J. Org. Chem.*, 1992, **57**, 3278-3286.
12. D. Belluš, *J. Am. Chem. Soc.*, 1978, **100**, 8026-8028.
13. L. Beverina and P. Salice, *Eur. J. Org. Chem.*, 2010, 1207-1225.
14. A. L. Tatarets, I. A. Fedyunyaeva, E. Terpetschnig and L. D. Patsenker, *Dyes and Pigments*, 2005, **64**, 125-134.
15. U. Mayerhöffer, M. Gsänger, M. Stolte, B. Fimmel and F. Würthner, *Chem. Eur. J.*, 2013, **19**, 218-232.
16. R. Borrelli, S. Ellena and C. Barolo, *PCCP*, 2014, **16**, 2390-2398.
17. J. Fu, L. A. Padilha, D. J. Hagan, E. W. Van Stryland, O. V. Przhonska, M. V. Bondar, Y. L. Slominsky and A. D. Kachkovski, *J. Opt. Soc. Am. B*, 2007, **24**, 67-76.
18. R. A. Negres, O. V. Przhonska, D. J. Hagan, E. W. Van Stryland, M. V. Bondar, Y. L. Slominsky and A. D. Kachkovski, *IEEE Journal of Selected Topics in Quantum Electronics*, 2001, **7**, 849-863.
19. S. Ohira, I. Rudra, K. Schmidt, S. Barlow, S. J. Chung, Q. Zhang, J. Matichak, S. R. Marder and J. L. Bredas, *Chem. Eur. J.*, 2008, **14**, 11082-11091.
20. U. Mayerhöffer, B. Fimmel and F. Wurthner, *Angew. Chem. Int. Ed.*, 2012, **51**, 164-167.
21. S. Webster, S. A. Odom, L. A. Padilha, O. V. Przhonska, D. Peceli, H. H. Hu, G. Nootz, A. D. Kachkovski, J. Matichak, S. Barlow, H. L. Anderson, S. R. Marder, D. J. Hagan and E. W. Van Stryland, *J. Phys. Chem. B*, 2009, **113**, 14854-14867.
22. S. Kuster and T. Geiger, *Dyes and Pigments*, 2012, **95**, 657-670.
23. A. L. Puyad, G. K. Chaitanya, A. Thomas, M. Paramasivam and K. Bhanuprakash, *J. Phys. Org. Chem.*, 2013, **26**, 37-46.
24. S. F. Völker, M. Renz, M. Kaupp and C. Lambert, *Chem.-Eur. J.*, 2011, **17**, 14147-14163.
25. K.-Y. Law, *Chem. Rev.*, 1993, **93**, 449-486.
26. J. Fabian, H. Nakazumi and M. Matsuoka, *Chem. Rev.*, 1992, **92**, 1197-1226.
27. V. B. Jipson and C. R. Jones, *J. Vac. Sci. Technol.*, 1981, **18**, 105-109.
28. M. Emmelius, G. Pawlowski and H. W. Vollmann, *Angew. Chem. Int. Edit. Engl.*, 1989, **28**, 1445-1471.
29. S. F. Völker, S. Uemura, M. Limpinsel, M. Mingebach, C. Deibel, V. Dyakonov and C. Lambert, *Macromol. Chem. Phys.*, 2010, **211**, 1098-1108.
30. A. Ajayaghosh, *Acc. Chem. Res.*, 2005, **38**, 449-459.
31. L. Hu, Y. F. Zhang, L. Nie, C. G. Xie and Z. Q. Yan, *Spectrochim. Acta Mol. Biomol. Spectrosc.*, 2013, **104**, 87-91.
32. S. Yagi, Y. Hyodo, M. Hirose, H. Nakazumi, Y. Sakurai and A. Ajayaghosh, *Org. Lett.*, 2007, **9**, 1999-2002.
33. A. Ajayaghosh, P. Chithra, R. Varghese and K. P. Divya, *Chem. Commun.*, 2008, 969-971.
34. R. R. Avirah, D. T. Jayaram, N. Adarsh and D. Ramaiah, *Organic & Biomolecular Chemistry*, 2012, **10**, 911-920.
35. M. Göppert-Mayer, *Ann. Phys. Berlin*, 1931, **401**, 273-294.

36. R. R. Birge and B. M. Pierce, *Int. J. Quant. Chem.*, 1986, **29**, 639-656.
37. M. Rumi and J. W. Perry, *Advances in Optics and Photonics*, 2010, **2**, 451-518.
38. B. Strehmel and V. Strehmel in *Advances in Photochemistry*, John Wiley & Sons, Inc., 2005, pp. 111-354.
39. W. Kaiser and C. G. B. Garrett, *Phys. Rev. Lett.*, 1961, **7**, 229-231.
40. M. Pawlicki, H. A. Collins, R. G. Denning and H. L. Anderson, *Angew. Chem. Int. Ed.*, 2009, **48**, 3244-3266.
41. F. Terenziani, C. Katan, E. Badaeva, S. Tretiak and M. Blanchard-Desce, *Adv. Mater.*, 2008, **20**, 4641-4678.
42. P. N. Butcher and D. Cotter, *The Elements of Nonlinear Optics*, Cambridge University Press, Cambridge, 1993.
43. C. Andraud, R. Fortrie, C. Barsu, O. Stéphan, H. Chermette and P. L. Baldeck in *Photoresponsive Polymers II*, eds. S. R. Marder and K.-S. Lee, Springer, Berlin Heidelberg, 2008, vol. 214.
44. M. Rumi, J. E. Ehrlich, A. A. Heikal, J. W. Perry, S. Barlow, Z. Y. Hu, D. McCord-Maughon, T. C. Parker, H. Rockel, S. Thayumanavan, S. R. Marder, D. Beljonne and J. L. Bredas, *J. Am. Chem. Soc.*, 2000, **122**, 9500-9510.
45. C. Katan, F. Terenziani, O. Mongin, M. H. V. Werts, L. Porres, T. Pons, J. Mertz, S. Tretiak and M. Blanchard-Desce, *J. Phys. Chem. A*, 2005, **109**, 3024-3037.
46. K. Kamada, K. Ohta, I. Yoichiro and K. Kondo, *Chem. Phys. Lett.*, 2003, **372**, 386-393.
47. R. W. Boyd, *Nonlinear Optics*, Elsevier, London, 3rd edn., 2008.
48. M. Rumi, S. Barlow, J. Wang, J. W. Perry and S. R. Marder in *Photoresponsive Polymers I*, eds. S. R. Marder and K. S. Lee, Springer-Verlag Berlin, Berlin, 2008, vol. 213, pp. 1-95.
49. T. Kogej, D. Beljonne, F. Meyers, J. W. Perry, S. R. Marder and J. L. Bredas, *Chem. Phys. Lett.*, 1998, **298**, 1-6.
50. M. A. C. Nascimento, *Chem. Phys.*, 1983, **74**, 51-66.
51. W. M. McClain, *Acc. Chem. Res.*, 1974, **7**, 129-135.
52. Peticola.W. L., *Annu. Rev. Phys. Chem.*, 1967, **18**, 233-260.
53. J. E. Lewis and M. Maroncelli, *Chem. Phys. Lett.*, 1998, **282**, 197-203.
54. G. S. He, L. S. Tan, Q. Zheng and P. N. Prasad, *Chem. Rev.*, 2008, **108**, 1245-1330.
55. M. Albota, D. Beljonne, J. L. Bredas, J. E. Ehrlich, J. Y. Fu, A. A. Heikal, S. E. Hess, T. Kogej, M. D. Levin, S. R. Marder, D. McCord-Maughon, J. W. Perry, H. Rockel, M. Rumi, C. Subramaniam, W. W. Webb, X. L. Wu and C. Xu, *Science*, 1998, **281**, 1653-1656.
56. O. Mongin, L. Porres, M. Charlot, C. Katan and M. Blanchard-Desce, *Chem. Eur. J.*, 2007, **13**, 1481-1498.
57. M. G. Kuzyk, *J. Chem. Phys.*, 2003, **119**, 8327-8334.
58. E. Collini, *PCCP*, 2012, **14**, 3725-3736.
59. M. Drobizhev, A. Karotki, Y. Dzenis, A. Rebane, Z. Suo and C. W. Spangler, *J. Phys. Chem. B*, 2003, **107**, 7540-7543.
60. S. Webster, J. Fu, L. A. Padilha, O. V. Przhonska, D. J. Hagan, E. W. Van Stryland, M. V. Bondar, Y. L. Slominsky and A. D. Kachkovski, *Chem. Phys.*, 2008, **348**, 143-151.
61. W. V. Moreshead, O. V. Przhonska, M. V. Bondar, A. D. Kachkovski, I. H. Nayyar, A. E. Masunov, A. W. Woodward and K. D. Belfield, *Journal of Physical Chemistry C*, 2013, **117**, 23133-23147.
62. D. Scherer, R. Dorfler, A. Feldner, T. Vogtmann, M. Schwoerer, U. Lawrentz, W. Grahn and C. Lambert, *Chem. Phys.*, 2002, **279**, 179-207.
63. D. Beljonne, W. Wenseleers, E. Zojer, Z. G. Shuai, H. Vogel, S. J. K. Pond, J. W. Perry, S. R. Marder and J. L. Bredas, *Adv. Funct. Mater.*, 2002, **12**, 631-641.
64. C. Katan, F. Terenziani, C. Le Droumaguet, O. Mongin, M. H. V. Werts, S. Tretiak and M. Blanchard-Desce, "*Branching of dipolar chromophores: effects on linear and nonlinear optical properties*", Proc. SPIE 5935, Linear and Nonlinear Optics of Organic Materials V, 2005.

65. F. Terenziani, C. Le Droumaguet, C. Katan, O. Mongin and M. Blanchard-Desce, *Chemphyschem*, 2007, **8**, 723-734.
66. C. Katan, S. Tretiak, M. H. V. Werts, A. J. Bain, R. J. Marsh, N. Leonczek, N. Nicolaou, E. Badaeva, O. Mongin and M. Blanchard-Desce, *J. Phys. Chem. B*, 2007, **111**, 9468-9483.
67. M. Sheik-Bahae, A. A. Said, T. H. Wei, D. J. Hagan and E. W. Van Stryland, *IEEE J. Quant. Electron.*, 1990, **26**, 760-769.
68. D. A. Oulianov, I. V. Tomov, A. S. Dvornikov and P. M. Rentzepis, *Optics Communications*, 2001, **191**, 235-243.
69. M. Kasha, *Discussions of the Faraday Society*, 1950, 14-19.
70. C. Xu and W. W. Webb, *J. Opt. Soc. Am. B*, 1996, **13**, 481-491.
71. M. Drobizhev, Y. Stepanenko, Y. Dzenis, A. Karotki, A. Rebane, P. N. Taylor and H. L. Anderson, *J. Phys. Chem. B*, 2005, **109**, 7223-7236.
72. N. S. Makarov, M. Drobizhev and A. Rebane, *Opt. Express*, 2008, **16**, 4029-4047.
73. N. S. Makarov, J. Campo, J. M. Hales and J. W. Perry, *Optical Materials Express*, 2011, **1**, 551-563.
74. P. Esherick, P. Zinsli and M. A. Elsayed, *Chem. Phys.*, 1975, **10**, 415-432.
75. P. K. Frederiksen, M. Jorgensen and P. R. Ogilby, *J. Am. Chem. Soc.*, 2001, **123**, 1215-1221.
76. S. R. Marder, *Chem. Commun.*, 2006, 131-134.
77. J. D. Bhawalkar, N. D. Kumar, C. F. Zhao and P. N. Prasad, *J. Clin. Las. Med. Sur.*, 1997, **15**, 201-204.
78. S. J. Andrasik, K. D. Belfield, M. V. Bondar, F. E. Hernandez, A. R. Morales, O. V. Przhonska and S. Yao, *Chemphyschem*, 2007, **8**, 399-404.
79. W. Denk, J. H. Strickler and W. W. Webb, *Science*, 1990, **248**, 73-76.
80. F. Helmchen and W. Denk, *Nature Methods*, 2005, **2**, 932-940.
81. J. R. Tumbleston, D. Shirvanyants, N. Ermoshkin, R. Janusziewicz, A. R. Johnson, D. Kelly, K. Chen, R. Pinschmidt, J. P. Rolland, A. Ermoshkin, E. T. Samulski and J. M. DeSimone, *Science*, 2015, **347**, 1349-1352.
82. C. N. LaFratta, J. T. Fourkas, T. Baldacchini and R. A. Farrer, *Angew. Chem. Int. Ed.*, 2007, **46**, 6238-6258.
83. B. Jia, J. Li and M. Gu, *Aust. J. Chem.*, 2007, **60**, 484-495.
84. K.-S. Lee, D.-Y. Yang, S. H. Park and R. H. Kim, *Polym. Adv. Technol.*, 2006, **17**, 72-82.
85. E. Walker and P. M. Rentzepis, *Nature Photon.*, 2008, **2**, 406-408.
86. D. A. Parthenopoulos and P. M. Rentzepis, *Science*, 1989, **245**, 843-845.
87. E. Walker, A. Dvornikov, K. Coblentz and P. Rentzepis, *Appl. Opt.*, 2008, **47**, 4133-4139.
88. E. Walker, A. Dvornikov, K. Coblentz, S. Esener and P. Rentzepis, *Opt. Express*, 2007, **15**, 12264-12275.
89. J. Frenkel, *Phys. Rev.*, 1931, **37**, 17-44.
90. G. H. Wannier, *Phys. Rev.*, 1937, **52**, 191-197.
91. N. F. Mott, *J. Chem. Soc. Faraday Trans.*, 1938, **34**, 500-506.
92. H. v. Amerongen, L. Valkunas and R. v. Grondelle in *Photosynthetic Excitons*, World Scientific, Singapur, 2002, ch. 3, pp. 73-118.
93. M. Kasha, *Radiat. Res.*, 1963, **20**, 55-71.
94. M. Kasha, H. R. Rawls and M. A. El-Bayoumi, *Pure Appl. Chem.*, 1965, **11**, 371-392.
95. E. G. McRea and M. Kasha in *Physical Processes in Radiation Biology*, eds. L. Augenstein, R. Mason and B. Rosenberg, Academic Press, New York, 1964.
96. U. Lawrentz, Diploma Thesis, Universität Braunschweig, 1996.
97. S. F. Völker and C. Lambert, *Chem. Mater.*, 2012, **24**, 2541-2553.
98. S. F. Völker, T. Dellermann, H. Ceymann, M. Holzapfel and C. Lambert, *J. Polym. Sci. A Polym. Chem.*, 2014, **52**, 890-911.
99. C. Brüning, E. Welz, A. Heilos, V. Stehr, C. Walter, B. Engels, S. F. Völker, C. Lambert and V. Engel, *Journal of Physical Chemistry C*, 2015, **119**, 6174-6180.
100. H. Ceymann, Diploma Thesis, Universität Würzburg, 2010.

101. W. Ziegenbein and H. E. Sprenger, *Angew. Chem. Int. Ed.*, 1966, **5**, 893-894.
102. P. H. Wöbkenberg, J. G. Labram, J. M. Swiecicki, K. Parkhomenko, D. Sredojevic, J. P. Gisselbrecht, D. M. de Leeuw, D. D. C. Bradley, J. P. Djukic and T. D. Anthopoulos, *J. Mater. Chem.*, 2010, **20**, 3673-3680.
103. K. Hafner, H. Kaiser and H. Patzelt, *Liebigs Ann. Chem.*, 1962, **656**, 24-33.
104. Y. Q. Xu, Z. Y. Li, A. Malkovskiy, S. G. Sun and Y. Pang, *J. Phys. Chem. B*, 2010, **114**, 8574-8580.
105. A. J. McKerrow, E. Buncel and P. M. Kazmaier, *Can. J. Chem.*, 1995, **73**, 1605-1615.
106. K. D. Volkova, V. B. Kovalska, A. L. Tatarets, L. D. Patsenker, D. V. Kryvorotenko and S. M. Yarmoluk, *Dyes and Pigments*, 2007, **72**, 285-292.
107. E. Clar, *J. Chem. Soc.*, 1950, 1823-1826.
108. M. Beer and H. C. Longuet-Higgins, *J. Chem. Phys.*, 1955, **23**, 1390-1391.
109. M. Porsch, G. Sigl-Seifert and J. Daub, *Adv. Mater.*, 1997, **9**, 635-639.
110. V. Hrobarikova, P. Hrobarik, P. Gajdos, I. Fitilis, M. Fakis, P. Persephonis and P. Zahradnik, *J. Org. Chem.*, 2010, **75**, 3053-3068.
111. P. Hrobarik, I. Sigmundova, P. Zahradnik, P. Kasak, V. Arion, E. Franz and K. Clays, *Journal of Physical Chemistry C*, 2010, **114**, 22289-22302.
112. W. Gottardi, *Mon. Chem.*, 1968, **99**, 815-822.
113. Guglielm.R, R. Meyer and C. Dupuy, *J. Chem. Educ.*, 1973, **50**, 413-415.
114. E. E. Sheepwash, P. A. Rowntree and A. L. Schwan, *J. Label. Comp. Radiopharm.*, 2008, **51**, 391-398.
115. R. Abbel, M. Woffs, R. A. A. Bovee, J. L. J. van Dongen, X. Lou, O. Henze, W. J. Feast, E. W. Meijer and A. Schenning, *Adv. Mater.*, 2009, **21**, 597-602.
116. C. J. Bennett, S. T. Caldwell, D. B. McPhail, P. C. Morrice, G. G. Duthie and R. C. Hartley, *Biorg. Med. Chem.*, 2004, **12**, 2079-2098.
117. V. Rapozzi, L. Beverina, P. Salice, G. A. Pagani, M. Camerin and L. E. Xodo, *J. Med. Chem.*, 2010, **53**, 2188-2196.
118. M. V. Reddington, *Bioconjugate Chem.*, 2007, **18**, 2178-2190.
119. F. Scherninski, V. Guyon and M.-N. Rager, US 08034626, 2011.
120. A. Toutchkine, V. Kraynov and K. Hahn, *J. Am. Chem. Soc.*, 2003, **125**, 4132-4145.
121. M. Balkenhohl, Bachelor Thesis, Julius-Maximilians-Universität, 2014.
122. S. F. Völker, A. Schmiedel, M. Holzapfel, K. Renziehausen, V. Engel and C. Lambert, *Journal of Physical Chemistry C*, 2014, **118**, 17467-17482.
123. W. W. Parson in *Modern Optical Spectroscopy*, Springer, 2009, p. 293.
124. H. Ceymann, A. Rosspeintner, M. H. Schreck, C. Mützel, A. Stoy, E. Vauthey and C. Lambert, *PCCP*, 2016, submitted.
125. C. Lambert, T. Scherpf, H. Ceymann, A. Schmiedel and M. Holzapfel, *J. Am. Chem. Soc.*, 2015, **137**, 3547-3557.
126. F. Zieschang, A. Schmiedel, M. Holzapfel, K. Ansorg, B. Engels and C. Lambert, *Journal of Physical Chemistry C*, 2013, **117**, 19816-19831.
127. K. Nishiyama and T. Okada, *J. Phys. Chem. A*, 1997, **101**, 5729-5735.
128. S. A. Kovalenko, J. Ruthmann and N. P. Ernsting, *J. Chem. Phys.*, 1998, **109**, 1894-1900.
129. M. D. Edington, R. E. Riter and W. F. Beck, *J. Phys. Chem. B*, 1997, **101**, 4473-4477.
130. K. Gibasiewicz, V. M. Ramesh, A. N. Melkozernov, S. Lin, N. W. Woodbury, R. E. Blankenship and A. N. Webber, *J. Phys. Chem. B*, 2001, **105**, 11498-11506.
131. H. Murakami, S. Kinoshita, Y. Hirata, T. Okada and N. Mataga, *J. Chem. Phys.*, 1992, **97**, 7881-7888.
132. P. Martinsson, J. A. I. Oksanen, M. Hilgendorff, P. H. Hynninen, V. Sundstrom and E. Akesson, *Chem. Phys. Lett.*, 1999, **309**, 386-394.
133. S. A. Kovalenko, N. P. Ernsting and J. Ruthmann, *J. Chem. Phys.*, 1997, **106**, 3504-3511.
134. T. J. Kang, J. W. Yu and M. Berg, *J. Chem. Phys.*, 1991, **94**, 2413-2424.
135. J. Knoester in *Proceedings of the International School of Physics "Enrico Fermi" Course CXLIX*, eds. V. M. Agranovich and G. C. La Rocca, IOS Press, Amsterdam, 2002, pp. 149-186.

136. C. Lambert, A. Schmiedel, M. Holzapfel, M. Schreck, L. Wittmann, unpublished results.
137. M. Glasbeek and H. Zhang, *Chem. Rev.*, 2004, **104**, 1929-1954.
138. T. Elsaesser and W. Kaiser, *Annu. Rev. Phys. Chem.*, 1991, **42**, 83-107.
139. A. Pigliucci, G. Duvanel, L. M. L. Daku and E. Vauthey, *J. Phys. Chem. A*, 2007, **111**, 6135-6145.
140. J. Arago and A. Troisi, *Phys. Rev. Lett.*, 2015, **114**, 026402.
141. H. Langhals, A. J. Esterbauer, A. Walter, E. Riedle and I. Pugliesi, *J. Am. Chem. Soc.*, 2010, **132**, 16777-16782.
142. C. Lambert, F. Koch, S. F. Völker, A. Schmiedel, M. Holzapfel, A. Humeniuk, M. I. S. Rohr, R. Mitric and T. Brixner, *J. Am. Chem. Soc.*, 2015, **137**, 7851-7861.
143. G. A. Olah, S. C. Narang, B. G. B. Gupta, R. Malhotra, *J. Org. Chem.*, 1979, **44**, 1247-1251.
144. J. R. Lakowicz, *Principles of Fluorescence Spectroscopy*, Springer, New York, NY, 3. (corr. at 4. print.) edn., 2010.
145. S. J. Strickler and R. A. Berg, *J. Chem. Phys.*, 1962, **37**, 814-822.
146. R. H. Dicke, *Phys. Rev.*, 1954, **93**, 99-110.
147. G. L. Celardo, G. G. Giusteri and F. Borgonovi, *Physical Review B*, 2014, **90**, 075113.
148. H. Fidder, J. Knoester and D. A. Wiersma, *J. Chem. Phys.*, 1991, **95**, 7880-7890.
149. Y. Shibata, S. Tateishi, S. Nakabayashi, S. Itoh and H. Tamiaki, *Biochemistry*, 2010, **49**, 7504-7515.
150. D. Gülen, *Photosynth. Res.*, 2006, **87**, 205-214.
151. P. Macak, Y. Luo, P. Norman and H. Ågren, *J. Chem. Phys.*, 2000, **113**, 7055-7061.
152. N. V. Tkachenko, *Optical Spectroscopy*, Elsevier, Amsterdam, 2006.
153. M. H. Schreck, A. Stoy, H. Marciniak, A. Schmiedel, M. Holzapfel, C. Lambert, unpublished results.
154. C. D. Entwistle and T. B. Marder, *Chem. Mater.*, 2004, **16**, 4574-4585.
155. T. S. Ahn, R. O. Al-Kaysi, A. M. Mueller, K. M. Wentz and C. J. Bardeen, *Rev. Sci. Instrum.*, 2007, **78**, 086105.
156. I. H. M. van Stokkum, D. S. Larsen and R. van Grondelle, *Biochim. Biophys. Acta*, 2004, **1658**, 262-262.
157. J. J. Snellenburg, S. P. Laptenok, R. Seger, K. M. Mullen and I. H. M. van Stokkum, *Journal of Statistical Software*, 2012, **49**, 1-22.
158. M. Steeger, Ph.D. Thesis, Julius-Maximilians-University Würzburg, 2015.
159. S. Dummling, E. Eichhorn, S. Schneider, B. Speiser and M. Wuerde, *Curr. Separations*, 1996, **15**, 53-56.
160. I. Noviandri, K. N. Brown, D. S. Fleming, P. T. Gulyas, P. A. Lay, A. F. Masters and L. Phillips, *J. Phys. Chem. B*, 1999, **103**, 6713-6722.
161. N. G. Connelly and W. E. Geiger, *Chem. Rev.*, 1996, **96**, 877-910.
162. V. V. Pavlishchuk and A. W. Addison, *Inorg. Chim. Acta*, 2000, **298**, 97-102.
163. D. Tsiplakides, D. Archonta and C. G. Vayenas, *Top. Catal.*, 2007, **44**, 469-479.
164. S. Amthor, C. Lambert, *J. Phys. Chem. A*, 2006, **110**, 1177-1189.
165. G. R. Fulmer, A. J. M. Miller, N. H. Sherden, H. E. Gottlieb, A. Nudelman, B. M. Stoltz, J. E. Bercaw and K. I. Goldberg, *Organometallics*, 2010, **29**, 2176-2179.
166. D. V. D. M. A. Shriver, *The manipulation of air-sensitive compounds.*, John Wiley & Sons, New York, 1968.
167. W. C. Still, M. Kahn and A. Mitra, *J. Org. Chem.*, 1978, **43**, 2923-2925.
168. K. Hafner, K.-P. Meinhardt, *Org. Synth. Coll.*, 1990, **7**, 15-18.
169. B. Q. Bao, L. Yuwen, X. W. Zhan and L. H. Wang, *J. Polym. Sci. A Polym. Chem.*, 2010, **48**, 3431-3439.
170. J. Cremer and P. Bauerle, *J. Mater. Chem.*, 2006, **16**, 874-884.
171. M. Matsui, H. Mase, J. Y. Jin, K. Funabiki, T. Yoshida and H. Minoura, *Dyes and Pigments*, 2006, **70**, 48-53.
172. U. Mayerhöffer, K. Deing, K. Gruss, H. Braunschweig, K. Meerholz and F. Würthner, *Angew. Chem. Int. Ed.*, 2009, **48**, 8776-8779.

173. Gaussian 09, Revision D.01, Frisch M. J., G. W. Trucks, H. B. Schlegel, G. E. Scuseria, M. A. Robb, J. R. Cheeseman, G. Scalmani, V. Barone, B. Mennucci, G. A. Petersson, H. Nakatsuji, M. Caricato, X. Li, H. P. Hratchian, A. F. Izmaylov, J. Bloino, G. Zheng, J. L. Sonnenberg, M. Hada, M. Ehara, K. Toyota, R. Fukuda, J. Hasegawa, M. Ishida, T. Nakajima, Y. Honda, O. Kitao, H. Nakai, T. Vreven, J. J. A. Montgomery, J. E. Peralta, F. Ogliaro, M. Bearpark, J. J. Heyd, E. Brothers, K. N. Kudin, V. N. Staroverov, R. Kobayashi, J. Normand, K. Raghavachari, A. Rendell, J. C. Burant, S. S. Iyengar, J. Tomasi, M. Cossi, N. Rega, J. M. Millam, M. Klene, J. E. Knox, J. B. Cross, V. Bakken, C. Adamo, J. Jaramillo, R. Gomperts, R. E. Stratmann, O. Yazyev, A. J. Austin, R. Cammi, C. Pomelli, J. W. Ochterski, R. L. Martin, K. Morokuma, V. G. Zakrzewski, G. A. Voth, P. Salvador, J. J. Dannenberg, S. Dapprich, A. D. Daniels, Ö. Farkas, J. B. Foresman, J. V. Ortiz, J. Cioslowski and D. J. Fox, Gaussian, Inc, Wallingford CT, 2009.
174. W. L. Liu, V. Settels, P. H. P. Harbach, A. Dreuw, R. F. Fink and B. Engels, *J. Comput. Chem.*, 2011, **32**, 1971-1981.

7 Table of Formulas

Precursors

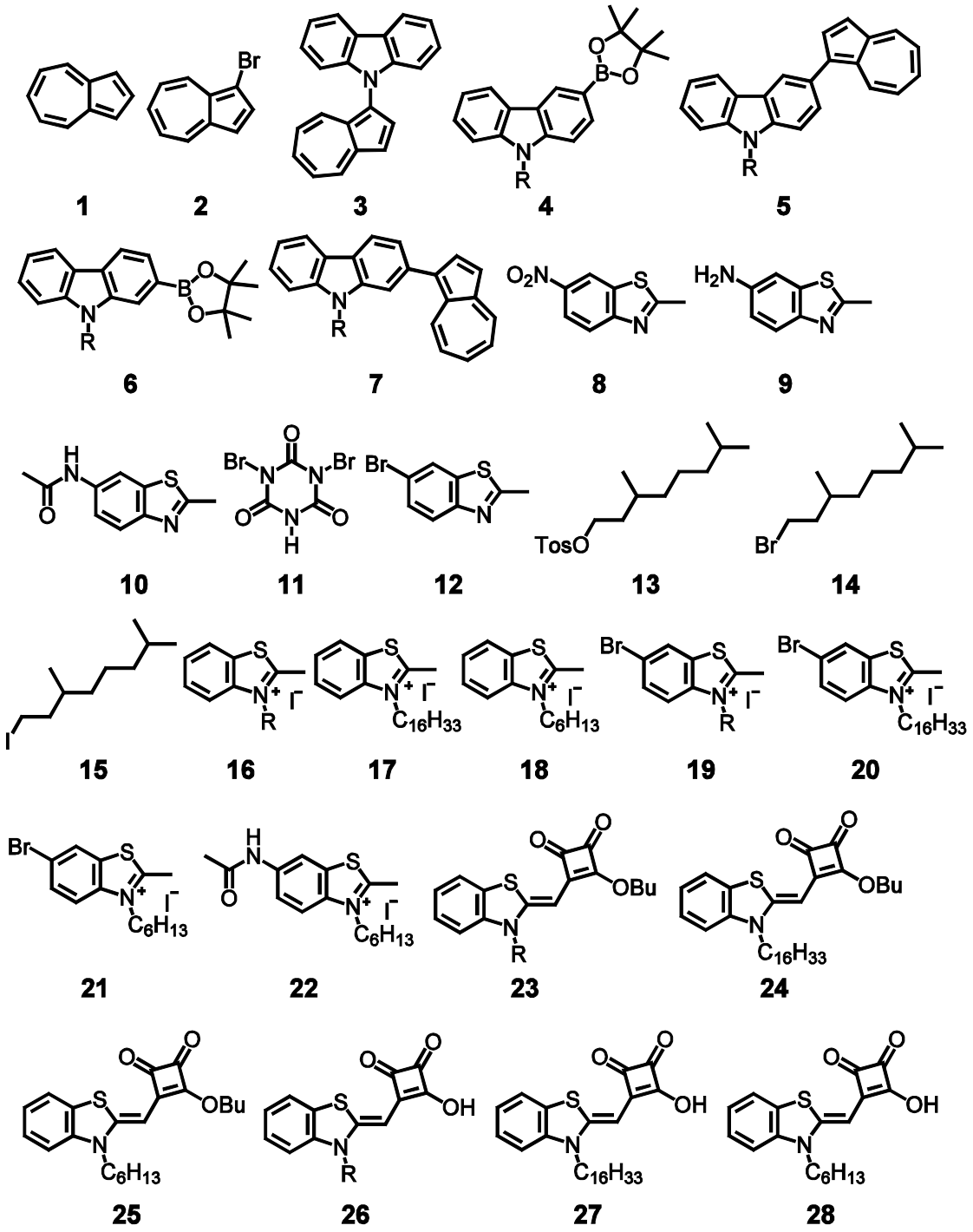

R = 3,7-dimethyloctyl

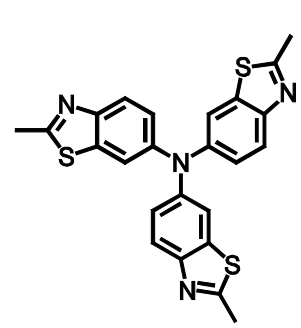

29

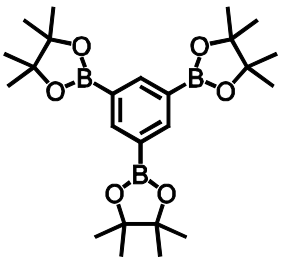

30

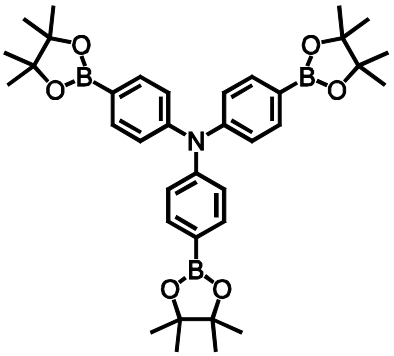

31

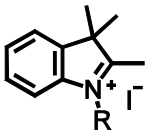

32

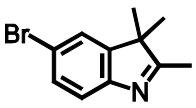

33

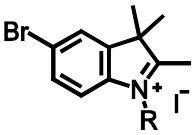

34

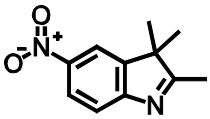

35

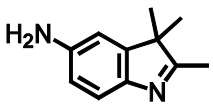

36

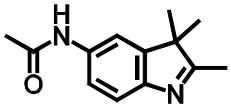

37

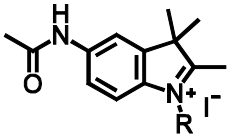

38

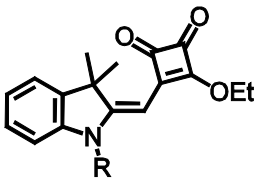

39

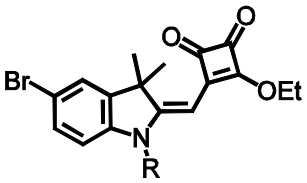

40

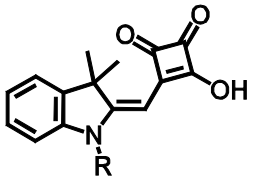

41

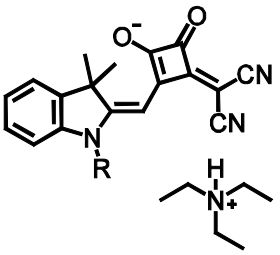

42

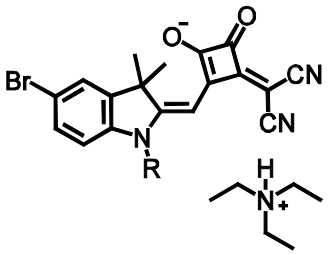

43

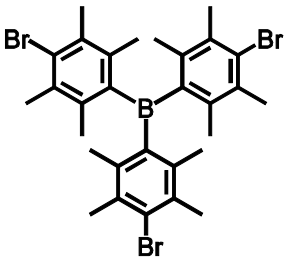

44

R = 3,7-dimethyloctyl

Azulene squaraines

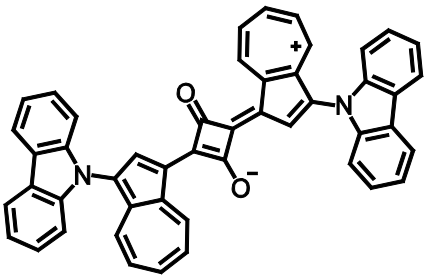

Az1

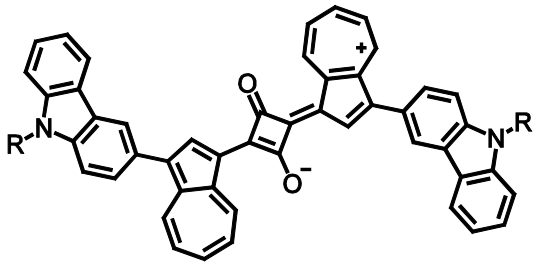

Az2

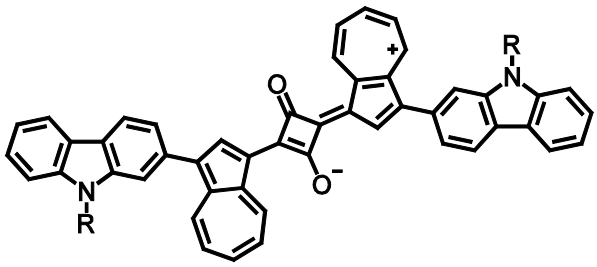

Az3

Benzothiazole squaraines

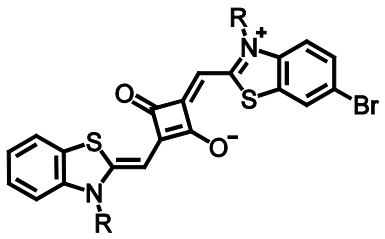

B1

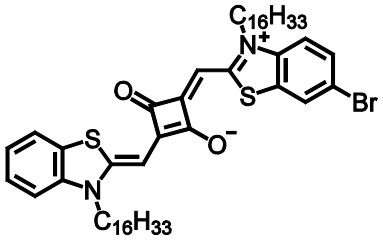

B2

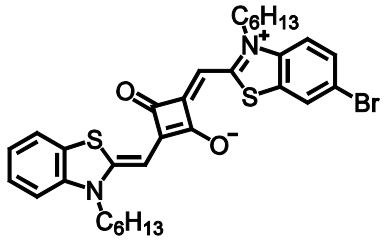

B3

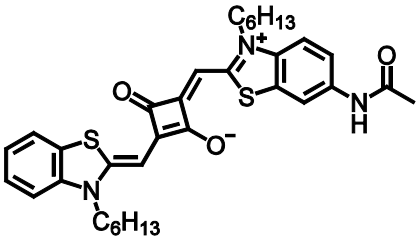

B4

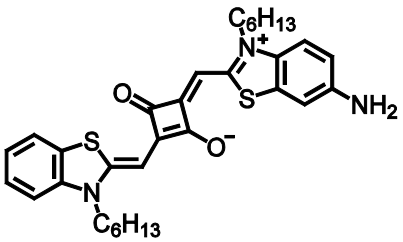

B5

R = 3,7-dimethyloctyl

Functionalised indolenine squaraines

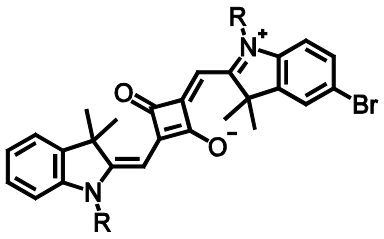

SQA-Br

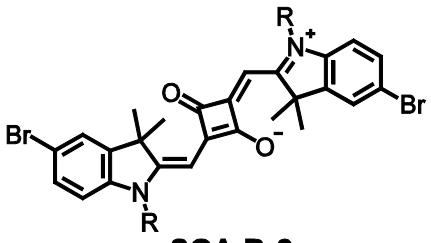

SQA-Br2

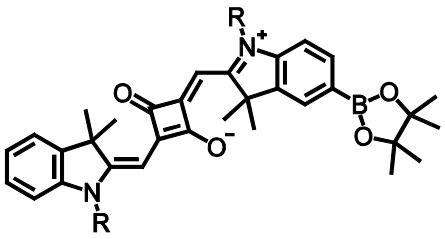

SQA-B

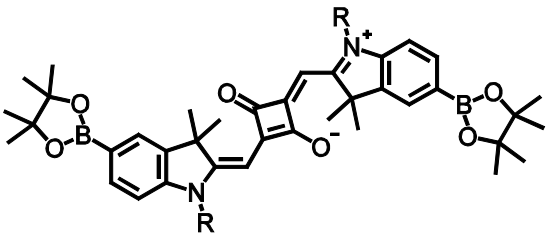

SQA-B$_2$

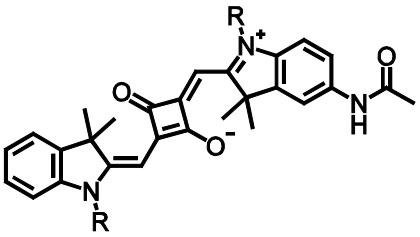

SQA-NHAc

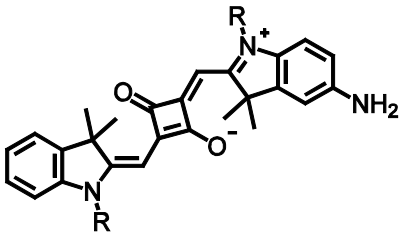

SQA-NH$_2$

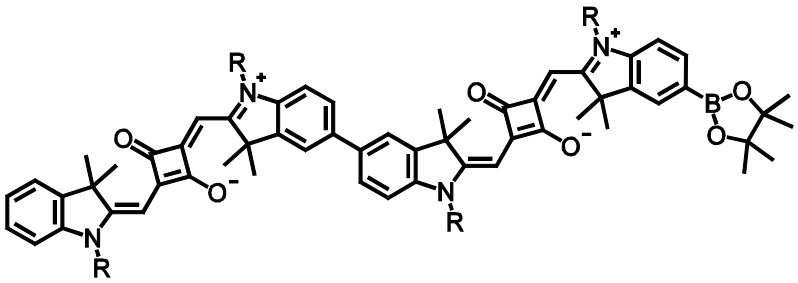

dSQA-B

R = 3,7-dimethyloctyl

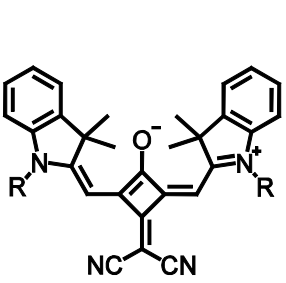

SQB

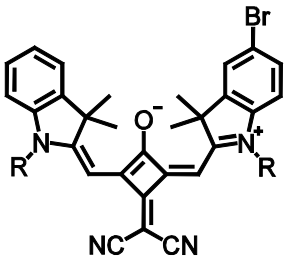

SQB-Br

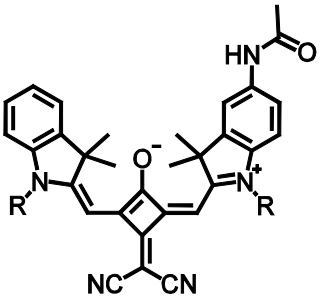

SQB-NHAc

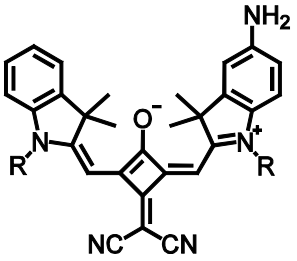

SQB-NH_2

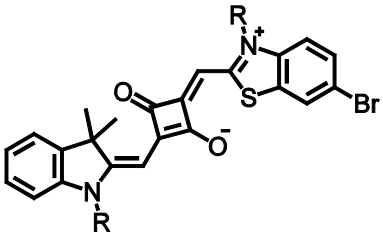

SQC-Br

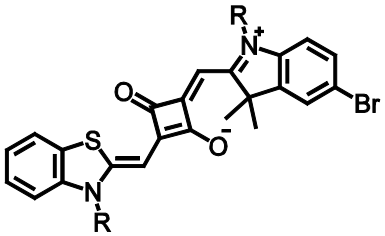

SQD-Br

Linear trans squaraines

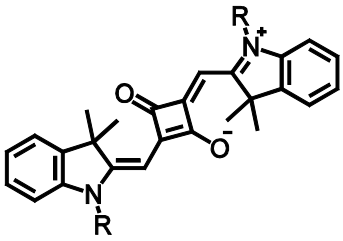

SQA

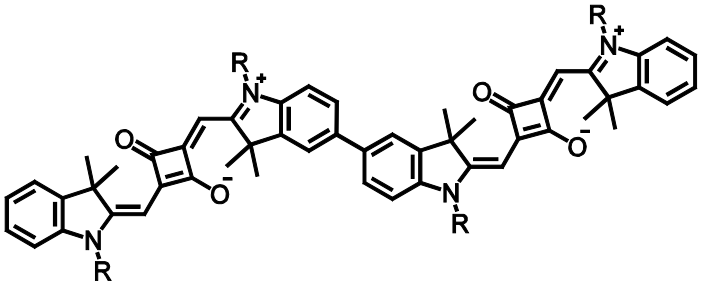

dSQA

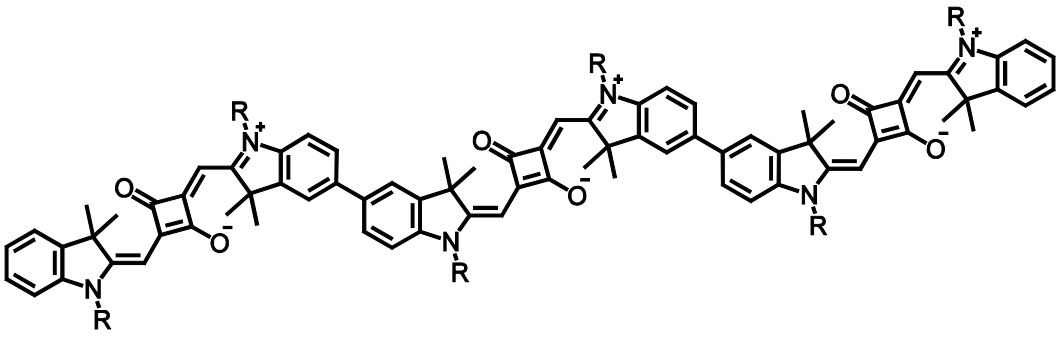

tSQA

R = 3,7-dimethyloctyl

Nitrogen core star-shaped squaraines

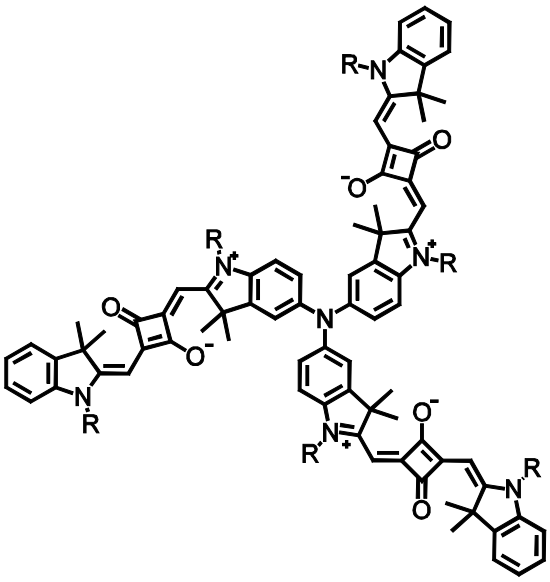

$(SQA)_3$-N

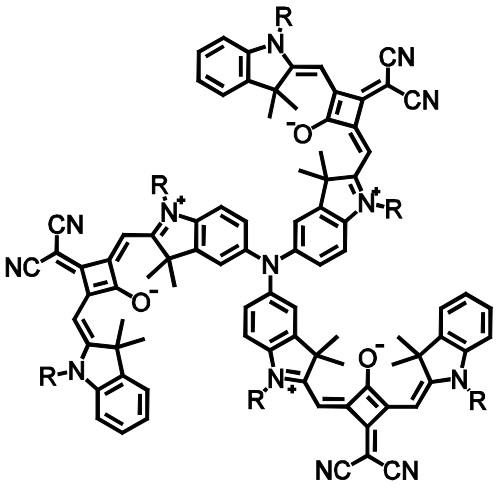

$(SQB)_3$-N

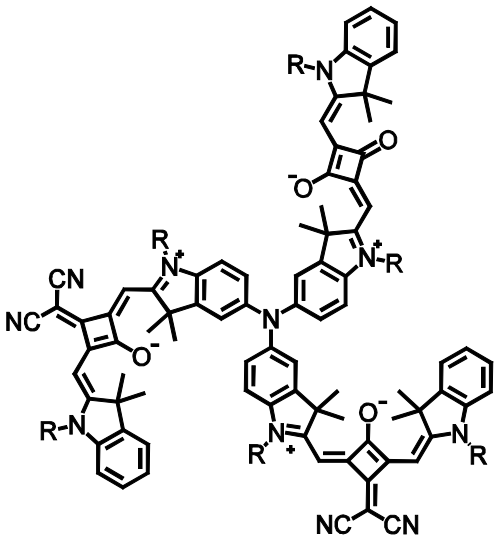

$(SQA)(SQB)_2$-N

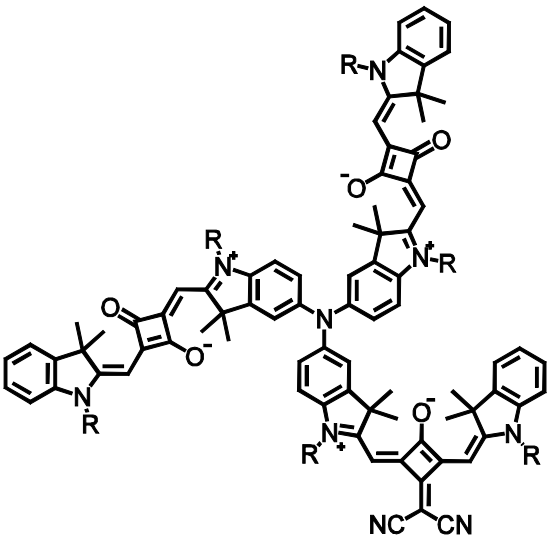

$(SQA)_2(SQB)$-N

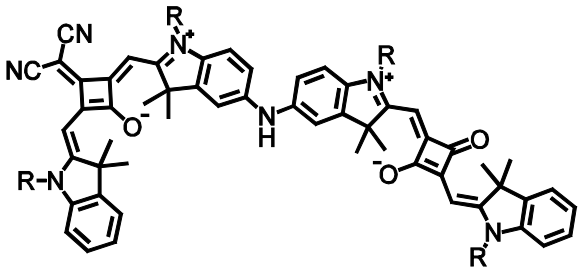

(SQA)(SQB)-NH

R = 3,7-dimethyloctyl

Triarylamine core star-shaped squaraines

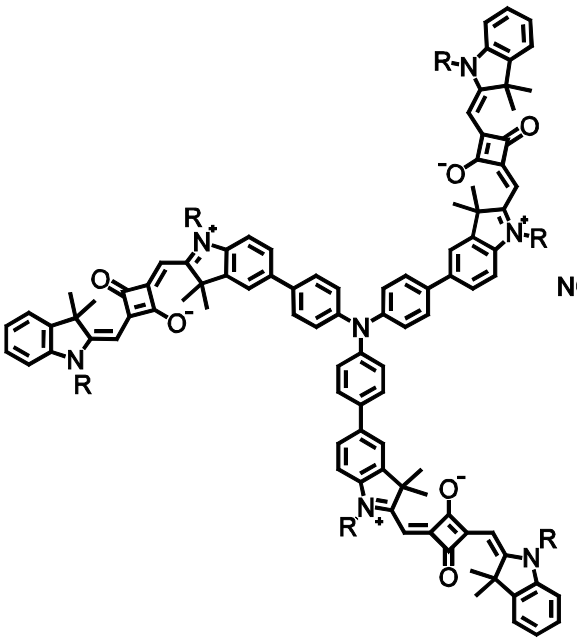

$(SQA)_3$-TAA

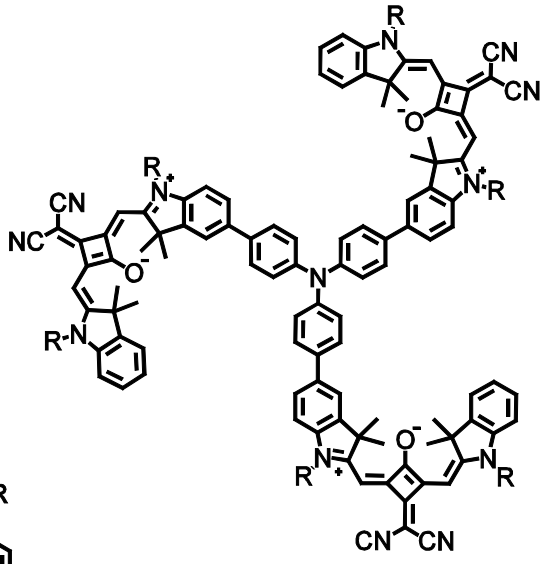

$(SQB)_3$-TAA

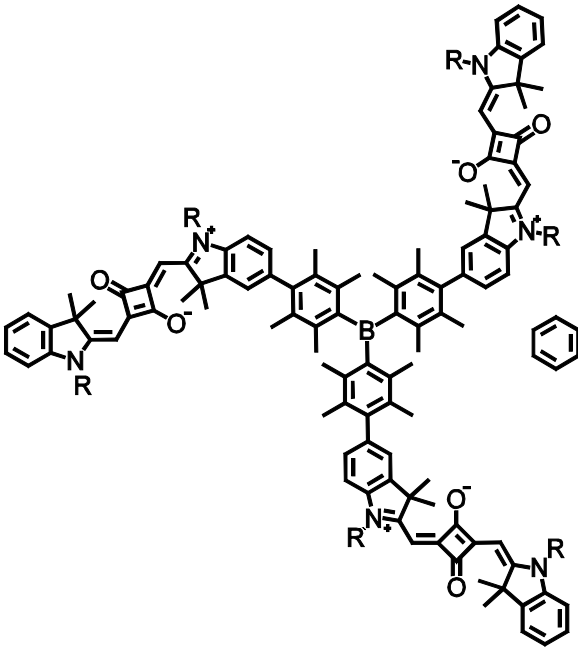

$(SQA)_3$-bor

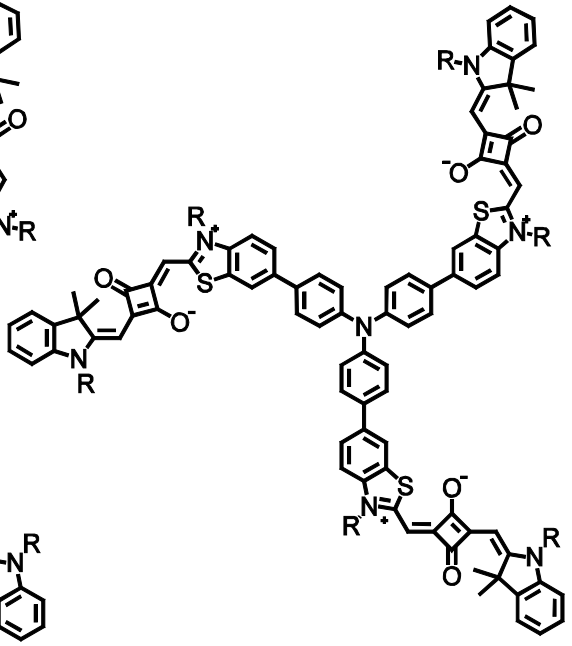

$(SQC)_3$-TAA

R = 3,7-dimethyloctyl

Benzene core star-shaped squaraines

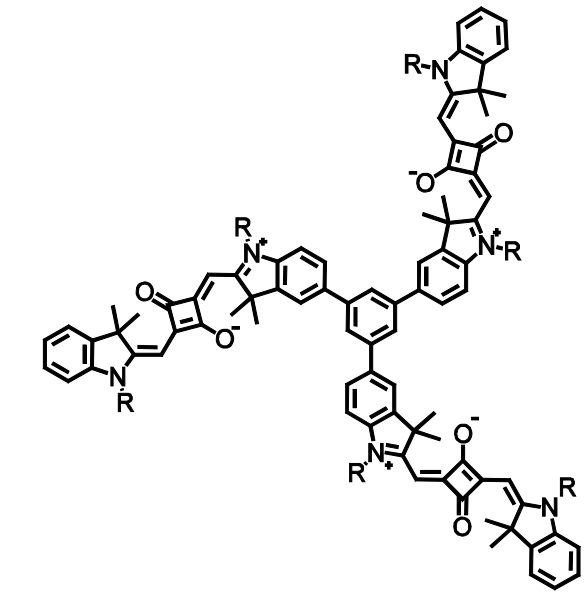

$(SQA)_3$-ben

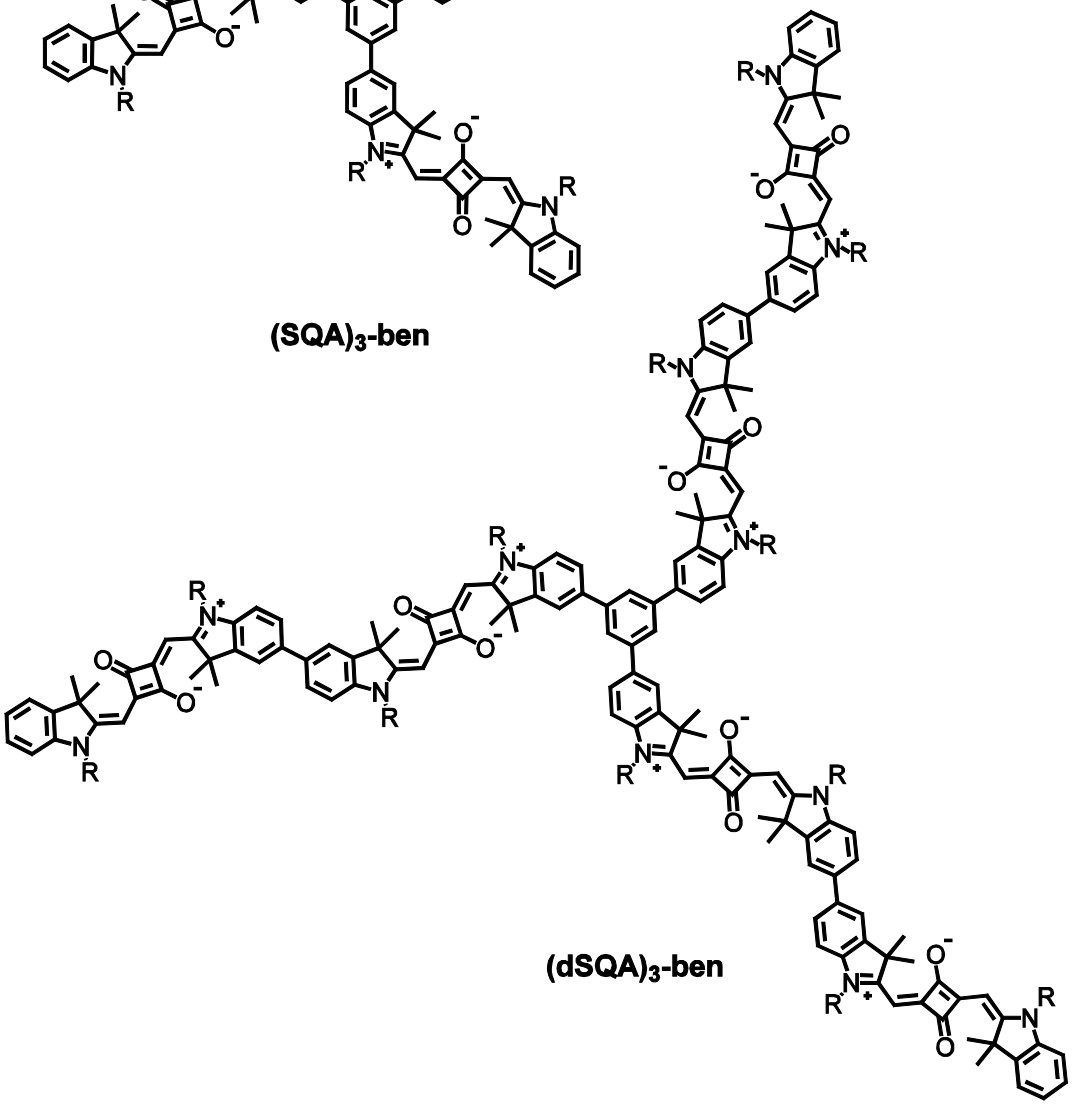

$(dSQA)_3$-ben

R = 3,7-dimethyloctyl

8 Zusammenfassung

Diese Arbeit beschreibt die Synthese von einigen linearen und stern-förmigen Squarain Superchromophoren die auf Indol Derivaten basieren. Außerdem werden sowohl deren lineare und nicht lineare spektroskopische Eigenschaften als auch ihr elektrochemisches Verhalten präsentiert. Der Versuch ähnliche Farbstoffe mit Benzothiazol Derivaten zu synthetisieren schlug leider fehl. Allerdings konnte ein stern-förmiges Trimer hergestellt und untersucht werden, dessen Äste aus einem gemischten Indol-Benzothiazol Squarain bestehen.

Die linearen spektroskopischen Eigenschaften, wie Rotverschiebung und die Verbreiterung der Absorption, aller Superchromophore konnten mit Hilfe der Exzitonen-Kopplungs Theorie erklärt werden. Die Heterochromophore **$(SQA)_2(SQB)$-N**, **$(SQA)(SQB)_2$-N** und **(SQA)(SQB)-NH** zeigten zusätzlich zu der typischen Squarain Fluoreszenz aus dem niedrigsten angeregten Zustand einige Besonderheiten die lokalisierten Zuständen zugeordnet werden konnten. Während die Farbstoffe mit einem Stickstoffkern lediglich geringe Fluoreszenzquantenausbeuten zeigen, zeigen die anderen Superchromophore im Vergleich mit den monomeren Squarainen teilweise erheblich größere Fluoreszenzquantenausbeuten.

Transiente Absorptionsspektroskopie Messungen der stern-förmigen Farbstoffe legen nahe, dass deren formell degenerierte S_1 Zustände wegen einer Abweichung von der C_3-Symmetrie aufspalten. Durch diese Abweichung bekommt auch der Übergang vom Grundzustand zum höchsten exzitonischen Zustand, der sich aus den S_1-Zuständen der Monomere ableiten lässt, ein merkliches Übergangsdipolmoment und kann daher in den linearen Absorptionsspektren beobachtet werden.

Die linearen Oligomere und die stern-förmigen Superchromophore die einen Benzol oder Triarylamin Kern haben zeigten mindestens additives, manchmal auch verstärkendes Verhalten in der Zweiphotonenabsorption. Zusätzlich zu den größeren molekularen Zweiphotonenabsorptions-Querschnitten sind auf Grund von Symmetriebrüchen und einer hohen Dichte von Zuständen die nicht linearen Absorptionsbanden merklich verbreitert.

Im Falle der Donor substituierten Azulen-Squaraine, war es nicht möglich wegen sterischen Gründen oder unstabilen Zwischenprodukten in der Synthese, das Gleichgewicht der cisoiden und der transoiden Struktur so zu verschieben das in Lösung nur noch eine der beiden Strukturen beobachtet wird.

9 Appendix

9.1 **Exciton Coupling Results** (see chapter 1.3)**:**

Exciton coupling of localised states leads to a set of exciton states (exciton manifold) whose eigenvalues ε_i and eigenvectors c_{ij} can be evaluated by solving the appropriate secular determinant. These are given for a linear homotrimer and all star-shaped trimers in Tables S1-S4. In these determinants we assume that the coupling J (instead of V_{ij}) between the localised states are all equal. The transition moments of the exciton states can then be expressed as linear combinations of the localised transition moments μ where the coefficients are those of the normalised eigenvectors.

Table S1 Exciton coupling results for **tSQA**.

Secular determinant:
$\begin{vmatrix} -\varepsilon & J & 0 \\ J & -\varepsilon & J \\ 0 & J & -\varepsilon \end{vmatrix} = 0$
eigenvalues, normalised eigenvectors, transition moments:
$\varepsilon_3 = \sqrt{2}J$
$c_{31} = \frac{1}{2}, \quad c_{32} = \frac{1}{\sqrt{2}}, \quad c_{33} = \frac{1}{2}$
$\hat{e}_{\mu_3} = c_{31}\mu_{\mathrm{SQA}}\begin{pmatrix}\cos\alpha_1\\ \sin\alpha_1\end{pmatrix} + c_{32}\mu_{\mathrm{SQA}}\begin{pmatrix}\cos\alpha_2\\ \sin\alpha_2\end{pmatrix} + c_{33}\mu_{\mathrm{SQA}}\begin{pmatrix}\cos\alpha_3\\ \sin\alpha_3\end{pmatrix}$
$\varepsilon_2 = -\sqrt{2}J$
$c_{21} = \frac{1}{2}, \quad c_{22} = -\frac{1}{\sqrt{2}}, \quad c_{23} = \frac{1}{2}$
$\hat{e}_{\mu_2} = c_{21}\mu_{\mathrm{SQA}}\begin{pmatrix}\cos\alpha_1\\ \sin\alpha_1\end{pmatrix} + c_{22}\mu_{\mathrm{SQA}}\begin{pmatrix}\cos\alpha_2\\ \sin\alpha_2\end{pmatrix} + c_{23}\mu_{\mathrm{SQA}}\begin{pmatrix}\cos\alpha_3\\ \sin\alpha_3\end{pmatrix}$
$\varepsilon_1 = 0$
$c_{11} = -\frac{1}{\sqrt{2}}, \quad c_{12} = 0, \quad c_{13} = \frac{1}{\sqrt{2}}$
$\hat{e}_{\mu_1} = c_{11}\mu_{\mathrm{SQA}}\begin{pmatrix}\cos\alpha_1\\ \sin\alpha_1\end{pmatrix} + c_{12}\mu_{\mathrm{SQA}}\begin{pmatrix}\cos\alpha_2\\ \sin\alpha_2\end{pmatrix} + c_{13}\mu_{\mathrm{SQA}}\begin{pmatrix}\cos\alpha_3\\ \sin\alpha_3\end{pmatrix}$
splitting between highest and lowest exciton level:
$\delta E_{\mathrm{trimer}} = 2\sqrt{2}J$

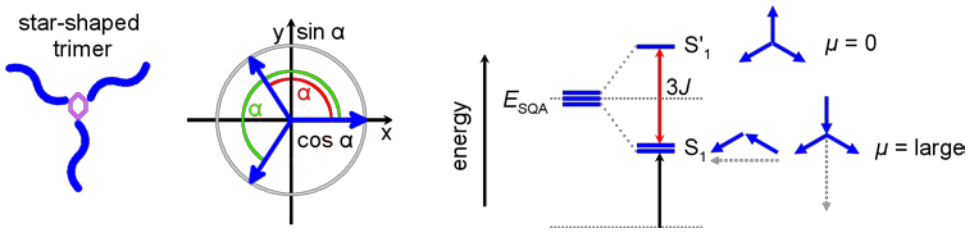

Figure S1 Orientation of a star-shaped trimer in a Cartesian coordinate system. On the right side the exciton eigenstates that are formed by exciton interaction are depicted, together with the localised transition dipole moments of the monomers (blue) and the resulting sum of the transition dipole moments (grey dashed).

Table S2 Exciton coupling results for star shaped homotrimers **(SQA)$_3$-ben**, **(SQA)$_3$-TAA**, **(SQB)$_3$-TAA** and **(SQA)$_3$N**.

Secular determinant:
$\begin{vmatrix} -\varepsilon & J & J \\ J & -\varepsilon & J \\ J & J & -\varepsilon \end{vmatrix} = 0$
eigenvalues, normalised eigenvectors, transition moments:
$\varepsilon_3 = 2J$
$c_{31} = \frac{1}{\sqrt{3}}, \quad c_{32} = \frac{1}{\sqrt{3}}, \quad c_{33} = \frac{1}{\sqrt{3}}$
$\hat{e}_{\mu_3} = c_{31}\mu_{SQA}\begin{pmatrix}\cos 240° \\ \sin 240°\end{pmatrix} + c_{32}\mu_{SQA}\begin{pmatrix}\cos 0° \\ \sin 0°\end{pmatrix} + c_{33}\mu_{SQA}\begin{pmatrix}\cos 120° \\ \sin 120°\end{pmatrix}$
$\varepsilon_2 = -J$
$c_{21} = -\frac{1}{\sqrt{2}}, \quad c_{22} = \frac{1}{\sqrt{2}}, \quad c_{23} = 0$
$\hat{e}_{\mu_2} = c_{21}\mu_{SQA}\begin{pmatrix}\cos 240° \\ \sin 240°\end{pmatrix} + c_{22}\mu_{SQA}\begin{pmatrix}\cos 0° \\ \sin 0°\end{pmatrix} + c_{23}\mu_{SQA}\begin{pmatrix}\cos 120° \\ \sin 120°\end{pmatrix}$
$\varepsilon_1 = -J$
$c_{11} = -\frac{1}{\sqrt{2}}, \quad c_{12} = 0, \quad c_{13} = \frac{1}{\sqrt{2}}$
$\hat{e}_{\mu_1} = c_{11}\mu_{SQA}\begin{pmatrix}\cos 240° \\ \sin 240°\end{pmatrix} + c_{12}\mu_{SQA}\begin{pmatrix}\cos 0° \\ \sin 0°\end{pmatrix} + c_{13}\mu_{SQA}\begin{pmatrix}\cos 120° \\ \sin 120°\end{pmatrix}$
splitting between highest and lowest exciton level:
$\delta E_{trimer} = 3J$

Table S3 Exciton coupling results for **$(SQA)_2(SQB)N$**.

Secular determinant:
$$\begin{vmatrix} \Delta E-\varepsilon & J & J \\ J & -\Delta E-\varepsilon & J \\ J & J & \Delta E-\varepsilon \end{vmatrix} = 0$$
eigenvalues, normalised eigenvectors, transition moments:
$$x = \sqrt{4\Delta E^2 + 4\Delta E J + 9J^2}$$
$$\varepsilon_3 = \frac{1}{2}(J + x)$$
$$c_{31} = \frac{-\frac{2\Delta E - J - x}{2J} + \frac{2\Delta E - 3J - x}{2\Delta E + 3J + x}}{\sqrt{1 + \left(\frac{2\Delta E - 3J - x}{2\Delta E + 3J + x}\right)^2 + \left(-\frac{2\Delta E - J - x}{2J} + \frac{2\Delta E - 3J - x}{2\Delta E + 3J + x}\right)^2}},$$ $$c_{32} = -\frac{2\Delta E - 3J - x}{(2\Delta E + 3J + x)\sqrt{1 + \left(\frac{2\Delta E - 3J - x}{2\Delta E + 3J + x}\right)^2 + \left(-\frac{2\Delta E - J - x}{2J} + \frac{2\Delta E - 3J - x}{2\Delta E + 3J + x}\right)^2}},$$ $$c_{33} = \frac{1}{\sqrt{1 + \left(\frac{2\Delta E - 3J - x}{2\Delta E + 3J + x}\right)^2 + \left(\frac{2\Delta E - J - x}{2J} + \frac{2\Delta E - 3J - x}{2\Delta E + 3J + x}\right)^2}}$$
$$\hat{e}_{\mu_3} = c_{31}\mu_{SQA}\begin{pmatrix}\cos 240^\circ \\ \sin 240^\circ\end{pmatrix} + c_{32}\mu_{SQB}\begin{pmatrix}\cos 0^\circ \\ \sin 0^\circ\end{pmatrix} + c_{33}\mu_{SQA}\begin{pmatrix}\cos 120^\circ \\ \sin 120^\circ\end{pmatrix}$$
$$\varepsilon_2 = \Delta E - J$$
$$c_{21} = -\frac{1}{\sqrt{2}}, \quad c_{22} = 0, \quad c_{23} = \frac{1}{\sqrt{2}}$$
$$\hat{e}_{\mu_2} = c_{21}\mu_{SQA}\begin{pmatrix}\cos 240^\circ \\ \sin 240^\circ\end{pmatrix} + c_{22}\mu_{SQB}\begin{pmatrix}\cos 0^\circ \\ \sin 0^\circ\end{pmatrix} + c_{23}\mu_{SQA}\begin{pmatrix}\cos 120^\circ \\ \sin 120^\circ\end{pmatrix}$$
$$\varepsilon_1 = \frac{1}{2}(J - x)$$
$$c_{11} = \frac{\frac{-2\Delta E + 3J - x}{-2\Delta E - 3J + x} - \frac{2\Delta E - J + x}{2J}}{\sqrt{1 + \left(\frac{-2\Delta E + 3J - x}{-2\Delta E - 3J + x}\right)^2 + \left(\frac{-2\Delta E + 3J - x}{-2\Delta E - 3J + x} - \frac{2\Delta E - J + x}{2J}\right)^2}},$$ $$c_{11} = -\frac{-2\Delta E + 3J - x}{(-2\Delta E - 3J + x)\sqrt{1 + \left(\frac{-2\Delta E + 3J - x}{-2\Delta E - 3J + x}\right)^2 + \left(\frac{-2\Delta E + 3J - x}{-2\Delta E - 3J + x} - \frac{2\Delta E - J + x}{2J}\right)^2}},$$ $$c_{13} = \frac{1}{\sqrt{1 + \left(\frac{-2\Delta E + 3J - x}{-2\Delta E - 3J + x}\right)^2 + \left(\frac{-2\Delta E + 3J - x}{-2\Delta E - 3J + x} - \frac{2\Delta E - J + x}{2J}\right)^2}}$$
$$\hat{e}_{\mu_1} = c_{11}\mu_{SQA}\begin{pmatrix}\cos 240^\circ \\ \sin 240^\circ\end{pmatrix} + c_{12}\mu_{SQB}\begin{pmatrix}\cos 0^\circ \\ \sin 0^\circ\end{pmatrix} + c_{13}\mu_{SQA}\begin{pmatrix}\cos 120^\circ \\ \sin 120^\circ\end{pmatrix}$$
splitting between highest and lowest exciton level:
$$\delta E_{\text{trimer}} = \sqrt{4\Delta E^2 + 4\Delta E J + 9J^2}$$

Table S4 Exciton coupling results for $(SQA)(SQB)_2N$.

Secular determinant:
$$\begin{vmatrix} -\Delta E-\varepsilon & J & J \\ J & \Delta E-\varepsilon & J \\ J & J & -\Delta E-\varepsilon \end{vmatrix} = 0$$
eigenvalues, normalised eigenvectors, transition moments:
$$x = \sqrt{4\Delta E^2 - 4\Delta E J + 9J^2}$$
$$\varepsilon_3 = \frac{1}{2}(J + x)$$
$$c_{31} = \frac{-\frac{-2\Delta E - J - x}{2J} + \frac{-2\Delta E - 3J - x}{-2\Delta E + 3J + x}}{\sqrt{1 + \left(\frac{-2\Delta E - 3J - x}{-2\Delta E + 3J + x}\right)^2 + \left(-\frac{-2\Delta E - J - x}{2J} + \frac{-2\Delta E - 3J - x}{-2\Delta E + 3J + x}\right)^2}},$$ $$c_{32} = -\frac{-2\Delta E - 3J - x}{(-2\Delta E + 3J + x)\sqrt{1 + \left(\frac{-2\Delta E - 3J - x}{-2\Delta E + 3J + x}\right)^2 + \left(-\frac{-2\Delta E - J - x}{2J} + \frac{-2\Delta E - 3J - x}{-2\Delta E + 3J + x}\right)^2}},$$ $$c_{33} = \frac{1}{\sqrt{1 + \left(\frac{-2\Delta E - 3J - x}{-2\Delta E + 3J + x}\right)^2 + \left(\frac{-2\Delta E - J - x}{2J} + \frac{-2\Delta E - 3J - x}{-2\Delta E + 3J + x}\right)^2}}$$
$$\hat{e}_{\mu_3} = c_{31}\mu_{SQB}\begin{pmatrix}\cos 240^\circ \\ \sin 240^\circ\end{pmatrix} + c_{32}\mu_{SQA}\begin{pmatrix}\cos 0^\circ \\ \sin 0^\circ\end{pmatrix} + c_{33}\mu_{SQB}\begin{pmatrix}\cos 120^\circ \\ \sin 120^\circ\end{pmatrix}$$
$$\varepsilon_2 = \frac{1}{2}(J - x)$$
$$c_{21} = \frac{\frac{2\Delta E + 3J - x}{2\Delta E - 3J + x} - \frac{-2\Delta E - J + x}{2J}}{\sqrt{1 + \left(\frac{2\Delta E + 3J - x}{2\Delta E - 3J + x}\right)^2 + \left(\frac{2\Delta E + 3J - x}{2\Delta E - 3J + x} - \frac{-2\Delta E - J + x}{2J}\right)^2}},$$ $$c_{22} = -\frac{2\Delta E + 3J - x}{(2\Delta E - 3J + x)\sqrt{1 + \left(\frac{2\Delta E + 3J - x}{2\Delta E - 3J + x}\right)^2 + \left(\frac{2\Delta E + 3J - x}{2\Delta E - 3J + x} - \frac{-2\Delta E - J + x}{2J}\right)^2}},$$ $$c_{23} = \frac{1}{\sqrt{1 + \left(\frac{2\Delta E + 3J - x}{2\Delta E - 3J + x}\right)^2 + \left(\frac{2\Delta E + 3J - x}{2\Delta E - 3J + x} - \frac{-2\Delta E - J + x}{2J}\right)^2}}$$
$$\hat{e}_{\mu_2} = c_{21}\mu_{SQB}\begin{pmatrix}\cos 240^\circ \\ \sin 240^\circ\end{pmatrix} + c_{22}\mu_{SQA}\begin{pmatrix}\cos 0^\circ \\ \sin 0^\circ\end{pmatrix} + c_{23}\mu_{SQB}\begin{pmatrix}\cos 120^\circ \\ \sin 120^\circ\end{pmatrix}$$
$$\varepsilon_1 = -\Delta E - J$$
$$c_{11} = -\frac{1}{\sqrt{2}}, \quad c_{12} = 0, \quad c_{13} = \frac{1}{\sqrt{2}}$$
$$\hat{e}_{\mu_1} = c_{11}\mu_{SQB}\begin{pmatrix}\cos 240^\circ \\ \sin 240^\circ\end{pmatrix} + c_{12}\mu_{SQA}\begin{pmatrix}\cos 0^\circ \\ \sin 0^\circ\end{pmatrix} + c_{13}\mu_{SQB}\begin{pmatrix}\cos 120^\circ \\ \sin 120^\circ\end{pmatrix}$$
splitting between highest and lowest exciton level:
$$\delta E_{\text{trimer}} = \frac{1}{2}\left(J + \sqrt{4\Delta E^2 - 4\Delta E J + 9J^2}\right) + \Delta E + J$$

9.2 Lifetime Distribution Analysis

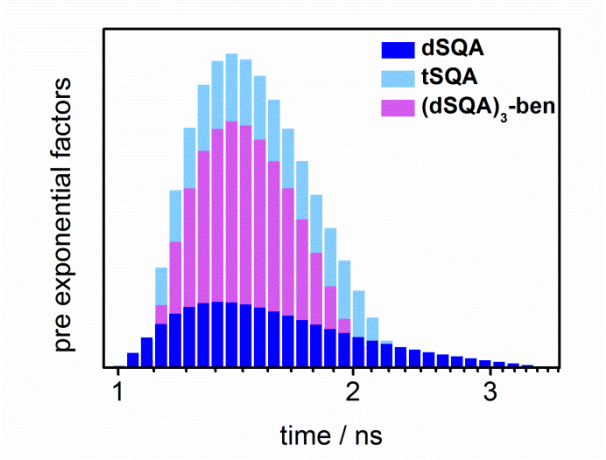

Fig. S2 Lifetime distribution analysis [software: FAST (version 3.4.2)] of the fluorescence spectra of **dSQA**, **tSQA** and **(dSQA)$_3$-ben** measured by TCSPC in toluene with excitation at 15200 cm^{-1}.

9.3 Anisotropy Spectra of the Fluorescence Upconversion Measurements

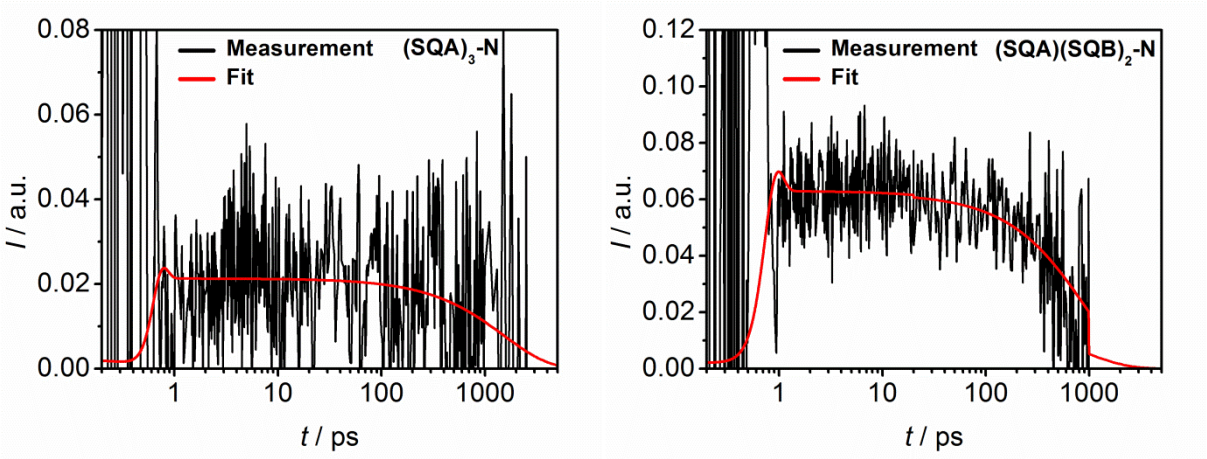

Fig. S3 Anisotropy spectra of the fluorescence upconversion measurements of **(SQA)$_3$-N** (left, pump at 16100 cm^{-1}, fluorescence at 13600 cm^{-1}) and **(SQA)(SQB)$_2$-N** (right, pump at 14400 cm^{-1}, fluorescence at 11100 cm^{-1}) in toluene.

9.4 TD-DFT Calculations[1]

TD-DFT calculations were performed using Gaussian 09[173]. Here we point out that the results of the quantum chemical calculations of exciton states strongly depend on the functional employed.[174] This is particularly true if CT states are involved. Thus, we consider the presented DFT computations more as an explanation of the findings rather than a confirmation.

Table S5 Excited state of **SQA** (D_{2h} symmetry) from TD-DFT computations at B3LYP/cc-pVTZ//B3LYP/6-31G* level of theory.

excited state	symmetry	energy (nm)	oscillator strength	
113 -> 114 0.71226 113 <- 114 -0.13147	singlet-B_U	2.3071 eV (537.40)	1.4096	<S**2>=0.000
n-π* 112 -> 114 0.70517	singlet-B_G	2.3705 eV (523.02)	0.0000	<S**2>=0.000
n-π* 109 -> 114 0.70524	singlet-A_U	3.3172 eV (373.76)	0.0000	<S**2>=0.000
111 -> 114 0.66393 113 -> 115 -0.12453 113 -> 117 0.19337	singlet-A_G	3.4354 eV (360.90)	0.0000	<S**2>=0.000
110 -> 114 0.70010	singlet-B_U	3.4944 eV 354.81	0.1662	<S**2>=0.000
111 -> 114 0.10036 113 -> 115 0.68142 113 -> 117 0.10737	singlet-A_G	3.6876 eV 336.22	0.0000	<S**2>=0.000
107 -> 114 -0.10127 113 -> 116 0.69411	singlet-B_U	3.6996 eV 335.13	0.0171	<S**2>=0.000
108 -> 114 0.26397 111 -> 114 -0.17741 113 -> 115 -0.10182 113 -> 117 0.61528	singlet-A_G	4.0100 eV 309.19	0.0000	<S**2>=0.000
108 -> 114 0.63864 113 -> 117 -0.25235	singlet-A_G	4.1310 eV 300.13	0.0000	<S**2>=0.000
107 -> 114 0.68987 113 -> 116 0.10772	singlet-B_U	4.1319 eV 300.06	0.0430	<S**2>=0.000

[1] The TD-DFT calculations were performed by *Dr. M. Holzapfel*.

Table S6 Excited state of **dSQA** (in C_2 symmetry) from TD-DFT computations at B3LYP/cc-pVTZ(aug at O)//B3LYP/cc-pVDZ level of theory.

excited state	symmetry	energy (nm)	oscillator strength	
224 -> 227 0.10023 225 -> 226 0.69923	singlet-B	1.9770 eV (627.15)	1.6513	<S**2>=0.000
224 -> 226 0.47050 225 -> 227 0.52664	singlet-A	2.0628 eV (601.05)	0.0007	<S**2>=0.000
224 -> 227 0.69670	singlet-B	2.2744 eV (545.13)	1.6905	<S**2>=0.000
224 -> 226 0.53186 225 -> 227 -0.47678 224 <- 226 -0.10004 225 <- 227 0.10115	singlet-A	2.3581 eV (525.77)	0.1540	<S**2>=0.000
n-π* 222 -> 227 0.46476 223 -> 226 0.52994	singlet-A	2.3786 eV (521.26)	0.0000	<S**2>=0.000
n-π* 222 -> 226 0.52997 223 -> 227 -0.46483	singlet-B	2.3786 eV (521.26)	0.0000	<S**2>=0.000
221 -> 226 0.68279 225 -> 228 0.12762	singlet-B	3.0941 eV (400.71)	0.0135	<S**2>=0.000
n-π* 222 -> 226 0.46674 223 -> 227 0.53061	singlet-B	3.1142 eV (398.13)	0.0000	<S**2>=0.000
n-π* 222 -> 227 0.53065 223 -> 226 0.46674	singlet-A	3.1142 eV (398.13)	0.0000	<S**2>=0.000
221 -> 227 0.68569 224 -> 228 0.12094	singlet-A	3.1895 eV (388.73)	0.0002	<S**2>=0.000
216 -> 227 -0.46096 217 -> 226 0.53256	singlet-B	3.3333 eV (371.95)	0.0000	<S**2>=0.000
216 -> 226 0.53134 217 -> 227 -0.46199	singlet-A	3.3334 eV (371.95)	0.0000	<S**2>=0.000
218 -> 227 0.14807 219 -> 226 0.51516 220 -> 227 -0.35877 225 -> 228 -0.24802	singlet-B	3.4505 eV (359.32)	0.1983	<S**2>=0.000
218 -> 226 -0.12075 219 -> 227 -0.34852 220 -> 226 0.56535 224 -> 228 -0.14235	singlet-A	3.4514 eV (359.23)	0.0061	<S**2>=0.000
219 -> 226 0.25809 221 -> 226 0.15091 225 -> 228 0.62145	singlet-B	3.5764 eV (346.67)	0.0457	<S**2>=0.000

Table S7 Excited state of **SQB** (C_{2v} symmetry) from TD-DFT computations at B3LYP/cc-pVTZ//B3LYP/6-31G* level of theory.

excited state	symmetry	energy (nm)	oscillator strength	
124 -> 126 0.16413 124 -> 126 0.69114 125 <- 126 -0.10893	singlet-B2	1.9407 eV (638.86)	0.5698	<S**2>=0.000
124 -> 126 0.68643 125 -> 126 -0.16850	singlet-B2	2.8668 eV (432.48)	0.8805	<S**2>=0.000
n-π* 122 -> 126 0.70549	singlet-B1	3.1167 eV (397.80)	0.0000	<S**2>=0.000
123 -> 126 0.66551 125 -> 128 -0.14424 125 -> 130 -0.15405	singlet-A1	3.3428 eV (370.90)	0.0243	<S**2>=0.000
123 -> 126 0.10239 125 -> 127 0.67837 125 -> 128 0.13174	singlet-A1	3.5429 eV (349.95)	0.2920	<S**2>=0.000
121 -> 126 0.19082 125 -> 129 0.67505	singlet-B2	3.7096 eV (334.22)	0.0077	<S**2>=0.000
120 -> 126 0.14043 125 -> 127 -0.14093 125 -> 128 0.60561 125 -> 130 -0.28127	singlet-A1	3.7335 eV (332.08)	0.0301	<S**2>=0.000
120 -> 126 -0.33747 123 -> 126 0.14624 124 -> 127 0.10001 125 -> 128 0.28759 125 -> 130 0.51296	singlet-A1	3.8566 eV (321.48)	0.0438	<S**2>=0.000
121 -> 126 0.67062 125 -> 129 -0.19645	singlet-B2	3.9129 eV (316.86)	0.0776	<S**2>=0.000
120 -> 126 0.59309 123 -> 126 0.11174 125 -> 130 0.34796	singlet-A1	3.9624 eV (312.90)	0.0119	<S**2>=0.000

9.5 List of Publications

1. *Localization/Delocalization of Charges in Bay-Linked Perylene Bisimides*, W. Jiang, C. Y. Xiao, L. X. Hao, Z. H. Wang, H. Ceymann, C. Lambert, S. Di Motta and F. Negri, *Chemistry-a European Journal*, 2012, **18**, 6764-6775.
2. *Synthesis, Electrochemical, and Optical Properties of Low Band Gap Homo- and Copolymers Based on Squaraine Dyes*, S. F. Völker, T. Dellermann, H. Ceymann, M. Holzapfel and C. Lambert, *J. Polym. Sci. A Polym. Chem.*, 2014, **52**, 890-911.
3. *Coupled Oscillators for Tuning Fluorescence Properties of Squaraine Dyes*, C. Lambert, T. Scherpf, H. Ceymann, A. Schmiedel and M. Holzapfel, *J. Am. Chem. Soc.*, 2015, **137**, 3547-3557.
4. *Localised and delocalised excitons in star-like squaraine homo- and heterotrimers*, H. Ceymann, M. Balkenhohl, A. Schmiedel, M. Holzapfel and C. Lambert, *PCCP*, 2016, **18**, 2646-2657.
5. *Decoupling charge transport and electroluminescence in a high mobility polymer semiconductor*, J. Harkin, K. Broch, M. H. Schreck, H. Ceymann, A. Stoy, C.-K. Yong, M. Nikolka, I. McCulloch, N. Stingelin, C. Lambert, H. Sirringhaus, *Adv. Mater.* 2016, DOI: 10.1002/adma.201600851.
6. *Cooperative Enhancement versus Additivity of Two-Photon-Absorption Cross Sections in Linear and Branched Squaraine Superchromophores,* H. Ceymann, A. Rosspeintner, M. H. Schreck, C. Mützel, A. Stoy, E. Vauthey and C. Lambert, *PCCP*, 2016, submitted.

9.6 Conference Contributions

1. Oral presentations:

1.1 Workshop of the Research Training School 1221 (GRK 1221), October **2012**, Schöntal, Germany.

1.2 Workshop of the DFG Forschergruppe 1809, Juni **2015**, Schöntal, Germany.

2. Posters:

2.1 Conference of the Research Training School (GRK 1221), September **2011**, Würzburg, Germany.

2.2 10^{th} International Symposium on Functional π-Electron Systems, October **2011**, Beijing, China.

2.3 Workshop of the Research Training School 1221 (GRK 1221), October **2012**, Schöntal, Germany.

2.4 26^{th} International Conference on Photochemistry (ICP 2013), July **2013**, Leuven, Belgium.

2.5 Conjugated Oligomers and Polymers (KOPO 2013), September **2013**, Retzbach, Germany.

2.6 Workshop of the Research Training School 1221 (GRK 1221), October **2013**, Kloster Banz, Germany.

2.6 XXVth IUPAC Symposium on Photochemistry, July **2014**, Bordeaux, France.

2.7 Conference of the Research Training School (GRK 1221), March **2015**, Würzburg, Germany.

2.8 Conjugated Oligomers and Polymers (KOPO 2015), September **2015**, Würzburg, Germany.